



UNIVERSITÄT
DES
SAARLANDES



Dynamic
Biomaterials

Tetrazole Methylsulfone - Thiol crosslinked hydrogels for automated and high-throughput 3D cell culture

Dissertation

zur Erlangung des Grades

des **Doktors der Naturwissenschaften**

der Naturwissenschaftlich-Technischen Fakultät

der Universität des Saarlandes

von

Adrián de Miguel Jiménez

Saarbrücken, July 2024

Tag des Kolloquiums: 01.10.2024

Dekan: N.N.

Berichterstatter: Prof. Dr. Aránzazu del Campo Bécares

Prof. Dr Karen Lienkamp

Akad. Mitglied: Dr. Sara Trujillo-Muñoz

Vorsitz: Prof. Dr.-Ing. Markus Gallei

Abstract

The understanding of diseases and the development of personalized therapies relies on the predictive potential of 3D cell culture models. Automation of the culture steps is crucial, for which in situ crosslinked hydrogels with adequate and tunable kinetics under physiological conditions are needed to temporally replace the natural 3D matrix. This Thesis investigates hydrogels formed by tetrazol methylsulfone (TzMS) derivatized star-polyethylene glycol and thiol-crosslinkers for automated 3D cell encapsulation, including precursor synthesis scale-up, characterization of their crosslinking kinetics and mechanical properties, and their semi-automated preparation with pipetting robots. The optimization of reaction and purification conditions allowed for an upscaling to 0.6-g scale of polymer precursor. The gelation kinetics and mechanical properties of the hydrogels were studied as a function of precursors stoichiometry, crosslinker architecture, biofunctionalization degree and pH. Tunability of gelation time and stiffness at pH 7.0 – 8.0 was explored for a cell-compatible hydrogel composition including the cell-adhesive ligand RGD and the enzyme-cleavable peptide VPM as crosslinker. A semi-automated pipetting protocol was set up to prepare 5 μ l hydrogels in a 384-well plate format, and statistical experimental design was used to systematically minimize variability. The results demonstrate the suitability and limitations of TzMS/thiol chemistry for in situ cell encapsulation.

Kurzzusammenfassung

Das Verständnis von Krankheiten und die Entwicklung personalisierter Therapien hängen von dem Fortschritt bei 3D-Zellkulturmodellen ab, bei denen *in situ* gebildete Hydrogele verwendet werden, um Zellen einzukapseln und die natürliche 3D-Matrix vorübergehend zu ersetzen. Von Vorteil sind Hydrogele mit kontrollierter Vernetzungskinetik, die in automatisierte Arbeitsabläufe implementiert werden können. Diese Dissertation befasst sich mit Hydrogelen, die aus Tetrazolmethylsulfon (TzMS)-derivatisiertem Stern-Polyethylenglykol mit kommerziellen thiolierten Vernetzern gebildet werden. Die bestehende fünfstufige Synthese und Aufreinigung der Hydrogel-Vorläufers wurde optimiert und hochskaliert. Die Vernetzungskinetik und mechanische Eigenschaften der Hydrogele wurden in Abhängigkeit von Stöchiometrie der Ausgangsstoffe, Vernetzerarchitektur, Biofunktionalisierungsgrad und pH-Wert untersucht. Die Einstellung von Vernetzungszeit und Steifigkeit wurden bei einem pH-Wert von 7,0 bis 8,0 für ein zellkompatibles Hydrogel mit dem zelladhäsiven Liganden RGD und dem enzymspaltbaren Peptid VPM als Vernetzer erforscht. Es wurde ein halbautomatisches Pipettierprotokoll für die Herstellung von 5 µl-Hydrogelen in einem 384-Well-Plattenformat erstellt, und die Variabilität mithilfe eines statistischer Versuchsplan systematisch minimiert. Die Ergebnisse zeigen die Eignung und die Grenzen der Thiol-TzMS-Chemie für die *in situ* Zellverkapselung.

Acknowledgements

The work presented in this thesis was conducted in the Dynamic Biomaterials group from the INM – Leibniz Institute for New Materials under the scientific mentorship of Prof. Dr. Aránzazu del Campo.

It has been a long but fruitful journey that I have accomplished in large part due to the constant support of many people. While I will mention everyone below, their recognition in this thesis only scratches the surface of my deep gratitude towards each and every one of them.

I am especially thankful to Prof. Dr. Aránzazu del Campo for providing me with the opportunity to join her multidisciplinary and international research group and pursue this exciting doctoral thesis. Her invaluable scientific guidance and continuous support have been instrumental throughout my doctoral research. Moreover, I extend my deepest appreciation to Dr. Samuel Pearson, whose supervision went beyond his obligations. His wise advice, both personally and professionally, along with his encouragement, was indispensable during this challenging path.

Additionally, I am also grateful to Dr. Julieta Paez for her contribution to establishing the foundations of the project that I continued during this thesis. Her scientific advice and support during my initial steps at INM were of great value.

I cannot proceed without thanking my exceptional office colleague, Stefan Brück. Since the beginning at INM, he has always been there to help and share his extensive knowledge accumulated over his scientific career. I could have never asked for a better office colleague, and I will always carry with me all his lessons and advice.

The last stages of a PhD thesis are usually the hardest. So, I especially want to thank my office colleague Therese for always being there during that part, whether it was a personal talk or a scientific discussion.

Throughout my time at INM, I have been fortunate to be surrounded by the bright and friendly scientists from the Dynamic Biomaterials group: Zahra, Qiyang, Maria

Villiou, Frano, Gülistan, Emmanuel, Syuzanna, Jennifer, Nguyen, Sandipan, Usama, Lara, Namine, Christopher, Britta, Krupansh, Kathrin, Simon, as well as Dr. Sara Trujillo Muñoz and Dr. Shrikrishnan Sankaran, who became group leaders during my stay at INM. Special recognition is also due to Martina Bonnard, the exceptional secretary of Dynamic Biomaterials group and ever better person. Her constant help and support during my time in Saarbrücken was undoubtedly very important to me.

I have had the good fortune to meet some very nice people, but also make wonderful friends who made my stay at INM (and in Saarbrücken) very enjoyable, including Minye, Mitchel, Shardul, María, Ana and Lola. Thank you very much for your support and for the great and unforgettable moments we have shared together.

Furthermore, I want to express my gratitude to all those at INM who have directly or indirectly contributed to this thesis, such as Dr. Claudia Fink-Straube and Ha Rimbach-Nguyen for their assistance with rapid and efficient analytical measurements, and Sabine Müller and Bernd Rus for their endless support with important paperwork.

Special thanks are reserved for my collaborators at IPF - Institute of Polymer Research, Dr. Nicholas Dennison and Dr. Maximilian Fusenig, who warmly welcomed me during my research stay in Dresden. They helped me immensely in laying the groundwork for the last chapter of this thesis, while also transferring valuable knowledge to me.

Finally, I want to thank the most significant people in my life, my family and friends, who have been the pillars of my mental health throughout this journey.

I want to start with who I sincerely believe is my other half, Rocío. I have so much to thank you for that I do not know where to begin. You were the main reason I embarked on this journey. It has been a hard path, but I would not change it if I could choose again. I have grown as a person and as a scientist, and I have grown in large part because you have believed in me all this time. I have always been able to count on your support and love, which have kept me going despite the difficulties. This is just a small sign of how grateful I am to have you by my side, so thank you, Rocío.

To my beloved family—my parents Lourdes and Javier, and my brother Daniel—your unconditional love and support have been my guiding light even from the distance.

Last but not least, I want to thank the people I consider my second family, my old friends Alberto, Borja, Carlos, Gloria, Irene, Javier, Kees and Santiago from Alameda de Osuna (Madrid, Spain), and Celso and Guillermo from Gijón (Asturias, Spain), as well as my friends from university Lucía, Mónica and Roberto. I do not know what would have become of me during this time away from home without their full support. I am very grateful to have such great friends who have pushed me toward the meaningful achievement of completing my PhD thesis.

Thank you all from the bottom of my heart.

To my dear grandmothers Lorenza and Aurora, and my aunt Adela, who are no longer with us, but will always be in my heart.

Table of contents

Kurzzusammenfassung	ii
Acknowledgements	iii
1 Motivation and objectives of this Thesis	1
2 State-of-the-art	8
2.1 Poly(ethyleneglycol)-based hydrogels.....	8
2.2 Crosslinking reactions to form hydrogels	10
2.2.1 Requirements to a crosslinking reaction for cell encapsulation	10
2.2.2 Physical crosslinking	11
2.2.3 Chemical crosslinking	12
2.3 Thiol-based crosslinking reactions for hydrogel formation	19
2.4 Thiol-Aryl methylsulfone (MS) crosslinking.....	24
2.5 Gelation of star-PEG hydrogel precursors and resulting networks ...	32
2.5.1 Kinetics of crosslinking	32
2.5.2 Network structure	34
2.6 Monitoring of gelation by rheology	37
2.7 High-throughput 3D cell culture	42
2.7.1 Automation of cell-encapsulated hydrogels for drug discovery	42
2.7.2 Process optimization with multiple parameters	45
3 Synthesis of the hydrogel precursor 4armPEG-Tetrazole Methylsulfone..	57
3.1 Introduction: optimization of reaction conditions and upscaling in organic synthesis	57
3.2 Objectives	58
3.3 Results	61
3.3.1 Optimization and upscaling of individual reaction steps.....	61
3.3.1.1 Methylation of the thiol group of Tz-1	61
3.3.1.2 Etherification of Tz-2 to introduce a Boc-protected amine and obtain Tz-3	64

3.3.1.3	Oxidation of methyl sulfide group	67
3.3.1.4	Boc deprotection	70
3.3.1.5	End-functionalization of PEG-4NHS to obtain PEG-4TzMS.....	75
3.3.1.6	Quantification of the degree of end-group functionalization and molecular weight (MW) of PEG-4TzMS	77
3.4	Discussion and outlook	79
3.5	Materials and general methods.....	88
3.5.1	Synthesis of PEG-4TzMS	89
3.5.2	Cost analysis.....	92
4	Rheological characterization of crosslinking kinetics and mechanical properties	96
5	Automated hydrogel preparation in pipetting robot	115
5.1	Introduction.....	115
5.1.1	Automated liquid handling in high throughput screening of pharmaceuticals 115	
5.1.2	Design of experiments (DoE) to identify working parameters and establish robust pipetting protocols at minimum effort.....	116
5.2	Objectives	118
5.3	Results and discussion	118
5.3.1	Steps in the development of an automated pipetting method	118
5.3.2	Design of the pipetting workflow	119
5.3.3	Programming of the pipetting robot	122
5.3.3.1	Liquid level detection of small volumes	123
5.3.3.2	Modularity of the pipetting method.....	125
5.3.3.3	Minimizing material waste	126
5.3.4	Pretesting of the pipetting parameters using water.....	126
5.3.5	Pipetting with hydrogel precursor solutions	127
5.3.6	Establishment of mixing parameters for PEG-4TzMS hydrogel preparation using a Design-of-Experiments approach	130
5.3.6.1	Selection of the fluorescent dyes for detection.....	131

5.3.6.2	Impact of flow rate, volume, and cycles on the mixing	133
5.3.7	Insights from the two consecutive dispensing steps into the 384-well plate 139	
5.3.7.1	Isolation of the final dispensing step by manual mixing	140
5.3.7.2	First dispensing effect: the impact of using sacrificial wells	141
5.3.7.3	Increasing viscosity: study on the effect of gelation time	144
5.3.7.4	Low precision dispensing: offsetting the even / odd difference at short gelation times by dispensing asymmetric volumes	148
5.4	Conclusions and outlook.....	151
5.5	Materials and methods.....	153
5.5.1	Materials and equipment	153
5.5.2	Methods.....	154
5.5.2.1	Programming the pipetting method for thiol-TzMS hydrogels automated preparation	154
5.5.2.2	Protocol optimization using blank aqueous solutions	158
5.5.2.3	Preparation of precursor solutions for hydrogel optimization ..	159
5.5.2.4	Protocol optimization for hydrogels	160
5.5.2.5	Assessment of hydrogel variability	160
5.5.2.6	Design of Experiments.....	161
5.5.2.7	Alternative protocol for the isolation of the final dispense into 384 well plate	161
5.5.2.8	Modifying the pipetting method for the study of sacrificial wells 162	
5.5.2.9	Setting different gelation times	162
6	Conclusions and outlook.....	164
7	List of publications	169

1 Motivation and objectives of this Thesis

The discovery and development of new drugs is a labor- and resource-intensive process that typically takes up to 15 years.¹ This process involves the identification of biologically active molecules from extensive compound libraries, followed by high-throughput screening (HTS) to evaluate the activity of the compounds in different in vitro biological scenarios.² HTS is done by automated robots for liquid handling, typically using 384- or 1536-well plates with volumes <10 μ l per well. Despite the streamlining of the screening process and the resulting savings in resources, there has not been a commensurate increase in the number of drugs approved. This is mainly due to the modest predictive output of current cell assays in 2D cell culture models, which are not sufficient to resemble the physiological complexity of the native tissues from the human body. 3D cell cultures using synthetic matrices that emulate the composition and physical properties of the natural extracellular matrix of tissues can overcome some of these limitations.³ HTS cell assays in 3D cultures require in situ forming hydrogels for cell encapsulation, with properties compatible with liquid handling systems and living organisms^{002E}

To be suitable for cell encapsulation, hydrogels need to fulfil a number of criteria. Primary considerations include their biocompatibility with the cells, and the controlled degradability of the three-dimensional network under physiological conditions. Precursor solutions with low viscosity are needed for accurate liquid transfer, effective mixing of reactants and cells and low shear forces during the mixing and transfer steps. The crosslinking mechanism should be efficient at mild, physiological conditions, and ideally be orthogonal to the physiological milieu. The crosslinking kinetics of the hydrogel is crucial for ensuring the uniformity of both the hydrogel structure and cell distribution during the encapsulation steps. If crosslinking occurs too rapidly, homogeneous mixing is not possible and cell aggregates will be heterogeneously distributed in the hydrogel, while if crosslinking is too slow, cells may sediment at the bottom of the hydrogel during the gelation process. For application in automated HTS formats for 3D cell culture, the crosslinking kinetics needs to be adapted to the time sequence of the pipetting, mixing and delivery steps of the handling robot. Systems whose crosslinking process can be tuned to accommodate to the hydrogel preparation sequence are desirable.

Physical and chemical crosslinking mechanisms have been used for cell encapsulation in hydrogels. Among chemical crosslinking mechanisms, thiol-mediated crosslinking reactions stand out due to several advantageous properties. Thiols can act as nucleophiles in substitution or addition reactions in comparison to other nucleophiles used for crosslinking, such as amines, thiols exhibit higher nucleophilicity at physiological conditions, making them more selective toward electrophiles. The reaction kinetics can be adjusted by changes in the pH, which controls the ratio of deprotonated thiol (thiolate) as more reactive species. Thiolated polymeric backbones and bioactive ligands are commercially available in different forms, and therefore accessible for functionalization of encapsulating matrices. Thiol groups are present in proteins containing cysteines, but only at low number and, therefore, do not significantly interfere with the crosslinking reaction. The stability of the resulting thioether bond varies based on the substituents involved in the reaction, allowing for customization of the hydrogel's properties, such as degradation rate.

Different types of thiol-mediated crosslinking reactions have been used for cell encapsulation: thiol-Michael addition, thiol-halogen ligation, thiol-epoxy opening, disulfide bond formation, split luciferin ligation, thiol-ene radical reaction, and thiol-aryl methylsulfone substitution. However, some of these reactions require basic conditions, (toxic) catalysts/oxidants, or even UV light for radical formation. Thiol-mediated reactions typically involve the nucleophilic attack of a thiol on an electrophile and are pH-dependent due to the stronger nucleophilicity of the deprotonated thiolate (S^-).

One of the most widely employed thiol-mediated reactions for 3D cell encapsulation in hydrogels is the thiol-Michael addition reaction, where the thiol (nucleophile) attacks an α , β -unsaturated carbonyl (electrophile). Among the most commonly used electrophiles for hydrogel formation, maleimide and vinyl sulfone stand out. The maleimide-mediated reaction is very fast (gelation time of seconds at $pH \geq 7$), which can lead to inhomogeneous pre-hydrogel mixtures and generates a product that is susceptible to Retro-Michael reaction and hydrolysis,⁴ making it unsuitable for long-term cell culture.⁵ Conversely, the vinyl sulfone-mediated reaction is considerably slower at physiological pH (several minutes to hours⁶), making it suitable for long-term cell culture due to the stability of the product towards hydrolysis.⁷ Other electrophiles, such as (meth)acrylates

or alkyne esters, require basic catalysts at physiological conditions and yield hydrolysis-unstable products. Recently, pyridazinediones have been introduced as alternative electrophiles in thiol-Michael addition crosslinking reactions, showing gelation times of less than 30 minutes at physiological pH and stability towards hydrolysis without undergoing the Retro-Michael reaction when using mono- or di-Br substituted pyridazinediones. Other thiol-mediated chemistries, such as thiol-halogen ligation (nucleophilic substitution of a halogen) and thiol-epoxy (nucleophilic opening of an epoxy ring), require basic conditions and often toxic catalysts such as the case of thiol-epoxy.⁸ Despite these drawbacks, hydrogels have been successfully formed using both approaches.^{9,10}

Disulfide bond formation has also been used for hydrogel crosslinking.¹¹ However, its relatively slow reaction kinetics at physiological pH¹² and the potential for thiol exchange reactions make it challenging for 3D cell encapsulation.

Another successful thiol-mediated reaction for hydrogel crosslinking is the split luciferin ligation, which involves (N-terminal)d-cysteine as the thiol source. Although it enables the formation of cell-encapsulated hydrogels with gelation times from seconds to minutes,¹³ the presence of d-cysteine in the physiological environment can cause interference, and the stability of the luciferin adduct decreases after 14 days, making it unsuitable for long-term cell culture.

Thiol-mediated photochemistry has been applied for hydrogel crosslinking through the thiol-ene reaction,^{14,15} a radical reaction initiated by light. While this approach offers fast kinetics and spatiotemporal control, the potential damage from UV light and free radicals to cells poses significant disadvantages.

Despite the application of various thiol-mediated chemistries for crosslinking 3D cell-encapsulated hydrogels, there is still a need for a crosslinking reaction that is tunable in kinetics, selective, and results in stable hydrogels suitable for long-term cell culture.

The thiol-aryl methylsulfone (MS) chemistry was introduced for the crosslinking of cell-encapsulated hydrogels by our group in 2020⁶ as an alternative to the widely used thiol-Michael addition reactions: thiol-maleimide (which crosslinks too fast) and thiol-vinyl

sulfone (which crosslinks too slow). The thiol-methylsulfone reaction exhibited intermediate crosslinking kinetics between the two systems at physiological conditions. Among tetra-arm polyethylene glycol (PEG)-MS precursors with different aryl MS groups (oxadiazole-MS, tetrazole-MS and benzothiazole-MS) the tetrazol-MS derivative exhibited a gelation time of 1.6 min under biologically relevant conditions, which was considered an appropriate time scale for in situ forming hydrogels for cell encapsulation.¹⁶ Moreover, thiol-methylsulfone hydrogels have demonstrated improved stability under cell conditions compared to maleimide hydrogels. They also exhibit suitable and tunable gelation kinetics, which facilitate complete mixing and result in homogeneous hydrogels, as well as cell distribution.⁶ Tetrazole-MS hydrogels were successfully tested for 3D cell encapsulation, demonstrating $\geq 90\%$ cell viability on day 7 (the maximum recorded duration).¹⁶ The positive results regarding their biocompatibility make these hydrogels a promising system for overcoming the limitations of the two widely employed thiol-chemistries for hydrogel crosslinking and 3D cell encapsulation: thiol-maleimide and thiol-vinyl sulfone systems.

Whereas maleimide and vinyl sulfone derivatized poly(ethylene glycol) hydrogel precursors for cell culture are commercially available at gram scale, aryl methylsulfone hydrogel precursors are not. The synthesis of the tetra-arm PEG tetrazole-MS (PEG-4TzMS) at 100 mg scale through a 5-step synthetic pathway had been established by our research group at the start of this Thesis (unpublished work). **To further test this system for medium to high-throughput 3D cell encapsulation, it was necessary to optimize and upscale the protocols to gram scale.** This includes more efficient synthesis steps, with higher yields, reduced reaction and purification times, and lower costs. This was the first goal of this Thesis (**Chapter 2**), to be achieved by screening alternative reaction parameters that impact time and yield, including temperature, concentration, stoichiometry, catalyst, solvent, pH, or stirring conditions. A transition to purification techniques compatible with larger scales, such as automated flash chromatography or precipitation, should also be explored and implemented where feasible. Alternative synthesis pathways should also be considered if the bottlenecks of the current strategy could not be overcome by optimizing the reaction conditions.

The understanding of the parameters influencing the kinetics of the crosslinking reaction is crucial for the implementation of a new cell encapsulation chemistry, as it directly influences the formation and homogeneity of the final hydrogel network and 3D cell culture. In addition, the final structure and mechanical properties of the final hydrogel can significantly affect cell function. Depending on the gelation kinetics, spatial inhomogeneities (at the 100 nm scale) in the hydrogel or non-homogeneous distribution of polymer units, and local inhomogeneities (at the molecular scale), such as connective defects like entanglements or dangling ends, may form. Those can affect the bioactivity of the hydrogel matrix as they can change the distribution of bioactive ligands and also the evolution of the mechanical properties of the matrix as it degrades during cell culture.^{17,18} Therefore, a systematic characterization and deep understanding of the compositional and reaction parameters affecting the crosslinking kinetics, particularly the gelation time, as well as the final mechanical properties, was important for the further development of MS-thiol hydrogels for cell-encapsulation.

For such studies, star-PEG polymers are convenient precursors since they can form fairly homogeneous hydrogels due to their symmetrical structure if the reaction kinetics is appropriate. For hydrogels forming with a stoichiometric A-B type crosslinking reactions between the end-groups of star-PEG chains, two different crosslinking regimes can be observed: diffusion-limited and reaction-limited. Diffusion-limited crosslinking leads to networks with inhomogeneities because the reaction between A and B occurs faster than the diffusion of the precursors, resulting in clusters with higher concentrations of specific reactive groups and local defects. In contrast, in reaction-limited crosslinking, such as in thiol-MS hydrogels, crosslinking proceeds slower than diffusion, allowing for even distribution and stepwise reaction of A and B, and producing a more orderly network with significantly reduced inhomogeneities.¹⁹ This regime is advantageous for cell encapsulating hydrogels.

The kinetics of crosslinking in thiol-MS (star-PEG) hydrogels, and therefore the crosslinking regime of a reactive precursor mixture, depends on external factors such as pH, which affects thiolate availability, and ionic strength, which can inhibit species diffusion due to shielding effects. By changing these parameters, reaction- or diffusion-limited hydrogels can be formed. The chemical nature of the MS unit, the concentration

of reactive groups and polymer and the length of the PEG backbone also impact the crosslinking kinetics. **The study of how compositional factors impact the gelation time of PEG-MS/thiol hydrogels under conditions used for cell encapsulation was the second objective of this Thesis (Chapter 3).** For this purpose, the crosslinking process and the mechanical properties of hydrogels should be monitored and studied by rheology. From these studies, the gelation time, as well as how it changes and can be tuned with the hydrogel precursor composition and gelation conditions, need to be quantified. Additionally, the final mechanical properties of the hydrogel should be determined. Building on the preliminary rheological studies conducted by our group on the conceptual hydrogel composition involving PEG-4TzMS and PEG-4SH as crosslinker, this thesis should progress from the initial conceptual formulation using PEG-4SH as a crosslinker to the final biologically relevant formulation, which involve pre-functionalizing the PEG backbone with a cell adhesive ligand (cyclo[RGDfC]) and using an enzymatically cleavable crosslinker (VPM). This rheological study should examine the effects of reactive group stoichiometry, polymer concentration, pH, crosslinker architecture, and chemical structure. Time sweep measurements recording the shear modulus (G^*), storage/elastic modulus (G'), and loss/viscous modulus (G'') over time should provide a detailed understanding of the hydrogel behavior during the crosslinking process. The obtained results should support the implementation of the in-situ hydrogel 3D cell encapsulation in automated medium/high-throughput workflows.

While medium/high-throughput experimentation is desired for drug discovery, the lack of validated polymer systems for 3D cell encapsulation compatible with automated instruments, such as liquid handling robots, hinders the development. Automated handling offers many advantages over manual approaches, such as parallel testing of high number of samples and conditions with increased reproducibility by eliminating human errors, standardized protocols, and enhanced accuracy and precision in the handling of very small volumes (down to 5 microliter scale). Therefore, developing and automating the preparation of in-situ forming hydrogels compatible with 3D cell encapsulation in liquid handling robots is highly desirable.

In this context, the 4th Chapter of this thesis focuses on transitioning from manual preparation (10 μ L hydrogels in a 15-well plate) to semi-automated preparation of 5

μ L thiol-MS hydrogels for 3D cell encapsulation in a 384-well plate format using an automated handling robot in order to validate the PEG-MS/thiol system for high throughput cell culture experiments. Based on the knowledge gained on gelation kinetics and hydrogel mechanics from rheological measurements, a realistic workflow of mixing and dispensing steps should be conceived and tested in terms of robustness and variability. To monitor reproducibility of the prepared hydrogels, different dyes will be included in the mixing solutions, and their concentrations should be tracked in the final hydrogels. The optimization process should follow a design of experiments (DOE) approach to quantify and visualize the impact of the different pipetting parameters on the variability of the volumes from the final hydrogels, as well as the interaction between the parameters. The study should provide a framework for understanding the influence of the multiple pipetting parameters involved in automated liquid handling, leading to more reliable and efficient automated pipetting workflows. Additionally, the reproducibility of the final hydrogel dispensed volumes will be optimized by studying and systematically reducing the variability of the dispensed volumes.

This Thesis aims to fill the gap of in-situ forming hydrogels suitable for automated medium/high-throughput 3D cell encapsulation workflows, as well as bridging the gap in the literature by providing a clear, reproducible protocol for transitioning from manual to semi-automated hydrogel preparation, facilitating the adoption of more efficient and standardized workflows in hydrogel-based 3D cell encapsulation.

2 State-of-the-art

2.1 Poly(ethyleneglycol)-based hydrogels

Hydrogels are polymeric materials capable of absorbing and retaining water. They are formed by hydrophilic polymeric chains which are either physically or chemically crosslinked into a three-dimensional network. Hydrogels are important materials in different biomedical contexts as carriers for drug delivery, dressings for wound healing, or scaffolds for cell culture and tissue engineering. For these applications, the polymeric chains need to be biocompatible.

Hydrogels can be classified as synthetic and natural depending on the source of origin of their backbone.^{20–22} Natural hydrogels are formed by polymers derived from natural sources such as gelatine or hyaluronic acid (HA) (animals), and alginate, starch or cellulose (plants). Synthetic hydrogels are artificially produced and can have different compositions depending on the monomer's chemical structure and macromolecular architecture.^{23,24} By using precursors of different chain length, architecture and functionality, hydrogels with tailored crosslinking degree and different network structures can be synthesized (**Figure 1**).

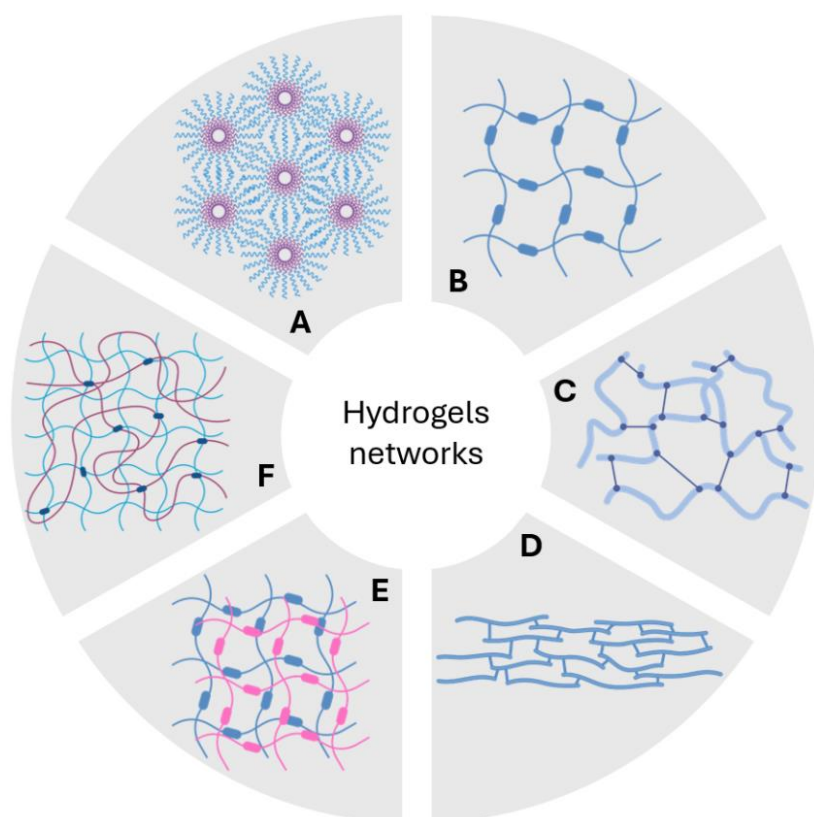
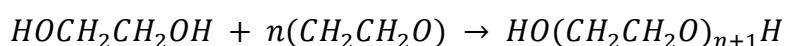


Figure 1. Network structure of different types of hydrogels **A**), Micellar structure (formed through crosslinking of self-assembled amphiphilic polymers)²⁵; **B**) Highly ordered and homogeneous structure (formed through stepwise crosslinking of star-shaped polymers)²⁶; **C**) Random and heterogeneous structure (formed through random crosslinking of linear polymers)²⁷; **D**) Fibrillar structure (formed through application of a tensile force after crosslinking of certain polymers like cellulose)²⁸, **E**) Interpenetrating networks structure (formed when a polymeric network is crosslinked within a previously crosslinked network), **F**) Co-network structure (formed through crosslinking of two or more different polymers).²⁷ Created with BioRender.

Poly(ethyleneglycol) (PEG) is one of the most common synthetic backbones used in hydrogels. PEG is usually synthesized by alkali alkoxide initiated, living anionic step-growth polymerization of ethylene oxide,²⁹ which consists in the exothermic reaction of ethylene oxide with ethylene glycol (**Equation 1**) in presence of a basic catalyst. By controlling the stoichiometry of species and the feeding of ethylene oxide, the molecular weight of the growing polymer chain increases linearly, and low polydispersity is achieved.



Equation 1. Polymerization reaction of linear PEG.

PEG is also available as multi-arm molecules, also known as star-PEGs, in which at least three linear PEG arms are connected to a central core. Star-PEGs are synthesized following the so called “core first” or “arms first” mechanism. “Core first” consists in using a multi-functional core such as glycerol (3-arm PEG product) or pentaerythritol (4arm PEG product) for reacting with ethylene oxide following a similar protocol as described in **Equation 1**. In “arms first” strategy, previously synthesized linear PEG molecules are attached to a multi-functional core.³⁰

PEG is commercially available in different molecular weights with a variety of chain architectures (e.g. multi-arm star shaped polymers with 4 or 8 arms) and reactive end group functionalities.⁷ This allows formation of PEG hydrogels with variable crosslinking density and via different polymerization reactions. PEG is interesting for biomedical

applications as it is inert, stable and non-toxic during body circulation, presenting a very low immunogenicity.^{31,32} PEG hydrogels can be modified with cell adhesive factors to improve cytocompatibility^{33,34} for their use in cell culture or tissue engineering,^{35,36} and crosslinked with enzyme-cleavable crosslinkers to incorporate biodegradability.^{36,37}

2.2 Crosslinking reactions to form hydrogels

To form a 3D network, polymeric precursors need to be crosslinked. This can be achieved by physical or chemical mechanisms, here particularized for PEG based hydrogel networks.

2.2.1 Requirements to a crosslinking reaction for cell encapsulation

Among the different applications of hydrogels, this Thesis focuses on hydrogels used as matrices to encapsulate cells and support their growth in vitro (cell culture or tissue engineering) and in vivo (cell therapies and regenerative medicine). For cell encapsulation, the formation of the 3D network occurs in the presence of living cells and, therefore, the crosslinking process needs to meet particular criteria:

- i. Cytocompatibility. The polymer precursors (including catalysts) and resulting products after crosslinking (including both network and side products) must be inert to cells, and the crosslinking process should work in conditions close to the physiological environment. This means aqueous medium, physiological pH ranging between 7.2 and 7.5, and a temperature range between 20-25°C (room temperature (rt)) and 40°C, with an ideal target of 37°C.³⁸ If light is employed to initiate the crosslinking reaction, preference should be given to visible light to prevent potential DNA damage.³⁹
- ii. Biorthogonality. The process should be biorthogonal and do not interact with biological moieties from the physiological environment.
- iii. Crosslinking kinetics within the time scale of minutes. The reaction should be slow enough to allow mixing of reactive precursors and cells at low shear rates, and fast enough to avoid cell sedimentation to the bottom of the hydrogel after mixing.
- iv. Efficient reaction. Reactive moieties from hydrogel precursors must react quantitatively to form a stable 3D network and avoid side reactions with non-crosslinked material.

- v. **Stability.** The bond resulting from the crosslinking reaction must be stable under cell culture conditions to allow long-term cell culture. Furthermore, the hydrogel precursors should be stable in storage.

The 3D network of cell-encapsulated hydrogels should degrade at a suitable rate to allow the expansion of the cells and the deposition of cell's own extracellular matrix (ECM). This can be achieved by introducing degradable crosslinks, which are sensitive to hydrolysis or enzymatic action. Alternatively, stable crosslinks can be used in combination with a degradable backbone, for example including peptides sensitive to matrix metalloproteinases.^{40,41}

In the following sections, both physical and chemical crosslinking strategies of relevance for crosslinking polymeric chains within a cell encapsulation context will be described.

2.2.2 Physical crosslinking

Physically crosslinked hydrogels form a 3D network through entanglements and/or reversible interactions between the polymeric chains. These interactions can be of different nature:

- i. **Ionic interactions**-mediated crosslinking occurs through opposite charged groups within the polymer chain, which can be initiated in situ by mixing the two polymers and changing the pH. Natural polymers incorporating ionizable moieties are commonly used for this type of physical hydrogels, having been used in combination with PEG to improve the final properties of the hydrogel.^{42,43}
- ii. **Hydrogen bonding** between polymer chains bearing moieties able to form H bonds. For example, PEG/poly(N-vinylpyrrolidone) (PVP) hydrogels have been prepared by using cyclodextrin molecules as hydrogen bonding linker between polymer chains.⁴⁴
- iii. **Stereo-complexation.** It involves the interaction between polymers with the same chemical composition (most cases) but differing stereochemistry, a common feature among natural molecules.^{45,46} Exploiting the stereo-complexation of poly(L-lactide) (PLLA) and poly(D-lactide) (PDLA) enantiomers, PEG/PLA copolymers have been used to produce physically crosslinked hydrogels.^{47,48}

- iv. **Hydrophobic interactions**, typically takes place between block copolymers containing hydrophilic and hydrophobic motifs,⁴⁹ referred to as amphiphiles (usually soluble in water at low temperatures). When the temperature increases, the hydrophobic motifs tend to aggregate to minimize the interactions with the surrounding water, forming micelles and micellar hydrogels.⁵⁰ The transition temperature at which this reorganization occurs depends on various factors, including the copolymer's concentration, the length of the hydrophobic chains, and the chemical structure of the molecule.⁵¹ A commercial polymer that forms physical hydrogels stabilized by hydrophobic interactions is the poloxamer PEOx-PPOy-PEOx or Pluronic, a copolymer formed by polypropylene oxide and polyethylene oxide (another name for polyethylene glycol) units.
- v. **Crystallization**, for example by freeze-thaw cycles, results in the partial alignment of polymer chains and subsequent formation of microcrystals. The final properties of the hydrogels depend on the crystallization process and the degree of crystallinity. It has been successfully applied to PVA/PEG systems.⁵²

The main advantage of physical crosslinking in the context of hydrogels for biomedical applications is that it does not require chemical agents.⁵³ Furthermore, physical interactions are reversible, giving physical hydrogels self-healing properties. However, non-covalent interactions are reversible and weaker than covalent bonds, which results in hydrogels with low mechanical properties.⁴⁵

Chemically crosslinked hydrogels form by covalent bonding between reactive functionalities incorporated in the polymeric precursors. These hydrogels usually present stronger networks than physically crosslinked. Examples of reactions used to synthesize chemically crosslinked hydrogels will be further described in the next section.

2.2.3 Chemical crosslinking

Chemically crosslinked hydrogels can be formed by two main mechanisms: chain-growth polymerization and step-growth polymerization.

Chain-growth polymerizations are addition reactions to a reactive (activated) species. In the context of hydrogels for cell encapsulation, most hydrogels polymerized by chain-growth mechanism start from (meth)acrylated monomers and are initiated by radical

active species. A radical initiated chain reaction has three major different steps: the initiation in which the radical is generated, typically by light or temperature, the propagation in which monomer molecules are added to the propagating radical, and the termination in which the kinetic chain reaction is stopped by reaction between two propagating radical species (**Figure 2**). Because of the stochastic nature of the propagation and termination steps, chain-growth polymerization renders heterogeneous networks that contain loops, entanglements, and/or dangling chains.⁵⁴ Hydrogel formation through chain-growth polymerization mechanism requires the presence of (co-)monomers with a reactive functionality ≥ 2 .

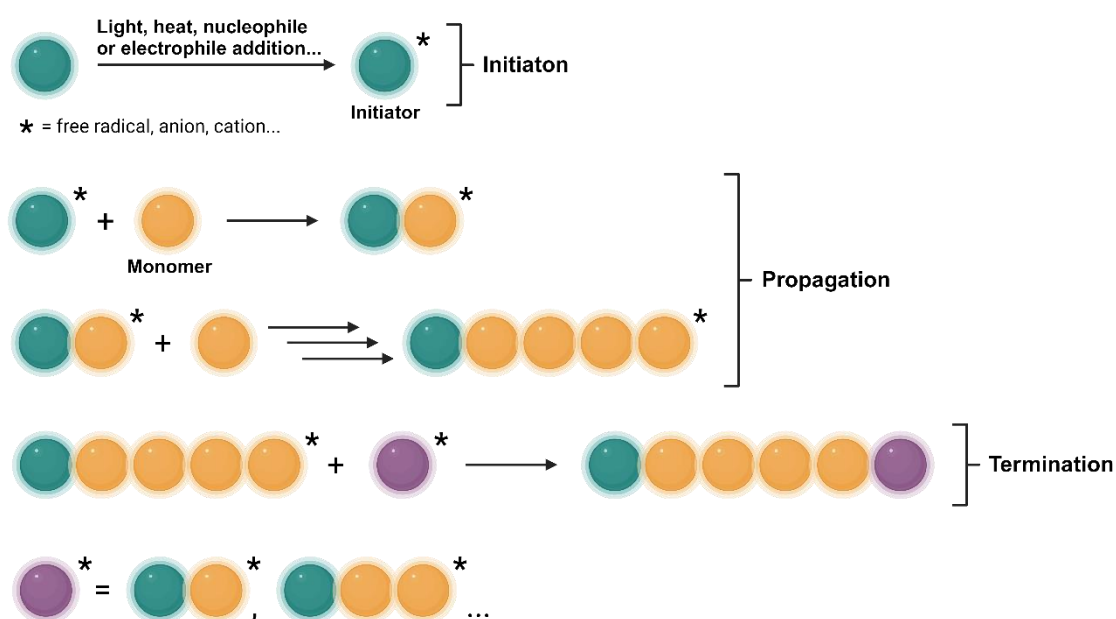


Figure 2. Chain-growth polymerization scheme constituted by three steps: initiation, propagation and termination (which may or not occur). The initiation can be triggered by light, heat, radiation, nucleophile addition to an electron withdrawing group (EWG), electrophile addition to an electron donating group (EDG), etc. Propagation takes place until two propagating molecules randomly react, during the so-called termination step. *Created with BioRender.*

Photo-initiated polymerization is commonly selected for chain-growth crosslinking reactions of cell-encapsulated hydrogels. However, the cytotoxicity of photo-initiators and exposure doses is an issue to consider.^{55–57} Cytocompatible photo-initiators like lithium phenyl(2,4,6-trimethylbenzoyl)phosphinate (LAP) that can be activated at visible

wavelengths are preferred.^{58,59} Yet, the use of visible light in chain-growth polymerization is not exempt of risks, since the formation of reactive oxygen species (ROS) through reaction of atmospheric oxygen with free radicals can cause oxidative stress to cells.³⁸

Hydrogel crosslinking through **step-growth polymerization** mechanism occurs when two macromonomers with complementary functional groups react stoichiometrically to form a larger molecule. In this type of polymerization, at least one of the macromonomers must contain functionality ≥ 3 in order to build a network (**Figure 3**).⁶¹ During the crosslinking, polymer chains with different lengths will be present and react with each other. The crosslinking stops when no reactive groups are left or do not encounter to react. Networks formed by step-growth crosslinking mechanism present less structural defects than those formed by chain-growth reactions.⁶²

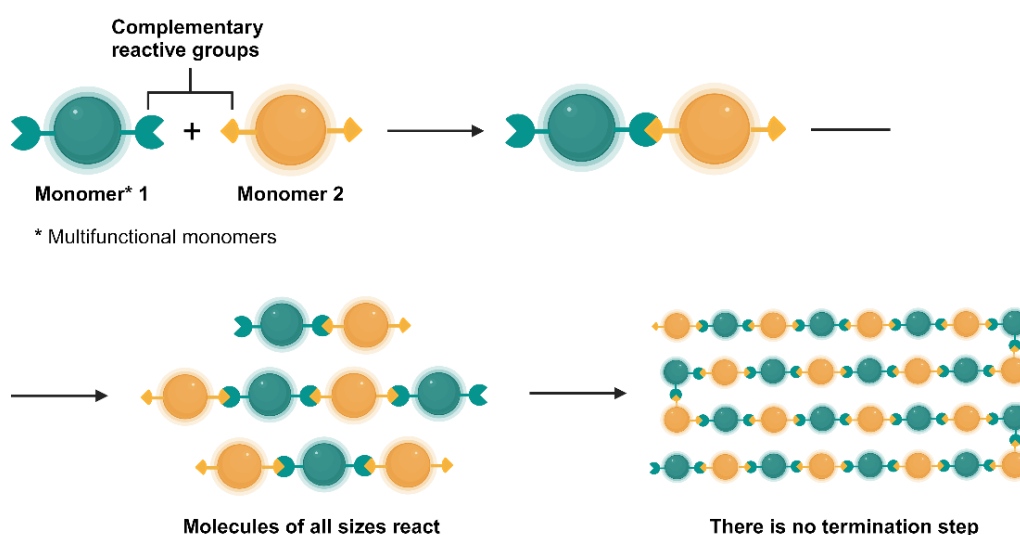


Figure 3. Step-growth polymerization scheme. Two (or more) complementary monomers, each bearing ≥ 2 reactive groups react stoichiometrically to form a polymer chain. *Created with BioRender.*

The most commonly used step-growth polymerization reactions for the synthesis of hydrogels are shown in **Figure 4** and described below.

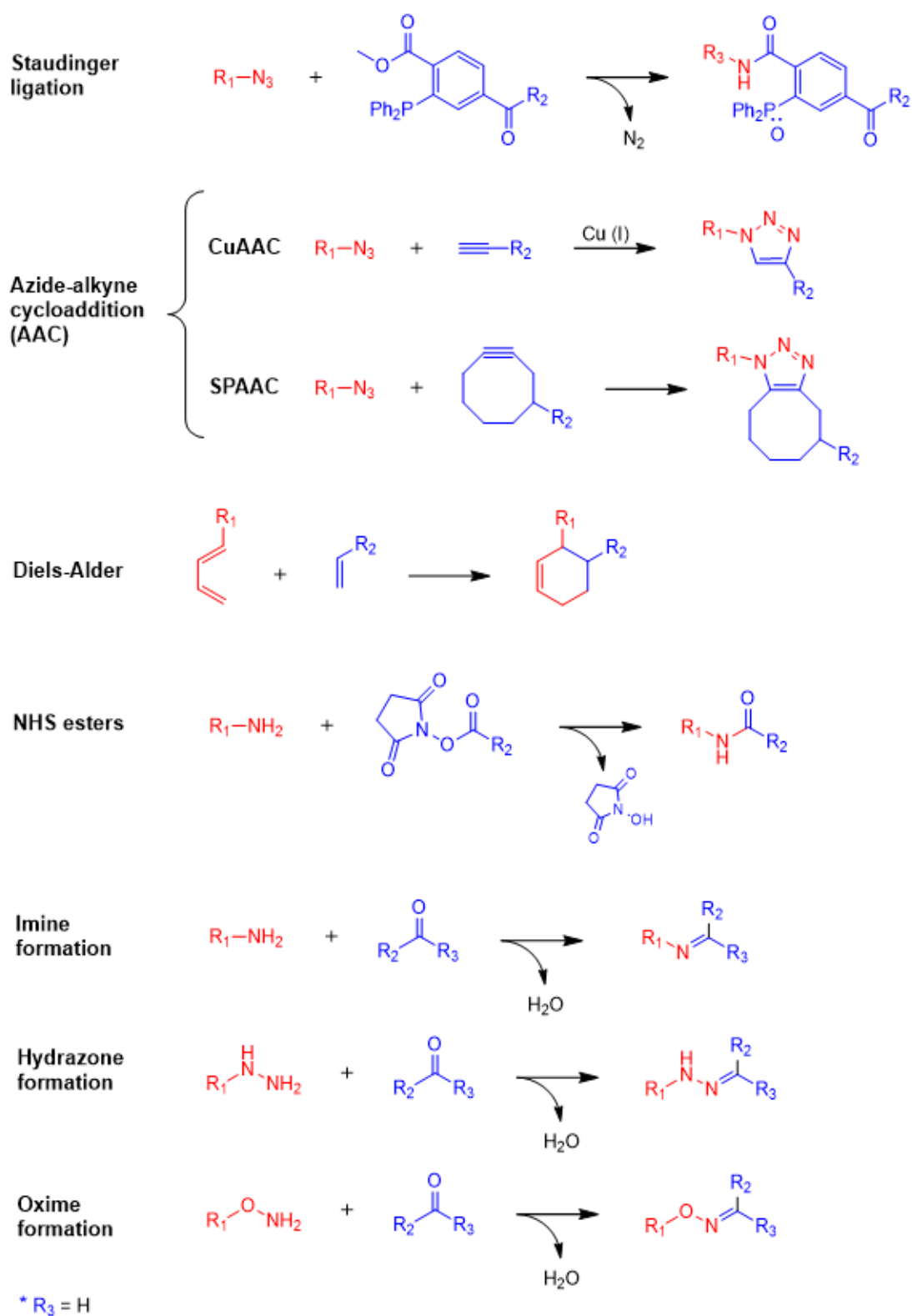


Figure 4. Most commonly used step-growth polymerization crosslinking reactions for the synthesis of cell-encapsulated hydrogels.⁶¹

Staudinger ligation is the reaction that occurs between an azide and a triaryl phosphine giving rise to an amide bond, and it was the first biorthogonal reaction that was developed.⁶³ The reaction is chemo selective under complex biological environments, making it highly compatible with in vitro and in vivo experiments.⁶⁴ However, its slow reaction kinetics, as well as the limited stability of the triaryl phosphine functional groups,⁶⁵ stand as a barrier to its use in the in situ preparation of hydrogels for cell encapsulation. Both natural⁶⁶ and synthetic⁶⁷ hydrogels have been developed based on the Staudinger ligation crosslinking reaction, necessitating ca. 20 h to ensure complete consumption of the reacting groups. To address the low conversion rate, hybrid systems have been developed by combining the Staudinger ligation reaction with another crosslinking mechanism, such as ionic crosslinking. An example of this hybrid approach is seen in alginate microgels, where the gelation process has been demonstrated to be compatible with islets and beta cells by Hall *et al.* 2011.⁶⁸

Azide-alkyne cycloaddition (AAC), consisting of the cycloaddition of monosubstituted azides to alkynes, is one of the most common bio-orthogonal crosslinking chemistries used for cell-encapsulated hydrogels.⁵¹ When it was first introduced, cytotoxic Cu(I) was used as catalyst.⁶⁹ Consequently, the reaction was not widely used for cell encapsulation. Using copper-binding ligands has been shown to reduce cytotoxicity for the CuAAC reaction in cell-encapsulating hydrogels.^{70,71}

To overcome the cytotoxicity of copper ions, strain-promoted alkyne-azide cycloaddition (SPAAC) was developed. Proceeding under physiological conditions without the addition of any catalyst,⁵⁰ SPAAC has been extensively used in hydrogels for cell encapsulation. Examples of this application include hydrogels based on the reaction between cyclooctyne- and azide-functionalized macromers,⁷²⁻⁷⁴ or bicyclononyne- and azide-functionalized PEG backbones.⁷⁵

Diels-Alder (DA) refers to the reaction between an electron-rich diene and an electron-deficient double bond. The DA reaction can be performed in water and does not require additional reagents or generate byproducts.⁵⁰ However, the reaction rate is relatively slow, with gelation times reaching > 50 min during the preparation of cell encapsulating hydrogels.⁷⁶

The slow kinetics of the DA reaction has been addressed by using the inverse electron demand Diels-Alder reaction, which in turn involves an electron-deficient diene and an electron-rich dienophile.⁷⁷ This method has been used for the preparation of cell-encapsulated hydrogels, including hydrogels crosslinked through reaction of tetrazine functionalized PEG macromers and di-norbornene peptides, with gelation occurring within minutes.⁷⁸ Tetrazine modified PEG macromers and cyclooctene crosslinkers have also been used in this context.⁷⁹

An interesting feature of DA crosslinking for cell encapsulation is its reversibility (controlled degradation). However, this requires temperatures between 30 and 80 °C,⁸⁰ which are not compatible with many cellular systems.

NHS ester reaction. The reaction of amines with NHS-activated carboxylic groups is widely used for hydrogel formation. It is biocompatible and chemoselective. In the reaction, N-hydroxysuccinimide (NHS) is formed as byproduct, which has slightly acidic behavior. The low hydrolytic stability of the NHS ester precursor, with a half-life of ca. 5 h at pH 7 and 0 °C, is a limitation of this reaction, as well as the possible reaction of the NHS ester with amines.

Imine, hydrazone and oxime formation through the reversible reaction of an amine (primary amines, hydrazines, or hydroxylamines) and a carbonyl group (aldehydes or ketones) have also been investigated as crosslinking reactions for the preparation of hydrogels in presence of cells. These reactions are carried out under physiological conditions with the release of water as the only byproduct.⁵⁰

Reaction of primary amines with a carbonyl group, also known as Schiff's base formation, results in the generation of an imine bond. An example of its application in hydrogel preparation is the system formed by reaction of chitosan with aldehyde-functionalized HA, effectively used in cartilage tissue engineering.⁸¹ Apart from the low hydrolytic stability of imine bonds, the reaction is not bioorthogonal, since amines are found in natural proteins and can interfere with the crosslinking reaction.

Systems based on the formation of hydrazones (reaction of hydrazine with a carbonyl group) and oximes (reaction of hydroxylamine with a carbonyl group) are more stable

towards hydrolysis and have also been implemented as a crosslinking mechanism for the preparation of hydrogels with stress relaxation properties. With an hydrolytic stability in between imines and oximes, hydrazone-based hydrogels such as the system developed through reaction of hydrazine and aldehyde functionalized PEG macromers,⁸² or the injectable hydrogel based on the crosslinking reaction between aldehyde and hydrazine modified HA⁸³ have been developed. Crosslinking reactions to form oximes are efficient and chemoselective. Although the oxime bond is generally highly stable in the physiological environment,⁸⁴ it can be reversed under acidic or basic pH conditions.⁸⁵ With a higher pH sensitivity than imine and hydrazone formation, gelation kinetics of oxime-based hydrogels can be effectively tuned by the pH⁸⁶ or by introducing a catalyst.⁸⁷ For instance, the gelation time between aldehyde functionalized macromers and aminoxy crosslinkers was reduced from several hours to several minutes at pH 7.4 by incorporating an aniline catalyst.⁸⁶

Enzyme-mediated ligation. Enzymes are proteins that catalyze chemical reactions in the physiological environment. Different systems using enzyme-mediated crosslinking have been developed for hydrogel-encapsulation of cells, including transglutaminases (TG),^{88,89} peroxidases,^{90,91} tyrosinase,⁹² thrombin, and phosphatases.⁹³

Transglutaminases catalyze the transfer of an acyl group between the α -carboxamide of a glutamine (acyl donor) and the ϵ -amino of a lysine (acyl acceptor) residue when the cofactor Ca^{2+} is present. This highly selective reaction has been widely applied for hydrogel crosslinking by polymerization of macromer precursors functionalized with the corresponding groups, such as modified PEG backbones with Gln and Lys peptides.⁹⁴

Peroxidases, among which the horseradish (HRP) and soybean peroxidases are the most extended for hydrogel preparation, catalyze the oxidative coupling between two phenolic molecules in presence of hydrogen peroxide (H_2O_2). During the radical-mediated reaction, a new carbon-carbon (C-C) bond is formed between the two carbons situated at the *ortho* position to the hydroxyl moiety from the two phenolic precursors. Additionally, the reaction can also occur between an *ortho*-carbon and the hydroxyl group from another phenol. An example of this mechanism is the enzymatically crosslinked hydrogel through reaction of phenol functionalized chitosan macromers in

presence of HRP within 10 sec to 4 min depending on the polymer concentration (3 to 1 % correspondingly for the indicated gelation times).⁹¹

Tyrosinases are enzymes that catalyze the oxidative reaction between phenol and catechol moieties. In contrast to peroxidase, this reaction occurs in absence of H₂O₂, thus it is a more cell-friendly approach. A few systems using tyrosine for hydrogel crosslinking have been developed for biomedical applications.^{95,96}

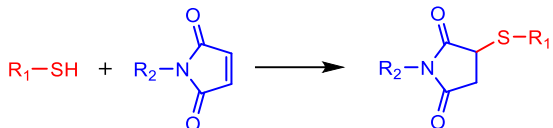
The oxidative conditions employed for certain enzymes may result in toxicity effects. Another drawback of enzymes is their relatively large size that hampers the enzyme diffusion during the gelation and can result in non-homogeneous networks.

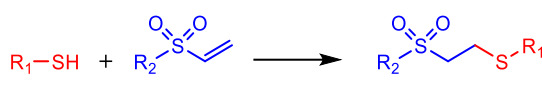
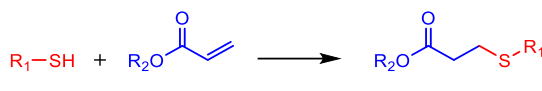
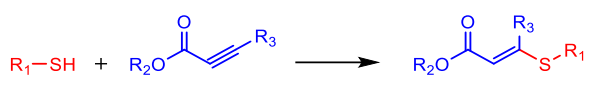
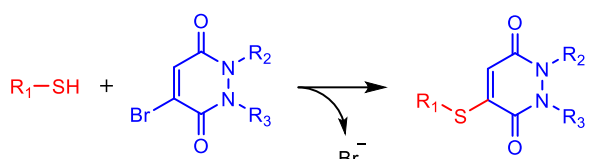
2.3 Thiol-based crosslinking reactions for hydrogel formation

In addition to the crosslinking reactions described in the previous section, a variety of hydrogels with interest for cell encapsulation have been used by crosslinking of thiol functionalized macromers with maleimides, vinyl sulfones, acrylates, alkyne esters, aryl methylsulfones, epoxy, alkenes or halo functionalized macromers and crosslinkers.

The **thiol-Michael addition** is a pH-dependent click reaction through the nucleophilic attack of a thiol to an electron deficient (electrophile) α , β -unsaturated carbonyl. Different electrophiles have been studied for crosslinking of cell-encapsulated hydrogels (**Table 1**).

Table 1. Thiol-based Michael addition reactions that are commonly used for the crosslinking of cell-encapsulated hydrogels.

Electrophile	Crosslinking reaction	Properties
Maleimide		<ul style="list-style-type: none"> - Efficient and highly selective. - Very fast at physiological pH. - Product susceptible to retro-Michael. - Low stability towards hydrolysis.

Vinyl sulfone	 $R_1-SH + R_2-SO_2-CH=CH_2 \longrightarrow R_2-SO_2-CH_2-CH_2-S-R_1$	<ul style="list-style-type: none"> - Highly selective. - Slow at physiological pH. - High stability towards hydrolysis.
(Meth)Acrylate	 $R_1-SH + R_2O-C(=O)-CH=CH_2 \longrightarrow R_2O-C(=O)-CH_2-CH_2-S-R_1$	<ul style="list-style-type: none"> - Need for a basic catalyst at physiological conditions. - Low stability towards hydrolysis.
Alkyne ester	 $R_1-SH + R_2O-C(=O)-C\equiv C-R_3 \longrightarrow R_2O-C(=O)-CH=C(R_3)-S-R_1$	<ul style="list-style-type: none"> - Need for a catalyst (base or nucleophile) at physiological conditions. - Relatively slow at physiological pH. - Di-substituted product may be obtained. - Low stability towards hydrolysis.
Pyridazinedione	 $R_1-SH + \text{Brominated Pyridazinedione} \longrightarrow \text{Thioether Pyridazinedione} + Br^-$	<ul style="list-style-type: none"> - Relatively fast at physiological pH. - Tunable stability towards retro-Michael by using substituted pyridazinediones. - Stable towards hydrolysis.

- Maleimides show fast kinetics ($k \sim 10^2 - 10^4 \text{ M}^{-1} \text{ s}^{-1}$,^{6,97} dependent on pH and reactants structure) and high selectivity in physiological conditions. The angle distortion of the C=C bond, the ring strain (108° vs ideal 109.47°), and the *cis*-conformation of the carbonyl groups from the maleimide ring have been proposed as the reasons for the rapid kinetics of the thiol-maleimide Michael-addition.⁹⁸ The fast reaction usually translates into gelation times of seconds ($\text{pH} \geq 7$) (also depending on multiple factors such as polymer structure, concentration, etc), resulting in non-homogeneous networks because of incomplete mixing. The final thioether succinimide bond in the crosslinked hydrogel is susceptible to retro-Michael or exchange reactions with other thiols present in the physiological

environment.⁴ Moreover, these bonds present low stability towards hydrolysis, not being suitable for long term cell culture.^{5,99}

- Vinyl sulfones react with thiols in a highly selective manner. The reaction rate ($k' \sim 10^{-4} - 10^{-3} \text{ s}^{-1}$,¹⁰⁰ dependent on pH and reactant structure) stands between maleimide and acrylates, being around 2 to 3 orders of magnitude lower than maleimide. This translates into gelation times of several minutes to hours.⁶ Long gelation times are accompanied by cell sedimentation,⁷ and obligates to continuously flip the hydrogel during crosslinking.¹⁰¹ The thioether bond is stable towards hydrolysis, making this crosslinking chemistry suitable for long-term cell culture.
- (Meth)Acrylates are commonly used electrophiles for thiol-Michael addition in polymers for hydrogel cell encapsulation. Contrary to maleimide and vinyl sulfone, it requires the presence of a base catalyst in physiological conditions.¹⁰² Additionally, the formed ester is prone to hydrolysis. Thus, this crosslinking chemistry has been applied for the development of hydrolytically degradable hydrogels. Methacrylates form hydrogels with higher hydrolytic stability, but they are less reactive than acrylates.
- Alkyne esters react with thiols in presence of a catalyst (base or nucleophile), similar to vinyl electrophiles, and usually results in high yields. It has been applied for the crosslinking reaction of multi-arm PEG macromers incorporating alkyne esters and thiol end-groups, resulting in gelation times of 30 min.¹⁰³ Depending on the reaction conditions (stoichiometry, catalyst and temperature) the mono- or di-substituted product can be obtained.^{98,103} The di-substituted product can undergo retro-Michael addition under basic medium or high temperatures, and has been applied for the preparation of injectable and self-healing hydrogels.¹⁰³ On the other hand, the ester bond present in the final product hydrolytically degrades over time (within few weeks), making this approach not suitable for long-term cell encapsulation.¹⁰⁴
- Pyridazinedione (PD)-thiol Michael-type addition was recently applied by Bahou *et al.* for the pH-dependent preparation of PEG hydrogels within minutes ($k_1 \sim 10^0 \text{ M}^{-1} \text{ s}^{-1}$). It was observed that different halogenation degree of the C=C bond (0, 1 or 2

bromides) from the pyridazinedione ring results in variable gelation times, with the di-functionalized being the fastest and the non-functionalized being the slowest.¹⁰⁵ The thioether bond formed after reaction may be susceptible to retro-Michael or thiol exchange depending on the degree of functionalization. While the reaction between the thiol and the non-functionalized pyridazinedione is dynamically reversible ($k_{-1} \sim 10^{-5} \text{ M}^{-1} \text{ s}^{-1}$), the mono- and di-functionalized PD do not show the same behavior. Thiol exchange resulting in network disruption and final hydrogel degradation occurs in presence of other thiols when the non- and mono-functionalized PD are selected, useful for stimuli-responsive hydrogels. In contrast, the bi-functionalized PD, presenting faster gelation kinetics, seems to be stable towards both retro-Michael and thiol exchange reactions, becoming a promising alternative for long-term cell-encapsulated hydrogels.

The **thiol-halogen ligation** is the substitution reaction between a thiol and a iodide or bromide functionalized macromers that requires basic conditions for gelation. Truong *et al.* developed a PEG-based hydrogel with tunable degradation rate by reacting multi-arm PEG-bromide/iodide with PEG-SH and obtained hydrogels within minutes at pH 7.8.⁹

The **thiol-epoxy** reaction involves the nucleophilic opening of an epoxy ring, but requires a toxic catalysts to activate the nucleophile.⁸ By using a diepoxy PEG and a multi-arm PEG crosslinker bearing eight thiols, Huynh *et al.* managed to successfully encapsulate hMSCs in a hydrogel without a catalyst.¹⁰

Disulfide bonds are formed by the oxidation of two thiol groups in the presence of mild oxidizers like atmospheric O_2 . Disulfide bond formation is a slow reaction (with an rate constant of $0.1\text{--}10 \text{ M}^{-1}\text{s}^{-1}$ at pH 7¹²) and requires long times for hydrogel formation. A faster alternative is the thiol-disulfide exchange reaction based on the nucleophilic substitution of a disulfide bond by a thiolate. Thus, a new disulfide bond is formed and a free thiol (or thione group, depending on reactant's chemical nature) group is released to the medium.^{12,108} Using pyridyl disulfide-modified HA and PEG-dithiols, Choh *et al.* successfully encapsulated different cell types in a hydrogel that formed within minutes.¹¹ The main drawback of this reaction is the release of thiolated-molecules, which can be

avoided by using cyclic disulfide molecules like 1,2-dithiolane, that reacts at neutral pH without releasing byproducts.

Disulfide bonds are mechanoresponsive and dissociate under mechanical stress associated with hydrogel swelling, resulting in hydrogel degradation.¹⁰⁹ Disulfide crosslinked hydrogels can be further degraded by glutathione, an anti-oxidant tripeptide present in the physiological environment of human cells.

The **split luciferin ligation** is a condensation reaction between 2-cyanobenzothiazole (CBT) and d-cysteine (d-Cys) and corresponds to the final step of D-Luciferin synthesis in fireflies. This reaction is fast, efficient and chemoselective in physiological conditions, as well as cytocompatible, being successfully applied for cell encapsulation in hydrogels.¹¹⁰ Menegatti *et al.* crosslinked CBT- and d-Cys modified hyaluronic acid within several minutes, resulting in a self-fluorescent hydrogel for wound adhesive and drug delivery.¹¹¹ Moreover, Jin *et al.* reacted CBT- and Cys-functionalized multiarm PEG macromers and demonstrated tunable gelation kinetics from seconds to minutes and good cytocompatibility.¹³

The **thiol-ene** reaction is a step-growth, radical-mediated reaction between a thiol and an alkene. This is the most extended photocrosslinking reaction involving thiol groups.¹¹² It starts by formation of a free radical that reacts with a thiol to form a thiyl radical. In turn, the latter reacts with an alkene, resulting in a new radical (from the alkene) that abstracts the proton from a thiol group to form a thioether, also releasing a new thiyl radical to the medium. The stepwise mechanism occurs by iterative formation of the thioether bond and the thiyl radical through a stoichiometric reaction until one of the reagents (thiol or alkene) is finished. While chain-growth polymerization is known because of its inhibition by oxygen and subsequent formation of ROS, thiol-ene can be propagated by these species, resulting in a lower concentration of ROS in the final hydrogel, and therefore less oxidative stress to cells.¹¹³ In addition, thiol-ene photopolymerization is more efficient than chain-growth and leads to more homogenous polymeric networks.¹¹⁴

Using unsaturated derivatives like (meth)acrylates, the reaction proceeds in a combination of step-growth and chain-growth polymerization, since free radicals from the photoinitiator can react with the thiol and acrylate, both serving as propagating

reactive species. Norbornene has been widely used as the unsaturated source in thiol-ene reactions because of its fast kinetics ($k=5.2 \times 10^7 \text{ M}^{-1} \text{ s}^{-1}$, propagation step rate constant from a computational study¹¹⁵). In addition, it does not undergo chain-growth polymerization unlike (meth)acrylates. Fairbanks *et al.* prepared a hydrogel by reacting 4arm PEG-norbornene and a chymotrypsin-degradable peptide with two cysteines through thiol-ene photochemistry.¹⁴ Unlike acrylates, norbornene molecules do not undergo homolytic photopolymerization, ensuring the step-growth mechanism.

The major advantage of step-growth photopolymerization is the possibility to have spatiotemporal control, allowing to modulate the internal structure and mechanical properties of the hydrogels when light is used as initiation source; exemplified by Anseth and coworkers, who demonstrated the potential of the thiol-ene crosslinking chemistry for cell encapsulation by controlling the peptides spatial arrangement in hydrogels.^{73,78} Another example of tuning mechanical properties by thiol-ene crosslinking reaction was presented by Zheng *et al.*, where after gelation through thiol-methacrylate Michael-type addition of dextran macromers, photopolymerization was applied as a secondary crosslinking method to increase the stiffness on-demand through reaction of remaining methacrylate groups.¹⁵

Under the same conditions, the impact of the thiol chemical structure on the reaction was also tested. While slightly different, high yields ($\geq 85 \%$) were obtained for all derivatives, proving the high effectiveness of the reaction towards different thiolated molecules.¹⁰⁶

2.4 Thiol-Aryl methylsulfone (MS) crosslinking

In search of more selective (towards thiols) alternatives to common reagents like iodoacetamides or N-substituted maleimides for protein blocking or bioconjugation, which are known to react with functionalities other than thiols under certain conditions,^{116,117} the thiol-aryl methylsulfone (MS) reaction was applied to selectively react with cysteine thiols in aqueous conditions.¹⁰⁶ This pH-dependent reaction occurs via nucleophilic aromatic substitution (S_NAr) of the methylsulfone moiety by a thiol group, with the subsequent release of methanesulfinic acid as byproduct. Due to the more nucleophilic profile of the thiolate species (deprotonated thiol), the reaction is faster at

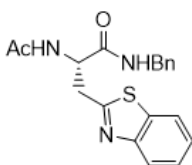
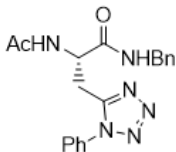
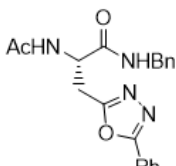
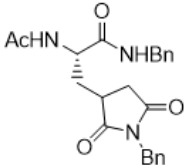
higher pHs, as happens with other thiol-mediated Michael additions such as thiol-maleimide.

MS derivatives are highly selective towards thiols under near physiological conditions, while other functional groups like amines or alcohols do not react with MS moiety under the same conditions. This specific reaction has been studied with different MS compounds, such as benzothiazole (Bt)-MS or oxadiazole (Ox)-MS, in presence of amino acids incorporating other reactive functionalities like amines and alcohols, both aromatic and aliphatic, as well as thioethers. Under near physiological conditions, no reaction was observed (monitored by TLC¹⁰⁶ or HPLC¹⁰⁷), confirming the high selectivity of the thiol-MS reaction.^{106,107}

Kinetics of the thiol-MS reaction can be tuned by modifying the chemical structure of the MS derivative, as many studies have proved.^{107,118–120} Different heteroaromatic rings have been attached to the MS moiety to analyze the impact on the reaction rate with cysteine derivatives, observing variations of 6 orders of magnitude under near physiological conditions. Thus, benzothiazole-MS ($0.52 \pm 0.02 \text{ M}^{-1} \text{ s}^{-1}$), phenyl tetrazole (Tz)-MS ($12.1 \pm 0.67 \text{ M}^{-1} \text{ s}^{-1}$), phenyl oxadiazole-MS ($451 \pm 46 \text{ M}^{-1} \text{ s}^{-1}$) and benzoxazole (Bo)-MS ($845 \pm 14 \text{ M}^{-1} \text{ s}^{-1}$) showed increasing reaction rate, with a protected cysteine, by varying the electron-withdrawing character of the heteroaromatic ring.¹¹⁸ Surprisingly, other substituents such as (phenyl)triazole, benzimidazole or thiadiazole did not react with the thiol derivative.^{107,118} Reaction rates of up to $8.7 \times 10^5 \text{ M}^{-1} \text{ s}^{-1}$ have been recorded by reacting glutathione (tripeptide containing cysteine amino acid), which is the most abundant intracellular antioxidant, with pyridine and pyrimidine derivatives.^{119,120} Moreover, modification of the substituent's chemical nature from the heteroaromatic ring, as well as their position within the ring, resulted in significant increasing of the reaction rate in pyrimidine (up to 7 orders of magnitude),¹⁰⁹ and Bt¹¹⁸ (up to 4 orders of magnitude) derivatives. In these cases, the mesomeric (-M) and inductive (-I) effects of stronger EWGs are hypothesized to be responsible for the higher reactivities towards thiols (nucleophile). On the contrary, changing the *p*-substituent of the phenyl Tz ring slightly altered the reaction rate (1 order of magnitude). With thiol-maleimide reaction rate being ca. $734 \text{ M}^{-1} \text{ s}^{-1}$,¹²¹ the thiol-MS stands as a good and tunable alternative in terms of kinetics.

Adducts from the thiol-MS reaction have shown greater stability than maleimide analogues in aqueous environment. The stability of the thioether product from the reaction of OxMS and cysteine was evaluated in basic (4 eq. of K_2CO_3 , THF/ H_2O 1:1, rt, 20 h) and acidic (THF/HCl aq 0.1 M 1:1, rt, 3 days) conditions, as well as in presence of glutathione (3 eq. of glutathione in THF/PBS 200 mM pH 7.4 2:3, 37 °C, 5 days). As seen in **Table 2**, the thioether bond from the MS derivatives (**14a-c**) was significantly more stable than the one from maleimide (**14d**) under all 4 conditions (A-D), being the BtMS **14a** slightly more stable than TzMS **14b** and OxMS **14c** derivatives.¹⁰⁷

Table 2. Stability test of methylsulfone aryl derivatives under different conditions: ^[a] (A) K_2CO_3 (4 eq.), THF/ H_2O (1:1), rt, 20 h; (B) THF/0.1 M HCl aq (1:1), rt, 3 days; (C) THF/PBS pH 4.0 200 mM (1:1), rt, 3 days; (D) glutathione (3 eq), THF/PBS pH 7.4 200 mM (2:3), 37 °C, 5 days; ^[b] Measured by HPLC (254 nm).¹⁰⁷ Reprinted (adapted) from Toda et al. 2013. Copyright © 2013 WILEY-VCH Verlag GmbH & Co. KGaA, Weinheim.

	Conjugate	Conditions ^[a]	% Remaining ^[b]
	14a	A	> 99
		B	> 99
		C	> 99
		D	94
	14b	A	88
		B	98
		C	> 99
		D	> 99
	14c	A	82
		B	> 99
		C	> 99
		D	99
	14d	A	2.7
		B	71
		C	69
		D	34

Stability of different unconjugated MS precursors has also been analyzed both in aqueous solution and in storage. Following their more reactive tendency, the BoMS and phenyl OxMS derivatives were relatively unstable towards hydrolysis in PBS buffer at pH 7.4 (analyzed after 4 and 24 h). In dry storage, solid BoMS was decomposed after 6 months at $-20\text{ }^{\circ}\text{C}$, while the OxMS lasted at least 1 year. On the other hand, phenyl tetrazole-MS and benzothiazole-MS derivatives were stable for more than a week under the same conditions, demonstrating relatively good stability in aqueous medium and potential high long-term stability in storage.¹¹⁸

The group of A. del Campo introduced the thiol-MS reaction for crosslinking with thiol terminated starPEGs and demonstrated the potential of this reaction for hydrogel cell encapsulation.⁶ Tetra-arm star-PEG was functionalized with OxMS through a 3-step synthetic pathway resulting in PEG-4OxMS macromers with $> 95\%$ substitution degree (**Figure 5a**). These were crosslinked to hydrogels with a tetra-arm PEG-SH crosslinker.

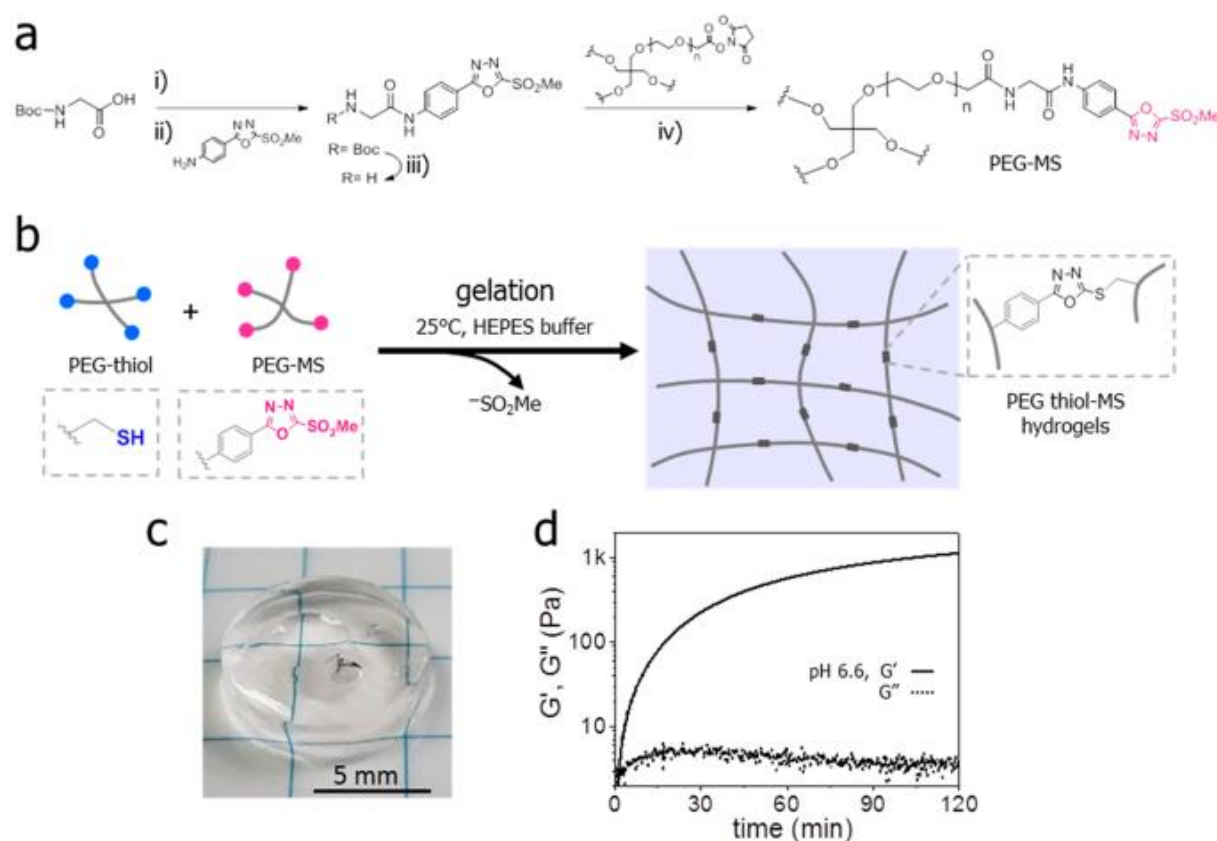


Figure 5. Chemical structure and properties of PEG-based thiol-OxMS hydrogels. (a) Synthetic pathway for the preparation of the PEG-OxMS macromer. Reagents and

conditions: (i) isobutyl chloroformate and NMM in THF/DMF (1:1, v/v), 0 °C, 30 min; (ii) room temperature, overnight; (iii) trifluoroacetic acid (TFA)/DCM (1:1, v/v), 0 °C, 30 min; (iv) DMF, NMM, room temperature, N₂, overnight. (b) Crosslinking scheme of the reaction between PEG-thiol and PEG-MS precursors resulting in the hydrogel 3D network with thioether bonds as crosslinking points. (c) Photograph of a swollen MS hydrogel. (d) Representative curves of storage (G') and loss (G'') modulus as a function of time during gelation. Conditions for (c,d): 5 wt % polymer, 10 mM HEPES buffer pH 6.6, T = 25 °C.⁶ Reprinted (adapted) with permission from Paez et al. 2020. Copyright 2012 American Chemical Society.

The gelation time of the thiol-OxMS hydrogel was tested and compared against the commonly used thiol-Mal and thiol-vinyl sulfone (VS) systems. The conditions for hydrogel formation were: 5 wt % polymer content, HEPES buffer 10 mM, 25 °C, [MS:SH] 1:1 molar ratio. The gelation was tested at different pHs (6.6 – 8.0) (**Table 3**). Thiol-OxMS hydrogels formed within seconds at pH ≥ 7.0 , similar to the thiol-maleimide system, while at pH 6.6 the gelation reaction slowed down to 4 minutes, in contrast to the 5 – 6 seconds of maleimide hydrogel. Under the same conditions, vinyl sulfone hydrogels formed within minutes, starting from 8 min at the higher pH (8.0) and reaching 190 min at the lowest (6.6).

Table 3. Gelation time defined as the time elapsed from the mixing of the two precursors until pipetting (manual micropipette equipped with 200 μ L tip) was not possible anymore. Conditions: precursor aliquots of 30 μ L each, 5 wt % polymer content, HEPES buffer 10 mM, T = 25 °C.⁶ Reprinted (adapted) with permission from Paez et al. 2020. Copyright 2012 American Chemical Society.

gel ^a	pH			
	8.0	7.5	7.0	6.6
thiol-Mal	<1 s	1–2 s	2–3 s	5–6 s
thiol-MS	3 s	6 s	12 s	4 min
thiol-VS	8 min	22 min	88 min	190 min

Fast kinetics of the Michael-type thiol-maleimide reaction often translates into poor mixing and consequent formation of microdomains within the final hydrogel,^{18,122}

decreasing hydrogel reproducibility. These inhomogeneities may in turn lead to abnormal cell behavior since topological and mechanical cues influence cell response.¹²³ In addition, cell distribution over the 3D hydrogel is also affected by fast gelation, meaning that only the upper layers of the construct are occupied by cells. To lower reaction rate and improve homogeneity, thiol-maleimide hydrogels are usually formed using alternative strategies such as lowering pH, which can compromise cell viability. Michael-type thiol-vinyl sulfone hydrogels present long gelation times at physiological pH (7.0 to 8.0), delivering homogeneous 3D networks after thorough mixing. However, cell sedimentation during gelation takes place and leads to inhomogeneous cell distribution.⁶

Thiol-methylsulfone (PEG)hydrogels emerged as a promising alternative to the thiol-maleimide and thiol-vinyl sulfone systems for hydrogel-encapsulation of cells. The gelation time of the PEG-OxMS derivative stands in between PEG Mal-MS and PEG VS-MS and allows better mixing and equal distribution of cells in the hydrogel (**Figure 6a, b**). To address the inertness of these PEG-based hydrogels towards cell adhesion, the PEG-MS precursor was biofunctionalized with the peptide cyclo(RGDfC). Furthermore, the dithiol peptide VPM, which can be enzymatically degraded (MMP-cleavable), was used as crosslinker to promote cell migration. MS hydrogels showed higher cell viability and stability than Mal, which was prematurely degraded. In contrast, cell migration out of the spheroids (cell aggregate) (**Figure 6e, f**) was higher in Mal hydrogels due to faster degradation of the networks, or higher pore size due to fast and irregular 3D network formation. In line with their previous results, cell migration in MS hydrogels was in between Mal and VS hydrogels.

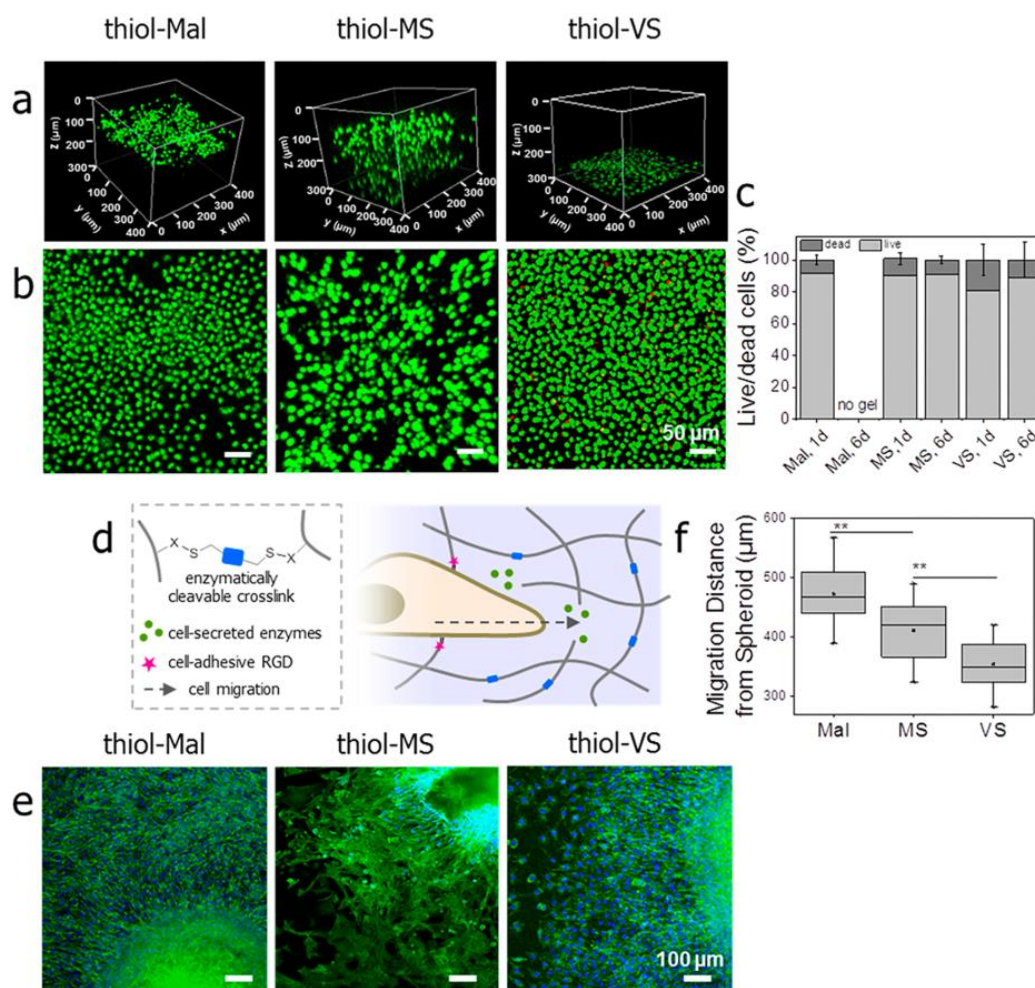


Figure 6. Cell studies of L929 fibroblasts in SH-MS PEG hydrogels containing VPM as enzymatically degradable dithiol crosslinker and RGD for cell adhesion. Conditions: 4 wt % PEG-X content, 1 mM cyclo(RGDfC), 3.14 mM VPM, in HEPES buffer 10 mM pH 8.0. (a, b) Z-stack showing cell distribution over the hydrogels with different compositions after 1 day of encapsulation; (c) cell viability quantification after 1 and 6 days after encapsulation; (d) scheme of encapsulated cell segregating enzymes that degrade the crosslinking points of the hydrogel allowing cell migration; (e) cell migration after 3 days of encapsulation (fluorescence images); (f) quantification of cell migration in hydrogels with different composition (mean \pm SD, ANOVA, Tukey-Kramer post hoc test $**p < 0.01$).⁶ Reprinted (adapted) with permission from Paez et al. 2020. Copyright 2012 American Chemical Society.

Despite the better stability of PEG-OxMS hydrogels over maleimide analogues, the fast crosslinking kinetics at near physiological conditions (5 wt % polymer content, HEPES pH

8.0 20 mM, rt) translated into low network homogeneity.¹⁶ In addition, hydrogel stability under cell culture conditions was less than 1 week. In order to lower the gelation kinetics and overcome the disadvantages derived from fast crosslinking, two other MS derivatives were tested against Ox: benzothiazole and phenyl tetrazole. Previously reported^{107,118} slower reaction rate of benzothiazole MS and phenyl tetrazole MS with cysteine derivatives also translated to PEG hydrogels, with gelation times of 4.6 min and 36 sec at pH 8.0 respectively (tetra arm PEG-SH crosslinker). Homogeneous networks were formed as a result of longer gelation times and more complete mixing processes.¹⁶ As expected,¹¹⁸ higher stability than OxMS (6 days) was also observed for both candidates under cell culture conditions (RPMI medium, pH 7.4, 37 °C), 16 days for PEG-TzMS 16 and 10 days for PEG-BtMS. Furthermore, both alternatives showed similar cell viability to Ox over 4 days of cell culture (> 90 %).¹⁶

Thiol-methylsulfone hydrogels fill the existing gap by overcoming some of the main drawbacks (cell homogeneous distribution and/or hydrogel stability) of the thiol-maleimide and thiol-vinyl sulfone chemistries, and it stands as a suitable alternative for 3D cell encapsulation applications.

Nevertheless, close attention must be paid to thiol-based crosslinking chemistries since thiols in aqueous conditions can form disulfide bonds. At physiological pH (7.0 to 8.0) the deprotonation of thiols is promoted and this accelerates disulfide formation in thiol-containing solutions. This reaction interferes with gelation in thiol-MS crosslinking. When thiols are slowly consumed by disulfide bonds, the stoichiometric ratio of the reactive functional groups is destabilized, and this prevents full crosslinking of the hydrogel precursor.¹²⁴ Incomplete crosslinking affects the mechanical properties and reproducibility of hydrogels. Lutolf and Hubbell reported a decrease of the storage modulus (G') at higher pH in a system using a dithiol peptide as crosslinker. They hypothesized that the consumption of free thiols during disulfide formation resulted in a disruption of the equimolar stoichiometry of the hydrogel crosslinking reaction. Thus, the formation of an incomplete network translated into a less stiff hydrogel (lower G').¹²⁵ During the development of their in situ thiol-mediated hydrogel, Bahou *et al.* observed an increasing viscosity when a multi-arm PEG-SH precursor was dissolved in absence of the crosslinker at pH 7.4 (PBS buffer). The viscosity was then attributed to disulfide formation

among starPEG-SH molecules.¹⁰⁵ Therefore, it is important to consider the disulfide formation as an interfering factor when working with thiol-mediated step growth polymerization.

2.5 Gelation of star-PEG hydrogel precursors and resulting networks

In theory, the symmetry of star-PEG polymers, together with stoichiometric crosslinking A-B type reaction between reactive end-groups leads to 3D networks with low inhomogeneities.^{118,11} However, the kinetics of the crosslinking reaction and the internal structure of the hydrogel's network influences the structure of the network and the final properties of hydrogels.

2.5.1 Kinetics of crosslinking

Two different regimes can be found in an A-B type end-group crosslinking reactions: diffusion-limited and reaction-limited (**Figure 7**). Reactions limited by diffusion result in networks with inhomogeneities because reaction between A and B is much faster than the diffusion itself. Thus, A and B will react when they encounter, even if diffusion did not reach equilibrium. Clusters in which there is more concentration of a certain reactive group will be formed, leading to local defects (**Figure 7c**). On the other hand, crosslinking reactions limited by the reaction, as it is the case of the thiol-MS hydrogels, have a reaction rate that is much slower than the diffusion. A and B can evenly diffuse through the mixture and react in a stepwise manner, resulting in an orderly network with significantly reduced inhomogeneities (**Figure 7f, g**).¹⁹

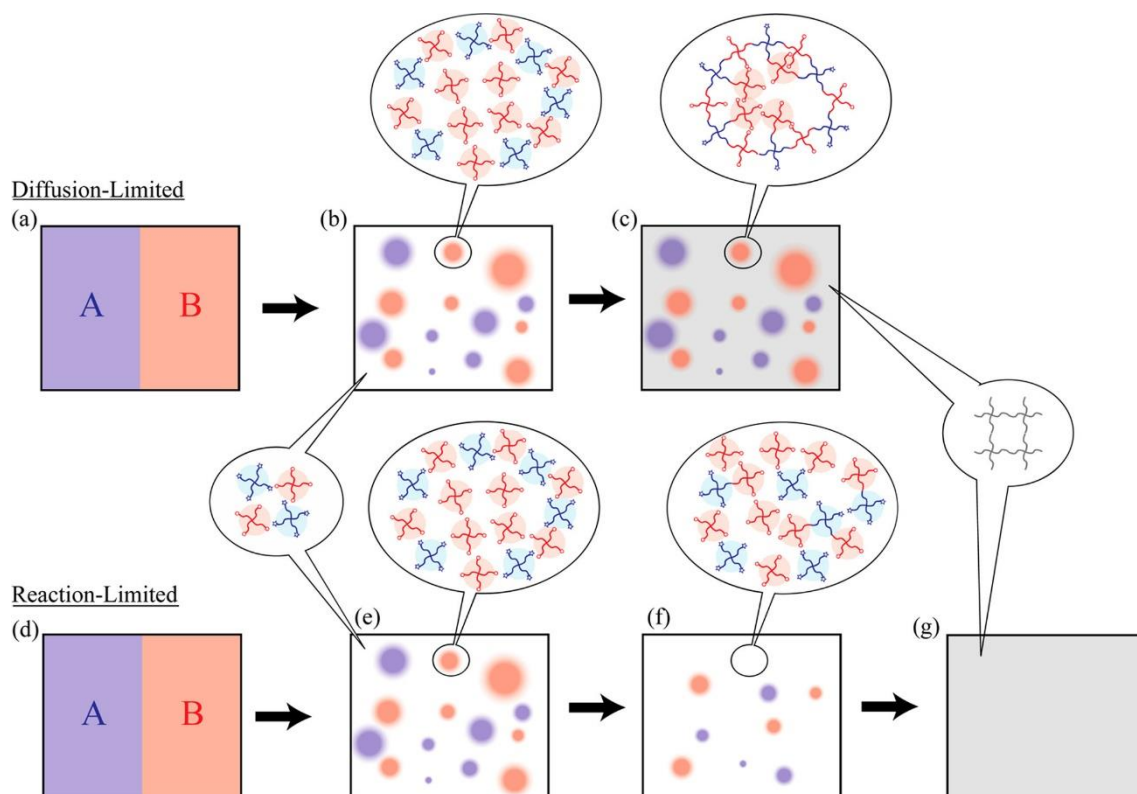


Figure 7. Comparison of the different stages of diffusion-limited (above) and reaction-limited (below) gelation reactions showing the situation: (a, d) before mixing, (b, e) after sufficient mixing, (f) beginning of the reaction, (c, g) end of the reaction.¹²⁴ Reprinted (adapted) with permission from Nishi *et al.* 2014. Copyright 2014 American Chemical Society.

Apart from the mechanism that governs the crosslinking reaction, other factors like pH significantly impacts the kinetics when ionizable species are involved in the crosslinking reaction, such as the thiolate molecule that acts as nucleophile in the thiol-MS reaction. In this case, the more basic the pH the higher the concentration of thiolate will be and therefore faster kinetics. Another factor that has a strong influence on kinetics is ionic strength, that at high values can inhibit the diffusion of species due to subsequent shielding of the charged species that are involved in the reaction by others that are not. Thus, ionic strength must be controlled to allow diffusion and encounter of reactive species. Kurazaku *et al.* developed a system with tunable kinetics mainly dependent on the pH and the ionic strength.^{19,126}

Furthermore, crosslinking kinetics heavily relies on other factors including the chemical nature of the reactive end-groups and the backbone. As highlighted in sections 2.2.3 and 2.3, reaction kinetics depends on the functional groups involved. This dependence largely relies upon the characteristics of atoms, such as their electronic configuration, atomic radius, etc. In addition, the chemical structure of the backbone may also impact the kinetics, since it defines its spatial configuration in solution, and therefore the availability of the end-groups, as well as the possible physical interactions between the backbone and the crosslinker, which may result in diminished reactivity of the latter. Kim *et al.* investigated the influence of using different multi-arm PEG backbones on the reaction kinetics. As seen in previous simulation studies using Monte Carlo prediction model of multi-arm polymers, an increasing number of arms results in their stretching. The reason is the higher density near the core, which reduces the interpenetration of other arms and leads to a higher number of reactive end-groups to be exposed for efficiently reacting with their complementary.⁷

Concentration of the backbone and therefore of the end-groups influences the crosslinking kinetics, and lastly to the network structure. In systems involving star-PEG macromers and short linear crosslinkers, when polymer concentration is too low, the complementary reacting molecules rarely encounter, and the efficiency of the crosslinking reaction is compromised. On the contrary, if the concentration is too high interpenetration or entanglement of polymer chains will occur, which could translate into unpredictable kinetics.¹²⁷ Extensively reported, the most suited polymer concentration for the efficient crosslinking of this type of systems is the overlap concentration, defined as the concentration at which the polymer chains start to connect with each other through small crosslinkers.^{127–129}

2.5.2 Network structure

As previously mentioned, star-PEG backbones have demonstrated to form highly ordered networks.^{18,130–133} Within this type of backbone, attention has been focused on the impact of stoichiometry of reactive groups, the polymer structure and content, and the overlap concentration on the homogeneity of the final mesh.

Stoichiometric ratio (1:1) of reactive end-groups is supposed to generate the highest number of crosslinking points, defined as the covalent bonds formed between two complementary reacting groups, thus resulting in a complete and homogeneous network. Additionally, altering parameters that produce an impact on the number of crosslinking points (e.g. varying the overall polymer content while keeping the stoichiometric ratio), would modify the network structure and therefore the stiffness and swelling ratio.¹²⁵

The structure of the backbone(s) dictates the final internal structure of the hydrogel. Star-PEG polymers lead to the formation of highly ordered networks characterized by uniformly spaced and distributed components, resulting in a homogeneous pore size. Nevertheless, these highly ordered networks are not exempt from inhomogeneities. Heterogeneity in hydrogels is classified into two different categories depending on the scale: global or spatial heterogeneity (100 nm scale) and local heterogeneity (1 nm scale). Spatial heterogeneity is defined as the non-homogeneous distribution of the polymer units. It produces refractive index (RI) deviations that scatters light, and it is detected through techniques like SANS. While spatial heterogeneities are the most common inhomogeneities in hydrogels, they are mostly suppressed in star-PEG systems due to the stepwise crosslinking process involving complementary chain end-groups.^{132,134} On the other hand, local heterogeneities, including trapped entanglements and connective defects (**Figure 8**), are formed by a low number of polymer chains. In this case, the topological inhomogeneities are detected by changes in the physical properties when comparing with model predictions.¹³² Still present due to the random encounter of reactive groups, local inhomogeneities are minimized through the complementary crosslinking reaction of chain end-groups.^{132,134}

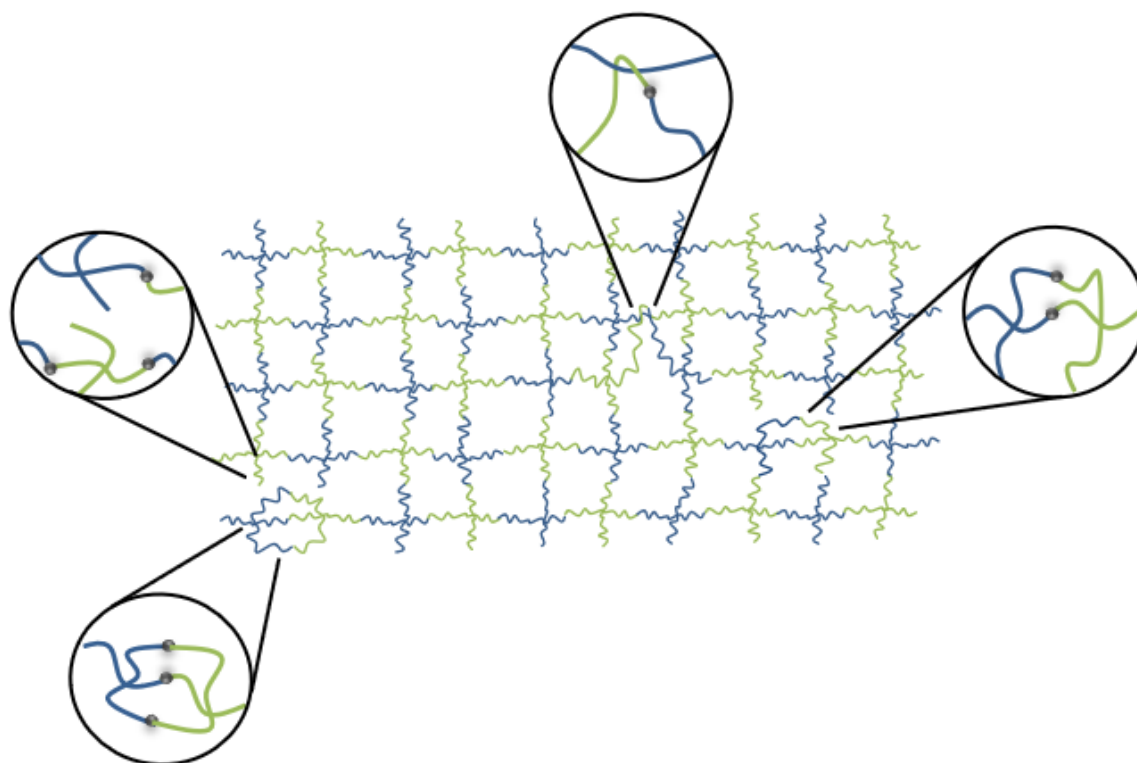


Figure 8. Schematic figure showing local inhomogeneities in a system involving two tetra-arm PEG polymers (blue and green) with complementary reactive end-groups. Entanglements, dangling ends and triple and double bonds between two single molecules (loops) are shown.

Furthermore, the low number of network defects in tetra-arm PEG hydrogels are partially explained by the highly ordered and numerous active crosslinking points, considered as connecting points with at least three bonds to the macroscopic hydrogel network.¹²⁵ In this type of hydrogels, all star-PEG molecules have the chance to become active crosslinking points. On the other hand, using linear crosslinkers in star-PEG hydrogels, while keeping the overall polymer content constant, results in a lower number of active crosslinking points when compared to their star-PEG homologous. As a result, a higher number of local inhomogeneities such as loops (**Figure 8**) may be introduced into the 3D network. However, these networks hold high interest for 3D cell encapsulation due to the possibility of using small degradable enzyme-sensitive sequences as crosslinkers. Li *et al.* investigated the formation of a well-defined and homogeneous network by using a tetra-arm PEG as backbone and a small linear crosslinker. For the preparation of their hydrogel, they applied the “bond percolation” model, which considers that all space is

uniformly pre-filled with complementary precursor molecules at the overlapping concentration. Crosslinking takes place by reaction of nearby reactive groups, following a reaction-limited mechanism. As a result, a highly ordered but flexible and near ideal network is formed.¹³⁴

Unlike star-PEG polymers, backbones incorporating multiple reactive groups within their chains result in less organized networks due to the stochastic crosslinking reactions between the different available reactive groups from the backbone and the crosslinker.

The crosslinking density and thus the network structure are directly proportional to the overall polymer content. Increased polymer content translates into a higher density of crosslinking points, resulting in a more densely packed network with smaller pore sizes. Consequently, a highly packed network also presents greater stiffness, as the network structure is intimately related to the mechanical/rheological properties of the hydrogel.^{135,136}

2.6 Monitoring of gelation by rheology

Viscoelastic materials such as hydrogels exhibit elastic (solid) and viscous (liquid) properties when subjected to deformation. To study the viscoelastic behavior of hydrogels, rheology, which is the science that studies the flow of matter, is often used.^{137,138} A rheometer is the instrument used to conduct these experiments, and two types can be found: controlled-stress and controlled-strain (**Figure 9**). In both types, the sample is placed between two different plates, upper and lower. In controlled-stress rheometers, the upper plate moves (applies a torque to control the stress or the strain) while the lower is static. On the other hand, in controlled-strain rheometers, both plates move (the lower moves at a certain speed while the upper measures the torsional force).¹³⁹

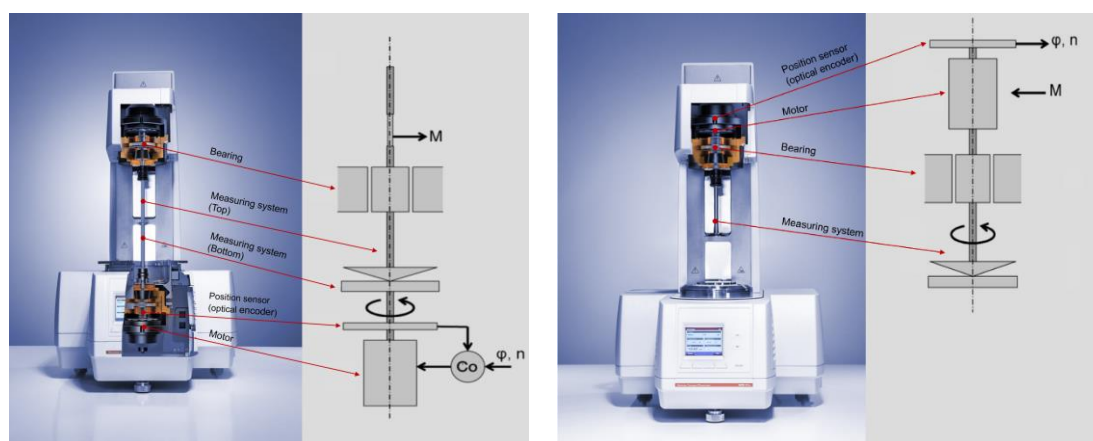


Figure 9. Strain-controlled (CR-) (left) and stress-controlled (CS) (right) rheometers. Figure reprinted/adapted from Anton Paar GmbH website (<https://wiki.anton-paar.com/en/basics-of-rheology/rheological-measurements/>).

In rheology, there are two different measuring methods that can be applied to the material under study: rotational and oscillatory. Rotational measurements are based on the constant rotation movement of the leading plate (upper or lower) in contact with the material under study, involving large deformations within the non-linear viscoelastic region of the material. In oscillatory measurements, a small sinusoidal deformation/oscillation is applied within the linear viscoelastic region of the sample, where the outputs do not depend on the employed strain or stress.^{140,141} While rotational measurements are often destructive, oscillatory are not due to the small deformation that is applied to the sample. This type of measurement is useful for studying processes that influence the structure of the sample, such as hydrogel crosslinking/gelation. For this, the strain must be small enough to not disturb the physical or chemical process.

Oscillation measurements (**Figure 10**) rely on the application of a shear deformation (or strain) to the material in form of a sinusoidal oscillation, $\gamma(t) = \gamma_0(\sin \omega t)$, where γ is the shear strain and ω is the angular frequency. The measured output in this case is the shear stress, $\tau(t) = \tau_A(\sin \omega t + \delta)$, where τ is the shear stress and δ is the phase angle, which is the shift between the two waves, stress and strain. In addition, shear stress can also be applied, and shear strain measured.

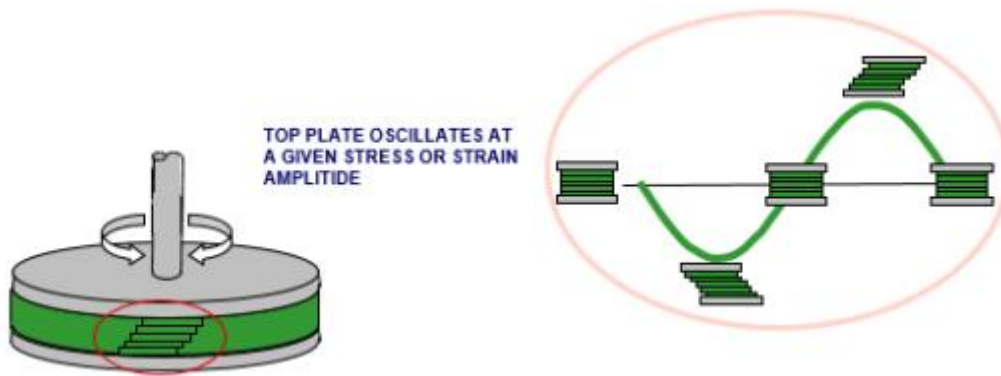


Figure 10. Sample (green) loaded between two parallel plates (top and bottom) to which a sinusoidal oscillatory shear deformation is applied. *Figure reprinted/adapted from “A Basic Introduction to Rheology”, ©2016 Malvern Instruments Limited.*

In case of a material with an ideal elastic behavior, strain and stress are in phase, which translates to $\delta = 0^\circ$. On the contrary, for a purely viscous material, a lag of $\delta = 90^\circ$ exists between strain and stress. Additionally, hydrogels, which present a viscoelastic behavior, have a phase shift angle $0 < \delta < 90^\circ$ (**Figure 11**).

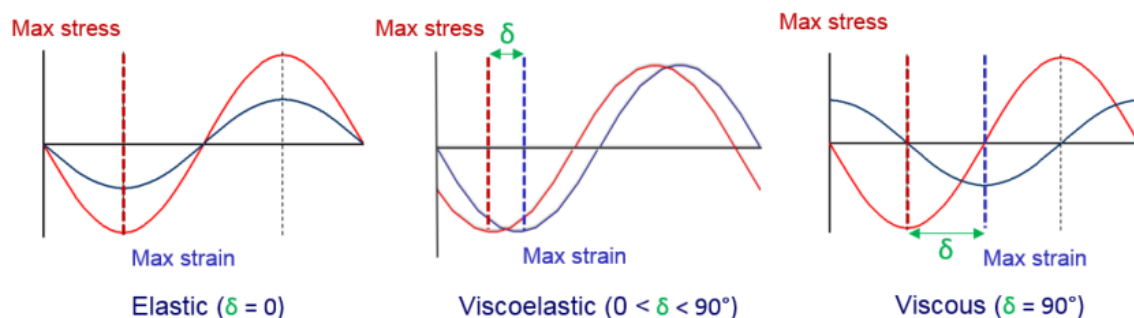


Figure 11. Scheme showing the relation existing between the stress and strain waves for a purely elastic (ideal solid), viscoelastic, and purely viscous (ideal liquid) material. *Figure reprinted/adapted from “A Basic Introduction to Rheology”, ©2016 Malvern Instruments Limited.*

The most important parameters that can be obtained from oscillation measurements regarding the viscoelastic properties of hydrogels are the complex shear modulus $G^* = \tau(t)/\gamma(t)$, the storage modulus G' , the loss modulus G'' , and the loss factor (or damping factor) $\tan \delta = G''/G'$. The complex modulus (G^*) is also referred as the stiffness or resistance to deformation of the material under study.^{142,143} The storage modulus (G') is a measure of the elastic behavior of the material and its capacity to store the deformation

energy, giving information about the amount of structure in the sample. On the other hand, the loss modulus (G'') is a measure of the viscous behavior, representing the energy dissipated/lost during the deformation. The loss factor is the ratio between the viscous and the elastic portions.¹⁴²

Within oscillatory measurements different types of tests can be performed, including amplitude sweep, frequency sweep, time sweep, temperature ramp and sweep.¹⁴⁴ In order to study the viscoelastic properties of a hydrogel, the measurements must be done within the so-called linear viscoelastic region (LVR), which is the amplitude region where G' and G'' are independent of the strain and have constant plateau values. In this region the elastic deformation is below the non-destructive deformation limit, meaning bonds are not broken. Sharma *et al.* studied the self-healing properties of chitosan-based hydrogels by monitoring the G' and G'' over time at the non-destructive deformation (strain) critical value. They observed an abrupt decrease (breaking of the 3D network bonds), after which a recovery of both G' and G'' took place (reformation of bonds), reaching values close to normal conditions.¹⁴⁵

The gelation process of a hydrogel can be monitored in oscillation rheology by performing a time sweep measurement, which consists of the monitorization of the material response over time to a constant oscillation amplitude, frequency, and temperature. It is commonly used to investigate potential structural changes of a material, such as the hydrogel's network crosslinking (gelation process). The time point in which the precursor solution (liquid) becomes a hydrogel (viscoelastic material) because of the formation of enough crosslinking points within the network is known as gelation point. In time sweep measurements, the gelation point is usually referred to as the time point in which $G' \geq G''$, when the elastic (solid) behavior dominates the viscous (liquid) one.¹⁴² As an example, Deng *et al.* studied the gelation time, occurring within a few minutes, of injectable hyaluronic acid/ carboxymethyl cellulose (HA/CMC) hydrogels at different conditions by observing the cross point between G' and G'' .¹⁴⁶ Thus, by performing time sweep tests, important parameters related to the internal structure of the hydrogel 3D network can be monitored, including the gelation time and the shear complex modulus G^* or stiffness. Moreover, to effectively study the gelation process, the measured output must be independent of the strain and therefore the stress, so the strain and oscillation frequency

inputs must belong to the LVR. These parameters are obtained by performing amplitude and frequency sweep measurements. Amplitude sweep test measures the response of the material under study to an increasing deformation and is conducted by varying the amplitude (strain or stress) while keeping the frequency and temperature constant. On the other hand, frequency sweep test measures the response of the material under study to an increasing oscillation frequency and is conducted by varying the frequency while keeping the amplitude and temperature constant.

Determining the gelation point of a hydrogel by monitoring G' and G'' over time has limitations. For instance, hydrogels whose crosslinking begins upon mixing precursors and present very short gelation times (few seconds), like thiol-maleimide, pose challenges. In such cases, the crossing point of G' and G'' is not observed, making it difficult or impossible to establish gelation time by rheology.¹⁴⁷ Additionally, when gelation is too fast, hydrogels are not suitable for 3D cell encapsulation because cell distribution and network formation will not be homogeneous, negatively affecting reproducibility. On the other hand, investigating the gelation time of systems with on-demand crosslinking, such as light-induced, is usually compatible with rheology.

Apart from the gelation process, other processes that may affect the internal structure of hydrogels, including evaporation of the solvent, swelling, or degradation (stability of the hydrogel), can be followed through time sweep measurements.¹⁴⁸ For example, the observation of no change in G' and G'' over time is considered a sign of hydrogel stability.

There are different acquisition factors that influence that govern the rheological studies of materials and must be optimized before the measurements, such as the geometries of the upper and lower plates, the gap (distance between the plates), and the solvent trap, which in turn depends on the solvent properties. In addition, both the mixing and the gelation process also play a vital role on the rheological output and must be controlled.

- i. Depending on the material and the type of measurement, geometries with different shapes, diameters and surfaces are available. The shape may be selected depending on the viscosity, the relaxation time and volume of the sample, e.g. cone upper plate is used for very low to high viscous liquids, while parallel flat upper plate is recommended for very low viscosity liquids to soft

solids. Regarding the diameter, the shear stress is dependent of it, $\sigma = 2M / \pi r^3$ (where M is the torque and r the moment arm, which is equivalent to the radius of the geometry), so it must be carefully selected. Moreover, all the sample must be in contact with the plates, avoiding both overfilling and insufficient sample volume. Finally, the surface is selected depending on the type of material under study and the possibility of it flipping or slipping between the plates during the measurements. Therefore, smooth or rough surfaces are available.

- ii. The gap is also related to the volume of the sample and the need for it to be in contact with the upper and lower plates. In addition, the shear rate is indirectly proportional to the gap, $\dot{\gamma} = \Omega \cdot r / h$ (where Ω is the angular velocity and h the gap distance).
- iii. A solvent trap is used to avoid solvent evaporation. In case of water evaporation, some rheological properties of the hydrogels, such as the G' , may be misunderstood since dry samples tend to have a higher stiffness (higher storage modulus). Therefore, in order to avoid water evaporation over time, solvent traps (isolation chamber + special upper geometry) loaded with water or/and a non-interfering sealant like silicon oil between the sample and the surroundings may be used.
- iv. Mixing must be sufficient to consider that the pre-hydrogel mixture is homogeneous, and the rheological output is therefore representative of the actual hydrogel behavior. An incomplete mixing results in heterogeneous networks and the subsequent altered mechanical properties.
- v. Gelation must be slow enough if it is intended to be monitored during the measurement. Fast gelation times, few seconds or less, are usually too short to be recorded.

2.7 High-throughput 3D cell culture

2.7.1 Automation of cell-encapsulated hydrogels for drug discovery

Cell-based high-throughput screening (HTS) assays are a common practice during the discovery and development of new drugs within the pharmaceutical industry.¹⁴⁹ Such assays serve to identify active molecules that modulate particular steps within a physiological pathway through their interaction with cellular targets or based on their

ability to provoke cellular responses. In that scenario, 3D cell culture models are expected to substitute 2D cell cultures in the near future, as their prediction potential increases as result of better encapsulation materials and coculture conditions.

High-throughput screening (HTS) formats (usually 384- or 1536-well plate format) are intrinsically linked to automation due to the multiple number of inputs and therefore outputs that are generated, as well as the need to obtain highly reproducible outcomes. While in its early stages, automated liquid handling is a promising technique that has been applied for cell-encapsulated hydrogels, requiring adaptation of the manual protocols to the needs and particularities of automated and standardized workflows.¹⁵⁰ Automation of 3D cell culture offers several advantages over the manual approach, such as higher accuracy, precision, and efficiency. Moreover, in combination with other promising technologies such as deep learning and AI, automation can lead to more standardized, reliable and reproducible 3D cell culture models.³

Automated liquid handling systems are devices that use a robotic arm equipped with single or multiple channels (micropipettes) that moves in the X, Y and Z axes in order to reach all positions within the deck layout. In case of multiple channels, two arrangements are available: parallel channels that move independently from each other (one can move while the others not), usually ranging from 1 to 8 channels, or parallel and equally distanced channels that are attached to a single head following a distribution like 96 and 384 well plates standard format (ANSI/SLAS). In the case of 96 or 384 channels heads, since the channels are all attached to the same head/module, they all move at the same time. This feature increases the flexibility of automated liquid handlers with instruments capable of working with both independent channels (up to 8) and 96/384 channels heads. Complexity of liquid handling robots goes from simple moving arms, just capable of moving in X, Y and Z axis and pipetting liquids, to sophisticated workstation that incorporate pipetting robotic arms (capable of transporting labware through the workstation), shakers, plate-tilting modules, heating and cooling modules, centrifuges, incubators, plate readers, simple or confocal microscope, etc. An example of this type of complex systems is the StemCellFactory workstation, developed by a German consortium, for the automated production, expansion and differentiation of induced pluripotent stem cells, as well as personalized stem cell-based drug prediction (by using

cells in suspension). Boussaad *et al.* also developed a multitask workstation incorporating an automated liquid handler, for the preparation and maintenance of 2D and 3D (organoids) cell culture models in suspension,¹⁵¹ with the subsequent decrease of workload.

In the field of hydrogels for cell encapsulation, Rimann *et al.* successfully translated a manual protocol for the 3D cell encapsulation of spheroids in dextran-based hydrogels to an automated liquid handling instrument. Moreover, in order to show the potential of automated liquid handling system in hydrogel cell encapsulation, they automatized not just the hydrogel preparation, but the medium exchange and the cell viability analysis. Similar viability in both manual and automated protocols was obtained, proving that the automated method is compatible with 3D cell culture and does not decrease cell survival. Additionally, they performed preliminary drug tests with Taxol (a natural product for cancer treatment), observing a similar effect on 3D cell cultures prepared through both techniques (manual and automated).¹⁵² Mabry *et al.* developed an automated high-throughput method for studying cell-matrix interactions by 3D encapsulation of vascular cells on peptide-functionalized PEG hydrogels with different properties. The introduction of an automated liquid pipettor compatible with medium/high-throughput allowed them to study the dynamically changing cell-matrix interactions in multiple conditions by varying the type and concentration of cell-adhesion motifs within the rows of the well plates, as well as performing post-gelation hydrogel modifications in different columns of the well plates through extra and unreacted end-groups.¹⁵³

Nevertheless, automation of high-throughput 3D cell culture assays presents challenges for its widespread adoption in areas such as drug discovery and development, including the complexity of the physiological architecture and the absence of suitable screening protocols. Thus, the incorporation of microfabrication techniques and high-throughput analytical tools is essential to assess the pharmacological and toxicological impacts of drugs in HTS 3D cell culture.

The adoption of automated techniques such as automated liquid handling involves the parallel manipulation of multiple parameters, as for example aspiration and dispensing speed and height, pipetted volumes, tip retracting speed, number of mixing cycles,

mixing speed, etc. As a result, when optimizing the process on automated liquid handling systems, effective and efficient methodologies like design of experiments (DOE) should be applied in order to save time and resources.

2.7.2 Process optimization with multiple parameters

Conventional process optimization involving multiple factors follows an iterative strategy referred to as one-factor-at-a-time (OFAT). This approach consists of changing the value of a particular factor while keeping the others fixed until the “optimal” value is found. Then, the described process is repeated with the rest of the factors. Nevertheless, OFAT strategies are inefficient and frequently result in imprecise outcomes. This is primarily due to the practice of drawing experimental conclusions after each trial run, comparing observed outcomes with previous results. Consequently, only two observations are employed to estimate the impact of each factor in each iteration, leading to misinterpretation. Regarded as a trial-and-error approach, the success of OFAT relies on luck, experience, and intuition. Additionally, another drawback is the lack of consideration for factor interactions, potentially resulting in the oversight of optimal settings for a certain factor.

Initially introduced by Sir Ronald Fischer in the 1920s for its application in agriculture, design of experiments (DOE) is a statistical methodology to plan, analyze, and interpret controlled experiments in order to evaluate the influence of various parameters. Since its introduction, it has been successfully applied to a wide variety of fields including combinatorial chemistry,¹⁵⁴ engineering,¹⁵⁵ the bioprocessing industry^{156,157} and drug discovery,^{158–160} where it serves as a tool for optimization processes.¹⁶¹ In this approach, the selection of experimental conditions involves varying multiple factors at the same time.¹⁶² Opposite to OFAT, all the design space, corresponding to the number of factors tested and delimited by their tested ranges of values (from the lowest to the highest), is explored. In addition, combinations of factors, that can be completely (full factorial design) or partially (fractional factorial design) investigated, reliably characterize the complete design space. Thus, DOE effectively reduces the required resources as it maximizes the information extracted from each experimental condition.¹⁵⁸

By reducing the substantial time and resources typically needed for complex biochemical and cell-based assays involving 3D cell culture, DOE strategies, when integrated with existing automated systems, pave the way for a more efficient and reliable high-throughput screening experimentation.

Bibliography

- (1) Singh, N.; Vayer, P.; Tanwar, S.; Poyet, J.-L.; Tsaïoun, K.; Villoutreix, B. O. Drug Discovery and Development: Introduction to the General Public and Patient Groups. *Front. Drug Discov.* **2023**, *3*. <https://doi.org/10.3389/fddsv.2023.1201419>.
- (2) Wildey, M. J.; Haunso, A.; Tudor, M.; Webb, M.; Connick, J. H. Chapter Five - High-Throughput Screening. In *Annual Reports in Medicinal Chemistry*; Goodnow, R. A., Ed.; Platform Technologies in Drug Discovery and Validation; Academic Press, 2017; Vol. 50, pp 149–195. <https://doi.org/10.1016/bs.armc.2017.08.004>.
- (3) Wang, Y.; Jeon, H. 3D Cell Cultures toward Quantitative High-Throughput Drug Screening. *Trends in Pharmacological Sciences* **2022**, *43* (7), 569–581. <https://doi.org/10.1016/j.tips.2022.03.014>.
- (4) Fontaine, S. D.; Reid, R.; Robinson, L.; Ashley, G. W.; Santi, D. V. Long-Term Stabilization of Maleimide-Thiol Conjugates. *Bioconjug Chem* **2015**, *26* (1), 145–152. <https://doi.org/10.1021/bc5005262>.
- (5) Ryan, C. P.; Smith, M. E. B.; Schumacher, F. F.; Grohmann, D.; Papaioannou, D.; Waksman, G.; Werner, F.; Baker, J. R.; Caddick, S. Tunable Reagents for Multi-Functional Bioconjugation: Reversible or Permanent Chemical Modification of Proteins and Peptides by Control of Maleimide Hydrolysis. *Chem Commun (Camb)* **2011**, *47* (19), 5452–5454. <https://doi.org/10.1039/c1cc11114k>.
- (6) Paez, J. I.; Farrukh, A.; Valbuena-Mendoza, R.; Włodarczyk-Biegun, M. K.; del Campo, A. Thiol-Methylsulfone-Based Hydrogels for 3D Cell Encapsulation. *ACS Appl. Mater. Interfaces* **2020**, *12* (7), 8062–8072. <https://doi.org/10.1021/acsami.0c00709>.
- (7) Kim, J.; Kong, Y. P.; Niedzielski, S. M.; Singh, R. K.; Putnam, A. J.; Shikanov, A. Characterization of the Crosslinking Kinetics of Multi-Arm Poly(Ethylene Glycol) Hydrogels Formed via Michael-Type Addition. *Soft Matter* **2016**, *12* (7), 2076–2085. <https://doi.org/10.1039/C5SM02668G>.
- (8) Cengiz, N.; Rao, J.; Sanyal, A.; Khan, A. Designing Functionalizable Hydrogels through Thiol–Epoxy Coupling Chemistry. *Chemical Communications* **2013**, *49* (95), 11191–11193. <https://doi.org/10.1039/C3CC45859H>.
- (9) Truong, V. X.; Donderwinkel, I.; Frith, J. E. Bioorthogonal Hydrogels by Thiol–Halide Click Crosslinking with Fast Gelation Time and Tunable Stability in Aqueous Media. *Journal of Polymer Science Part A: Polymer Chemistry* **2019**, *57* (18), 1872–1876. <https://doi.org/10.1002/pola.29267>.
- (10) Huynh, C. T.; Liu, F.; Cheng, Y.; Coughlin, K. A.; Alsberg, E. Thiol-Epoxy “Click” Chemistry to Engineer Cytocompatible PEG-Based Hydrogel for siRNA-Mediated Osteogenesis of hMSCs. *ACS Appl Mater Interfaces* **2018**, *10* (31), 25936–25942. <https://doi.org/10.1021/acsami.8b07167>.
- (11) Choh, S.-Y.; Cross, D.; Wang, C. Facile Synthesis and Characterization of Disulfide-Cross-Linked Hyaluronic Acid Hydrogels for Protein Delivery and Cell Encapsulation. *Biomacromolecules* **2011**, *12* (4), 1126–1136. <https://doi.org/10.1021/bm101451k>.
- (12) Nagy, P. Kinetics and Mechanisms of Thiol–Disulfide Exchange Covering Direct Substitution and Thiol Oxidation-Mediated Pathways. *Antioxid Redox Signal* **2013**, *18* (13), 1623–1641. <https://doi.org/10.1089/ars.2012.4973>.

- (13) Jin, M.; Koçer, G.; Paez, J. I. Luciferin-Bioinspired Click Ligation Enables Hydrogel Platforms with Fine-Tunable Properties for 3D Cell Culture. *ACS Appl. Mater. Interfaces* **2022**, *14* (4), 5017–5032. <https://doi.org/10.1021/acsami.1c22186>.
- (14) Fairbanks, B. D.; Schwartz, M. P.; Halevi, A. E.; Nuttelman, C. R.; Bowman, C. N.; Anseth, K. S. A Versatile Synthetic Extracellular Matrix Mimic via Thiol-Norbornene Photopolymerization. *Adv Mater* **2009**, *21* (48), 5005–5010. <https://doi.org/10.1002/adma.200901808>.
- (15) Zheng, Y.; Han, M. K. L.; Jiang, Q.; Li, B.; Feng, J.; Campo, A. del. 4D Hydrogel for Dynamic Cell Culture with Orthogonal, Wavelength-Dependent Mechanical and Biochemical Cues. *Materials Horizons* **2020**, *7* (1), 111–116. <https://doi.org/10.1039/C9MH00665F>.
- (16) Paez, J. I.; de Miguel-Jiménez, A.; Valbuena-Mendoza, R.; Rathore, A.; Jin, M.; Gläser, A.; Pearson, S.; del Campo, A. Thiol-Methylsulfone-Based Hydrogels for Cell Encapsulation: Reactivity Optimization of Aryl-Methylsulfone Substrate for Fine-Tunable Gelation Rate and Improved Stability. *Biomacromolecules* **2021**, *22* (7), 2874–2886. <https://doi.org/10.1021/acs.biomac.1c00256>.
- (17) Kharkar, P. M.; Kiick, K. L.; Kloxin, A. M. Designing Degradable Hydrogels for Orthogonal Control of Cell Microenvironments. *Chem Soc Rev* **2013**, *42* (17), 7335–7372. <https://doi.org/10.1039/c3cs60040h>.
- (18) Xue, B.; Tang, D.; Wu, X.; Xu, Z.; Gu, J.; Han, Y.; Zhu, Z.; Qin, M.; Zou, X.; Wang, W.; Cao, Y. Engineering Hydrogels with Homogeneous Mechanical Properties for Controlling Stem Cell Lineage Specification. *Proc Natl Acad Sci U S A* **2021**, *118* (37), e2110961118. <https://doi.org/10.1073/pnas.2110961118>.
- (19) Nishi, K.; Fujii, K.; Katsumoto, Y.; Sakai, T.; Shibayama, M. Kinetic Aspect on Gelation Mechanism of Tetra-PEG Hydrogel. *Macromolecules* **2014**, *47* (10), 3274–3281. <https://doi.org/10.1021/ma500662j>.
- (20) Ho, T.-C.; Chang, C.-C.; Chan, H.-P.; Chung, T.-W.; Shu, C.-W.; Chuang, K.-P.; Duh, T.-H.; Yang, M.-H.; Tyan, Y.-C. Hydrogels: Properties and Applications in Biomedicine. *Molecules* **2022**, *27* (9), 2902. <https://doi.org/10.3390/molecules27092902>.
- (21) Lin, X.; Zhao, X.; Xu, C.; Wang, L.; Xia, Y. Progress in the Mechanical Enhancement of Hydrogels: Fabrication Strategies and Underlying Mechanisms. *Journal of Polymer Science* **2022**, *60* (17), 2525–2542. <https://doi.org/10.1002/pol.20220154>.
- (22) Simionescu, B. C.; Ivanov, D. Natural and Synthetic Polymers for Designing Composite Materials. In *Handbook of Bioceramics and Biocomposites*; Antoniac, I. V., Ed.; Springer International Publishing: Cham, 2016; pp 233–286. https://doi.org/10.1007/978-3-319-12460-5_11.
- (23) Chai, Q.; Jiao, Y.; Yu, X. Hydrogels for Biomedical Applications: Their Characteristics and the Mechanisms behind Them. *Gels* **2017**, *3* (1), 6. <https://doi.org/10.3390/gels3010006>.
- (24) Gyles, D. A.; Castro, L. D.; Silva, J. O. C.; Ribeiro-Costa, R. M. A Review of the Designs and Prominent Biomedical Advances of Natural and Synthetic Hydrogel Formulations. *European Polymer Journal* **2017**, *88*, 373–392. <https://doi.org/10.1016/j.eurpolymj.2017.01.027>.
- (25) Bhusari, S.; Hoffmann, M.; Herbeck-Engel, P.; Sankaran, S.; Wilhelm, M.; Campo, A. del. Rheological Behavior of Pluronic/Pluronic Diacrylate Hydrogels Used for Bacteria Encapsulation in Engineered Living Materials. *Soft Matter* **2024**, *20* (6), 1320–1332. <https://doi.org/10.1039/D3SM01119D>.
- (26) Lust, S. T.; Hoogland, D.; Norman, M. D. A.; Kerins, C.; Omar, J.; Jowett, G. M.; Yu, T. T. L.; Yan, Z.; Xu, J. Z.; Marciano, D.; da Silva, R. M. P.; Dreiss, C. A.; Lamata, P.; Shipley, R. J.; Gentleman, E. Selectively Cross-Linked Tetra-PEG Hydrogels Provide Control over Mechanical Strength with Minimal Impact on Diffusivity. *ACS Biomater. Sci. Eng.* **2021**, *7* (9), 4293–4304. <https://doi.org/10.1021/acsbiomaterials.0c01723>.

- (27) Liang, J.; Dijkstra, P. J.; Poot, A. A.; Grijpma, D. W. Hybrid Hydrogels Based on Methacrylate-Functionalized Gelatin (GelMA) and Synthetic Polymers. *Biomedical Materials & Devices* **2023**, *1* (1), 191–201. <https://doi.org/10.1007/s44174-022-00023-2>.
- (28) Guo, Y. Z.; Nakajima, T.; Mredha, Md. T. I.; Guo, H. L.; Cui, K.; Zheng, Y.; Cui, W.; Kurokawa, T.; Gong, J. P. Facile Preparation of Cellulose Hydrogel with Achilles Tendon-like Super Strength through Aligning Hierarchical Fibrous Structure. *Chemical Engineering Journal* **2022**, *428*, 132040. <https://doi.org/10.1016/j.cej.2021.132040>.
- (29) Herzberger, J.; Niederer, K.; Pohlit, H.; Seiwert, J.; Worm, M.; Wurm, F. R.; Frey, H. Polymerization of Ethylene Oxide, Propylene Oxide, and Other Alkylene Oxides: Synthesis, Novel Polymer Architectures, and Bioconjugation. *Chem. Rev.* **2016**, *116* (4), 2170–2243. <https://doi.org/10.1021/acs.chemrev.5b00441>.
- (30) Zhao, X.; Si, J.; Huang, D.; Li, K.; Xin, Y.; Sui, M. Application of Star Poly(Ethylene Glycol) Derivatives in Drug Delivery and Controlled Release. *Journal of Controlled Release* **2020**, *323*, 565–577. <https://doi.org/10.1016/j.jconrel.2020.04.039>.
- (31) Wang, Z.; Ye, Q.; Yu, S.; Akhavan, B. Poly Ethylene Glycol (PEG)-Based Hydrogels for Drug Delivery in Cancer Therapy: A Comprehensive Review. *Advanced Healthcare Materials* **2023**, *12* (18), 2300105. <https://doi.org/10.1002/adhm.202300105>.
- (32) Tang, G.; Zhou, B.; Li, F.; Wang, W.; Liu, Y.; Wang, X.; Liu, C.; Ye, X. Advances of Naturally Derived and Synthetic Hydrogels for Intervertebral Disk Regeneration. *Front Bioeng Biotechnol* **2020**, *8*, 745. <https://doi.org/10.3389/fbioe.2020.00745>.
- (33) Cambria, E.; Renggli, K.; Ahrens, C. C.; Cook, C. D.; Kroll, C.; Krueger, A. T.; Imperiali, B.; Griffith, L. G. Covalent Modification of Synthetic Hydrogels with Bioactive Proteins via Sortase-Mediated Ligation. *Biomacromolecules* **2015**, *16* (8), 2316–2326. <https://doi.org/10.1021/acs.biomac.5b00549>.
- (34) Nimmo, C. M.; Shoichet, M. S. Regenerative Biomaterials That “Click”: Simple, Aqueous-Based Protocols for Hydrogel Synthesis, Surface Immobilization, and 3D Patterning. *Bioconjugate Chem.* **2011**, *22* (11), 2199–2209. <https://doi.org/10.1021/bc200281k>.
- (35) Lin, C.-C.; Anseth, K. S. PEG Hydrogels for the Controlled Release of Biomolecules in Regenerative Medicine. *Pharm Res* **2009**, *26* (3), 631–643. <https://doi.org/10.1007/s11095-008-9801-2>.
- (36) Caliani, S. R.; Burdick, J. A. A Practical Guide to Hydrogels for Cell Culture. *Nat Methods* **2016**, *13* (5), 405–414. <https://doi.org/10.1038/nmeth.3839>.
- (37) Burdick, J. A.; Murphy, W. L. Moving from Static to Dynamic Complexity in Hydrogel Design. *Nat Commun* **2012**, *3*, 1269. <https://doi.org/10.1038/ncomms2271>.
- (38) Echalié, C.; Valot, L.; Martínez, J.; Mehdi, A.; Subra, G. Chemical Cross-Linking Methods for Cell Encapsulation in Hydrogels. *Materials Today Communications* **2019**, *20*, 100536. <https://doi.org/10.1016/j.mtcomm.2019.05.012>.
- (39) Madl, C. M.; Heilshorn, S. C. Bioorthogonal Strategies for Engineering Extracellular Matrices. *Advanced Functional Materials* **2018**, *28* (11), 1706046. <https://doi.org/10.1002/adfm.201706046>.
- (40) Hu, J.; Zhang, G.; Liu, S. Enzyme-Responsive Polymeric Assemblies, Nanoparticles and Hydrogels. *Chemical Society Reviews* **2012**, *41* (18), 5933–5949. <https://doi.org/10.1039/C2CS35103J>.
- (41) Zhu, J.; Marchant, R. E. Design Properties of Hydrogel Tissue-Engineering Scaffolds. *Expert Rev Med Devices* **2011**, *8* (5), 607–626. <https://doi.org/10.1586/erd.11.27>.
- (42) Nam, S.; Stowers, R.; Lou, J.; Xia, Y.; Chaudhuri, O. Varying PEG Density to Control Stress Relaxation in Alginate-PEG Hydrogels for 3D Cell Culture Studies. *Biomaterials* **2019**, *200*, 15–24. <https://doi.org/10.1016/j.biomaterials.2019.02.004>.
- (43) Buranachai, T.; Praphairaksit, N.; Muangsinsin, N. Chitosan/Polyethylene Glycol Beads Crosslinked with Tripolyphosphate and Glutaraldehyde for Gastrointestinal Drug Delivery. *AAPS PharmSciTech* **2010**, *11* (3), 1128–1137. <https://doi.org/10.1208/s12249-010-9483-z>.

- (44) Kirmic Cosgun, S. N.; Ceylan Tuncaboylu, D. Cyclodextrin-Linked PVP/PEG Supramolecular Hydrogels. *Carbohydrate Polymers* **2021**, *269*, 118278. <https://doi.org/10.1016/j.carbpol.2021.118278>.
- (45) Bustamante-Torres, M.; Romero-Fierro, D.; Arcentales-Vera, B.; Palomino, K.; Magaña, H.; Bucio, E. Hydrogels Classification According to the Physical or Chemical Interactions and as Stimuli-Sensitive Materials. *Gels* **2021**, *7* (4), 182. <https://doi.org/10.3390/gels7040182>.
- (46) Tsuji, H. Poly(Lactide) Stereocomplexes: Formation, Structure, Properties, Degradation, and Applications. *Macromol Biosci* **2005**, *5* (7), 569–597. <https://doi.org/10.1002/mabi.200500062>.
- (47) Hiemstra, C.; Zhong, Z.; Li, L.; Dijkstra, P. J.; Feijen, J. In-Situ Formation of Biodegradable Hydrogels by Stereocomplexation of PEG-(PLLA)₈ and PEG-(PDLA)₈ Star Block Copolymers. *Biomacromolecules* **2006**, *7* (10), 2790–2795. <https://doi.org/10.1021/bm060630e>.
- (48) Mao, H.; Wang, C.; Chang, X.; Cao, H.; Shan, G.; Bao, Y.; Pan, P. Poly(Lactic Acid)/Poly(Ethylene Glycol) Stereocomplexed Physical Hydrogels Showing Thermally-Induced Gel–Sol–Gel Multiple Phase Transitions. *Mater. Chem. Front.* **2018**, *2* (2), 313–322. <https://doi.org/10.1039/C7QM00502D>.
- (49) Chang, H.; Li, C.; Huang, R.; Su, R.; Qi, W.; He, Z. Amphiphilic Hydrogels for Biomedical Applications. *J. Mater. Chem. B* **2019**, *7* (18), 2899–2910. <https://doi.org/10.1039/C9TB00073A>.
- (50) Guiseppi-Elie, A. Electroconductive Hydrogels: Synthesis, Characterization and Biomedical Applications. *Biomaterials* **2010**, *31* (10), 2701–2716. <https://doi.org/10.1016/j.biomaterials.2009.12.052>.
- (51) Hoare, T. R.; Kohane, D. S. Hydrogels in Drug Delivery: Progress and Challenges. *Polymer* **2008**, *49* (8), 1993–2007. <https://doi.org/10.1016/j.polymer.2008.01.027>.
- (52) Ahmed, A. S.; Mandal, U. K.; Taher, M.; Susanti, D.; Jaffri, J. M. PVA-PEG Physically Cross-Linked Hydrogel Film as a Wound Dressing: Experimental Design and Optimization. *Pharm Dev Technol* **2018**, *23* (8), 751–760. <https://doi.org/10.1080/10837450.2017.1295067>.
- (53) Xue, X.; Hu, Y.; Wang, S.; Chen, X.; Jiang, Y.; Su, J. Fabrication of Physical and Chemical Crosslinked Hydrogels for Bone Tissue Engineering. *Bioactive Materials* **2022**, *12*, 327–339. <https://doi.org/10.1016/j.bioactmat.2021.10.029>.
- (54) Li, C.; Wang, Z.; Wang, Y.; He, Q.; Long, R.; Cai, S. Effects of Network Structures on the Fracture of Hydrogel. *Extreme Mechanics Letters* **2021**, *49*, 101495. <https://doi.org/10.1016/j.eml.2021.101495>.
- (55) Mironi-Harpaz, I.; Wang, D. Y.; Venkatraman, S.; Seliktar, D. Photopolymerization of Cell-Encapsulating Hydrogels: Crosslinking Efficiency versus Cytotoxicity. *Acta Biomater* **2012**, *8* (5), 1838–1848. <https://doi.org/10.1016/j.actbio.2011.12.034>.
- (56) Bryant, S. J.; Nuttelman, C. R.; Anseth, K. S. Cytocompatibility of UV and Visible Light Photoinitiating Systems on Cultured NIH/3T3 Fibroblasts in Vitro. *J Biomater Sci Polym Ed* **2000**, *11* (5), 439–457. <https://doi.org/10.1163/156856200743805>.
- (57) Williams, C. G.; Malik, A. N.; Kim, T. K.; Manson, P. N.; Elisseff, J. H. Variable Cytocompatibility of Six Cell Lines with Photoinitiators Used for Polymerizing Hydrogels and Cell Encapsulation. *Biomaterials* **2005**, *26* (11), 1211–1218. <https://doi.org/10.1016/j.biomaterials.2004.04.024>.
- (58) Ooi, H. W.; Mota, C.; Ten Cate, A. T.; Calore, A.; Moroni, L.; Baker, M. B. Thiol-Ene Alginate Hydrogels as Versatile Bioinks for Bioprinting. *Biomacromolecules* **2018**, *19* (8), 3390–3400. <https://doi.org/10.1021/acs.biomac.8b00696>.
- (59) McCall, J. D.; Anseth, K. S. Thiol–Ene Photopolymerizations Provide a Facile Method To Encapsulate Proteins and Maintain Their Bioactivity. *Biomacromolecules* **2012**, *13* (8), 2410–2417. <https://doi.org/10.1021/bm300671s>.
- (60) Schieber, M.; Chandel, N. S. ROS Function in Redox Signaling and Oxidative Stress. *Curr Biol* **2014**, *24* (10), R453–462. <https://doi.org/10.1016/j.cub.2014.03.034>.

- (61) Gao, Y.; Peng, K.; Mitragotri, S. Covalently Crosslinked Hydrogels via Step-Growth Reactions: Crosslinking Chemistries, Polymers, and Clinical Impact. *Advanced Materials* **2021**, *33* (25), 2006362. <https://doi.org/10.1002/adma.202006362>.
- (62) Malkoch, M.; Vestberg, R.; Gupta, N.; Mespouille, L.; Dubois, P.; Mason, A. F.; Hedrick, J. L.; Liao, Q.; Frank, C. W.; Kingsbury, K.; Hawker, C. J. Synthesis of Well-Defined Hydrogel Networks Using Click Chemistry. *Chem Commun (Camb)* **2006**, No. 26, 2774–2776. <https://doi.org/10.1039/b603438a>.
- (63) Saxon, E.; Bertozzi, C. R. Cell Surface Engineering by a Modified Staudinger Reaction. *Science* **2000**, *287* (5460), 2007–2010. <https://doi.org/10.1126/science.287.5460.2007>.
- (64) Prescher, J. A.; Dube, D. H.; Bertozzi, C. R. Chemical Remodelling of Cell Surfaces in Living Animals. *Nature* **2004**, *430* (7002), 873–877. <https://doi.org/10.1038/nature02791>.
- (65) Sletten, E. M.; Bertozzi, C. R. From Mechanism to Mouse: A Tale of Two Bioorthogonal Reactions. *Acc Chem Res* **2011**, *44* (9), 666–676. <https://doi.org/10.1021/ar200148z>.
- (66) Gattás-Asfura, K. M.; Stabler, C. L. Chemoselective Cross-Linking and Functionalization of Alginate via Staudinger Ligation. *Biomacromolecules* **2009**, *10* (11), 3122–3129. <https://doi.org/10.1021/bm900789a>.
- (67) Sallouh, O.; Weberskirch, R. Facile Formation of Hydrogels by Using Functional Precursor Polymers and the Chemoselective Staudinger Coupling. *Polymer* **2016**, *86*, 189–196. <https://doi.org/10.1016/j.polymer.2016.01.066>.
- (68) Hall, K. K.; Gattás-Asfura, K. M.; Stabler, C. L. Microencapsulation of Islets within Alginate/Poly(Ethylene Glycol) Gels Cross-Linked via Staudinger Ligation. *Acta Biomater* **2011**, *7* (2), 614–624. <https://doi.org/10.1016/j.actbio.2010.07.016>.
- (69) Ossipov, D. A.; Hilborn, J. Poly(Vinyl Alcohol)-Based Hydrogels Formed by “Click Chemistry.” *Macromolecules* **2006**, *39* (5), 1709–1718. <https://doi.org/10.1021/ma052545p>.
- (70) Hong, V.; Steinmetz, N. F.; Manchester, M.; Finn, M. G. Labeling Live Cells by Copper-Catalyzed Alkyne-Azide Click Chemistry. *Bioconjug Chem* **2010**, *21* (10), 1912–1916. <https://doi.org/10.1021/bc100272z>.
- (71) Soriano Del Amo, D.; Wang, W.; Jiang, H.; Besanceney, C.; Yan, A. C.; Levy, M.; Liu, Y.; Marlow, F. L.; Wu, P. Biocompatible Copper(I) Catalysts for in Vivo Imaging of Glycans. *J Am Chem Soc* **2010**, *132* (47), 16893–16899. <https://doi.org/10.1021/ja106553e>.
- (72) DeForest, C. A.; Sims, E. A.; Anseth, K. S. Peptide-Functionalized Click Hydrogels with Independently Tunable Mechanics and Chemical Functionality for 3D Cell Culture. *Chem. Mater.* **2010**, *22* (16), 4783–4790. <https://doi.org/10.1021/cm101391y>.
- (73) DeForest, C. A.; Anseth, K. S. Cytocompatible Click-Based Hydrogels with Dynamically-Tunable Properties Through Orthogonal Photoconjugation and Photocleavage Reactions. *Nat Chem* **2011**, *3* (12), 925–931. <https://doi.org/10.1038/nchem.1174>.
- (74) DeForest, C. A.; Tirrell, D. A. A Photoreversible Protein-Patterning Approach for Guiding Stem Cell Fate in Three-Dimensional Gels. *Nat Mater* **2015**, *14* (5), 523–531. <https://doi.org/10.1038/nmat4219>.
- (75) Zhan, H.; Löwik, D. W. P. M. A Hybrid Peptide Amphiphile Fiber PEG Hydrogel Matrix for 3D Cell Culture. *Advanced Functional Materials* **2019**, *29* (16), 1808505. <https://doi.org/10.1002/adfm.201808505>.
- (76) Yu, F.; Cao, X.; Li, Y.; Zeng, L.; Zhu, J.; Wang, G.; Chen, X. Diels–Alder Crosslinked HA/PEG Hydrogels with High Elasticity and Fatigue Resistance for Cell Encapsulation and Articular Cartilage Tissue Repair. *Polym. Chem.* **2014**, *5* (17), 5116–5123. <https://doi.org/10.1039/C4PY00473F>.
- (77) Knall, A.-C.; Slugovc, C. Inverse Electron Demand Diels–Alder (iEDDA)-Initiated Conjugation: A (High) Potential Click Chemistry Scheme. *Chem. Soc. Rev.* **2013**, *42* (12), 5131–5142. <https://doi.org/10.1039/C3CS60049A>.

- (78) Alge, D. L.; Azagarsamy, M. A.; Donohue, D. F.; Anseth, K. S. Synthetically Tractable Click Hydrogels for Three-Dimensional Cell Culture Formed Using Tetrazine-Norbornene Chemistry. *Biomacromolecules* **2013**, *14* (4), 949–953. <https://doi.org/10.1021/bm4000508>.
- (79) Zhang, H.; Dicker, K. T.; Xu, X.; Jia, X.; Fox, J. M. Interfacial Bioorthogonal Cross-Linking. *ACS Macro Lett.* **2014**, *3* (8), 727–731. <https://doi.org/10.1021/mz5002993>.
- (80) Koehler, K. C.; Anseth, K. S.; Bowman, C. N. Diels–Alder Mediated Controlled Release from a Poly(Ethylene Glycol) Based Hydrogel. *Biomacromolecules* **2013**, *14* (2), 538–547. <https://doi.org/10.1021/bm301789d>.
- (81) Tan, H.; Chu, C. R.; Payne, K. A.; Marra, K. G. Injectable in Situ Forming Biodegradable Chitosan-Hyaluronic Acid Based Hydrogels for Cartilage Tissue Engineering. *Biomaterials* **2009**, *30* (13), 2499–2506. <https://doi.org/10.1016/j.biomaterials.2008.12.080>.
- (82) McKinnon, D. D.; Domaille, D. W.; Cha, J. N.; Anseth, K. S. Biophysically Defined and Cytocompatible Covalently Adaptable Networks as Viscoelastic 3D Cell Culture Systems. *Adv Mater* **2014**, *26* (6), 865–872. <https://doi.org/10.1002/adma.201303680>.
- (83) Purcell, B. P.; Lobb, D.; Charati, M. B.; Dorsey, S. M.; Wade, R. J.; Zellars, K. N.; Doviak, H.; Pettaway, S.; Logdon, C. B.; Shuman, J. A.; Freels, P. D.; Gorman, J. H.; Gorman, R. C.; Spinale, F. G.; Burdick, J. A. Injectable and Bioresponsive Hydrogels for On-Demand Matrix Metalloproteinase Inhibition. *Nat Mater* **2014**, *13* (6), 653–661. <https://doi.org/10.1038/nmat3922>.
- (84) Ulrich, S.; Boturnyn, D.; Marra, A.; Renaudet, O.; Dumy, P. Oxime Ligation: A Chemoselective Click-Type Reaction for Accessing Multifunctional Biomolecular Constructs. *Chemistry* **2014**, *20* (1), 34–41. <https://doi.org/10.1002/chem.201302426>.
- (85) Kalia, J.; Raines, R. T. Hydrolytic Stability of Hydrazones and Oximes. *Angew Chem Int Ed Engl* **2008**, *47* (39), 7523–7526. <https://doi.org/10.1002/anie.200802651>.
- (86) Lin, F.; Yu, J.; Tang, W.; Zheng, J.; Defante, A.; Guo, K.; Wesdemiotis, C.; Becker, M. L. Peptide-Functionalized Oxime Hydrogels with Tunable Mechanical Properties and Gelation Behavior. *Biomacromolecules* **2013**, *14* (10), 3749–3758. <https://doi.org/10.1021/bm401133r>.
- (87) Wang, S.; Nawale, G. N.; Oommen, O. P.; Hilborn, J.; Varghese, O. P. Influence of Ions to Modulate Hydrazone and Oxime Reaction Kinetics to Obtain Dynamically Cross-Linked Hyaluronic Acid Hydrogels. *Polym. Chem.* **2019**, *10* (31), 4322–4327. <https://doi.org/10.1039/C9PY00862D>.
- (88) Yung, C. W.; Wu, L. Q.; Tullman, J. A.; Payne, G. F.; Bentley, W. E.; Barbari, T. A. Transglutaminase Crosslinked Gelatin as a Tissue Engineering Scaffold. *J Biomed Mater Res A* **2007**, *83* (4), 1039–1046. <https://doi.org/10.1002/jbm.a.31431>.
- (89) Davis, N. E.; Ding, S.; Forster, R. E.; Pinkas, D. M.; Barron, A. E. Modular Enzymatically Crosslinked Protein Polymer Hydrogels for in Situ Gelation. *Biomaterials* **2010**, *31* (28), 7288–7297. <https://doi.org/10.1016/j.biomaterials.2010.06.003>.
- (90) Kim, K. S.; Park, S. J.; Yang, J.-A.; Jeon, J.-H.; Bhang, S. H.; Kim, B.-S.; Hahn, S. K. Injectable Hyaluronic Acid-Tyramine Hydrogels for the Treatment of Rheumatoid Arthritis. *Acta Biomater* **2011**, *7* (2), 666–674. <https://doi.org/10.1016/j.actbio.2010.09.030>.
- (91) Jin, R.; Moreira Teixeira, L. S.; Dijkstra, P. J.; Karperien, M.; van Blitterswijk, C. A.; Zhong, Z. Y.; Feijen, J. Injectable Chitosan-Based Hydrogels for Cartilage Tissue Engineering. *Biomaterials* **2009**, *30* (13), 2544–2551. <https://doi.org/10.1016/j.biomaterials.2009.01.020>.
- (92) Chen, T.; Embree, H. D.; Brown, E. M.; Taylor, M. M.; Payne, G. F. Enzyme-Catalyzed Gel Formation of Gelatin and Chitosan: Potential for in Situ Applications. *Biomaterials* **2003**, *24* (17), 2831–2841. [https://doi.org/10.1016/s0142-9612\(03\)00096-6](https://doi.org/10.1016/s0142-9612(03)00096-6).
- (93) Teixeira, L. S. M.; Feijen, J.; van Blitterswijk, C. A.; Dijkstra, P. J.; Karperien, M. Enzyme-Catalyzed Crosslinkable Hydrogels: Emerging Strategies for Tissue Engineering. *Biomaterials* **2012**, *33* (5), 1281–1290. <https://doi.org/10.1016/j.biomaterials.2011.10.067>.

- (94) Ehrbar, M.; Rizzi, S. C.; Schoenmakers, R. G.; Miguel, B. S.; Hubbell, J. A.; Weber, F. E.; Lutolf, M. P. Biomolecular Hydrogels Formed and Degraded via Site-Specific Enzymatic Reactions. *Biomacromolecules* **2007**, *8* (10), 3000–3007. <https://doi.org/10.1021/bm070228f>.
- (95) Lee, S. H.; Lee, Y.; Lee, S.-W.; Ji, H.-Y.; Lee, J.-H.; Lee, D. S.; Park, T. G. Enzyme-Mediated Cross-Linking of Pluronic Copolymer Micelles for Injectable and in Situ Forming Hydrogels. *Acta Biomater* **2011**, *7* (4), 1468–1476. <https://doi.org/10.1016/j.actbio.2010.11.029>.
- (96) Chen, T.; Embree, H. D.; Wu, L.-Q.; Payne, G. F. In Vitro Protein-Polysaccharide Conjugation: Tyrosinase-Catalyzed Conjugation of Gelatin and Chitosan. *Biopolymers* **2002**, *64* (6), 292–302. <https://doi.org/10.1002/bip.10196>.
- (97) Smith, N. J.; Rohlfing, K.; Sawicki, L. A.; Kharkar, P. M.; Boyd, S. J.; Kloxin, A.; Fox, J. M. Fast, Irreversible Modification of Cysteines through Strain Releasing Conjugate Additions of Cyclopropenyl Ketones. *Org Biomol Chem* **2018**, *16* (12), 2164–2169. <https://doi.org/10.1039/c8ob00166a>.
- (98) Nair, D. P.; Podgórski, M.; Chatani, S.; Gong, T.; Xi, W.; Fenoli, C. R.; Bowman, C. N. The Thiol-Michael Addition Click Reaction: A Powerful and Widely Used Tool in Materials Chemistry. *Chem. Mater.* **2014**, *26* (1), 724–744. <https://doi.org/10.1021/cm402180t>.
- (99) Forte, N.; Livanos, M.; Miranda, E.; Morais, M.; Yang, X.; Rajkumar, V. S.; Chester, K. A.; Chudasama, V.; Baker, J. R. Tuning the Hydrolytic Stability of Next Generation Maleimide Cross-Linkers Enables Access to Albumin-Antibody Fragment Conjugates and Tri-scFvs. *Bioconjugate Chem.* **2018**, *29* (2), 486–492. <https://doi.org/10.1021/acs.bioconjchem.7b00795>.
- (100) Wang, H.; Cheng, F.; Li, M.; Peng, W.; Qu, J. Reactivity and Kinetics of Vinyl Sulfone-Functionalized Self-Assembled Monolayers for Bioactive Ligand Immobilization. *Langmuir* **2015**, *31* (11), 3413–3421. <https://doi.org/10.1021/la504087a>.
- (101) Headen, D. M.; García, J. R.; García, A. J. Parallel Droplet Microfluidics for High Throughput Cell Encapsulation and Synthetic Microgel Generation. *Microsyst Nanoeng* **2018**, *4* (1), 1–9. <https://doi.org/10.1038/micronano.2017.76>.
- (102) Khan, A. H.; Cook, J. K.; Wortmann, W. J.; Kersker, N. D.; Rao, A.; Pojman, J. A.; Melvin, A. T. Synthesis and Characterization of Thiol-Acrylate Hydrogels Using a Base-Catalyzed Michael Addition for 3D Cell Culture Applications. *J Biomed Mater Res B Appl Biomater* **2020**, *108* (5), 2294–2307. <https://doi.org/10.1002/jbm.b.34565>.
- (103) Worch, J. C.; Stubbs, C. J.; Price, M. J.; Dove, A. P. Click Nucleophilic Conjugate Additions to Activated Alkynes: Exploring Thiol-Yne, Amino-Yne, and Hydroxyl-Yne Reactions from (Bio)Organic to Polymer Chemistry. *Chem Rev* **2021**, *121* (12), 6744–6776. <https://doi.org/10.1021/acs.chemrev.0c01076>.
- (104) Truong, V. X.; Tsang, K. M.; Forsythe, J. S. Nonswelling Click-Cross-Linked Gelatin and PEG Hydrogels with Tunable Properties Using Pluronic Linkers. *Biomacromolecules* **2017**, *18* (3), 757–766. <https://doi.org/10.1021/acs.biomac.6b01601>.
- (105) Bahou, C.; Spears, R. J.; Ramírez Rosales, A. M.; Rochet, L. N. C.; Barber, L. J.; Stankevich, K. S.; Miranda, J. F.; Butcher, T. C.; Kerrigan, A. M.; Lazarov, V. K.; Grey, W.; Chudasama, V.; Spicer, C. D. Hydrogel Cross-Linking via Thiol-Reactive Pyridazinediones. *Biomacromolecules* **2023**. <https://doi.org/10.1021/acs.biomac.3c00290>.
- (106) Zhang, D.; Devarie-Baez, N. O.; Li, Q.; Lancaster, J. R.; Xian, M. Methylsulfonyl Benzothiazole (MSBT): A Selective Protein Thiol Blocking Reagent. *Org Lett* **2012**, *14* (13), 3396–3399. <https://doi.org/10.1021/ol301370s>.
- (107) Toda, N.; Asano, S.; Barbas, C. F. Rapid, Stable, Chemoselective Labeling of Thiols with Julia-Kociński Like Reagents: A Serum-Stable Alternative to Maleimide-Based Protein Conjugation. *Angew Chem Int Ed Engl* **2013**, *52* (48), 10.1002/anie.201306241. <https://doi.org/10.1002/anie.201306241>.

- (108) Hermanson, G. T. Chapter 3 - The Reactions of Bioconjugation. In *Bioconjugate Techniques (Third Edition)*; Hermanson, G. T., Ed.; Academic Press: Boston, 2013; pp 229–258. <https://doi.org/10.1016/B978-0-12-382239-0.00003-0>.
- (109) Lee, J.; Silberstein, M. N.; Abdeen, A. A.; Kim, S. Y.; Kilian, K. A. Mechanochemical Functionalization of Disulfide Linked Hydrogels. *Mater. Horiz.* **2016**, *3* (5), 447–451. <https://doi.org/10.1039/C6MH00091F>.
- (110) Zheng, Z.; Chen, P.; Li, G.; Zhu, Y.; Shi, Z.; Luo, Y.; Zhao, C.; Fu, Z.; Cui, X.; Ji, C.; Wang, F.; Huang, G.; Liang, G. Mechanistic Study of CBT-Cys Click Reaction and Its Application for Identifying Bioactive N-Terminal Cysteine Peptides in Amniotic Fluid †Electronic Supplementary Information (ESI) Available: General Methods; Synthesis and Characterization; HPLC Conditions; Schemes S1 and S2; Fig. S1–S29; Tables S1 and S2. See DOI: 10.1039/C6sc01461e Click Here for Additional Data File. *Chem Sci* **2017**, *8* (1), 214–222. <https://doi.org/10.1039/c6sc01461e>.
- (111) Menegatti, S.; Ruocco, N.; Kumar, S.; Zakrewsky, M.; Sanchez De Oliveira, J.; Helgeson, Matthew. E.; Leal, G. L.; Mitragotri, S. Synthesis and Characterization of a Self-Fluorescent Hyaluronic Acid–Based Gel for Dermal Applications. *Advanced Healthcare Materials* **2015**, *4* (15), 2297–2305. <https://doi.org/10.1002/adhm.201500619>.
- (112) Fairbanks, B. D.; Macdougall, L. J.; Mavila, S.; Sinha, J.; Kirkpatrick, B. E.; Anseth, K. S.; Bowman, C. N. Photoclick Chemistry: A Bright Idea. *Chem. Rev.* **2021**, *121* (12), 6915–6990. <https://doi.org/10.1021/acs.chemrev.0c01212>.
- (113) Roberts, J. J.; Bryant, S. J. Comparison of Photopolymerizable Thiol-Ene PEG and Acrylate-Based PEG Hydrogels for Cartilage Development. *Biomaterials* **2013**, *34* (38), 9969–9979. <https://doi.org/10.1016/j.biomaterials.2013.09.020>.
- (114) Lin, C.-C.; Raza, A.; Shih, H. PEG Hydrogels Formed by Thiol-Ene Photo-Click Chemistry and Their Effect on the Formation and Recovery of Insulin-Secreting Cell Spheroids. *Biomaterials* **2011**, *32* (36), 9685–9695. <https://doi.org/10.1016/j.biomaterials.2011.08.083>.
- (115) Northrop, B. H.; Coffey, R. N. *Thiol–Ene Click Chemistry: Computational and Kinetic Analysis of the Influence of Alkene Functionality*. ACS Publications. <https://doi.org/10.1021/ja305441d>.
- (116) Yang, Z.; Attygalle, A. B. LC/MS Characterization of Undesired Products Formed during Iodoacetamide Derivatization of Sulfhydryl Groups of Peptides. *Journal of Mass Spectrometry* **2007**, *42* (2), 233–243. <https://doi.org/10.1002/jms.1157>.
- (117) Chen, X.; Wu, H.; Park, C.-M.; Poole, T. H.; Keceli, G.; Devarie-Baez, N. O.; Tsang, A. W.; Lowther, W. T.; Poole, L. B.; King, S. B.; Xian, M.; Furdul, C. M. Discovery of Heteroaromatic Sulfones As a New Class of Biologically Compatible Thiol-Selective Reagents. *ACS Chem Biol* **2017**, *12* (8), 2201–2208. <https://doi.org/10.1021/acscchembio.7b00444>.
- (118) Motiwala, H. F.; Kuo, Y.-H.; Stinger, B. L.; Palfey, B. A.; Martin, B. R. Tunable Heteroaromatic Sulfones Enhance In-Cell Cysteine Profiling. *J. Am. Chem. Soc.* **2020**, *142* (4), 1801–1810. <https://doi.org/10.1021/jacs.9b08831>.
- (119) Pichon, M. M.; Drelinkiewicz, D.; Lozano, D.; Moraru, R.; Hayward, L. J.; Jones, M.; McCoy, M. A.; Allstrum-Graves, S.; Balourdas, D.-I.; Joerger, A. C.; Whitby, R. J.; Goldup, S. M.; Wells, N.; Langley, G. J.; Herniman, J. M.; Baud, M. G. J. Structure–Reactivity Studies of 2-Sulfonylpyrimidines Allow Selective Protein Arylation. *Bioconjugate Chem.* **2023**, *34* (9), 1679–1687. <https://doi.org/10.1021/acs.bioconjchem.3c00322>.
- (120) Lipka, B. M.; Honeycutt, D. S.; Bassett, G. M.; Kowal, T. N.; Adamczyk, M.; Cartnick, Z. C.; Betti, V. M.; Goldberg, J. M.; Wang, F. Ultra-Rapid Electrophilic Cysteine Arylation. *J. Am. Chem. Soc.* **2023**, *145* (43), 23427–23432. <https://doi.org/10.1021/jacs.3c10334>.
- (121) Saito, F.; Noda, H.; Bode, J. W. Critical Evaluation and Rate Constants of Chemoselective Ligation Reactions for Stoichiometric Conjugations in Water. *ACS Chem Biol* **2015**, *10* (4), 1026–1033. <https://doi.org/10.1021/cb5006728>.

- (122) Guo, Y.; Gu, J.; Jiang, Y.; Zhou, Y.; Zhu, Z.; Ma, T.; Cheng, Y.; Ji, Z.; Jiao, Y.; Xue, B.; Cao, Y. Regulating the Homogeneity of Thiol-Maleimide Michael-Type Addition-Based Hydrogels Using Amino Biomolecules. *Gels* **2021**, *7* (4), 206. <https://doi.org/10.3390/gels7040206>.
- (123) Darling, N. J.; Hung, Y.-S.; Sharma, S.; Segura, T. Controlling the Kinetics of Thiol-Maleimide Michael-Type Addition Gelation Kinetics for the Generation of Homogenous Poly(Ethylene Glycol) Hydrogels. *Biomaterials* **2016**, *101*, 199–206. <https://doi.org/10.1016/j.biomaterials.2016.05.053>.
- (124) Stewart, S. A.; Coulson, M. B.; Zhou, C.; Burke, N. a. D.; Stöver, H. D. H. Synthetic Hydrogels Formed by Thiol-Ene Crosslinking of Vinyl Sulfone-Functional Poly(Methyl Vinyl Ether-Alt-Maleic Acid) with α,ω -Dithio-Polyethyleneglycol. *Soft Matter* **2018**, *14* (41), 8317–8324. <https://doi.org/10.1039/C8SM01066H>.
- (125) Lutolf, M. P.; Hubbell, J. A. Synthesis and Physicochemical Characterization of End-Linked Poly(Ethylene Glycol)-Co-Peptide Hydrogels Formed by Michael-Type Addition. *Biomacromolecules* **2003**, *4* (3), 713–722. <https://doi.org/10.1021/bm025744e>.
- (126) Kurakazu, M.; Katashima, T.; Chijiishi, M.; Nishi, K.; Akagi, Y.; Matsunaga, T.; Shibayama, M.; Chung, U.; Sakai, T. Evaluation of Gelation Kinetics of Tetra-PEG Gel. *Macromolecules* **2010**, *43* (8), 3935–3940. <https://doi.org/10.1021/ma100176f>.
- (127) Liu, W.; Gong, X.; Zhu, Y.; Wang, J.; Ngai, T.; Wu, C. Probing Sol-Gel Matrices and Dynamics of Star PEG Hydrogels Near Overlap Concentration. *Macromolecules* **2019**, *52* (22), 8956–8966. <https://doi.org/10.1021/acs.macromol.9b01489>.
- (128) Wang, J.; Zhang, F.; Tsang, W. P.; Wan, C.; Wu, C. Fabrication of Injectable High Strength Hydrogel Based on 4-Arm Star PEG for Cartilage Tissue Engineering. *Biomaterials* **2017**, *120*, 11–21. <https://doi.org/10.1016/j.biomaterials.2016.12.015>.
- (129) Zhang, H.; Wehrman, M. D.; Schultz, K. M. Structural Changes in Polymeric Gel Scaffolds Around the Overlap Concentration. *Front Chem* **2019**, *7*, 317. <https://doi.org/10.3389/fchem.2019.00317>.
- (130) Lutolf, M. P.; Lauer-Fields, J. L.; Schmoekel, H. G.; Metters, A. T.; Weber, F. E.; Fields, G. B.; Hubbell, J. A. Synthetic Matrix Metalloproteinase-Sensitive Hydrogels for the Conduction of Tissue Regeneration: Engineering Cell-Invasion Characteristics. *Proc Natl Acad Sci U S A* **2003**, *100* (9), 5413–5418. <https://doi.org/10.1073/pnas.0737381100>.
- (131) Matsunaga, T.; Sakai, T.; Akagi, Y.; Chung, U.; Shibayama, M. Structure Characterization of Tetra-PEG Gel by Small-Angle Neutron Scattering. *Macromolecules* **2009**, *42* (4), 1344–1351. <https://doi.org/10.1021/ma802280n>.
- (132) Sakai, T. Experimental Verification of Homogeneity in Polymer Gels. *Polym J* **2014**, *46* (9), 517–523. <https://doi.org/10.1038/pj.2014.28>.
- (133) Okihara, M.; Okuma, K.; Kawamura, A.; Miyata, T. Photoresponsive Gelation of Four-Armed Poly(Ethylene Glycol) with Photodimerizable Groups. *Gels* **2022**, *8* (3). <https://doi.org/10.3390/gels8030183>.
- (134) Li, X.; Nakagawa, S.; Tsuji, Y.; Watanabe, N.; Shibayama, M. Polymer Gel with a Flexible and Highly Ordered Three-Dimensional Network Synthesized via Bond Percolation. *Sci Adv* **2019**, *5* (12), eaax8647. <https://doi.org/10.1126/sciadv.aax8647>.
- (135) Oyen, M. L. Mechanical Characterisation of Hydrogel Materials. *International Materials Reviews* **2014**. <https://doi.org/10.1179/1743280413Y.0000000022>.
- (136) Wu, Y.; Liu, T.; Shi, Y.; Wang, H. Dramatically Enhancing Mechanical Properties of Hydrogels by Drying Reactive Polymers at Elevated Temperatures to Introduce Strong Physical and Chemical Crosslinks. *Polymer* **2022**, *249*, 124842. <https://doi.org/10.1016/j.polymer.2022.124842>.
- (137) Yan, C.; J. Pochan, D. Rheological Properties of Peptide -Based Hydrogels for Biomedical and Other Applications. *Chemical Society Reviews* **2010**, *39* (9), 3528–3540. <https://doi.org/10.1039/B919449P>.

- (138) Otero-Espinar, F. J.; Fernández-Ferreiro, A.; González-Barcia, M.; Blanco-Méndez, J.; Luardo, A. Stimuli Sensitive Ocular Drug Delivery Systems. In *Drug Targeting and Stimuli Sensitive Drug Delivery Systems*; Elsevier, 2018; pp 211–270. <https://doi.org/10.1016/B978-0-12-813689-8.00006-9>.
- (139) Fernanda, P. Chapter 11 - Methods Used in the Study of the Physical Properties of Fats. In *Structure-Function Analysis of Edible Fats (Second Edition)*; Marangoni, A. G., Ed.; AOCS Press, 2018; pp 313–385. <https://doi.org/10.1016/B978-0-12-814041-3.00011-3>.
- (140) Solar, C.; Palacio, D.; Sánchez, S.; Urbano, B. F.; Solar, C.; Palacio, D.; Sánchez, S.; Urbano, B. F. OSCILLATORY STRAIN SWEEPS OF HYDROGELS FROM METHACRYLATED ALGINATE MACROMONOMERS: ASSESSMENT OF SYNTHESIS AND ACQUISITION VARIABLES. *Journal of the Chilean Chemical Society* **2019**, *64* (3), 4542–4546. <https://doi.org/10.4067/S0717-97072019000304542>.
- (141) Marin, G. Rheological Measurements: Oscillatory, Rotational, and Pressure Flows. In *Rheological Fundamentals of Polymer Processing*; Covas, J. A., Agassant, J. F., Diogo, A. C., Vlachopoulos, J., Walters, K., Eds.; NATO ASI Series; Springer Netherlands: Dordrecht, 1995; pp 139–160. https://doi.org/10.1007/978-94-015-8571-2_6.
- (142) Mezger, T. G. *The Rheology Handbook: For Users of Rotational and Oscillatory Rheometers*; Vincentz Network GmbH & Co KG, 2006.
- (143) Kulkarni, V. S.; Shaw, C. Chapter 9 - Rheological Studies. In *Essential Chemistry for Formulators of Semisolid and Liquid Dosages*; Kulkarni, V. S., Shaw, C., Eds.; Academic Press: Boston, 2016; pp 145–182. <https://doi.org/10.1016/B978-0-12-801024-2.00009-1>.
- (144) Yuan, Q.; Lu, X.; Khayat, K. H.; Feys, D.; Shi, C. Small Amplitude Oscillatory Shear Technique to Evaluate Structural Build-up of Cement Paste. *Mater Struct* **2016**, *50* (2), 112. <https://doi.org/10.1617/s11527-016-0978-2>.
- (145) Sharma, S.; Kumar, A.; Deepak; Kumar, R.; Rana, N. K.; Koch, B. Development of a Novel Chitosan Based Biocompatible and Self-Healing Hydrogel for Controlled Release of Hydrophilic Drug. *International Journal of Biological Macromolecules* **2018**, *116*, 37–44. <https://doi.org/10.1016/j.ijbiomac.2018.05.020>.
- (146) Deng, S.; Li, X.; Yang, W.; He, K.; Ye, X. Injectable in Situ Cross-Linking Hyaluronic Acid/Carboxymethyl Cellulose Based Hydrogels for Drug Release. *J Biomater Sci Polym Ed* **2018**, *29* (13), 1643–1655. <https://doi.org/10.1080/09205063.2018.1481005>.
- (147) Balakrishnan, B.; Soman, D.; Payanam, U.; Laurent, A.; Labarre, D.; Jayakrishnan, A. A Novel Injectable Tissue Adhesive Based on Oxidized Dextran and Chitosan. *Acta Biomater* **2017**, *53*, 343–354. <https://doi.org/10.1016/j.actbio.2017.01.065>.
- (148) Stojkov, G.; Niyazov, Z.; Picchioni, F.; Bose, R. K. Relationship between Structure and Rheology of Hydrogels for Various Applications. *Gels* **2021**, *7* (4), 255. <https://doi.org/10.3390/gels7040255>.
- (149) Worthington, P.; Drake, K. M.; Li, Z.; Napper, A. D.; Pochan, D. J.; Langhans, S. A. Implementation of a High-Throughput Pilot Screen in Peptide Hydrogel-Based Three-Dimensional Cell Cultures. *SLAS Discov* **2019**, *24* (7), 714–723. <https://doi.org/10.1177/2472555219844570>.
- (150) Doulgkeroglou, M.-N.; Di Nubila, A.; Niessing, B.; König, N.; Schmitt, R. H.; Damen, J.; Szilvassy, S. J.; Chang, W.; Csontos, L.; Louis, S.; Kugelmeier, P.; Ronfard, V.; Bayon, Y.; Zeugolis, D. I. Automation, Monitoring, and Standardization of Cell Product Manufacturing. *Frontiers in Bioengineering and Biotechnology* **2020**, *8*.
- (151) Boussaad, I.; Cruciani, G.; Bolognin, S.; Antony, P.; Dording, C. M.; Kwon, Y.-J.; Heutink, P.; Fava, E.; Schwamborn, J. C.; Krüger, R. Integrated, Automated Maintenance, Expansion and Differentiation of 2D and 3D Patient-Derived Cellular Models for High Throughput Drug Screening. *Sci Rep* **2021**, *11* (1), 1439. <https://doi.org/10.1038/s41598-021-81129-3>.

- (152) Rimann, M.; Angres, B.; Patocchi-Tenzer, I.; Braum, S.; Graf-Hausner, U. Automation of 3D Cell Culture Using Chemically Defined Hydrogels. *J Lab Autom.* **2014**, *19* (2), 191–197. <https://doi.org/10.1177/2211068213508651>.
- (153) Mabry, K. M.; Schroeder, M. E.; Payne, S. Z.; Anseth, K. S. Three-Dimensional High-Throughput Cell Encapsulation Platform to Study Changes in Cell-Matrix Interactions. *ACS Appl. Mater. Interfaces* **2016**, *8* (34), 21914–21922. <https://doi.org/10.1021/acsami.5b11359>.
- (154) Kirsten, G.; Maier, W. F. Strategies for the Discovery of New Catalysts with Combinatorial Chemistry. *Applied Surface Science* **2004**, *223* (1), 87–101. [https://doi.org/10.1016/S0169-4332\(03\)00911-5](https://doi.org/10.1016/S0169-4332(03)00911-5).
- (155) Ilzarbe, L.; Álvarez, M. J.; Viles, E.; Tanco, M. Practical Applications of Design of Experiments in the Field of Engineering: A Bibliographical Review. *Quality and Reliability Engineering International* **2008**, *24* (4), 417–428. <https://doi.org/10.1002/qre.909>.
- (156) Kumar, V.; Bhalla, A.; Rathore, A. S. Design of Experiments Applications in Bioprocessing: Concepts and Approach. *Biotechnol Prog* **2014**, *30* (1), 86–99. <https://doi.org/10.1002/btpr.1821>.
- (157) Shekhawat, L. K.; Godara, A.; Kumar, V.; Rathore, A. S. Design of Experiments Applications in Bioprocessing: Chromatography Process Development Using Split Design of Experiments. *Biotechnol Prog* **2019**, *35* (1), e2730. <https://doi.org/10.1002/btpr.2730>.
- (158) N. Politis, S.; Colombo, P.; Colombo, G.; M. Rekkas, D. Design of Experiments (DoE) in Pharmaceutical Development. *Drug Development and Industrial Pharmacy* **2017**, *43* (6), 889–901. <https://doi.org/10.1080/03639045.2017.1291672>.
- (159) Montgomery, D. C. *Design and Analysis of Experiments*; John Wiley & Sons, 2017.
- (160) Chen, X. C.; Zhou, L.; Gupta, S.; Civoli, F. Implementation of Design of Experiments (DOE) in the Development and Validation of a Cell-Based Bioassay for the Detection of Anti-Drug Neutralizing Antibodies in Human Serum. *J Immunol Methods* **2012**, *376* (1–2), 32–45. <https://doi.org/10.1016/j.jim.2011.11.004>.
- (161) Jankovic, A.; Chaudhary, G.; Goia, F. Designing the Design of Experiments (DOE) – An Investigation on the Influence of Different Factorial Designs on the Characterization of Complex Systems. *Energy and Buildings* **2021**, *250*, 111298. <https://doi.org/10.1016/j.enbuild.2021.111298>.
- (162) Niedz, R.; Evens, T. Design of Experiments (DOE)—History, Concepts, and Relevance to in Vitro Culture. *In Vitro Cellular & Developmental Biology - Plant* **2016**, *52*, 547–562. <https://doi.org/10.1007/s11627-016-9786-1>.

3 Synthesis of the hydrogel precursor 4armPEG-Tetrazole Methylsulfone

The adoption of high-throughput screening (HTS) formats and big data approaches in biological experimentation requires cell culture precursors to be accessible at sufficient scale. In this context, the upscaling of the synthesis of 4arm PEG-tetrazole methylsulfone (PEG-4TzMS) hydrogel precursor was the first targeted objective of this PhD Thesis. This upscaling was necessary for the establishment of medium/high-throughput automated 3D culture protocols in Chapter 5. The existing synthesis protocol was developed by Dr. Julieta Paez and Aditi Rathore based on a reported synthesis protocol by N. Toda et al. in 2013.⁸

3.1 Introduction: optimization of reaction conditions and upscaling in organic synthesis

The optimization of the reaction time and yield of a synthesis pathway is a standard step in chemical processes to minimize cost and waste. Experimental parameters that may impact the time and yield of a reaction include temperature, concentration, stoichiometry, catalyst, solvent, pH, labware, and stirring conditions. In an optimization process, the influence of these parameters is analyzed to identify the most favorable reaction conditions.¹ In academic research, the optimization of synthetic processes is often pursued through the one-factor-at-a-time (OFAT) approach, which involves the iterative modification of individual parameters while keeping the others fixed until the “best” value is identified. The fine chemical and pharmaceutical industry often use statistical methods, like design of experiments (DOE), in which several parameters and their interrelations are evaluated at once.² Optimization efforts also extend to the work-up and purification processes. Alternative synthesis pathways might also be considered in this process to reduce synthesis steps or to avoid expensive reactants.

Reaction upscaling comprises adapting an optimized synthesis pathway to accommodate larger quantities of compounds. Upscaling requires consideration of:

- i. Availability and costs of precursor, reagents and solvents.
- ii. Toxicity of the reactants/reagents and (by)products.

- iii. Reaction kinetics and proper mixing to maintain efficiency of the reaction and avoid extended reaction times.
- iv. Effective and efficient heat management to avoid unsafe overheating and byproduct formation.³
- v. Laboratory equipment to accommodate the reaction.
- vi. Waste generation to minimize environmental impact.⁴

The upscaling of the purification step also needs special attention. Whereas manual or high-performance liquid chromatography (HPLC) can be a reasonable choice for sub gram scale, at larger scales these methods often become unfeasible in terms of time and costs.⁵ At larger scales, purification by washing, extraction, precipitation or recrystallization are preferred. However, these methods can be challenging in purification processes from complex mixtures, since they rely on finding solvent combinations where impurities and the desired compound have contrasting solubilities. When chromatography is unavoidable, automated flash chromatography systems can upscale purification. These allow continuous loading of the crude, higher flowrates, automated eluant profiles and product detection. Material and eluent consumption is also lower since carrier materials with smaller particle size (i.e. higher surface area⁶) and reusable cartridges can be used.⁷

3.2 Objectives

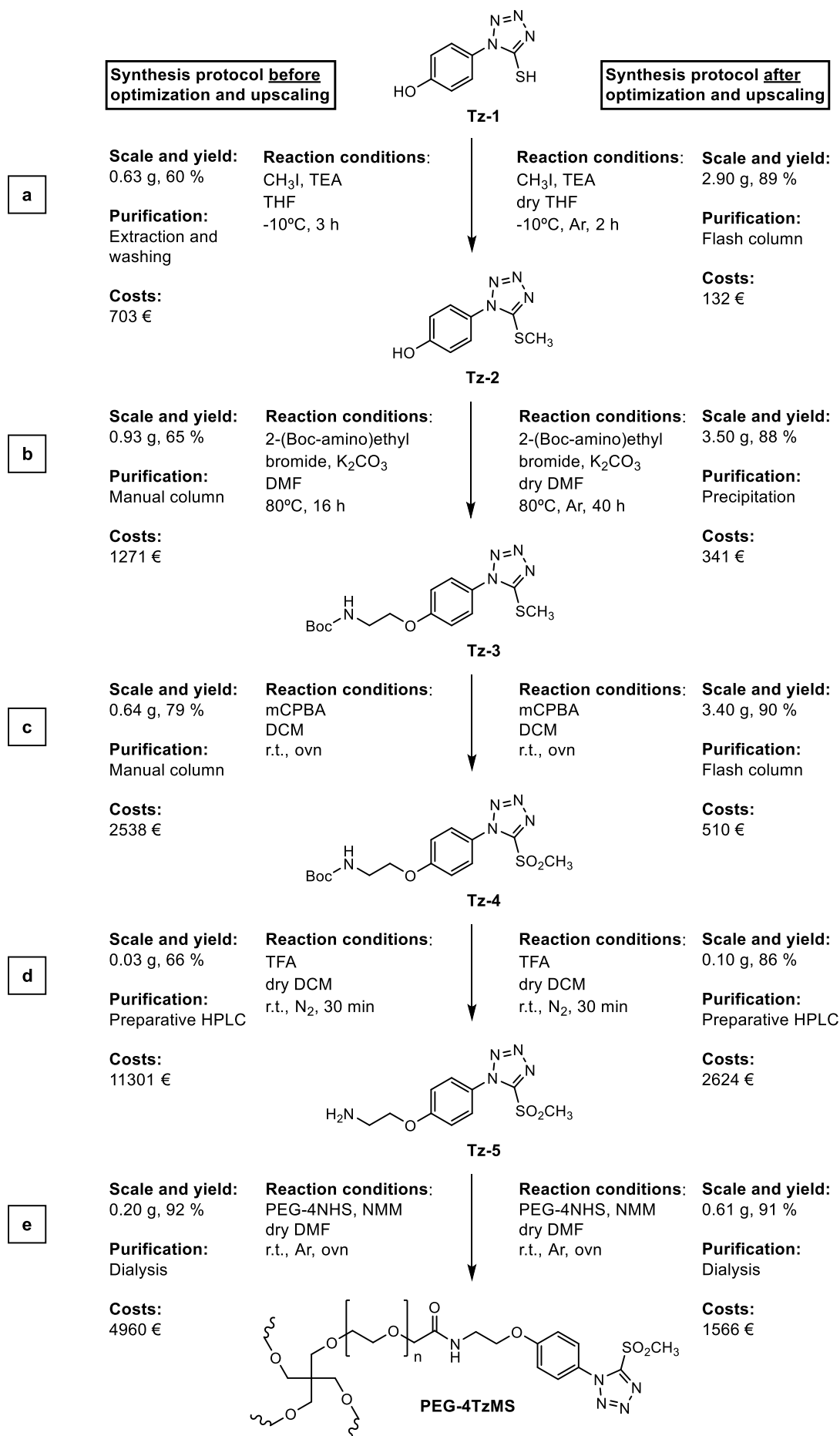
The existing protocol for the synthesis of PEG-4TzMS started from the commercially available 1-(4-Hydroxyphenyl)-5-mercapto-1H-tetrazole (Tz-1) and involved 5 steps (**Scheme 1**): methylation of the thiol, etherification of the phenol to introduce a Boc-protected amine, oxidation of the sulfide to sulfone, deprotection of the primary amine, and coupling of the free amine to the NHS-activated ester of the commercially available 4arm polyethylene glycol succinimidyl carboxymethyl ester (PEG-4NHS) (**Scheme 1**). In the available protocol, step **a** was performed at 630-mg scale and 60 % yield, step **b** at 930-mg scale and 65 % yield and step **c** at 640-mg scale and 79 % yield. For step **d**, 20-mg scale was used due to purification difficulties of Tz-5 (yield 66 %). The final step **e** was performed at 200-mg scale with 92 % yield. The overall yield of the synthesis of Tz-5 was 25 %.

The present work targeted the improvement of the overall yield (Tz-5 synthesis) > 25 % and the upscaling of PEG-4TzMS (**e**) to \geq 1-g scale. The strategy involved:

- i. Optimization of reaction conditions to increase individual yields.
- ii. Increasing the scale of the reaction.
- iii. Simplification of the purification.

With the optimization and scale-up, a reduction in the cost of PEG-4TzMS synthesis was expected. Therefore, the cost of the synthesis (raw materials, manpower and lab use) was monitored and is also described in the following sections.

Synthesis of the hydrogel precursor 4armPEG-Tetrazole Methylsulfone



Scheme 1. 5-step synthetic pathway of PEG-4TzMS: **a)** methylation, **b)** coupling of Boc-amine by etherification, **c)** oxidation, **d)** Boc-amine deprotection, and **e)** coupling of the free amine to the starPEG end groups. The described yields and scale refer to the existing protocols at the beginning of this Thesis and to the optimized protocol. The yield and scales of the individual steps are also presented.

3.3 Results

3.3.1 Optimization and upscaling of individual reaction steps

3.3.1.1 Methylation of the thiol group of Tz-1

The first step of the synthesis pathway involves the methylation of the thiol group from Tz-1 via an S_N2 reaction (reaction **a** from **Scheme 1**). This type of substitution reactions is influenced by the nature of the nucleophile that shares its electrons (size, number of electrons and polarizability), the leaving group (size, electronegativity and resonance) and the solvent that stabilize all species in solution (solvation of the nucleophile through intermolecular interactions).

The thiol from Tz-1 ($pK_a = 6.1$) is more acidic than the phenol moiety ($pK_a = 10.2$) (pK_a was calculated based on the partial charge distribution from the molecule with the pK_a plugin from MarvinSketch⁹), making it more susceptible to deprotonation and subsequent activation to thiolate in basic conditions.¹⁰ Moreover, thiolates present a stronger nucleophilic character than alkoxides due to their higher polarizability. As a result, the thiolate is expected to act as better nucleophile in this reaction. The weak base triethylamine (TEA) is used to deprotonate the thiol and not the phenol, resulting in a higher reaction rate of the thiolate-mediated substitution.⁸ Intermolecular interactions between the solvent and the nucleophile, such as strong ion-dipole interactions between protic solvents and negatively charged nucleophiles, result in lower nucleophilicity due to the less accessible nucleophile being surrounded by solvent molecules. Thus, using polar aprotic solvents like tetrahydrofuran (THF) as in our case, can dissolve the nucleophile and minimize the intermolecular interactions, favoring the S_N2 reaction.¹¹

In the available protocol, the reaction was performed at 0.63-g scale over 3 h. Tz-2 was isolated in 60 % yield after extraction with ethyl acetate (EtOAc) and washing with brine (water plus NaCl). The overall cost of step **a** under the described conditions was ca. 703 € per g of Tz-2 (**Figure 1**) (calculation method described in experimental section 3.5.2).

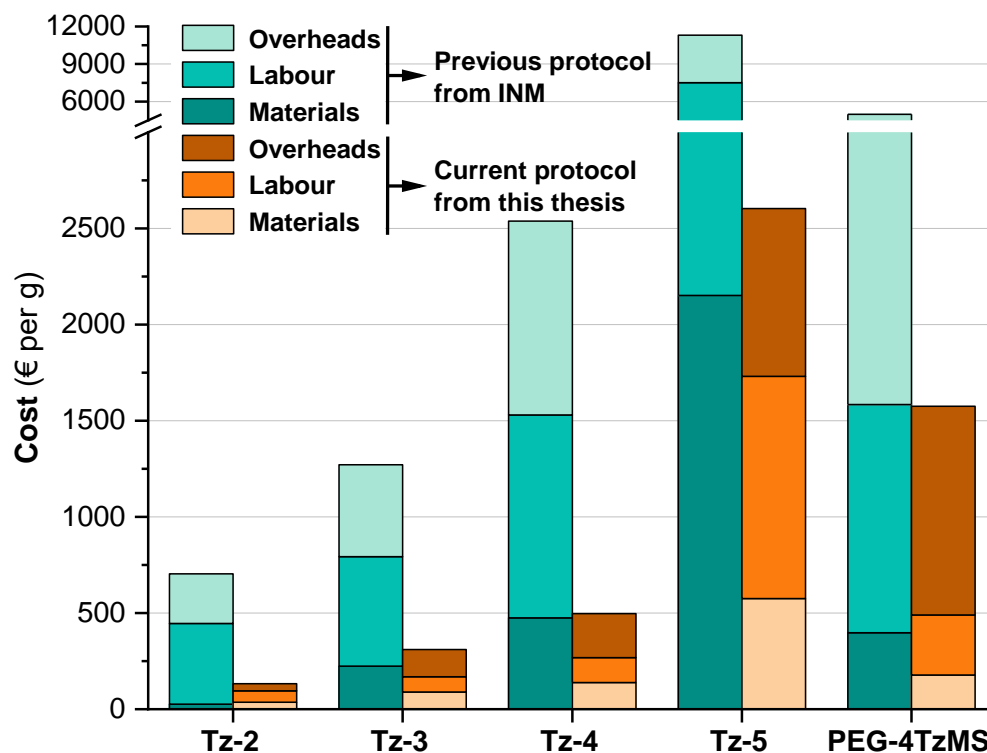


Figure 1. Stacked plot showing the synthesis cost of intermediates Tz-2 – Tz-5 and PEG-TzMS before (blue color scale) and after (orange color scale) optimization and scale-up. Each stack from a column corresponds to the different factors that influence the cost: materials, labour (active man-hours) and overheads (full-time use of lab). The costs of subsequent steps are cumulative, i.e. they contain the costs of the necessary previous steps.

The reaction was initially tested at 0.2 and 0.5 g scales. Since the yield of 60 % was partially attributed to the hydrolysis of the methyl iodide, dry THF and inert conditions were used (as described by Motiwala *et al.*¹²). To avoid potential loss of compound during the washing steps after extraction with EtOAc, the crude was purified by manual

chromatography. A yield of 68 % was obtained. By using flash chromatography for purification, an 89 % yield was obtained at 2.9-g scale.

Manual chromatography column was performed with a solvent mixture of 1:1 EtOAc/n-hexane (Hx), necessitating ca. 3.5 hours for complete elution of Tz-1. When purified by automated flash chromatography, a gradient from 0 to 50 % EtOAc was used. The desired compound Tz-1 was eluted ($t_R = 2 \text{ min } 44 \text{ s}$) with a 1:1 EtOAc/Hx mixture as eluent, while the only impurity (remaining starting material) observed by normal thin layer chromatography (TLC) was successfully separated ($t_R = 2 \text{ min}$). The use of automated flash chromatography allowed a shortening in the purification time to ca. 1.5 hour and a saving of 50 % in solvent consumption.

To compare with the original purification method, the reaction crude was also worked-up by the alternative method, using extraction with ethyl acetate and subsequent washing with brine and water, drying over magnesium sulfate (MgSO_4) and filtering by gravity. While similar time was needed for the alternative work-up (ca. 1 h) in comparison with the purification by flash chromatography, the solvent usage was significantly decreased (80 % less EtOAc). In addition, the purification method was greener because water and brine were used instead of n-Hexane and the usage of EtOAc was minimized. According to the proton nuclear magnetic resonance ($^1\text{H NMR}$) spectrum, both methods lead to similar purity ($\approx 100 \%$). The small peak at 2.9 ppm corresponds to water traces (**Figure 2**).⁸ A yield of 82 % (2.6-g scale) was reached after purification by extraction and washing vs. 89 % (2.9-g scale) yield obtained when purifying by flash chromatography. The costs of the reaction were ca. 132 € per g of Tz-2 when using flash column (**Figure 1**), and ca. 114 € per g when using purification by extraction and washing. The difference in costs between the two purification methods is due to the lower purification time (30 min) and solvent usage in the purification by washing and extraction. This method was considered the most appropriate one.

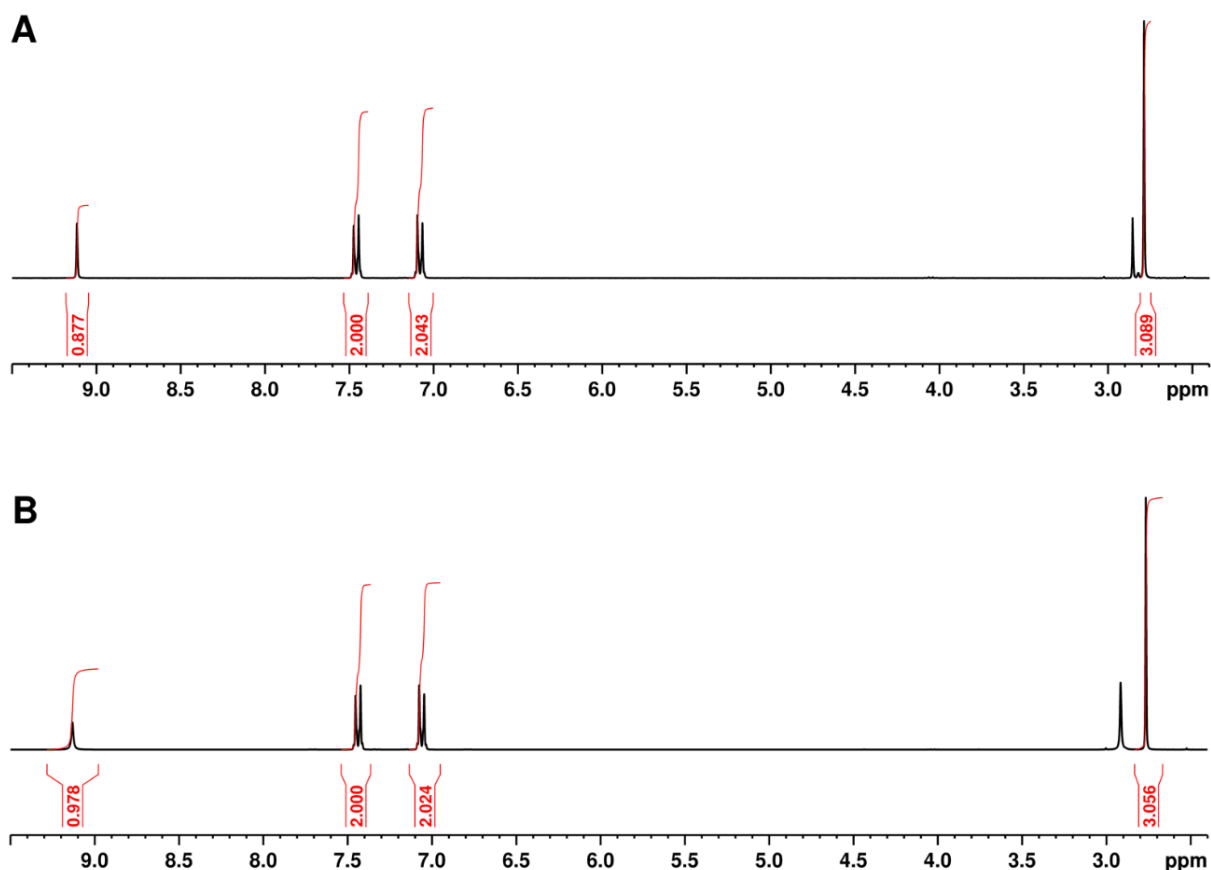


Figure 2. ^1H NMR spectra (300 MHz, acetone- d_6) of **A**) Tz-2 after alternative work-up, and **B**) Tz-2 after purification by flash chromatography.

3.3.1.2 Etherification of Tz-2 to introduce a Boc-protected amine and obtain Tz-3

The second step in the synthetic pathway is a Williamson etherification in which the phenol from Tz-2 undergoes a $\text{S}_{\text{N}}2$ reaction with an alkyl bromide containing a Boc-protected amine (reaction **b** in **Scheme 1**). After deprotonation by the potassium carbonate (K_2CO_3) base, the resulting phenolate acts as nucleophile. DMF is used as polar aprotic solvent to favor the $\text{S}_{\text{N}}2$ reaction.

In the available protocol, 1.2 and 1.5 eq. of the bromide were compared, as well as temperatures going from 60 to 80°C. The higher number of equivalents and temperature in DMF over ca. 16 h were found to increase the yield from 60 to 65 % (**b-0**). The cumulative cost of Tz-3 (taking into consideration the synthesis costs of Tz-2) under these conditions was ca. 1271 € per g of Tz-3 (**Figure 1**).

Different reaction conditions and scales were tested (**Table 1**) during the optimization process. In order to minimize the amount of bromide derivative 1.2 eq. were used under

the same reaction conditions as previous work in the group, resulting in a low conversion rate (20 mol%) and low yield (13 %) (reaction **b-1**). Increasing the bromide equivalents to 1.5 eq. (reaction **b-2**) was not sufficient to obtain full conversion overnight (< 50 mol%), so the reaction time was extended for another 24 h. After 40 h the conversion was still incomplete (70 mol%). To speed up the reaction, 0.3 more equivalents of the bromide derivative were added, and the reaction was left for another 24 h. After 64 h the conversion increased to 87 mol%. 24 extra hours (88 h total) resulted in a final conversion of 95 mol%. Because the slow conversion rate was partially attributed to hydrolysis of the bromide derivative, inert conditions were used in reaction **b-3**. A higher excess of the bromide derivative was added after 16 h of reaction. Following a reaction time of 40 h, > 95 mol% conversion was achieved after purification by flash chromatography. To improve the yield, purification by precipitation and washing was tested (**b-4**). The yield was increased from 67 to 88 %. The ¹H NMR of Tz-3 is shown in **Figure 3**.

Table 1. Reaction conditions and purification methods of reaction **b** at different scales.

Reaction	Scale	Bromide (eq.)	Solvent	Reaction time	Inert atm.	Conversion (mol%)	Purification method	Yield
b-0	0.93-g	1.5	DMF	16 h	No	> 95	Manual column	65 %
b-1	0.4-g	1.2	DMF	16 h	No	20	Manual column	13 %
b-2	1.6-g	1.5 + 0.3	Extra pure DMF	88 h	No	95	Manual column	67 %
b-3	3.3-g	1.5 + 0.7	Dry DMF	40 h	Yes	> 95	Flash column	67 %
b-4	3.5-g	1.5 + 1.4	Dry DMF	40 h	Yes	> 95	Precipitation	88 %

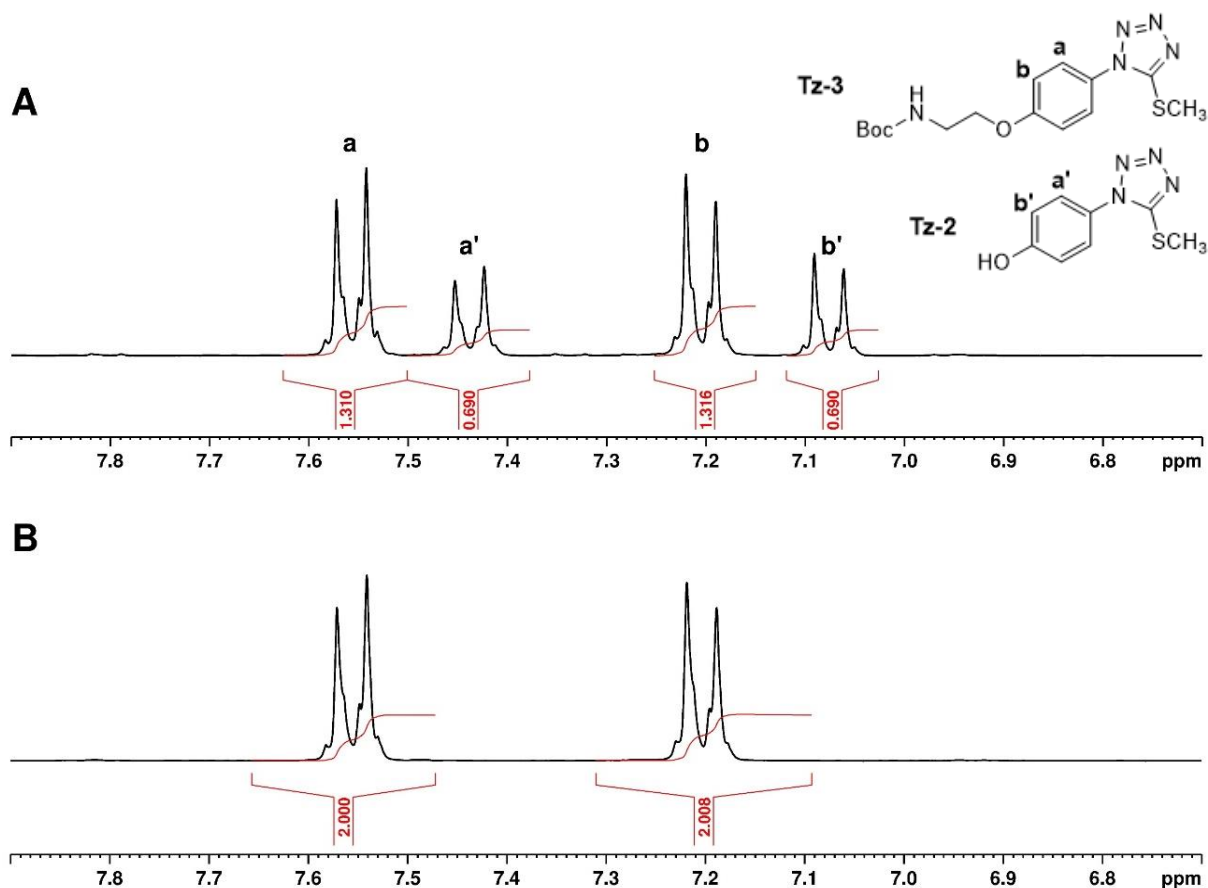


Figure 3. ^1H NMR spectra (300 MHz, acetone- d_6) of A) Aromatic signals from the etherification reaction crude (2.4-g scale) after 24 hours, where two pairs of multiplets corresponding to Tz-2 (starting material) at 7.44 and 7.08 ppm, and Tz-3 (final product) at 7.55 and 7.20 ppm are observed, and B) Aromatic signals from the Boc-amine coupling reaction crude after 40 hours and addition of 1.5 extra equivalents of the protected amine, where all Tz-2 (starting material) is consumed.

The substitution of the chromatographic purification by a faster (1 vs 1.7 h) and higher-yielding precipitation method also resulted in a greener purification with the usage of water (instead of EtOAc) and 83 % less n-Hexane. The alternative method consisted of 4 steps:

1. Precipitation of the reaction product by cooling the reaction mixture to 4°C .
2. Filtration and washing of the precipitate with cold water.
3. Stirring the precipitate in Hx to dissolve nonpolar impurities.
4. Filtration and drying of the final product.

Along with the successful optimization of the reaction conditions to maximize conversion of the starting material Tz-2, the alternative purification method allowed for isolation of pure ($\approx 100\%$, **Figure 4**) Tz-3 product in an 88% yield, which was directly used in the next step.

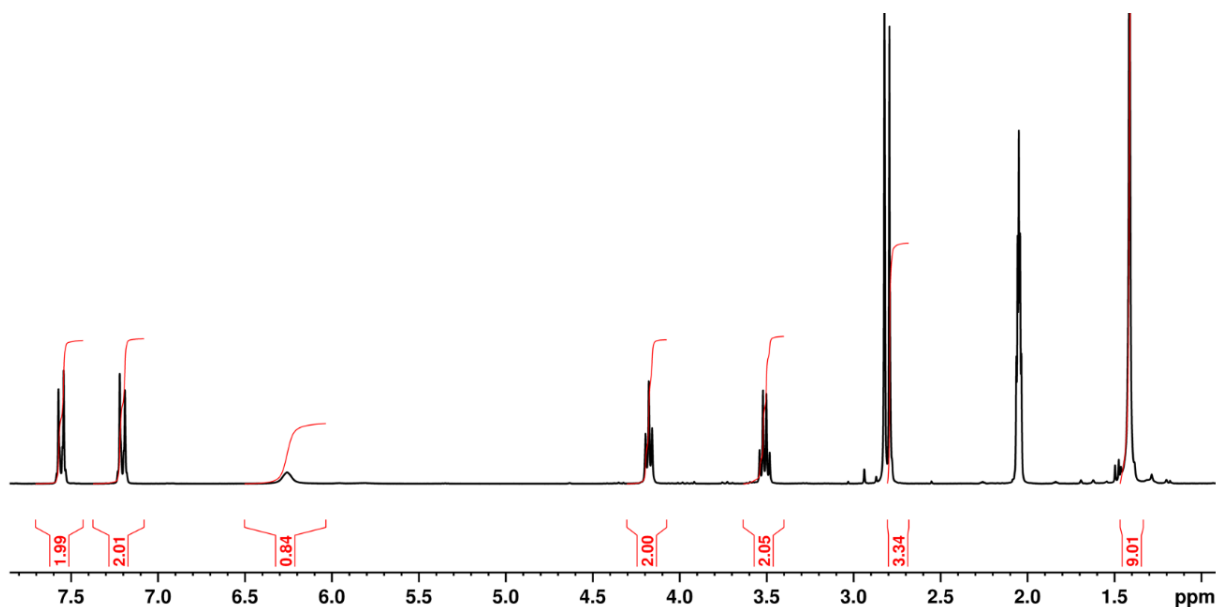


Figure 4. ^1H NMR spectra (300 MHz, acetone- d_6) of isolated Tz-3 after improved work-up (signals at 2.84 and 2.05 ppm correspond to water and non-deuterated acetone traces correspondingly).

In this step, the costs for the synthesis of Tz-3 decreased to ca. 341 € per g after optimization and scale-up (**Figure 1**). While the total process time of step **b** (including reaction and purification) increased from 24 to 48 h after upscaling, the higher scale and yield are the dominant factors because significantly more product is generated.

3.3.1.3 Oxidation of methyl sulfide group

The third step of the synthesis involves the oxidation of the methyl sulfide to methylsulfone using meta-chloroperoxybenzoic (mCPBA) as the oxidant (reaction **c** from **Scheme 1**).⁸ The use of non-flammable solvent like dichloromethane (DCM) and slow addition of reagents is necessary due to the strong oxidant character of mCPBA. Room temperature is used for complete oxidation to sulfone.¹³

The available oxidation protocol at 0.64-g scale used an excess of mCPBA (5 equivalents) overnight.¹⁴ The oxidant (mCPBA) was added at 0°C and kept at room temperature

overnight. The product was isolated after column chromatography in 79 % yield (purity not specified). Under these conditions, the overall costs of step **c** were calculated to ca. 2538 € per g of Tz-4 (**Figure 1**).

This reaction was upscaled (**Table 2**) using the same protocol. Purification by flash chromatography allowed an increase in the yield to 90 % at 3.4-g scale after purification.

Table 2. Scale and purification methods in which reaction **c** was attempted.

Scale	Purification method	Yield	Purity (wt%)
1.5-g	Manual chromatography column	81 %	90 %
1.2-g	Flash chromatography	91 %	84 %
2.9-g	Flash chromatography	89 %	88 %
3.4-g	Flash chromatography	90 %	95 %

Purification time was decreased from 4 to 1.5 h with a 50 % reduction in solvent usage by switching from manual to flash column. Optimization of the eluant profile to a gradient from 10:90 to 35:65 EtOAc/Hx gave an improved separation of Tz-4 from the remaining starting material and impurities (**Figure 5**). Thus, purity of the isolated Tz-4 improved from 84 %, before optimization, to 95 %, while yield remained at 90 %.

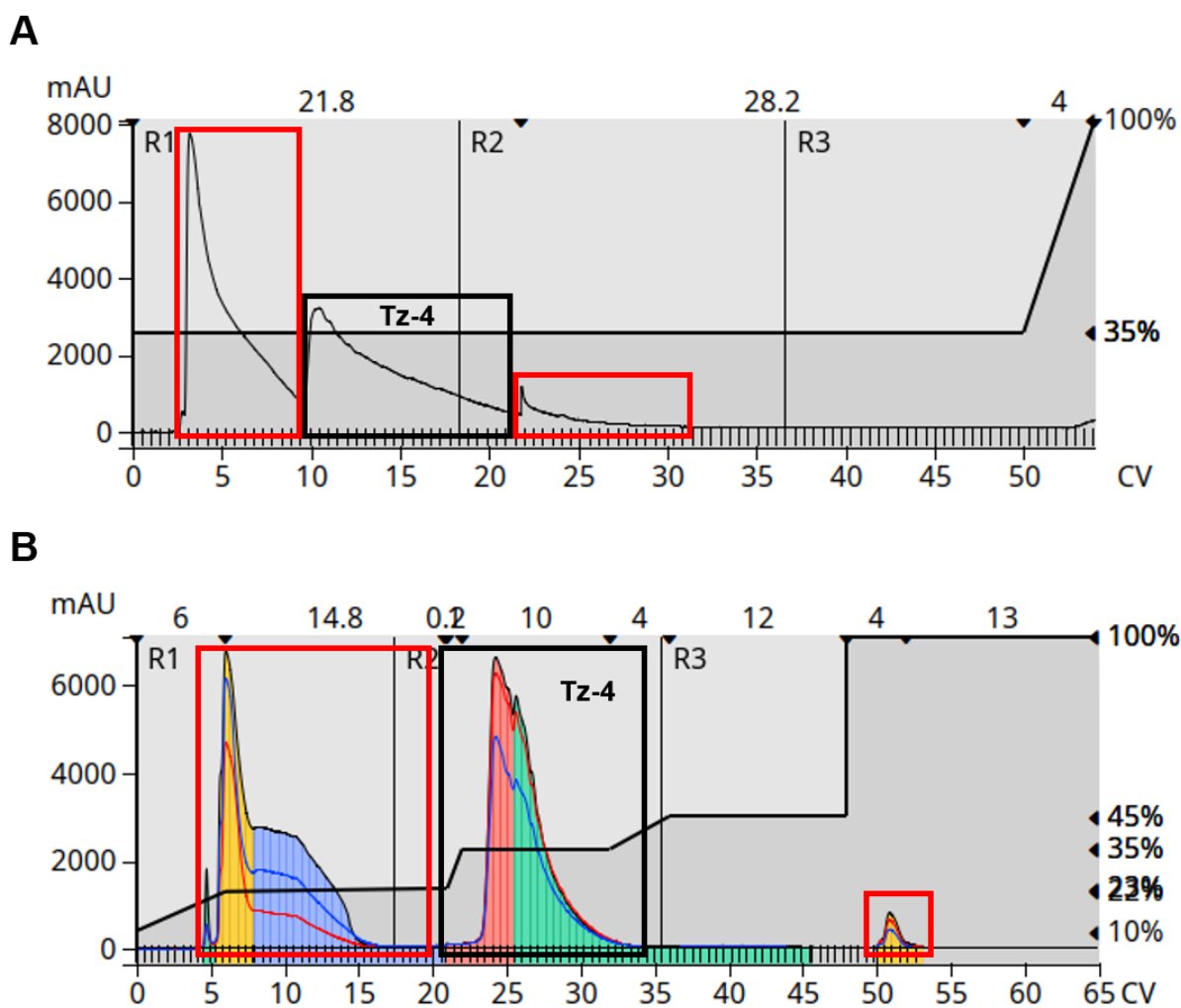


Figure 5. Chromatograms from flash chromatography purification of reaction **c**, showing the column volume (CV) on the X axis and intensity as milliabsorbance units (mAU) on the Y axis. A) Purification of reaction at 3.0-g scale using a 35:65 EtOAc/Hx mixture for elution with poor separation of impurities and desired product Tz-4; B) purification of reaction at 3.5-g scale using a EtOAc/Hx mixture gradient for much better separation of impurities (CV 4 to 5 and 50 to 53) and remaining reactant (CV 6 to 17) from Tz-4 (CV 23 to 34) (colors signaling the different detected peaks are just displayed in B due to a software update).

The costs of this reaction after optimization of the purification process and upscaling decreased to ca. 510 € per g of Tz-4 (**Figure 1**). Overheads cost is higher than labour after scale-up because the automated purification by flash column allowed for a lower workload, in comparison with the situation from previous protocol.

3.3.1.4 Boc deprotection

The fourth step of the synthesis consists of the deprotection of the primary amine by acid-mediated removal of the Boc protecting group (reaction **d** from **Scheme 1**). This deprotection had been performed at 30-mg scale with a yield of 66 % and 60 % purity. The formation over time of an unknown byproduct (40 mol% in this attempt) was the reason for the low purity and yield. The calculated reaction cost for step **e** under these conditions was 11301 € per g of Tz-5 (**Figure 1**).

The byproduct was detected in ^1H NMR spectroscopy by the shift of the integral corresponding to the methylene proton triplet from 4.3 to 3.7 ppm (**Figure 6**). To minimize byproduct formation, the purified compound was reacted with PEG-4NHS directly after evaporation of the HPLC solvent. The presence of the byproduct did not interfere with the following step **e** (PEG functionalization). No change in the signal of the methylsulfone's (MS) methyl group (3.6 ppm) was seen by ^1H NMR, meaning that the byproduct formation did not involve attack of the MS unit by the free amine. However, since the signal from the methylene protons next to the amine group seemed to be the only one affected by the byproduct formation (**Figure 6**), it was hypothesized that the amine could be involved in the byproduct formation.

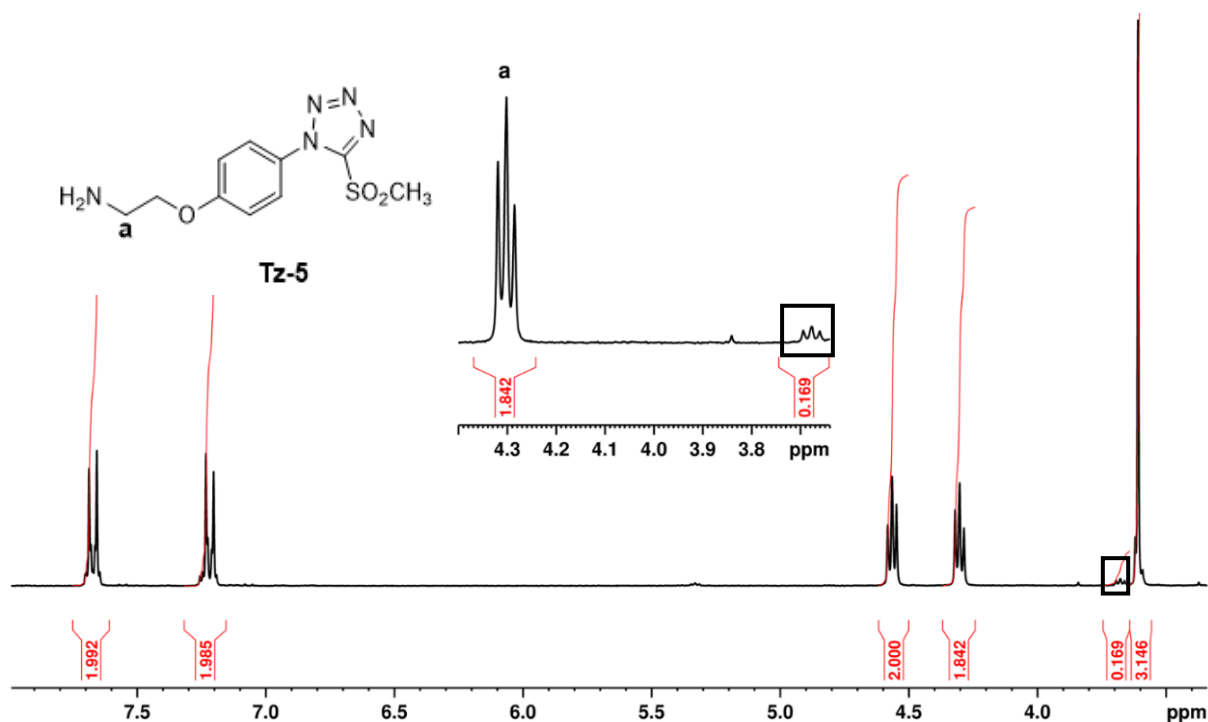


Figure 6. ^1H NMR spectra (300 MHz, acetone- d_6) of the deprotected amine (Tz-5) after purification by preparative HPLC. A 8.5 % loss of the -CH₂ (a) integral (4.3 ppm) can be observed, along with the emergence of a new triplet at 3.68 ppm (marked on the spectrum) from the byproduct.

The formation rate of the byproduct was monitored by ^1H NMR spectroscopy under acidic and basic conditions. Addition of 1.0 eq. of trifluoroacetic acid (TFA) to Tz-5 in deuterated acetone did not lead to any difference in the byproduct content (40 mol%) after 24 h. Addition of deuterated pyridine showed 60 mol% byproduct content after 24 h in the presence of pyridine, indicating that the byproduct is promoted in basic media where the amine is the prevalent form. The chemical identity of the byproduct could not be resolved from the NMR spectrum.

The deprotected amine Tz-5 was purified by preparative HPLC using columns with a maximum loading capacity of ca. 200 mg, which establishes the upper limit of the reaction scale. A maximum of 160-mg of Tz-4 was used to avoid saturation of the column. The reaction crude was rapidly handled and purified to minimize formation of the byproduct. As studied by ^1H NMR, the byproduct starts forming during the reaction (\approx 10 mol% in the crude) and increases further during the purification process to ca. 10 – 20 mol %. Purified by preparative HPLC, the final compound Tz-5 was successfully isolated

with a yield of 86 % and an 83 mol% (0.1-g scale). As a result, overall yield of precursor Tz-5 synthesis was increased from 25 to 59 %. While still the costliest step of the synthetic pathway, the reaction costs of step **d** were decreased from 11301 to 2624 € per g of Tz-5 by upscaling from 30-mg to 100-mg scale (same total time but higher amount of product), as well as lower production costs from previous steps (**Figure 1**).

To further upscale purification, flash chromatography of the product was attempted (**Table 3**). A reverse phase (C18 silica) and the same eluent profile as in the purification by HPLC was attempted, but the desired product was not identified.

Table 3. Purification methods used for the isolation of compound Tz-5. Eluents mixture, retention time and byproduct concentration from the isolated material is shown. Preparative HPLC N = 5, while rest of purification methods N = 1.

Purification method	Solvent mixture for elution of Tz-5	Retention time (min)	Byproduct concentration after purification (mol%)
Preparative HPLC (reverse phase)	63:37 Solvent A/Solvent B	14	10 – 20
Flash Chromatography (reverse phase)	-	-	-
Flash Chromatography (amine functionalized stationary phase)	90:10 EtOAc/Hx	90	100
Flash Chromatography (normal phase)	16:84 MeOH/DCM	20	78
Flash Chromatography (normal phase)	5:95 MeOH/DCM + TEA 1.5 v/v%	7.3	21

Normal phase flash chromatography was then targeted. TLC (normal phase) of Tz-5 in EtOAc/Hx mixtures and EtOAc (100 %) showed no elution, which was attributed to the interaction between the silanol groups of the carrier material and the free amine group of Tz-5. To minimize these interactions, flash chromatography with NH₂-functionalized stationary phase (propylamine groups) was used, along with a mixture 90:10 EtOAc/Hx. Only the byproduct ($t_R = 1$ h 33 min) was eluted (¹H NMR), supporting the observed enhancement of the byproduct formation in presence of amines. By using solvent

mixtures with higher polarity (MeOH/DCM) Tz-5 could be eluted at 2 and 5 % MeOH ($R_f = 0.1$ and $R_f = 0.2$ respectively). A gradient from 2:98 to 20:80 MeOH/DCM proved best for the elution of Tz-5 ($t_R = 20$ min, 16:84 MeOH/DCM) in flash chromatography. After purification, the isolated mixture contained 78 mol% of byproduct (^1H NMR). The ^1H NMR spectrum showed additional peaks that could not be attributed to the desired compound (**Figure 7B**).

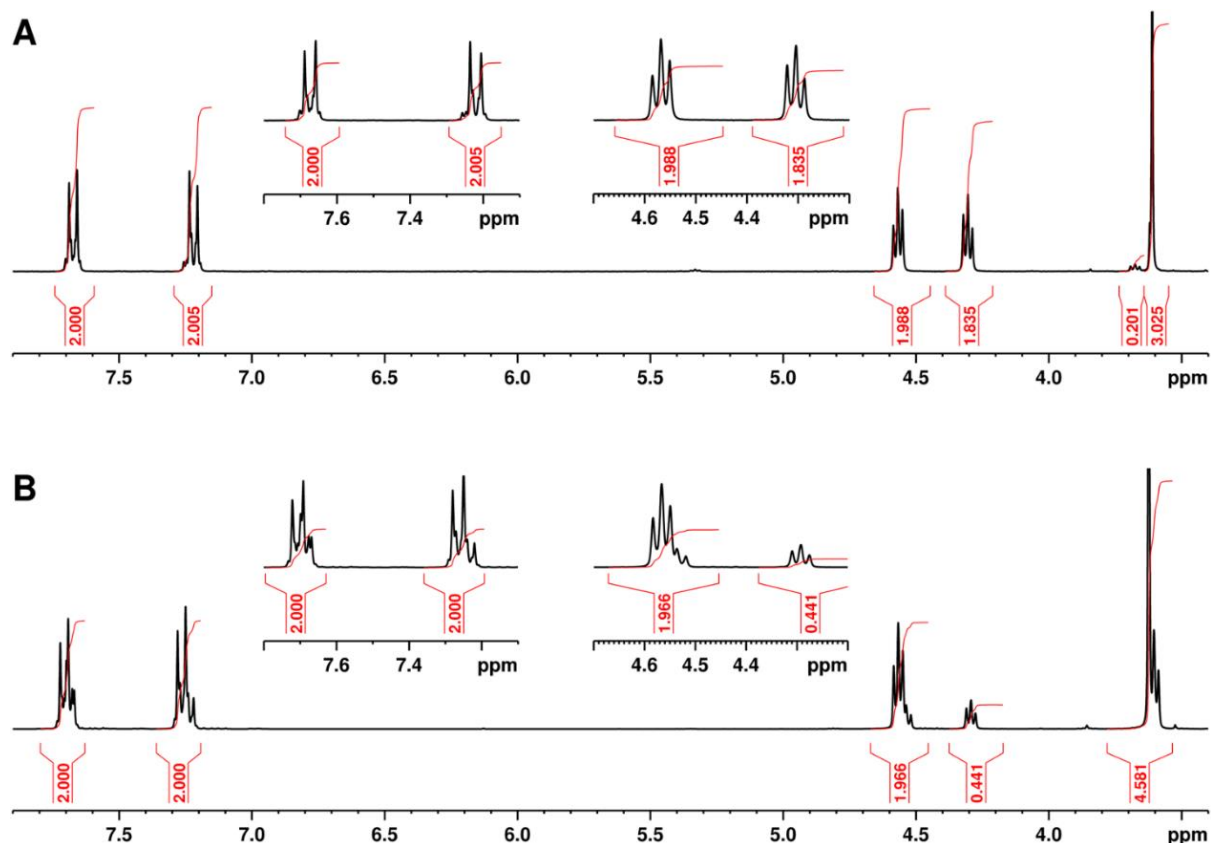


Figure 7. ^1H NMR spectra (300 MHz, acetone- d_6) of **A**) the deprotected amine (Tz-5) after purification by preparative HPLC showing a loss of 9.0 % of the $-\text{CH}_2$ integral (4.3 ppm), **B**) the deprotected amine (Tz-5) after purification by flash chromatography (elution at 15:85 MeOH/DCM) showing a loss of 78.0 % of the $-\text{CH}_2$ integral (4.3 ppm) and new peaks on both the aromatic (7.8 – 7.1 ppm) and the aliphatic regions (4.7 – 4.2 ppm), as seen in the zoomed sections.

The impact of the purification method on the byproduct generation was analyzed by splitting a crude batch in two parts and purifying one half by flash chromatography and the other half by preparative HPLC in parallel. HPLC generated 15 mol% of byproduct (**Figure 8A**), while flash column contained ca. 50 mol% (**Figure 8B**). The extra peaks

detected in both the aromatic (7.4 and 7.15 ppm) and aliphatic (4.45 ppm) regions were observed in the compound eluted through flash chromatography (**Figure 8B**). The spectrum from the product isolated by HPLC showed no new signals. It was concluded that these extra peaks from the isolated product after flash chromatography purification with MeOH/DCM solvent mixture were associated with the purification step and not with the synthesis protocol. The small difference in the purification time between flash column (30 min) and preparative HPLC (40 min) suggests that time was not the primary factor contributing to the greater amount of byproduct.

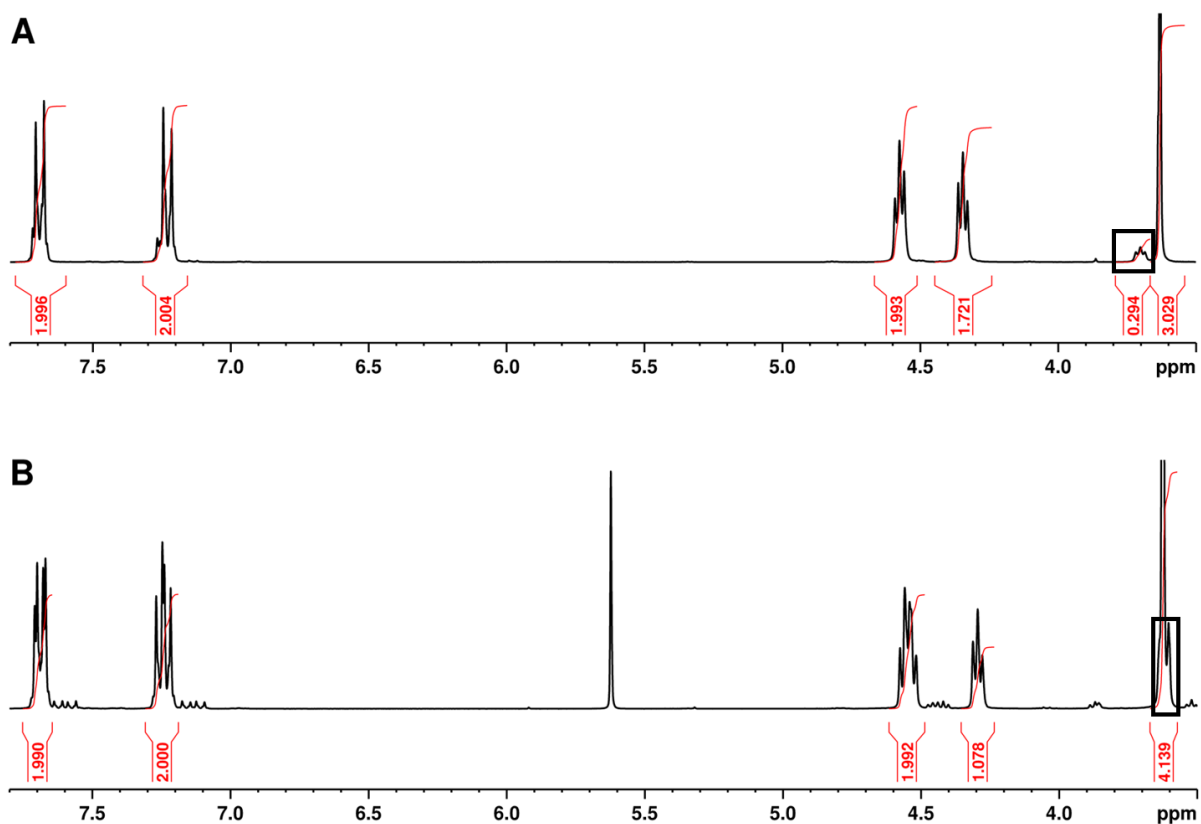


Figure 8. ^1H NMR spectra (300 MHz, acetone- d_6) of Tz-5 from same reaction batch **A**) after purification by preparative HPLC (15 mol% byproduct, peak at 3.7 ppm), **B**) after purification by flash chromatography (elution at 10:90 MeOH/DCM) (50 mol% byproduct, peak at 3.6 ppm overlapped by methyl signal); extra peaks on both the aromatic (7.8 – 7.1 ppm) and the aliphatic regions (4.7 – 4.35 ppm) are observed. (Singlet at 5.6 ppm belongs to remaining DCM traces from eluents mixture).

To improve purification and decrease the retention time (byproduct concentration increases over time), neutralization of the silanol groups from the silica carrier was done

in the flash column. Neutralization avoids acid-base interactions between the amine and the silanols from the stationary phase. The eluant (3:97 MeOH/DCM) was supplemented with triethylamine (1.5 v/v%), resulting in the elution of Tz-5 at $t_R = 8$ min with good separation from major impurities (**Figure 9**).

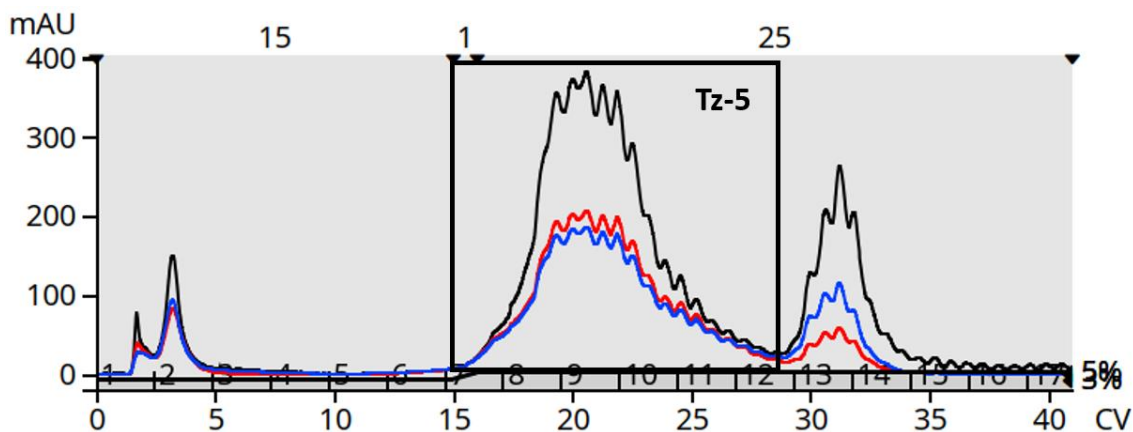


Figure 9. Chromatogram of Tz-5 after purification by flash chromatography (3:95 – 5:95 MeOH/DCM gradient + 1.5 v/v% TEA). Separation of Tz-5 peak from prominent impurities can be appreciated.

The byproduct content in the isolated material decreased from 50 – 78 mol% to 22 mol% after optimization of flash column purification. While still present, the amount of byproduct formed during this purification was successfully reduced to levels similar to the default purification by preparative HPLC (10 – 20 mol%). Moreover, the byproduct content (22 mol%) is comparable to the 20 mol% formed after exposition of Tz-5 to pyridine, another tertiary amine like the TEA used for neutralization of the silica during flash column purification. The previously mentioned new peaks were still observed in the ^1H NMR spectra. Tz-5 isolated by both flash column and HPLC was coupled to PEG-4NHS as described in section 3.3.1.5.

3.3.1.5 End-functionalization of PEG-4NHS to obtain PEG-4TzMS

The last step of the synthesis is the coupling of the amine group from Tz-5 to 4arm polyethylene glycol succinimidyl carboxymethyl ester (reaction **e** from **Scheme 1**). The reaction was done in inert conditions to prevent hydrolysis of the N-hydroxysuccinimide (NHS) groups. N-methylmorpholine (NMM) was used as proton scavenger to avoid

acidification of the media and subsequent decrease of the free amine (from Tz-5) nucleophilicity. 2.5 eq. of Tz-5 per 1 eq. of end-group were used.

The available reaction protocol performed at 0.2-g scale and using 2.5 eq. of Tz-5 gave PEG-4TzMS with a degree of functionalization > 95 % and 92 % yield after purification by dialysis. The costs for step **d** were ca. 4960 € per g of PEG-4TzMS (**Figure 1**).

Attempts to perform the reaction with 1.25 equivalents resulted in a lower degree of functionalization (75 %). 2.50 equivalents of Tz-5 per polymer end-group continued to be used for the scale-up to maximize functionalization. By using Tz-5 with ca. 15 mol% byproduct (purified by preparative HPLC), PEG-4NHS with a degree of functionalization of 98 % and 91 % yield was successfully synthesized at 0.61-g scale (**Figure 10**). The costs of this step decreased to 1566 € per g of PEG-4TzMS (**Figure 1**).

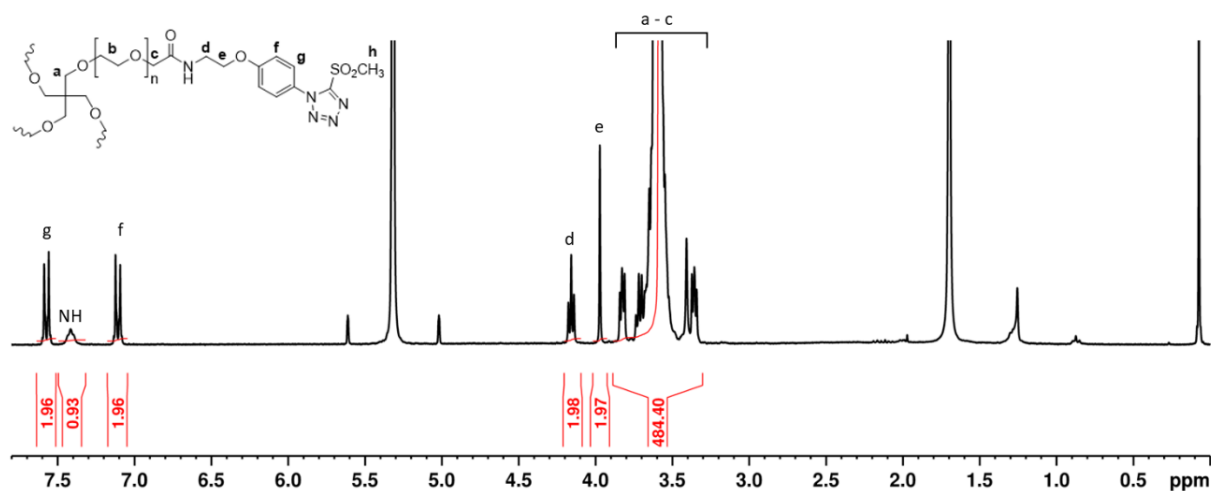


Figure 10. ^1H NMR spectra (300 MHz, acetone- d_6) of PEG-4TzMS after final coupling of the free amine (Tz-5) (solvent traces: $\text{DCM-}d_2$ (5.3 ppm), water (1.7 ppm), tetramethylsilane (0.0 ppm)).

The small impurities (new peaks observed in the ^1H NMR spectra, **Figure 7B**) after successful elution of Tz-5 by flash column did not interfere in the coupling to PEG-4NHS. PEG-4TzMS from reaction of PEG-4NHS with Tz-5 (purified by flash column), incorporating 20 mol% byproduct as well as the other undefined small impurities, was isolated with a degree of functionalization of 91 % (**Figure 11B**). While the conversion % of NHS to MS groups was ≈ 100 %, the lower degree of functionalization of the final polymer resulted from the partially hydrolyzed (9 %) starting material (peak **b** at 4.1 ppm

from **Figure 11A**). Thus, the coupling of Tz-5 after purification by flash chromatography proved to be successful.

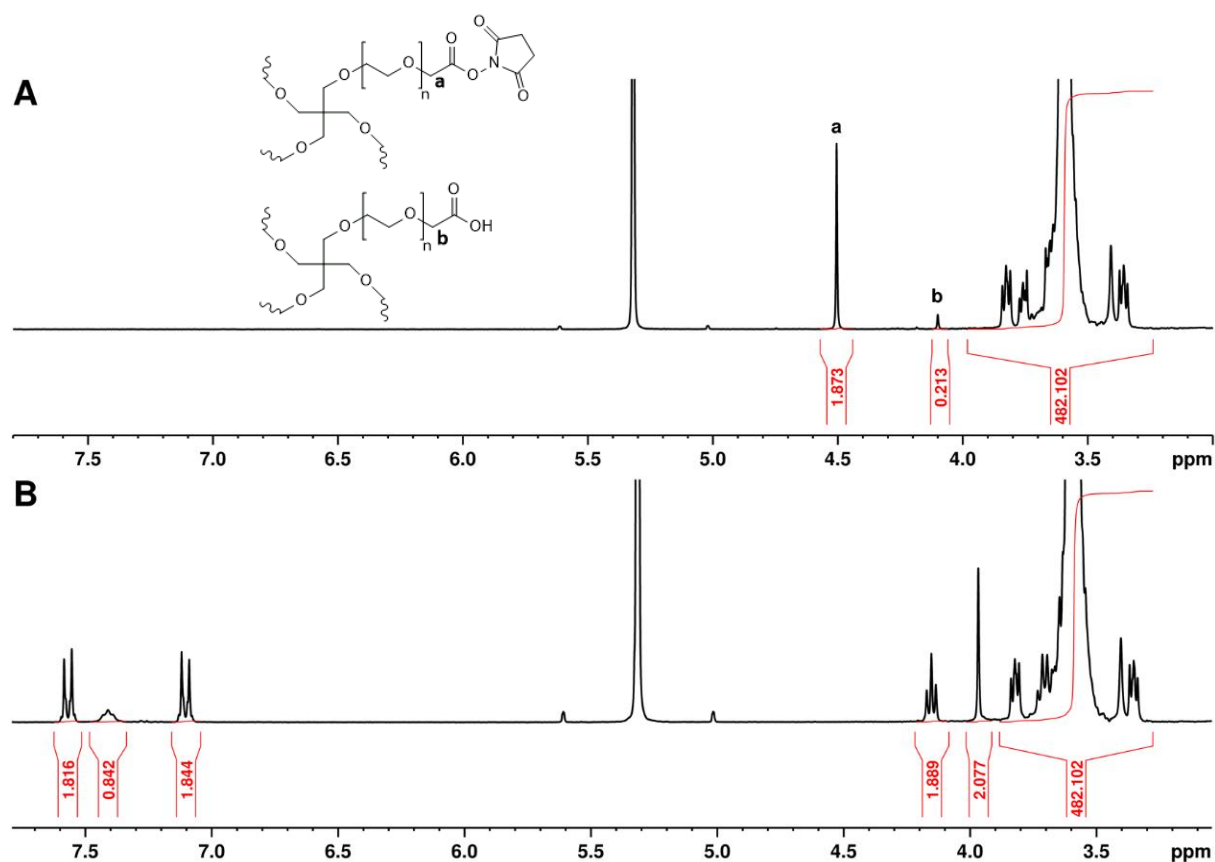


Figure 11. ^1H NMR spectra (300 MHz, acetone- d_6) of A) partially (9 %) hydrolyzed PEG-4NHS showing the two distinctive peaks: peak “a” (4.5 ppm) corresponds to the -CH₂ group from the non-hydrolyzed component, while peak “b” (4.1 ppm) corresponds to the hydrolyzed starting material, B) PEG-4TzMS after functionalization with the isolated Tz-5 (purified by flash chromatography).

3.3.1.6 Quantification of the degree of end-group functionalization and molecular weight (MW) of PEG-4TzMS

To determine the molecular weight and degree of functionalization of PEG-TzMS, the signals of the ^1H NMR spectra from PEG-4NHS (**Figure 12A**) and PEG-4TzMS (**Figure 12B**) were compared. The degree of functionalization of PEG-4NHS (F_{NHS}) was taken from the certificate of analysis of the provider and used to set the integral of the two methylene protons at 4.5 ppm (c), i.e. $I_c = 2 \times F_{\text{NHS}}$. In the spectrum of the PEG-4NHS in **Figure 12A**, $I_c = 2 \times 0.984 = 1.968$. The integral for signals “a” and “b” ($I_{a,b}$), which correspond to the

protons from the core and the repeat units of PEG, was used to establish the number of repeat units “n”, i.e. $n = (I_{a,b} - I_a) / 4 = (474.802 - 13.00) / 4 = 118.2$. Then, the molecular weight of the starting material was calculated assuming that non-functionalized end-groups were carboxylic acid (-COOH). A molecular weight of 21.6 kDa was obtained.

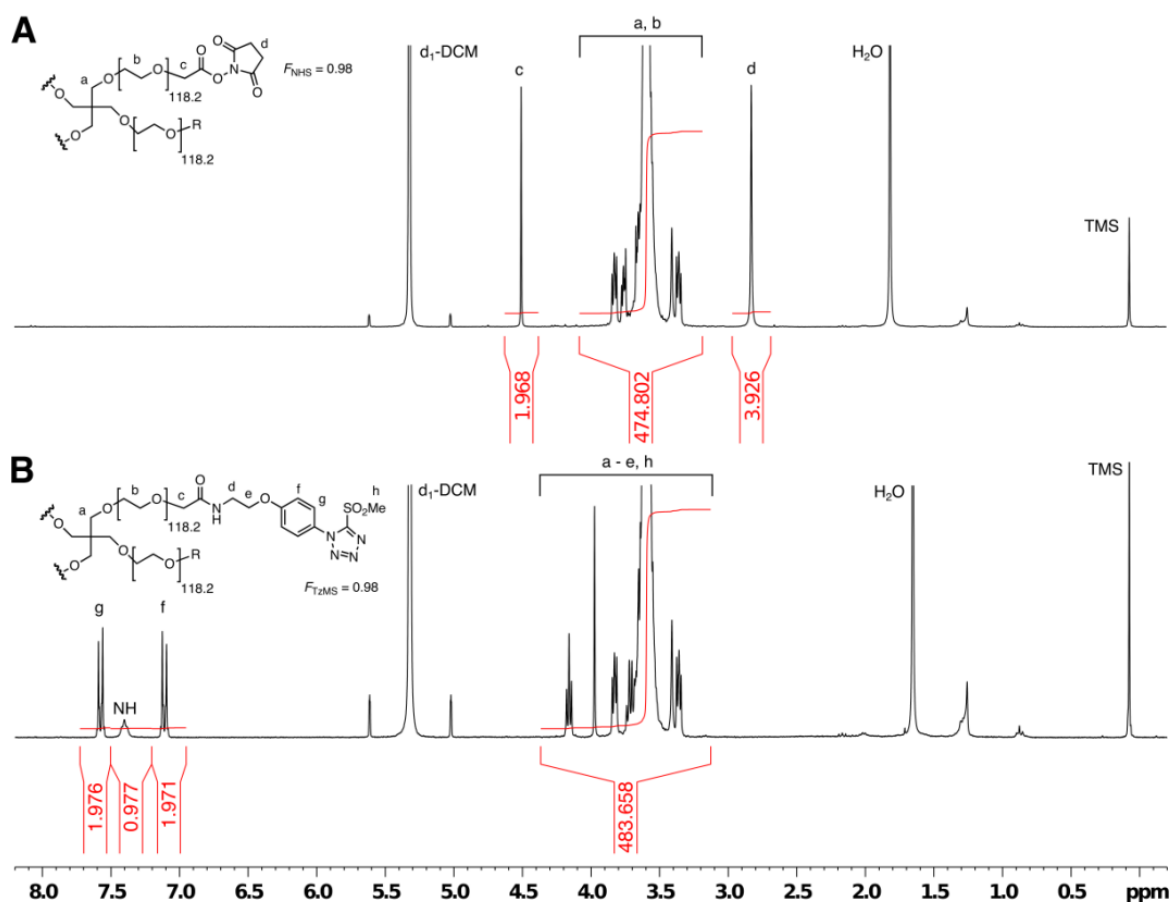


Figure 12. ¹H NMR spectra of A) commercial PEG-4NHS and B) synthesized PEG-4TzMS. Reprinted from de Miguel-Jiménez et al. © 2022 Macromolecular Bioscience published by Wiley-VCH GmbH.

In the NMR spectra of PEG-4TzMS (**Figure 12B**), the $I_{(a+b)}$ value from **Figure 12A** was used to set the integral of the backbone signals, considering that additional signals (“c”, “d”, “e”, and “h”) contributed by the TzMS part of the molecule. This gave an integral of 483.658 for “a – e, h” protons. Note that this assumes that all the NHS groups had been converted to TzMS groups. Since signals from protons “c”, “d”, “e”, and “h” are negligible compared with I_{a+b} , this assumption is reasonable even if conversion was not quantitative. The F_{TzMS} was then calculated from the signals of the aromatic protons “f”

and “g” (7.1 and 7.6 ppm), i.e. $F_{\text{TzMS}} = (I_f + I_g) / 4 = (1.971 + 1.976) / 4 = 0.986$, which was considered as 0.984 because it cannot exceed F_{NHS} indicated in the COA by the supplier. Same as with PEG-4NHS, the M_w was obtained, resulting in a molecular weight of 22.2 kDa.¹³

The calculated molecular weight from the starting material via the explained method differed from the value stated by the commercial supplier (21.6 vs 20.4 kDa). The molecular weight determination via the ^1H NMR analysis is important to define the stoichiometry of the prepolymer in the hydrogel mixture for full crosslinking in PEG-4TzMS hydrogels.

3.4 Discussion and outlook

In this chapter, the optimization of the 5-step synthetic pathway to obtain the hydrogel precursor PEG-4TzMS was achieved. **Table 4** compares the reaction and purification conditions as well as the yield and scale of each step. Given the stability issues described with Tz-5, the upscaled synthesis to 3.0-g stock of Boc-protected Tz-4 is considered a useful scale for the experimental purpose of this Thesis. This compound can be stored and used for subsequent reactions at smaller scale. In the present work, a batch size of 0.6 g of functionalized polymer with > 95 % functionalization degree was achieved. MS hydrogels for medium/high-throughput cell cultures are prepared at 5 wt%, so one 0.6-g batch of PEG-4TzMS is enough material to prepare six 384-well plates containing 5 μL hydrogels in each well. Further upscaling of the two last steps might be possible using flash chromatography for the purification of Tz-5.

Table 4. Reactions **a** – **e** (**Scheme 1**) from PEG-4TzMS synthetic pathway with conditions before and after upscaling. The purification method and the respective yield after purification is shown.

Step	Upscaling	Scale (g)	Reaction conditions	Purification method	Yield (%)
Methylation (step a)	Before	0.63	-10°C, THF, 3 h	Manual chromatography	60
	After	2.9	-10°C, inert atmosphere, dry THF, 1.5 – 2 h	Extraction and washing	82*
Etherification (step b)	Before	0.93	1.5 eq., 80°C, DMF, 16 h	Manual chromatography	65

	After	3.5	2.9 eq., 80°C, inert atmosphere, dry DMF, 40 h	Precipitation and washing	88
Oxidation (step c)	Before	0.64	r.t., DCM, ovn	Manual chromatography	79
	After	3.4	r.t., DCM, ovn	Flash chromatography	90
Deprotection (step d)	Before	0.020	r.t., DCM, 30 min	Preparative HPLC	66
	After	0.10	r.t., DCM, 30 min	Preparative HPLC**	86
PEG coupling (step e)	Before	0.20	r.t., DMF, NMM, ovn	Dialysis	92
	After	0.61	r.t., DMF, NMM, ovn	Dialysis	91

* Yield after purification by flash chromatography at 3.0-g scale was 89 %.

** Purification was successfully translated to flash chromatography at 0.040-g scale.

Primary alkyl halides such as methyl iodide (MeI) (from reaction **a**, **Scheme 1**) and 2-(Boc-amino)ethyl bromide (from reaction **b**, **Scheme 1**) are susceptible to hydrolysis in neutral or basic aqueous conditions, and this reaction is promoted by temperature.^{14,15} Traces of water in non-aqueous solvents like THF (≤ 0.05 % water; data from Sigma Aldrich) or DMF (≤ 0.15 % water; data from Sigma Aldrich), air, and labware can be responsible for certain hydrolysis degree in the reaction mixture. Thus, inert atmosphere was applied to reactions **a** and **b**. Although water traces (≤ 1.8 mmol of water vs 15.4 mmol of MeI) were present in reaction **a** at 3.0-g scale, barely no hydrolysis of the methyl iodide could be expected due to the slow kinetics of this reaction.¹⁰ On the other hand, the electron-withdrawing character of the *N*-Boc group¹⁶ from the bromide derivative, the high temperature (80 – 85°C), as well as the higher water content in DMF solvent (≤ 8.3 mmol of water vs 20.9 mmol of 2-[Boc-amino]ethyl bromide at 3-g scale) and basic medium¹⁵ from reaction **b**, could translate into hydrolysis of 2-(Boc-amino)ethyl bromide at some extent. Thus, the yield improvement from 67 to 88 % achieved in our experiments is partially explained by using inert conditions.

The reaction time was extended from 16 to 40 h in reaction **b**, along with an increase of the bromide derivative equivalents (from 1.5 to 1.5 + 1.4), resulting in > 95 % consumption of Tz-2 (limiting reactant). Increasing the reaction time resulted in slower conversion rate compared to addition of more equivalents of the bromide derivative, which seems to be critical for achieving full conversion faster. Thus, the reaction time could be decreased

by adding 3 eq. of the bromide derivative at the start. In order to further decrease the reaction time and improve efficiency of the etherification, a stronger base like sodium hydride could be used to easily deprotonate and activate the phenol,¹⁷ though low temperatures and careful control would be necessary due to exothermic reaction in sodium hydride (NaH)/DMF and NaH/THF mixtures.¹⁸ Sodium iodide (NaI), commonly used as catalyst (in DMF solvent) for the replacement of the bromide as better leaving group in the iodide form¹⁹ (higher atom size = better stabilization of electrons) could also be used to accelerate the reaction.

The implementation of automated flash chromatography for the purification of the product from reaction **c** allowed faster, greener and more effective purification. Although chromatographic instruments require a higher investment than manual chromatography, a cost saving of ca. 114 € was acknowledged in reaction **c**. Purification of the crudes from reactions **a** and **b** in the optimized protocols took place by extraction and precipitation correspondingly. These processes resulted in shorter purification processes, lower solvent consumption and cheaper instrumentation, also translating into cost saving of ca. 81 € per purification in step **a**, and ca. 115 € in step **b**.

The overall cost decreased from 4960 to 1565 € per g of PEG-4TzMS after reaction optimization was influenced by the higher scale of the reactions, which lead to a reduction in the required labour and laboratory use for producing the same amount of PEG-4TzMS.

The formation of a byproduct during deprotection of the Boc-amine Tz-4 and after purification of the free amine precursor Tz-5 was a major bottleneck in the synthesis process. The transition to a chromatographic purification technique using neutralized normal silica as stationary phase, allowed for upscaling with 22% formation of the undesired byproduct which, however, did not interfere in the subsequent reaction, where a high conversion degree (≈ 100 %) was obtained. This is of significance since the formation of the byproduct cannot be avoided with the current protocol.

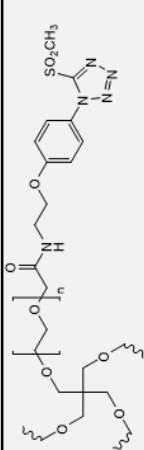
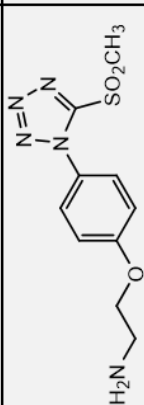
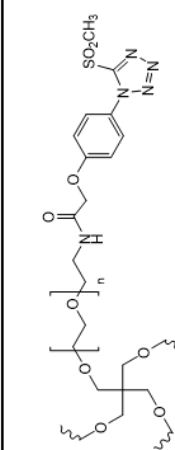
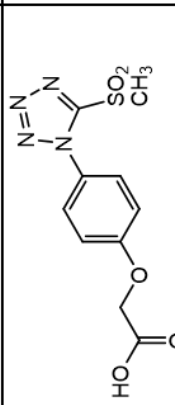
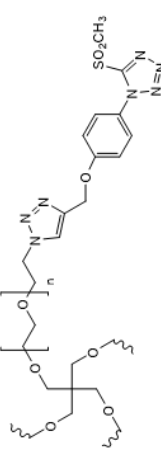
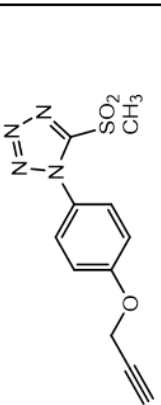
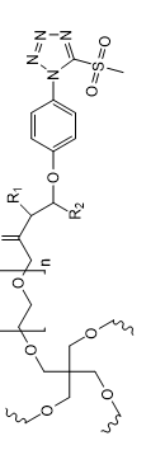
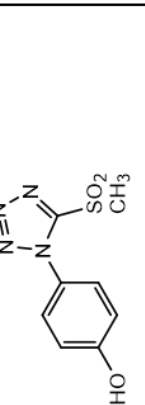
To further upscale the process and avoid the instability issues of Tz-5 intermediate, alternative synthetic pathways can also be envisaged. Relevant specific conditions to take into account for the design of the pathway are:

- i. **The need to obtain >95% end-group functionality in PEG-4TzMS** to achieve high crosslinking and stability of the final network. High yielding and orthogonal click reactions²⁰ are preferred to obtain a high degree of functionalization.
- ii. **Comparable reaction rate of PEG-4TzMS with thiols.** The *p*-substituent on the aryl TzMS ring influences the reaction rate of MS with thiols¹⁰, so molecular designs that maintain the ether group of Tz-5 should be considered first. Changes in molecular structure more distant from the TzMS group should have a negligible impact on reaction rate, giving scope for different chemistries for attachment of the TzMS unit to PEG.
- iii. **Comparable or better stability of precursors and formed hydrogels against hydrolysis or enzymatic degradation.** Hydrogel stability is partially dependent on the bond between the TzMS-containing molecule and the PEG backbone. In this context, ethers or amides are preferred vs. esters.

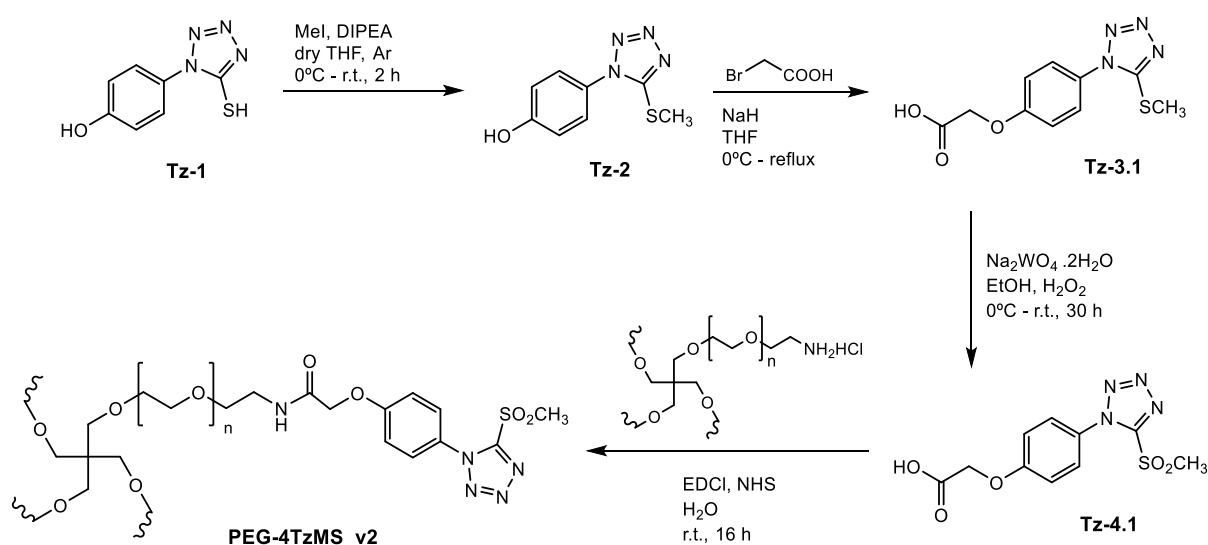
The current synthetic pathway that has been presented in this thesis ends with a highly functional (> 95 %) PEG-4TzMS. Phenol-TzMS has a reaction rate of $6.03 \pm 0.55 \text{ M}^{-1} \text{ s}^{-1}$ under aqueous conditions (pH 7.5)^{10,21,22}, which translates into a crosslinking time of 1.6 min with VPM crosslinker at pH 7.5.¹³ While precursor Tz-5 is not stable in storage over time (byproduct formation), Tz-4 is stable over a year (at least). However, deprotection of Tz-4 and subsequent purification before functionalization of PEG is needed, which results in a less efficient process than having Tz-5 in stock for the final coupling. On the other hand, the NHS group from PEG-4NHS is sensitive to hydrolysis. Regarding the hydrogel stability, the current PEG-4TzMS forms a network (with VPM crosslinker) that is stable under cell culture conditions (cell medium, pH 7.4, 37 °C) for 15 days.²¹ The phenol precursor Tz-1 costs 3.3 € per g (TCI) and the PEG-4NHS costs 88 € per g (JenKem). Furthermore, the total reaction time (excluding purification time) of the 5-step synthesis is 75 h, while the active man-hours are 28 h. This translates into an overall cost of 1565 € per g of synthesized PEG-4TzMS. The safety of the current synthesis is relatively high in terms of non-violent reactions.

In this section, 3 alternative pathways for the synthesis of 4arm PEG-tetrazol methylsulfone, that could potentially meet the 3 selection criteria, are presented (**Table 5**).

Table 5. Comparison of key aspects from current synthesis of PEG-4TzMS and proposed alternative pathways.

	Final structure	Key intermediate	Synthetic pathway steps	Starting material cost (€ per g)	Stability of intermediate
Current synthesis			5	<u>Tetrazole</u> derivative: 3.3 <u>PEG</u> derivative: 88	PEG-4NHS sensitive to hydrolysis and amine-TzMS unstable over time (unknown if reversible)
Alternative pathway 1			4	<u>Tetrazole</u> derivative: 3.3 <u>PEG</u> derivative: 40	PEG-4NH ₂ salt hydrolytically stable and TzMS-phenoxyacetic acid potentially less reactive than amine Tz-5
Alternative pathway 2			4	<u>Tetrazole</u> derivative: 3.3 <u>PEG</u> derivative: 104	PEG-4Azide and alkyne-TzMS both stable towards hydrolysis
Alternative pathway 3			3	<u>Tetrazole</u> derivative: 3.3 <u>PEG</u> derivative: 109	PEG-4Epoxide more hydrolytically stable and phenol-TzMS present higher stability than free amine Tz-5

Alternative pathway 1. Interchanging the main functionalities of Tz-5 (amine) and PEG-4NHS (activated acid derivative as an ester) is a straight-forward alternative. For that, a carboxylic acid like bromoacetic acid is coupled to the phenol group of Tz-2 (**Scheme 2**), following the procedure described by Luo X., *et al.* 2013.¹⁷ The oxidation allows for the final coupling of the carboxylic acid of Tz-4.1 to the cheaper PEG-4NH₂ (HCL salt) in presence of a coupling agent like carbodiimide hydrochloride (EDCI) and N-hydroxysuccinimide (NHS) in water during 24 h. This coupling has been successfully tested with hyaluronic acid.²³

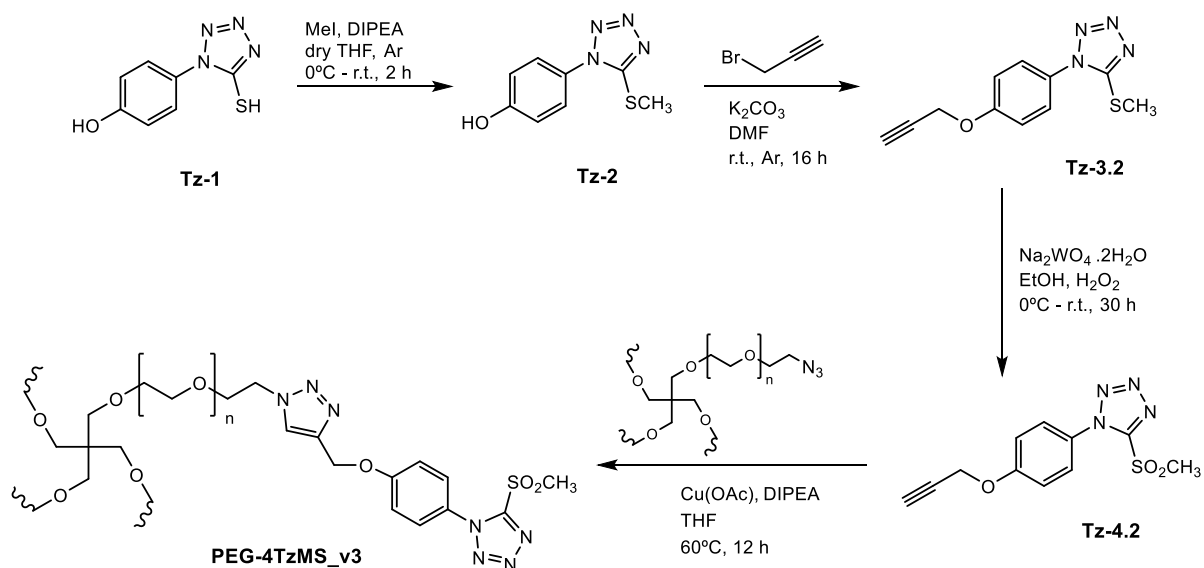


Scheme 2. Proposed synthetic pathway for the preparation of PEG-4TzMS through the coupling of PEG-4NH₂ with TzMS-phenoxyacetic acid (Tz-4.1).

Bian *et al.*²³ achieved a 61 % functionalization degree with HA 0.1 MDa. While significantly lower than current synthesis (> 95 %), the solubility of HA in water is lower than PEG (5-50 vs 100-670 mg/mL; data from Creative PEGWorks and Merck respectively), which could translate in a more effective reaction and higher functionalization degree when working with PEG. Moreover, other coupling reagents are used in literature, such as N,N'-dicyclohexylcarbodiimide (DCC)/4-Dimethylaminopyridine (DMAP) or hexafluorophosphate azabenzotriazole tetramethyl uronium (HATU)/ N, N-Diisopropyletilamina (DIPEA). The crosslinking reaction with thiolated molecules should not be significantly affected due to the use of the same phenol precursor Tz-1 (ether bond is maintained). Non-activated carboxylic acids, like phenoxyacetic acid precursor Tz-4.1,

usually present low reactivity so Tz-4.1 would potentially be more stable than Tz-5. PEG-4NH₂ is stable towards hydrolysis, unlike PEG-4NHS. The cost of the precursors is similar, as Tz-1 is also used in the current synthesis, and PEG-4NH₂ is slightly cheaper than PEG-4NHS (88 € per g) at 40 € per g (JenKem). In terms of time, the total reaction time of this 4-step pathway is ca. 48 h (excluding step 2 due to reaction time omission in protocol¹⁷), vs 75 h of current synthesis. While less toxic organic solvents are used, precautions must be taken when handling sodium hydride (NaH) since it reacts violently in contact with water.

Alternative Pathway 2. Another promising option is the azide-alkyne cycloaddition,^{24,25} which is a highly efficient and selective click-reaction (**Scheme 3**).^{24,26,27} The copper-catalyzed reaction between a mono-substituted alkyne and an azide, both stable towards hydrolysis, results in a 1,2,3-triazol. The alkyne moiety can be incorporated to the phenol following the protocol described by Motiwala *et al.*¹⁰ After oxidation of the sulfide following the same protocol, the alkyne-TzMS is reacted with the commercially available PEG-4Azide in presence of copper (II) acetate (Cu(OAc)) as catalyst and DIPEA, which presents quantitative conversion after 12 h (**Scheme 3**).²⁸ The remaining copper can be then removed (to avoid later contamination) through simple washing or dialysis with ethylenediaminetetraacetic acid (EDTA) solutions.^{29,30} Moreover, Cu(0) wire is also used as catalyst to avoid further removal of copper impurities after reaction.³¹



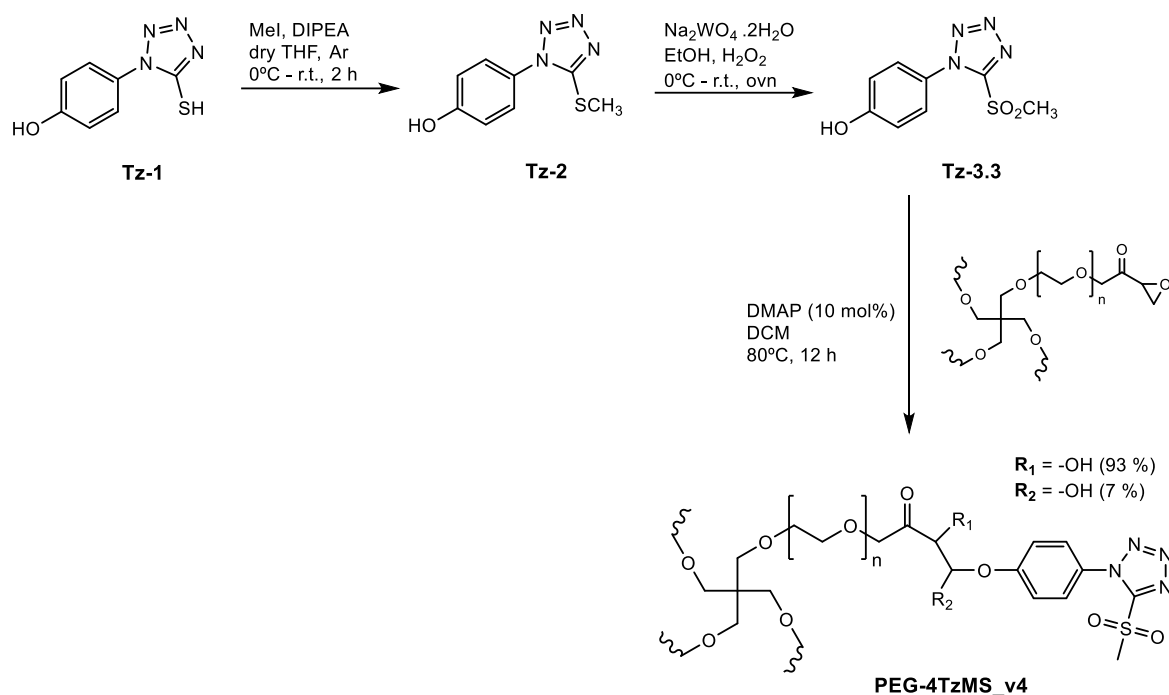
Scheme 3. Proposed synthetic pathway for the preparation of PEG-4TzMS through the coupling of PEG-4Azide and alkyne-TzMS (Tz-4.2).

Quantitative conversion to the triazol group is achieved, meaning that a high degree of functionalization comparable to current synthesis could be achieved (no yield is indicated in the source,²⁸ so degree of functionalization cannot be estimated). As previous alternative, Tz-1 is also used in this pathway as synthesis precursor, so crosslinking kinetics between functionalized PEG and thiols are not expected to be significantly affected (ether bond is maintained). While storage stability is expected from Tz-4.2, azides like PEG-4Azide must be kept away from light (activation into highly reactive intermediates³²) to avoid side reactions. On the other hand, these two precursors should not be prone to hydrolysis in normal storage conditions. The costs of these precursors is also similar to the current synthesis, being the same for Tz-1, and 104 € per g for PEG-4Azide (JenKem), which is slightly more expensive than PEG-4NHS (88 € per g). Alternative pathway 2 involves 4 steps and an overall reaction time of 60 h (vs 75 h of current synthesis). In terms of safety, attention should be paid to copper from last step due to high toxicity, as well as the violent decomposition of certain azides at high temperatures (> 100°C), which highly depends on the structure.³³

Alternative pathway 3. Another alternative approach involves the nucleophilic opening of an epoxide ring as crosslinking reaction (**Scheme 4**). After methylation of the thiol, the resulting methyl sulfide is oxidated following the same conditions described in previous synthesis, that were successfully employed in presence of Tz-2 by Chen *et al.*²² A highly regioselective epoxide opening in presence of the catalyst DMAP at 80°C during 12 h³⁴ is then used to react PEG-4Epoxide with Tz-3.3. With a high conversion of 94 %, the two regioisomers are formed in a 93 and 7 mol% (**Scheme 4**). Apart from the regioisomers, the new chiral C (not indicated in **Scheme 4**) incorporating hydroxyl moiety could result in an enantiomeric mixture.

Additionally, while the epoxide is relatively stable in normal storage conditions, it may be sensitive to hydrolysis in acidic or basic media. Nevertheless, epoxides are much more stable than NHS-esters towards hydrolysis.³⁵

Synthesis of the hydrogel precursor 4armPEG-Tetrazole-Methylsulfone



Scheme 4. Proposed synthetic pathway for the preparation of PEG-4TzMS through the nucleophilic ring opening of PEG-4Epoxide with phenol-TzMS (Tz-3.3).

A high conversion of 94 % was achieved by Brunelli *et al.*³⁴ in the selective epoxide opening with phenol derivatives. Thus, a high degree of functionalization could be expected in this reaction too (no yield is indicated in the source, so degree of functionalization cannot be estimated). Crosslinking kinetics of the final PEG product with thiols should not be significantly affected due to using the same phenol Tz-1 as synthetic precursor (ether bond is maintained). Regarding stability, phenol derivative Tz-3.3 is expected to be very stable in storage conditions due to observed high stability of Tz-1 and Tz-2. Epoxides are relatively stable in normal storage conditions, but hydrolysis may occur under acidic or basic media. Nevertheless, epoxides are much more stable than NHS-esters towards hydrolysis.³⁵ Costs, as in previous pathways, remains similar, with Tz-1 at 3.3 € per g and PEG-4Epoxide at 80 \$ per g (Laysan Bio), which is slightly cheaper than PEG-4NHS (88 € per g). Alternative pathway 3 consists of 3 steps and a total reaction time of 30 h (vs 75 h of current synthesis). Regarding safety, no violent reactions or dangerous reactants/reagents are used in this synthetic pathway.

3.5 Materials and general methods

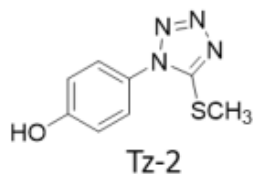
Chemicals and solvents were purchased from Fluka Chemie AG (Taufkirchen, DE), Merck KGaA (Darmstadt, DE), ABCR (Karlsruhe, DE), AcrosOrganics (Geel, BE), TCI (Tokyo, JP) and Sigma-Aldrich Chemie GmbH (Steinheim, DE). Solvents had p.a. purity and were used as purchased. 4arm (20 kDa), polyethyleneglycol (PEG) polymers functionalized with thiol (PEG-SH) and succinimidyl carboxymethyl ester (PEG-NHS) were purchased from Jenkem (Beijin, CN).

TLC plates (ALUGRAM® SIL G/UV254) and silica gel for column chromatography (60 Å pore size, 63-200 µm particle size) were obtained from Macherey-Nagel, (Düren, DE). TLC plates were observed under 254 or 365 nm light. HPLC analysis and purification of the compounds were performed with a HPLC JASCO 4000 (Tokyo, JP) equipped with a diode array, UV/Vis detector and fraction collector. Reprosil C18 columns were used for semi-preparative (250 × 25 mm) and analytical (250 × 5 mm) runs. Solvent gradients using a combination of the following eluents were used: solvent A (MilliQ water + 0.1% TFA) and solvent B (95% acetonitrile (CAN)/5% MilliQ water + 0.1% TFA), with runs over 40 min duration. Automated flash chromatography, using a Biotage® Selekt system equipped with UV/Vis detector and fraction collector, was performed for the purification of some intermediates. Purification of modified polymers was performed by dialysis against acetone and water, using a Spectra/Por 3 dialysis tubing (molecular weight cut-off $M_wCO = 3.5$ kDa) from Repligen (Massachusetts, US), and solvent was renewed at least 4 times.

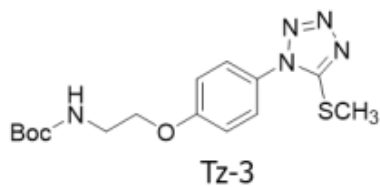
Deuterated solvents were obtained from Deutero GmbH Germany (Kastellaun, DE). Solution 1H NMR spectra were recorded at 25 °C (298 K) on a Bruker Avance 300 MHz, and the solvent residual peak (S.R.P.) was employed as internal reference. The chemical shifts (δ) are informed in parts per million and the coupling constants in Hz. The following abbreviations are used: s-singlet, d-doublet, t-triplet, q-quartet, m-multiplet. The degree of substitution of PEG polymer was calculated by end-group determination. To this purpose, the integral of the signal corresponding to the PEG backbone (3.70-3.40 ppm) was set to 440 H and compared with the integral of the protons corresponding to the bound molecule (the aromatic protons at $\delta = 8.0$ -7.0 ppm and the methylene at $\delta = 4.2$

ppm). Functionalization degrees of >90% and yields of >80% were obtained in all cases. Data was analyzed and plotted with TopSpin.

3.5.1 Synthesis of PEG-4TzMS

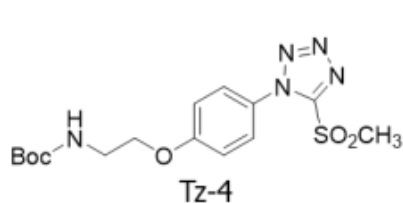


1-(4-Hydroxyphenyl)-5-methylthio-1H-tetrazole (Tz-2). A protocol previously reported by Toda *et al.*¹ was followed, with some modifications. 1-(4-Hydroxyphenyl)-5-mercapto-1H-tetrazole (3.00 g, 15.4 mmol, 1 eq.) was dissolved in THF (65 mL) and the solution was cooled to -10°C using a bath of dry ice in acetone. To this solution, TEA (2.58 mL, 18.5 mmol, 1.2 eq.) and methyl iodide (0.96 mL, 15.4 mmol, 1 eq.) were added, and the reaction mixture was stirred for 3 h at -10°C. The course of the reaction was monitored every 30 min by TLC (50% EtOAc/hexane). When all the starting reactant was consumed (ca 3 h), the reaction mixture was quenched by adding 1 M HCl and allowed to reach room temperature. The organic layer was extracted with EtOAc and then with brine, dried over magnesium sulfate, filtered to remove solids and evaporated. The solid residue was then purified by flash chromatography (45% EtOAc in hexane) and the expected product was obtained in high purity as a white solid (2.90 g, yield= 88 %), and used directly for the next step. Spectroscopic characterization data matched reported values in the literature. ESI-MS⁺: 209.0 (M+H), 439.2 (2M+Na). ¹H NMR (300 MHz, acetone-d₆, δ [ppm]) = 9.13 (1H, s, -OH); 7.46 (2H, dd, J₁= 8.5 Hz, J₂= 1.5 Hz, -CH Ar); 7.08 (2H, dd, J₁= 8.5 Hz, J₂= 1.5 Hz, -CH Ar); 2.79 (3H, s, -SMe). ¹³C NMR (125 MHz, acetone-d₆, δ [ppm]) = 160.00, 155.97, 126.97, 126.27, 117.12, 15.29.



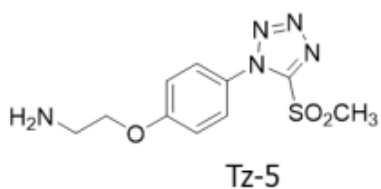
tert-butyl (2-(4-(5-(methylthio)-1H-tetrazol-1-yl)phenoxy)ethyl)carbamate (Tz-3). Compound Tz-2 (2.38 g, 11.5 mmol, 1 eq.) was dissolved in DMF (82 mL), followed by the addition of 2-(Boc-amino)ethyl bromide (3.86 g, 17.2 mmol, 1.50 eq.) and K₂CO₃ (5.24 g, 37.9 mmol, 3.30 eq.) at room temperature. The reaction mixture was stirred at 80°C overnight. Then, another equivalent of 2-(Boc-amino)ethyl bromide was added and again, the reaction was stirred at 80°C overnight. Reaction completion was confirmed by ¹H NMR spectroscopy. The reaction mixture was cooled to 4°C, leading to precipitation of the desired compound. The precipitate was vacuum filtered, washed with cold water, and stirred in a n-Hexane

bath to dissolve non-polar impurities. The residue was again vacuum filtered and dried. The pure product was obtained as a white powder without further purification (3.55 g, yield = 87 %). ESI-MS+: 352.2 (M+H). ¹H NMR (300 MHz, acetone-d₆, δ [ppm]) = 7.60-7.52 (2H, m, -CH Ar); 7.24-7.17 (2H, m, -CH Ar); 6.26 (1H, m, -NH amide), 4.18 (2H, t, S-20 J= 5.7 Hz, -CH₂O), 3.55-3.47 (2H, m, -CH₂NH), 2.79 (3H, s, -SMe), 1.41 (3H, s, -tBu Boc). ¹³C NMR (75 MHz, acetone-d₆, δ [ppm]) = 161.15, 156.73, 156.01, 127.38, 126.87, 116.38, 78.89, 68.23, 40.49, 28.60, 15.38.



tert-butyl (2-(4-(5-(methylsulfonyl)-1H-tetrazol-1-yl)phenoxy)ethyl)carbamate (Tz-4). Compound Tz-3 (3.50 g, 10.0 mmol, 1 eq.) was dissolved in dry DCM (233 mL) and cooled down to 0°C with an ice bath, followed by

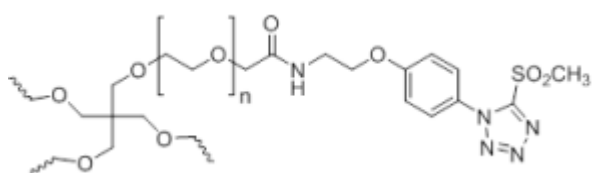
addition of mCPBA (8.59 g, 49.8 mmol, 5 eq.) as a solid. The reaction mixture was stirred overnight at room temperature. The course of the reaction was monitored by mass and ¹H NMR spectroscopy of an aliquot of the reaction mixture, since TLC and analytical HPLC proved not useful because of the similarity in the elution of starting reactant and product (i.e. they both had similar R_f or R_t in a variety of eluents). The reaction mixture was then filtered to remove solids and evaporated. The residue was subjected to flash chromatography (gradient 20-50% EtOAc in n-Hexane) to afford the pure product as a colorless sticky solid (3.44 g, yield = 90 %). ESIMS+: 422.0 (M+K), 687.2 (2M-SO₂Me). ¹H NMR (300 MHz, acetone-d₆, δ [ppm]) = 7.76-7.59 (2H, m, -CH Ar); 7.29-7.12 (2H, m, -CH Ar); 6.27 (1H, m, -NH amide), 4.19 (2H, t, J= 5.6 Hz, -CH₂O), 3.62 (3H, s, -SO₂Me), 3.52 (2H, q, J= 5.6 Hz, -CH₂N), 1.41 (3H, s, -tBu Boc). ¹³C NMR (75 MHz, acetone-d₆, δ [ppm]) = 161.89, 156.86, 155.38, 128.29, 126.88, 116.14, 115.91, 78.99, 68.25, 44.20, 40.54, 28.56.



2-(4-(5-(methylsulfonyl)-1H-tetrazol-1-yl)phenoxy)ethan-1-amine (Tz-5). Compound Tz-4 (0.160 g, 0.56 mmol, 1 eq.) was dissolved in dry DCM (3 mL) and purged with nitrogen. After addition of a DCM/TFA 1:1

mixture (4 mL) the reaction was stirred under inert atmosphere (without nitrogen flow to avoid evaporation of DCM) at room temperature. When consumption of starting reagent was observed (ca. 30-45 min as checked by TLC in 50% EtOAc/hexane), the solvent was

evaporated under strong nitrogen stream and the residue was purified by preparative HPLC (method: 20B to 95 B, 280 nm; r.t.: 12-14 min). The pure product was obtained as a colorless sticky solid (0.102 g, yield = 86 %) and was used for the next reaction immediately. ESI-MS⁺: 284.0 (M+H). ¹H NMR (300 MHz, acetone-d₆, δ [ppm]) = 7.72-7.67 S-21 (2H, m, -CH Ar); 7.27-7.22 (2H, m, -CH Ar); 4.56 (2H, t, J= 5.0 Hz, -CH₂O), 4.35 (2H, t, J= 5.0 Hz, -CH₂NH₂), 3.63 (3H, s, -SO₂Me). ¹³C NMR (75 MHz, acetone-d₆, δ [ppm]) = 161.05; 155.40; 128.40; 127.51; 116.06; 66.07; 47.60; 44.23.



Synthesis of PEG-4TzMS: Freshly prepared compound Tz-5 (0.092 g, 325 μmol, 10 eq.) and N-methylmorpholine (12.8 μL, 117 μmol, 3.6 eq.) were dissolved in dry DMF (2 mL), purged with nitrogen and stirred for 15 min. 20kDa, 4arm PEG-NHS (0.65 g, 32.5 μmol, 1 eq.) was dissolved in dry DMF (3 mL) and added to above solution under argon stream. The mixture was stirred overnight at room temperature under inert atmosphere (without constant Ar stream), then dialyzed in acetone and water, and freeze-dried. A white solid polymer was obtained and characterized by ¹H NMR in DCM-d₂. Functionalization degree was calculated as >95 % and yield was 91 % (0.614 g). The polymer prepared this way proved stable as solid upon >6 months storage at -20°C (evidenced by no changes in ¹H NMR spectrum). ¹H NMR (500 MHz, DCM-d₂, δ [ppm]) = 7.60-7.54 (m, -CH Ar), 7.41 (pseudo-t, -NH), 7.14-7.07 (m, -CH Ar), 4.16 (t, J= 5.5 Hz, -CH₂O), 3.97 (s, -OCH₂C=O PEG); 3.74-3.41 (m, PEG core, -CH₂NH and -SO₂Me group).

*Disclaimer: Text from sections 3.5 (enumerating the materials and methods) and 3.5.1 (describing the reaction protocols) are taken/adapted from my published work: “Thiol-Methylsulfone-Based Hydrogels for Cell Encapsulation: Reactivity Optimization of Aryl-Methylsulfone Substrate for Fine-Tunable Gelation Rate and Improved Stability”– Paez *et al.* - Biomacromolecules – ACS Publications. <https://pubs.acs.org/doi/10.1021/acs.biomac.1c00256> (published 06.06.2021). Reprinted (adapted) with permission from Paez *et al.* Copyright 2021 American Chemical Society.

3.5.2 Cost analysis

Cost of the synthetic pathway was calculated based on:

- i. **Materials.** Amount and commercial price (at the moment of writing this thesis) of raw materials (e.g. **Table 6** for step **a** and **Table 7** for step **b**).

Table 6. Materials data and their costs from the first step of the synthesis (step **a**) after optimization and upscaling (flash chromatography purification). “Cost” column shows the total cost of material that is used at the scale and yield that is indicated in section 3.3.1.1.

	M _w (Da)	Eq	Moles	Density	Amount	Unit	€ per unit	Cost
Tz-1	194.21	1.0	0.015	-	3.00	g	3.60	10.80
MeI	141.94	1.0	0.015	2.28	0.96	mL	0.72	0.69
TEA	101.19	1.2	0.019	0.73	2.58	mL	0.13	0.34
THF	-				65.00	mL	0.040	2.61
EtOAc	-				495.00	mL	0.037	13.28
Hx	-				605.00	mL	0.077	46.46
Cartridge	-				1.00	piece	23.80	23.80

Table 7. Materials data and their costs from the second step of the synthesis (step **b**) after optimization and upscaling (precipitation purification). “Cost” column shows the total cost of material that is used at the scale and yield that is indicated in section 3.3.1.2, including in this case the costs of producing Tz-2 in step **a**.

	M _w (Da)	Eq	Moles	Density	Amount	Unit	€ per unit	Cost
Tz-2	207.25	1.0	0.012	-	2.38	g	132.09	314.38
BocNH_Et_Br	224.10	2.5	0.029	-	6.43	g	32.40	208.45
K₂CO₃	138.21	3.3	0.038	-	5.24	g	0.13	0.68
DMF	-				82.00	mL	0.062	5.08
EtOAc	-				0	mL	0.037	0
Hx	-				200.00	mL	0.077	15.36
Cartridge	-				0	piece	23.80	0

- ii. **Labour.** Active time spent in the lab (e.g. reaction set-up, monitoring, work-up, purification, drying and analysis) and salary of a PhD student (24.17 € per h).
- iii. **Overheads.** Total lab time (from the initial set-up of the reaction to having the pure compound ready for storage) and the cost of using the installations at Leibniz Institute for New Materials (INM) (10.42 € per h).
- iv. **Yield.**

The reaction protocols described in this section were employed to quantify the materials used in each reaction and their associated costs. Subsequently, taking into account the individual yield, the cost of the resultant product at a given scale (whether before or after upscaling), as well as the cost per gram was calculated. Finally, taking into consideration the active man-hours and the total lab use per reaction, the overall cost of each reaction was determined (**Table 6**). In the case of steps **b – e** an adjustment was made to include the production cost of the previous step. Thus, the material costs of Tz-2 – PEG-4TzMS incorporated the production cost of the tetrazole-containing synthesis precursor (e.g. synthesis cost of Tz-2 from step **a** was incorporated in material cost of subsequent step **b**) (**Table 7**).

Bibliography

- (1) Toda, N.; Asano, S.; Barbas, C. F. Rapid, Stable, Chemoselective Labeling of Thiols with Julia-Kociński Like Reagents: A Serum-Stable Alternative to Maleimide-Based Protein Conjugation. *Angew Chem Int Ed Engl* **2013**, *52* (48), 10.1002/anie.201306241. <https://doi.org/10.1002/anie.201306241>.
- (2) Shields, B. J.; Stevens, J.; Li, J.; Parasram, M.; Damani, F.; Alvarado, J. I. M.; Janey, J. M.; Adams, R. P.; Doyle, A. G. Bayesian Reaction Optimization as a Tool for Chemical Synthesis. *Nature* **2021**, *590* (7844), 89–96. <https://doi.org/10.1038/s41586-021-03213-y>.
- (3) Taylor, C. J.; Pomberger, A.; Felton, K. C.; Grainger, R.; Barecka, M.; Chamberlain, T. W.; Bourne, R. A.; Johnson, C. N.; Lapkin, A. A. A Brief Introduction to Chemical Reaction Optimization. *Chem. Rev.* **2023**, *123* (6), 3089–3126. <https://doi.org/10.1021/acs.chemrev.2c00798>.
- (4) Hendershot, D. C.; Sarafinas, A. Safe Chemical Reaction Scale Up. *Chem. Health Saf.* **2005**, *12* (6), 29–35. <https://doi.org/10.1016/j.chs.2005.07.011>.
- (5) Bonneau, M.; Lavenn, C.; Ginet, P.; Otake, K.; Kitagawa, S. Upscale Synthesis of a Binary Pillared Layered MOF for Hydrocarbon Gas Storage and Separation. *Green Chem.* **2020**, *22* (3), 718–724. <https://doi.org/10.1039/C9GC03561C>.
- (6) Fernando, G. S. N.; Sergeeva, N. N.; Frutos, M. J.; Marshall, L. J.; Boesch, C. Novel Approach for Purification of Major Betalains Using Flash Chromatography and Comparison of Radical Scavenging and Antioxidant Activities. *Food Chemistry* **2022**, *385*, 132632. <https://doi.org/10.1016/j.foodchem.2022.132632>.
- (7) Roge, A. B.; Firke, S. N.; Kawade, R. M.; Sarje, S. K.; Vadvalkar, S. M. BRIEF REVIEW ON: FLASH CHROMATOGRAPHY. 2.
- (8) Sandesh, J. S. S.; Shyamala; Swapana, K.; Balaiah, S.; Sharma, J. V. C. A REVIEW ON FLASH CHROMATOGRAPHY AND ITS PHARMACEUTICAL APPLICATIONS. *Journal of Biomedical and Pharmaceutical Research* **2021**, *10* (1), 120–124. <https://doi.org/10.32553/jbpr.v10i1.850>.
- (9) Szegezdi, J.; Csizmadia, F. A Method for Calculating the pKa Values of Small and Large Molecules.
- (10) Danehy, J. P.; Parameswaran, K. N. Acidic Dissociation Constants of Thiols. *J. Chem. Eng. Data* **1968**, *13* (3), 386–389. <https://doi.org/10.1021/je60038a025>.
- (11) Carey, F. A.; Sundberg, R. J. *Advanced Organic Chemistry: Part A: Structure and Mechanisms*; Springer Science & Business Media, 2007.

- (12) Motiwala, H. F.; Kuo, Y.-H.; Stinger, B. L.; Palfey, B. A.; Martin, B. R. Tunable Heteroaromatic Sulfones Enhance In-Cell Cysteine Profiling. *J. Am. Chem. Soc.* **2020**, *142* (4), 1801–1810. <https://doi.org/10.1021/jacs.9b08831>.
- (13) Kakarla, R.; Dulina, R. G.; Hatzenbuehler, N. T.; Hui, Y. W.; Sofia, M. J. Simple and Efficient Method for the Oxidation of Sulfides to Sulfoxides: Application to the Preparation of Glycosyl Sulfoxides. *J. Org. Chem.* **1996**, *61* (23), 8347–8349. <https://doi.org/10.1021/jo961478h>.
- (14) Koo, S.; Ahn, K.; Byeon, S.; Yang, J.; Ji, M.; Choi, S. Selective Oxidation of Sulfides by the Use of an Oxidant System Consisting of Lithium Molybdenate Niobate and Hydrogen Peroxide. WO2001062719A1, August 30, 2001. <https://patents.google.com/patent/WO2001062719A1/en> (accessed 2023-10-10).
- (15) de Miguel-Jiménez, A.; Ebeling, B.; Paez, J. I.; Fink-Straube, C.; Pearson, S.; del Campo, A. Gelation Kinetics and Mechanical Properties of Thiol-Tetrazole Methylsulfone Hydrogels Designed for Cell Encapsulation. *Macromolecular Bioscience* **2023**, *23* (2), 2200419. <https://doi.org/10.1002/mabi.202200419>.
- (16) Ogg, R. A. Jr. The Hydrolysis of Methyl Iodide. *J. Am. Chem. Soc.* **1938**, *60* (8), 2000–2001. <https://doi.org/10.1021/ja01275a507>.
- (17) Mabey, W.; Mill, T. Critical Review of Hydrolysis of Organic Compounds in Water under Environmental Conditions. *Journal of Physical and Chemical Reference Data* **1978**, *7* (2), 383–415. <https://doi.org/10.1063/1.555572>.
- (18) Ragnarsson, U.; Grehn, L. Dual Protection of Amino Functions Involving Boc. *RSC Advances* **2013**, *3* (41), 18691–18697. <https://doi.org/10.1039/C3RA42956C>.
- (19) Luo, X.; Ma, X.; Lebreux, F.; Markó, I. E.; Lam, K. Electrochemical Methoxymethylation of Alcohols – a New, Green and Safe Approach for the Preparation of MOM Ethers and Other Acetals. *Chem. Commun.* **2018**, *54* (71), 9969–9972. <https://doi.org/10.1039/C8CC05843A>.
- (20) Yang, Q.; Sheng, M.; Henkelis, J. J.; Tu, S.; Wiensch, E.; Zhang, H.; Zhang, Y.; Tucker, C.; Egeh, D. E. Explosion Hazards of Sodium Hydride in Dimethyl Sulfoxide, N,N-Dimethylformamide, and N,N-Dimethylacetamide. *Org. Process Res. Dev.* **2019**, *23* (10), 2210–2217. <https://doi.org/10.1021/acs.oprd.9b00276>.
- (21) Davis, O. A.; Bull, J. A. Synthesis of Di-, Tri-, and Tetrasubstituted Oxetanes by Rhodium-Catalyzed O=H Insertion and C=C Bond-Forming Cyclization. *Angew Chem Int Ed Engl* **2014**, *53* (51), 14230–14234. <https://doi.org/10.1002/anie.201408928>.
- (22) Wong, C.-H.; Zimmerman, S. C. Orthogonality in Organic, Polymer, and Supramolecular Chemistry: From Merrifield to Click Chemistry. *Chem. Commun.* **2013**, *49* (17), 1679–1695. <https://doi.org/10.1039/C2CC37316E>.
- (23) Paez, J. I.; de Miguel-Jiménez, A.; Valbuena-Mendoza, R.; Rathore, A.; Jin, M.; Gläser, A.; Pearson, S.; del Campo, A. Thiol-Methylsulfone-Based Hydrogels for Cell Encapsulation: Reactivity Optimization of Aryl-Methylsulfone Substrate for Fine-Tunable Gelation Rate and Improved Stability. *Biomacromolecules* **2021**, *22* (7), 2874–2886. <https://doi.org/10.1021/acs.biomac.1c00256>.
- (24) Chen, X.; Wu, H.; Park, C.-M.; Poole, T. H.; Keceli, G.; Devarie-Baez, N. O.; Tsang, A. W.; Lowther, W. T.; Poole, L. B.; King, S. B.; Xian, M.; Furdui, C. M. Discovery of Heteroaromatic Sulfones As a New Class of Biologically Compatible Thiol-Selective Reagents. *ACS Chem Biol* **2017**, *12* (8), 2201–2208. <https://doi.org/10.1021/acscchembio.7b00444>.
- (25) Bian, S.; He, M.; Sui, J.; Cai, H.; Sun, Y.; Liang, J.; Fan, Y.; Zhang, X. The Self-Crosslinking Smart Hyaluronic Acid Hydrogels as Injectable Three-Dimensional Scaffolds for Cells Culture. *Colloids and Surfaces B: Biointerfaces* **2016**, *140*, 392–402. <https://doi.org/10.1016/j.colsurfb.2016.01.008>.
- (26) Echalié, C.; Valot, L.; Martínez, J.; Mehdi, A.; Subra, G. Chemical Cross-Linking Methods for Cell Encapsulation in Hydrogels. *Materials Today Communications* **2019**, *20*, 100536. <https://doi.org/10.1016/j.mtcomm.2019.05.012>.

- (27) Gao, Y.; Peng, K.; Mitragotri, S. Covalently Crosslinked Hydrogels via Step-Growth Reactions: Crosslinking Chemistries, Polymers, and Clinical Impact. *Advanced Materials* **2021**, *33* (25), 2006362. <https://doi.org/10.1002/adma.202006362>.
- (28) Zhao, Y.; Chai, Z.; Zeng, Q.; Zhang, W.-X. Overview of 1,5-Selective Click Reaction of Azides with Alkynes or Their Synthetic Equivalents. *Molecules* **2023**, *28* (3), 1400. <https://doi.org/10.3390/molecules28031400>.
- (29) Chen, G.; Tao, L.; Mantovani, G.; Admiral, V.; Burt, D. P.; Macpherson, J. V.; Haddleton, D. M. Synthesis of Azide/Alkyne-Terminal Polymers and Application for Surface Functionalisation through a [2 + 3] Huisgen Cycloaddition Process, "Click Chemistry." *Soft Matter* **2007**, *3* (6), 732–739. <https://doi.org/10.1039/B618325E>.
- (30) Fong, D.; Andrews, G. M.; Adronov, A. Functionalization of Polyfluorene-Wrapped Carbon Nanotubes via Copper-Mediated Azide–Alkyne Cycloaddition. *Polym. Chem.* **2018**, *9* (21), 2873–2879. <https://doi.org/10.1039/C8PY00377G>.
- (31) Presolski, S. I.; Hong, V. P.; Finn, M. G. Copper-Catalyzed Azide–Alkyne Click Chemistry for Bioconjugation. *Curr Protoc Chem Biol* **2011**, *3* (4), 153–162. <https://doi.org/10.1002/9780470559277.ch110148>.
- (32) Haldón, E.; Nicasio, M. C.; Pérez, P. J. Copper-Catalysed Azide–Alkyne Cycloadditions (CuAAC): An Update. *Org. Biomol. Chem.* **2015**, *13* (37), 9528–9550. <https://doi.org/10.1039/C5OB01457C>.
- (33) Gracia, E.; García, M. T.; De Lucas, A.; Rodríguez, J. F.; Gracia, I. Copper Wire as a Clean and Efficient Catalyst for Click Chemistry in Supercritical CO₂. *Catalysis Today* **2020**, *346*, 65–68. <https://doi.org/10.1016/j.cattod.2018.12.021>.
- (34) Zhang, Y.; Tan, J.; Chen, Y. Visible-Light-Induced Protein Labeling in Live Cells with Aryl Azides. *Chem. Commun.* **2023**, *59* (17), 2413–2420. <https://doi.org/10.1039/D2CC06987C>.
- (35) Schock, M.; Bräse, S. Reactive & Efficient: Organic Azides as Cross-Linkers in Material Sciences. *Molecules* **2020**, *25* (4), 1009. <https://doi.org/10.3390/molecules25041009>.
- (36) Brunelli, N. A.; Long, W.; Venkatasubbaiah, K.; Jones, C. W. Catalytic Regioselective Epoxide Ring Opening with Phenol Using Homogeneous and Supported Analogues of Dimethylaminopyridine. *Top Catal* **2012**, *55* (7), 432–438. <https://doi.org/10.1007/s11244-012-9822-2>.
- (37) Seurnyck-Servoss, S. L.; Baird, C. L.; Rodland, K. D.; Zangar, R. C. Surface Chemistries for Antibody Microarrays. *FBL* **2007**, *12* (10), 3956–3964. <https://doi.org/10.2741/2362>.

4 Rheological characterization of crosslinking kinetics and mechanical properties

Title: Gelation Kinetics and Mechanical Properties of Thiol-Tetrazole Methylsulfone Hydrogels Designed for Cell Encapsulation

Published in: Macromolecular bioscience (on 01 December 2022)

Authors: Adrián de Miguel-Jiménez, Bastian Ebeling, Julieta I. Paez, Claudia Fink-Straube, Samuel Pearson, Aránzazu del Campo

Citation: de Miguel-Jiménez, A., Ebeling, B., Paez, J. I., Fink-Straube, C., Pearson, S., & Del Campo, A. (2023). Gelation Kinetics and Mechanical Properties of Thiol-Tetrazole Methylsulfone Hydrogels Designed for Cell Encapsulation. *Macromolecular bioscience*, 23(2), 2200419, doi/10.1002/mabi.202200419.

Author's Contribution:

- Adrián de Miguel-Jiménez: Designed and performed most experiments, Data interpretation, Validation, Formal analysis, Investigation, Writing (Original draft, review and editing).
- Bastian Ebeling: Performed computational studies, Data interpretation, Writing.
- Julieta I. Paez: Data interpretation, Writing - review & editing.
- Claudia Fink-Straube: Performed mass spectrometry characterization, Data interpretation.
- Samuel Pearson: Data interpretation, Writing - review & editing, Supervision.
- Aránzazu del Campo: Original idea, Data interpretation, Writing - review & editing, Supervision, Funding acquisition.

Gelation Kinetics and Mechanical Properties of Thiol-Tetrazole Methylsulfone Hydrogels Designed for Cell Encapsulation

Adrián de Miguel-Jiménez, Bastian Ebeling, Julieta I. Paez, Claudia Fink-Straube, Samuel Pearson,* and Aránzazu del Campo*

Hydrogel precursors that crosslink within minutes are essential for the development of cell encapsulation matrices and their implementation in automated systems. Such timescales allow sufficient mixing of cells and hydrogel precursors under low shear forces and the achievement of homogeneous networks and cell distributions in the 3D cell culture. The previous work showed that the thiol-tetrazole methylsulfone (TzMS) reaction crosslinks star-poly(ethylene glycol) (PEG) hydrogels within minutes at around physiological pH and can be accelerated or slowed down with small pH changes. The resulting hydrogels are cytocompatible and stable in cell culture conditions. Here, the gelation kinetics and mechanical properties of PEG-based hydrogels formed by thiol-TzMS crosslinking as a function of buffer, crosslinker structure and degree of TzMS functionality are reported. Crosslinkers of different architecture, length and chemical nature (PEG versus peptide) are tested, and degree of TzMS functionality is modified by inclusion of RGD cell-adhesive ligand, all at concentration ranges typically used in cell culture. These studies corroborate that thiol/PEG-4TzMS hydrogels show gelation times and stiffnesses that are suitable for 3D cell encapsulation and tunable through changes in hydrogel composition. The results of this study guide formulation of encapsulating hydrogels for manual and automated 3D cell culture.

1. Introduction

Hydrogels have broad use as biomaterials, ranging from scaffolds for fundamental cell studies to translational products in sprayable, injectable, and implantable formats.^[1] They are particularly appealing for generating cell-laden constructs as 3D cultures or cell-based therapeutic products. Crosslinking of liquid precursors is performed in the presence of the cells, and the networks can be designed with features that emulate the native extracellular environment.^[2] Hydrogel matrices that allow reliable and automatable 3D cell encapsulation are important in these contexts.


The properties of the crosslinking reaction are fundamental for successful 3D cell encapsulation. The reaction needs to i) work at near-physiological conditions, ii) proceed at a rate that permits complete mixing and homogeneous cell suspension, iii) reach completion in the presence of other reactive groups in the biological milieu, iv) form linkages that are stable over a desired timescale, and v) be cytocompatible. To reach widespread adoption, the

pre-polymers bearing the crosslinkable groups should also be easily attained and stable in storage.

A. de Miguel-Jiménez, J. I. Paez, C. Fink-Straube, S. Pearson, A. del Campo
 INM – Leibniz Institute for New Materials
 Campus D2 2, 66123 Saarbrücken, Germany
 E-mail: samuel.pearson@leibniz-inm.de;
 aranzazu.delcampo@leibniz-inm.de

A. de Miguel-Jiménez, A. del Campo
 Chemistry Department
 Saarland University
 66123 Saarbrücken, Germany
 B. Ebeling
 Kuraray Europe GmbH
 Advanced Interlayer Solutions
 Competence Center for Innovation & Technology
 Mülheimer Str. 26, 53840 Troisdorf, Germany

J. I. Paez
 Current address: Department of Developmental BioEngineering
 Technical Medical Centre
 University of Twente
 Enschede The Netherlands

 The ORCID identification number(s) for the author(s) of this article can be found under <https://doi.org/10.1002/mabi.202200419>

© 2022 The Authors. Macromolecular Bioscience published by Wiley-VCH GmbH. This is an open access article under the terms of the Creative Commons Attribution-NonCommercial License, which permits use, distribution and reproduction in any medium, provided the original work is properly cited and is not used for commercial purposes.

DOI: 10.1002/mabi.202200419

We recently demonstrated that thiol-methylsulfone (MS) coupling chemistry is promising for 3D cell encapsulation, with starPEG-based derivatives meeting all the above criteria and thereby surpassing some of the limitations of the commonly used thiol/maleimide (Mal) and thiol/vinylsulfone (VS) crosslinking systems.^[3,4] The three tested MS candidates – oxadiazole (OxMS), tetrazole (TzMS) and benzothiazole (BtMS) – reliably formed hydrogels that were cytocompatible, with L929 fibroblasts demonstrating >92% viability after 7 days culture.^[4] Encapsulated fibroblast spheroids showed cell spreading and active migration indicating both recognition of cell-adhesive RGD ligands and degradation of the matrix metalloproteinase (MMP)-cleavable peptidic bonds provided by the VPM crosslinker.^[3] More sensitive human umbilical vein endothelial cells demonstrated >94% viability after 1 day,^[3] showing comparable cytocompatibility to other prevalent PEG-based gelation systems.^[5] Thiol/MS crosslinking of PEG-based gels therefore proved suitable for various 3D cell encapsulation scenarios on the basis of cell viability, morphogenesis, and migration studies. The three MS candidates showed differences in gelation rate, stability in long-term cell culture, and ease and cost of synthesis, with the TzMS derivative emerging as the leading option across all of these metrics. PEG-4TzMS gels formed on a minutes timescale at pH 7.5.^[4] The thiol-TzMS gels were the most stable of the three derivatives, enduring for 15 days under cell culture conditions.^[4] The TzMS-derivatized PEG polymers could also be synthesized cheaply on gram scale, and showed excellent stability in storage and in aqueous solution.

The rheological study of crosslinking kinetics and mechanical properties of PEG-4TzMS was performed on hydrogels with 20 kDa PEG-4SH as a model crosslinker.^[4] However, in cell encapsulation and culture studies precursors need to be pre-functionalized with adhesive ligands and crosslinked with degradable peptides of different length and functionality, which influence the gelation kinetics and final properties of the hydrogel. These parameters are adjusted in cell cultures to meet the needs of individual cell types, and their impact in the gelation process and the network properties are important to understand.^[6] Recent studies highlight the implications of gelation rate in the local gel homogeneity, and its consequences for the mechanics of the network and reproducibility of the final cell experiments.^[7] Along this line, the present work compares the gelation kinetics and final mechanical properties of PEG-4TzMS-based hydrogels using PEG-4SH, linear PEG-dithiols and VPM as crosslinkers, and with incorporation of cell-adhesive ligand RGD prior to crosslinking. Different pH and buffering conditions are explored as additional handles to control the gelation process. We aim to facilitate the establishment of cell culture models based on PEG-TzMS hydrogels by illustrating how compositional changes might impact the quality and properties of the final networks.

2. Results

Hydrogels in this work are based on 20 kDa 4-arm starPEG end-functionalized with TzMS groups at degrees of functionalization, denoted F_{TzMS} , of >95%.^[3] Crosslinking was achieved with PEG-4SH (20 kDa) or dithiols of different molar masses and either PEG or peptidic backbones. For each crosslinker, the degree

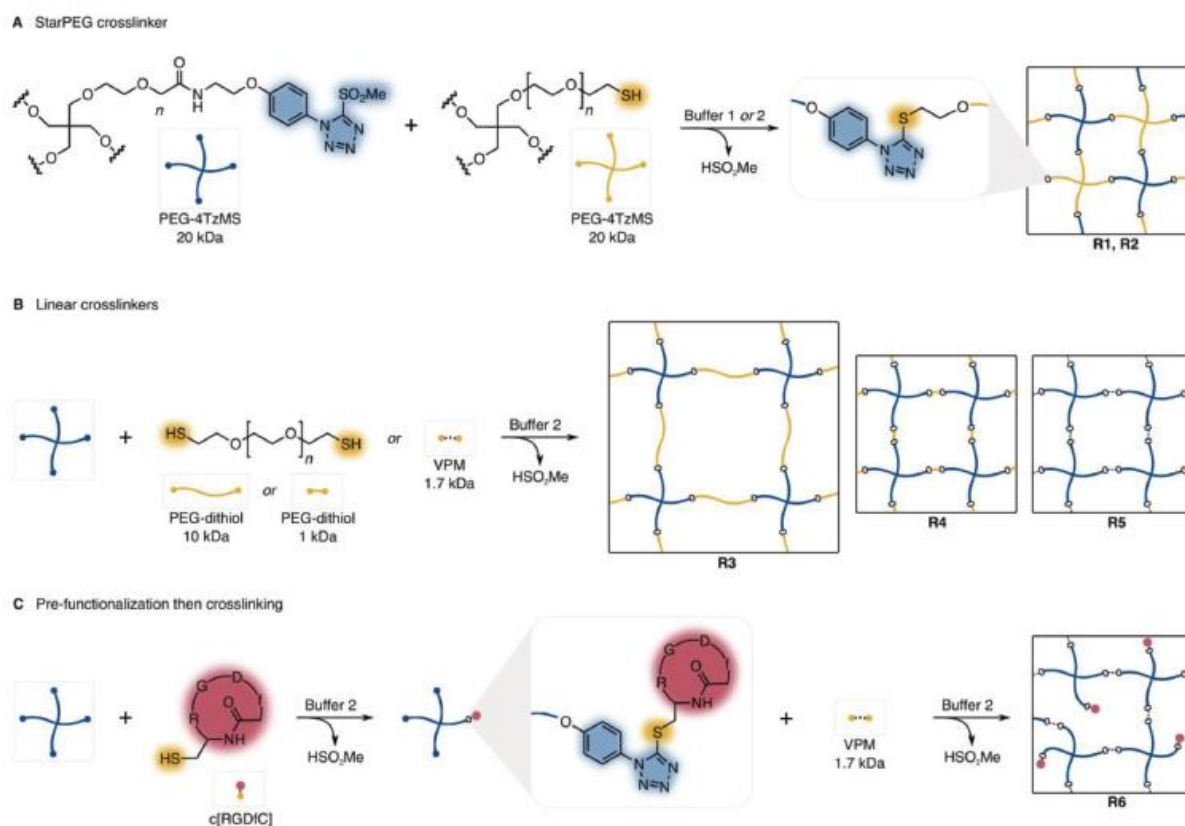
of thiol functionalization is represented by F_{SH} . For the rheology measurements, PEG-4TzMS and thiol solutions in the corresponding buffer were mixed directly on the rheometer plate at 25 °C, and the evolution of shear storage (G') and loss (G'') moduli was monitored throughout crosslinking. The addition sequence, volume, and mixing protocol are important for reproducibility and are detailed in the experimental section. All rheology curves start at 1 min, which was the time needed for mixing of the gel precursor solution and launch of the instrument. To compare crosslinking kinetics among the different formulations, we selected the time required for $G' > 50$ Pa (denoted t_{50Pa}) as a proxy for the gelation onset, since the conventionally used^[8] crossover of G' and G'' was not always observed. The value of G' at minute 40 (G'_{40min}) was taken as a measure of the crosslinking degree achieved at different pH values within a given formulation, and for comparing the stiffness across the different hydrogel formulations.

All experiments in our study were performed keeping the total polymer content in the hydrogels at 5.0% w/v. This is a typical polymer concentration used for cell encapsulation with 20 kDa starPEGs.^[3,5,6] The concentration of the individual precursors was fixed such that $[SH]:[MS] = 1:1$. The exact stoichiometry was calculated for each polymer batch considering the degree of functionalization and the molar mass from ¹H NMR analysis of the PEG precursors (Figures S1 and S2 and Table S1, Supporting Information) or the purity degree from HPLC analysis in the case of the peptide reactants (Table S2, Supporting Information). We anticipate that this procedure leads to hydrogels with higher G' values than when using the molar mass and end group determination taken from the suppliers' material data sheets for the calculation.^[4] An exact 1:1 ratio of reactive groups should lead to more complete crosslinking and fewer network defects.^[9]

2.1. The Importance of Buffer Selection

The thiol-MS reaction is sensitive to pH in two ways (Scheme 1). First, the initial pH of the medium affects the concentration of the nucleophilic thiolate as reactive intermediate. Higher initial reaction rates are therefore expected at higher pH values. Second, the methanesulfinic acid byproduct of the thiol-MS reaction can lead to a progressive decline in pH value during the reaction if the proton concentration exceeds the buffering capacity of the medium. This can slow down the reaction and reduce the conversion (i.e., crosslinking) degree.^[3] We therefore first tested the pH progression during gelation in our working conditions and searched for a buffer system that could maintain a stable pH.

In our experiments, precursor solutions were prepared at the target pH values. Initial experiments were performed by crosslinking PEG-4TzMS with PEG-4SH in 10 mM HEPES buffer at pH 8.0, 7.5, and 7.0 (R1, Table 1). In these conditions, we observed lower initial gelation rate and less stiff gels at lower initial pH values (Figure 1A), as reflected in the higher t_{50Pa} and lower G'_{40min} values (Table 1). pH monitoring of separate solutions with the same compositions as the rheology experiments showed a sharp decline in the pH of the reaction mixtures within 1 min of mixing, followed by a slower decline over the remainder of the 40 min measurement time (Figure 1A). Over the 40 min reaction time, decreases of >1.6 pH units in the pH 7.0 system,



Scheme 1. Overview of representative networks formed by PEG-4TzMS reaction with A) PEG-4SH, B) Linear crosslinkers PEG-dithiol (10 and 1 kDa) and VPM, and C) c[RGDfC] as a prefunctionalization step before reaction with VPM. **R1–R6** refer to the rheology experiments in Table 1. Buffer 1 = 10 mM HEPES, Buffer 2 = 20 mM HEPES + 40 mM sodium bicarbonate, VPM = GCRDVPMSMRGGDRCG peptide.

0.9 pH units in the pH 7.5 system, and 0.8 pH units in the pH 8.0 system were observed. These results indicate that at the reactive group concentrations used in **R1**, the buffering capacity of 10 mM HEPES was insufficient to combat the generated methanesulfonic acid and maintain stable pH values. The expected trend of slower gelation at lower initial pH values is therefore amplified by the subsequent drops in pH value, which were more dramatic at lower initial pH values since pH declines significantly below the optimum buffering range for HEPES ($pK_a \approx 7.6$).^[10] The slow reaction at pH 7.0 meant t_{50Pa} exceeded 10 min, and the G'_{40min} of just 650 Pa shows that the crosslinking degree in this system was far inferior to those at higher pH values, due to the combined effects of low initial pH and declining pH as crosslinking proceeded.

To maintain a stable pH during crosslinking, we adopted a buffering system containing 20 mM HEPES and 40 mM sodium bicarbonate. Bicarbonate buffers are the most prevalent for cell culture, and concentrations from 22 mM (i.e., physiological concentration) to 44 mM are standard.^[11] HEPES concentrations up to 25 mM are typically included in 3D cell culture medium to provide additional buffering capacity to bicarbonate. The buffer concentrations in this work are therefore within cytocompati-

ble ranges. During the gelation of PEG-4TzMS and PEG-4SH using this buffer (**R2**, Table 1) considerably smaller pH drops of <0.3 pH units were observed (Figure 1B). At a given initial pH value, t_{50Pa} was shorter and G'_{40min} was higher than in experiments using 10 mM HEPES (**R1**). At pH 7.0 for example, t_{50Pa} decreased from 11.1 (**R1**) to 3.0 min (**R2**), and G'_{40min} increased from 660 to 5590 Pa. These results confirm that the slower kinetics and lower conversions at lower initial pH values in **R1** are a result of declining pH value throughout crosslinking. Interestingly, higher values of G'_{40min} were obtained with decreasing pH value in **R2**; G'_{40min} was 3560 Pa at pH 8.0, 4690 Pa at pH 7.5, and 5590 Pa at pH 7.0. In line with previous work, we hypothesize that the slower crosslinking rate at lower pH leads to formation of a more homogeneous and complete network that achieves higher stiffness values by limiting the extent to which the reaction proceeds during the mixing phase wherein the reactive partners are inhomogeneously distributed.^[3] In contrast, G'_{40min} in **R1** was lowest at pH 7.0 because this system exhibited the greatest decline in pH value and the reaction became prohibitively slow. The 20 mM HEPES and 40 mM sodium bicarbonate buffer was used for the remaining experiments in this paper.

Table 1. Experimental parameters and results of the rheology experiments performed in this work.

# ^{a)}	PEG-4TzMS [% w/v]	c[RGDFC] [mM]	$F_{TzMS,final}$ [%] ^{b)}	[MS] _{final} [mM]	Crosslinker [% w/v]	[SH] _{theor} ^{c)} [mM]	[SH]:[MS] _{theor}	[P] _{total} [% w/v]	Buffer ^{d)}	pH _{initial}	t_{50Pa} [min] ^{e)}	G'_{40min} [Pa]
R1	2.55	-	98.3	4.40	20 kDa PEG-4SH 2.49	4.48	1.02	5.04	1	8.0	1.2 ± 0.1	4208 ± 480
										7.5	2.9 ± 0.1	3694 ± 140
										7.0	11.1 ± 0.4	650 ± 29
R2	2.54	-	96.4	4.39	20 kDa PEG-4SH 2.49	4.39	1.00	5.03	2	8.0	<1	3560 ± 895
										7.5	1.2 ± 0.2	4685 ± 692
										7.0	3.0 ± 0.3	5590 ± 937
R3	2.37	-	96.4	4.24	10 kDa PEG-dithiol 2.66	4.24	1.00	5.03	2	8.0	2.2 ± 0.2	1013 ± 289
										7.5	3.8 ± 0.1	967 ± 146
R4	4.50	-	96.4	8.14	1 kDa PEG-dithiol 0.56	8.14	1.00	5.06	2	8.0	<1	2422 ± 161
										7.5	1.8 ± 0.1	3080 ± 486
R5	4.43	-	96.4	7.74	VPM 0.65	7.74	1.00	5.08	2	8.0	<1	840 ± 233
										7.5	1.6 ± 0.2	1149 ± 348
R6	4.46	1.29	83.3 ^{f)}	6.55	VPM 0.54	6.20	0.95	4.98 ^{g)}	2	8.0	<1	321 ± 94
										7.5	4.1 ± 0.9	272 ± 125
										7.0	6.3 ± 1.1	243 ± 147

^{a)} Rheometer settings: $T = 25$ °C, $V_{total} = 36.0$ μ L, gap = 300 μ m, strain = 1%, frequency = 1 Hz; ^{b)} $F_{TzMS,final}$ = degree of functionality of the starPEG immediately prior to crosslinking, i.e., the percentage of end groups that bear the TzMS function; ^{c)} This theoretical value is the expected thiol content of the crosslinkers based on ¹H NMR spectroscopy (PEG-based crosslinkers) and HPLC (VPM) analyses; ^{d)} Buffer 1: 10 mM HEPES. Buffer 2: 20 mM HEPES + 40 mM sodium bicarbonate; ^{e)} Values < 1 min indicate that the G' was above 50 kPa at the 1 min timepoint; ^{f)} Value determined by ¹H NMR spectroscopy of isolated polymer; ^{g)} Overall mass does not consider the mass contributed by the c[RGDFC] ligand.

2.2. The Influence of Crosslinker Architecture and Molar Mass

Linear dithiol crosslinkers and degradable peptides terminated with cysteine residues are often used in the formulation of PEG-based hydrogels for cell culture.^[12,13] We compared the gelation kinetics and the properties of PEG-4TzMS hydrogels crosslinked with linear dithiols of two different molar masses: a 10 kDa PEG-dithiol (**R3**, Table 1), which offers the same thiol content per unit mass as the PEG-4SH but without the star structure, and a 1 kDa PEG-dithiol (**R4**, Table 1) which is shorter than the 10 kDa analog, but has similar length to a typical MMP-degradable peptide crosslinker. Finally, experiments with the 1.7 kDa degradable peptide VPM bearing two cysteines (**R5**, Table 1) were also performed.

Hydrogels with 10 kDa PEG-dithiol as crosslinker (**R3**) presented longer t_{50Pa} and smaller G'_{40min} values than **R2** hydrogels crosslinked with PEG-4SH (Figure 1C, Table 1). This agrees with the lower concentration of network points (Scheme 1). Only the star PEG-4TzMS molecule, which is present at 2.4% w/v, can contribute network points after crosslinking, with the 2.6% w/v of linear 10 kDa PEG-dithiol serving only as a connector between stars. Hydrogels crosslinked with 1 kDa PEG-dithiol (**R4**) showed faster crosslinking and higher final stiffnesses than **R3** hydrogels (Figure 1D, Table 1). The molar concentration of reactive groups present in the **R4** systems was almost double that in **R3** (for a constant polymer total concentration of 5% w/v), and this translated to a faster rise in G' . The **R4** systems also had almost twice the concentration of PEG-4TzMS than the **R3** hydrogels (Table 1). The higher concentration of network points explains the higher G'_{40min} values.

During crosslinking of **R4** hydrogels at pH 8.0, an initial drop of 0.4–0.5 pH units was observed (Figure 1D). This is due to the relatively high concentration of reactive groups generating considerable amounts of methanesulfonic acid in the beginning of the crosslinking process. The initial decline in pH was less pronounced at pH 7.5, presumably due to the lower initial rate of acid generation and the better buffering ability of the HEPES component of the buffer at pH 7.5 given its pKa of ≈ 7.6 .^[10] Hydrogels containing the peptidic dithiol crosslinker VPM (**R5**) showed similar t_{50Pa} to hydrogels crosslinked with 1 kDa PEG-dithiol (**R4**), but approximately threefold lower G'_{40min} values (Figure 1E, Table 1). The reactive group concentration, the PEG-4TzMS mass content, and the concentration of network points in **R5** are $\approx 10\%$ lower than in **R4**, which partially explain the lower stiffness of the final hydrogel. Deviation from expected 1:1 reactive group stoichiometry in the VPM system could also lower the stiffness, and is explored in Section 2.4.

2.3. The Effect of Pre-Functionalization with Cell-Adhesive Ligand

To serve as artificial matrices for 3D cell culture, PEG hydrogels need to be biofunctionalized with cell-adhesive moieties such as the RGD peptide.^[14,15] In our system, thiolated bioactive molecules can be incorporated into the gel network by pre-incubation with the PEG-4TzMS pre-polymer. This step consumes reactive sites, and is expected to affect t_{50Pa} and G'_{40min} values by decreasing the concentration of MS groups available for crosslinking. The higher the adhesive ligand content, the lower the reactive sites available for crosslinking.

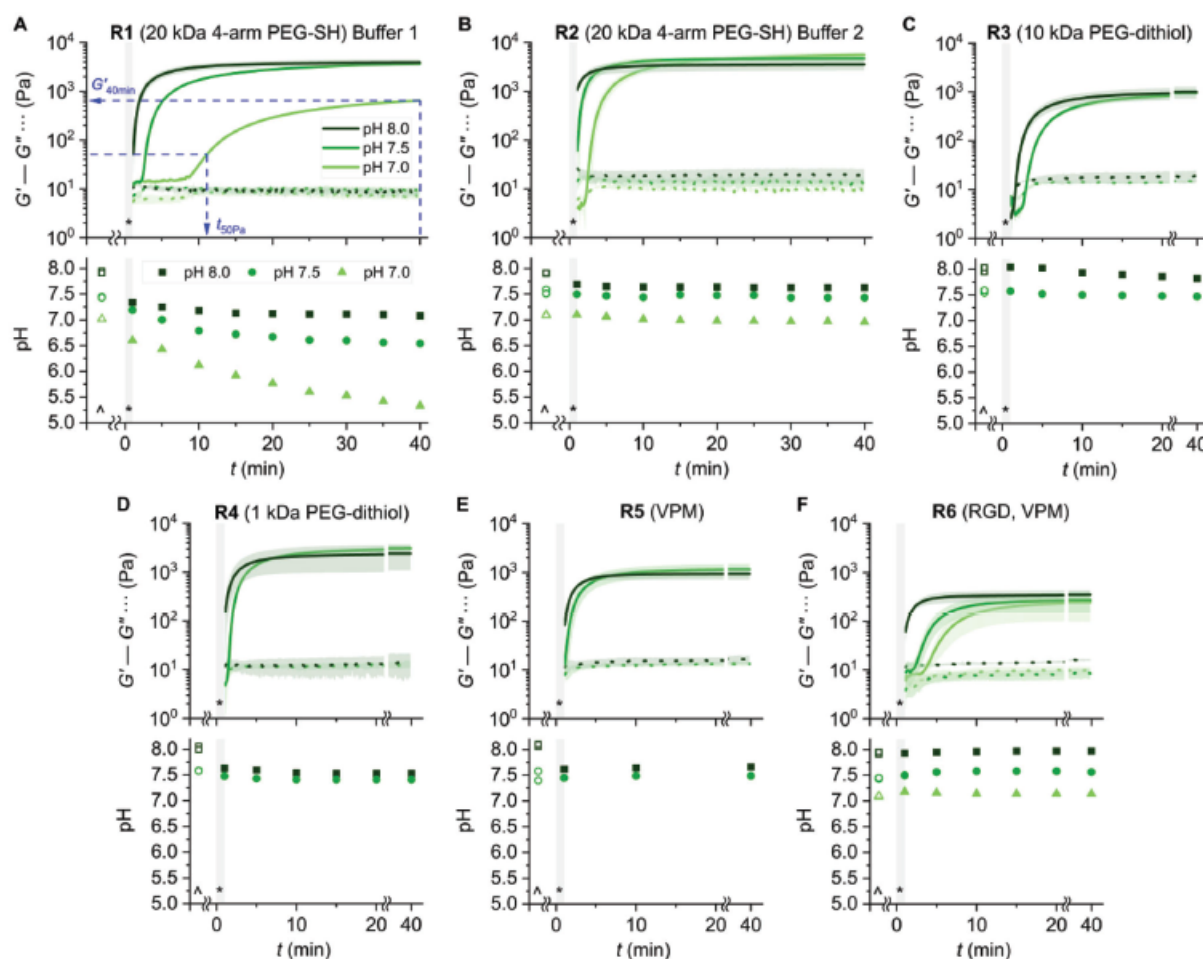


Figure 1. Rheology and pH monitoring during gelation of PEG-4TzMS and crosslinkers. A) R1, B) R2, C) R3, D) R4, E) R5, and F) R6, conditions in Table 1; $N = 3$ at all pH values for rheology, except R6 for which $N = 4$. $N = 1$ for all pH tracking points. $\hat{\ast}$ = time period for solution mixing and rheometer launch (60 s). $\hat{\ast}$ = time period before mixing during which pH values of precursor solutions were measured.

We explored the effect of $c[\text{RGDfC}]$ incorporation on the gelation rate and final mechanical properties of resulting hydrogels. In the following, we express ligand content in terms of the degree of functionality of the TzMS units (F_{TzMS}), i.e., the proportion of end groups carrying the TzMS function, since this accounts for any variability in the degree of functionality of precursor polymers. PEG-4TzMS ($F_{\text{TzMS}} = 0.964$) was incubated with $c[\text{RGDfC}]$ at a molar ratio that targeted $F_{\text{TzMS}} = 0.80$ after complete reaction. ^1H NMR spectroscopy analysis confirmed that $c[\text{RGDfC}]$ (Figure 2A) was covalently attached to PEG-4TzMS (Figure 2B), with the aromatic proton signal “b” at 7.6 ppm shifting 0.1 ppm upfield upon thiol substitution of the MS group (Figure 2C). A similar shift in the 7.6 ppm proton signal upon thiol substitution was also observed for model substitutions with mercaptoethanol (data not shown). Integration of the aromatic proton signals in Figure 2C showed incorporation of the $c[\text{RGDfC}]$ ligand to give F_{TzMS} of 0.83, which is slightly higher than the expected value of 0.80 and indicates that a portion of the feed $c[\text{RGDfC}]$ ($\approx 20\%$) was not incorporated into the 4-arm starPEG.

The gelation of hydrogels crosslinked with VPM after functionalization with $c[\text{RGDfC}]$ (R6) was then characterized. $t_{50\text{Pa}}$ ranged from just over 1 min at pH 8.0 to 4 min at pH 7.5 and 6 min at pH 7.0. These $t_{50\text{Pa}}$ values are significantly longer than in the non-biofunctionalized hydrogel R5, in agreement with the lower number of reactive groups available for building the network. In line with this argument, $G'_{40\text{min}}$ was also approximately threefold lower (Table 1), reaching 240–320 Pa across the three tested pH values. In decreasing the overall proportion of end groups with TzMS functions, the prefunctionalization step changes the distribution of PEG molecules bearing 0, 1, 2, 3, and 4 terminal TzMS groups. The expected distributions can be determined theoretically and depend on the reaction conditions for the (de)functionalization of arms. The resulting distributions were deduced for the limiting cases of diffusion and reaction control by simulations (see Supporting Information for details). Figure 3 shows the mean distributions for both studied systems with the black vertical bars indicating the possible range defined by the limiting cases. In PEG-4TzMS ($F_{\text{TzMS}} = 0.964$, Figure 3A),

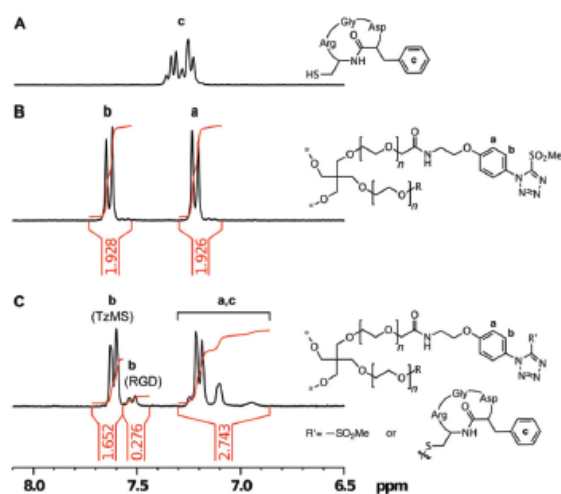


Figure 2. ^1H NMR spectra (300 MHz, D_2O) of A) c[RGDFc], B) PEG-4TzMS, and C) the purified polymer after reaction with c[RGDFc] to give $F_{\text{TzMS}} = 0.83$. Reaction conditions: pH 8.0, 20 mM HEPES with 40 mM sodium bicarbonate, 1 h reaction time.

96.4–99.3% of the stars bear 3 or 4 TzMS groups and can therefore generate network points during crosslinking. After RGD functionalization ($F_{\text{TzMS}} = 0.833$, Figure 3B), 13.2–15.0% of stars carry ≤ 2 TzMS functions. Species with 2 active arms (10.9–11.6% of stars) can act only as linear chain extenders during the crosslinking process with VPM and are not able to contribute network points, and species with only one active arm (1.6–3.1% of stars) can only be incorporated into the network as terminal units. Only the 85.0–86.7% of remaining stars (3 or 4 arms bearing TzMS) can introduce network points when reacted with VPM.

2.4. Maximizing $G'_{40\text{min}}$ by Varying the Reactive Group Stoichiometry with VPM Crosslinkers

Throughout this work, a 1:1 stoichiometry between SH and MS was imposed, since consumption of all reactive partners would form the most complete network with the highest stiffness. Modest deviations from 1:1 stoichiometry in other step-growth hydrogels have been shown to significantly decrease the stiffness.^[16,17] The significantly lower $G'_{40\text{min}}$ values obtained when using VPM versus 1 kDa PEG-dithiol prompted us to check the relationship between stoichiometry and final stiffness. We analyzed R6 systems with variable [SH]:[MS] ratio from 0.93 up to 1.31 at pH 7.0 by preparing identical stock solutions to those used for previous rheology experiments (Figure 1) and adding different volume ratios of the two solutions to the rheometer. An increase in $G'_{40\text{min}}$ was observed with increasing VPM concentration, reaching a fourfold higher $G'_{40\text{min}}$ value at 17% excess VPM (Figure 4A) compared to 1:1 stoichiometry. A similar study performed on the R5 system at pH 8.0 showed a peak in $G'_{40\text{min}}$ at 40% excess VPM (Figure 4B). Note that these experiments were performed by starting with identical stock solutions of the starPEG and crosslinker, and adding these solutions in different volume ratios to the rheometer plate. At [SH]:[MS] ratios above 1, the total polymer concentration (5.0% w/v at 1:1 stoichiometry) declines,

reaching 4.3% w/v at [SH]:[MS] = 1.4. The higher $G'_{40\text{min}}$ values observed at excess VPM were therefore obtained despite slightly lower overall polymer contents. The results confirm that a significantly higher ratio of VPM to MS groups is required to maximize hydrogel stiffness. In contrast, hydrogels crosslinked with PEG-dithiol crosslinkers (R3 and R4 systems) showed a maximum $G'_{40\text{min}}$ at [SH]:[MS] = 1 (Figure 4C; Figure S3, Supporting Information), and excess dithiol resulted in hydrogels with significantly lower stiffness. The increase in stiffness at excess VPM contents suggests that a competing reaction such as disulfide formation could be decreasing the availability of crosslinking (thiol) functions.

We checked disulfide bond formation in commercial VPM by using liquid chromatography/electrospray ionization quadrupole time-of-flight mass spectrometry (LC/ESI QTOF-MS). A VPM stock solution with identical composition to the precursor solution at pH 8.0 in R5 was used for this experiment. According to the detected m/z values, three main species were detected from the beginning of the experiment: VPM, linear VPM dimer and cyclic VPM species (Figure S4, Supporting Information). VPM in its 3+ state was the dominant component. The preference for the 3+ state arises from the three arginine residues in the structure that are protonated at the tested pH value. The cyclic VPM species containing disulfide(s) and zero available thiols could be unimeric, dimeric, (etc.) since these would exhibit the same m/z value. Differentiation of these species would require a more elaborate LC protocol to separate them chromatographically prior to mass spectrometry analysis. The proportion of thiols locked up in disulfides was calculated from the counts (Figure S5, Supporting Information) since detector counts are proportional to the molar concentration of each species in solution. Initially, 2.2–5.3% of the thiol groups was in the form of disulfide bonds, and this number reached 7.2–14.2% over the next 60 min at pH 8.0 (Figure 5). The rheology experiments typically require ≈ 10 min between VPM solution preparation and mixing with PEG-4TzMS. The thiol concentration was therefore likely to be already 3–6% lower than theoretical values in R5 and R6 at the beginning of the network formation. Significant here is the fact that the linear VPM dimer is still capable of reacting with MS groups and contributing to crosslinking, since it contains a thiol at each end, while the cyclic VPM dimer cannot react with any MS groups. This ability to compensate for functional group loss by adding excess crosslinker is unique to systems where the loss occurs through coupling reactions, since monofunctional species that could only contribute dangling ends to the network are absent. The need for excess VPM to attain peak $G'_{40\text{min}}$ values (Figure 4) can then be partially attributed to the competing disulfide reaction in the precursor solutions uptaking part of the thiols, although the required excess of VPM was higher than accounted for by disulfide formation determined here.

3. Discussion

On the molecular scale, 3D polymer networks are inherently heterogeneous, exhibiting dangling ends, loops, double or triple links (in star-shape polymers), and entanglements because of the stochastic cross-linking reaction processes.^[18] These molecular defects result in a nonuniform distribution of polymer chains

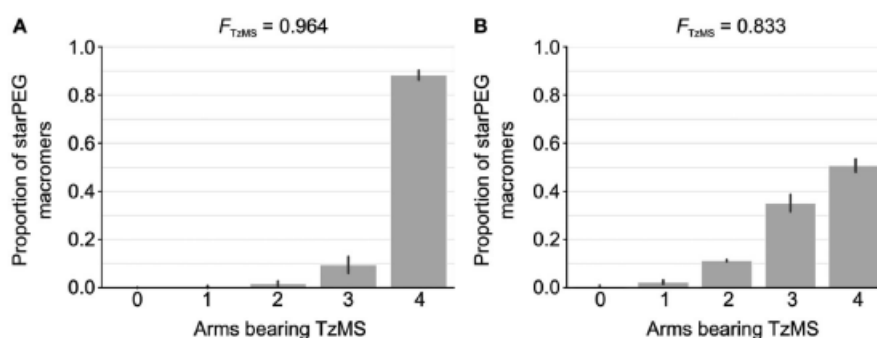


Figure 3. Proportion of starPEG macromers bearing 0, 1, 2, 3, and 4 TzMS groups at the chain ends for A) $F_{TzMS} = 0.964$, and B) $F_{TzMS} = 0.833$ obtained by functionalization of the polymer in A) with c[RGDFc] under the limiting cases of pure diffusion- and reaction-control. The vertical bars show the range of possibly attainable values according to these two limiting cases.

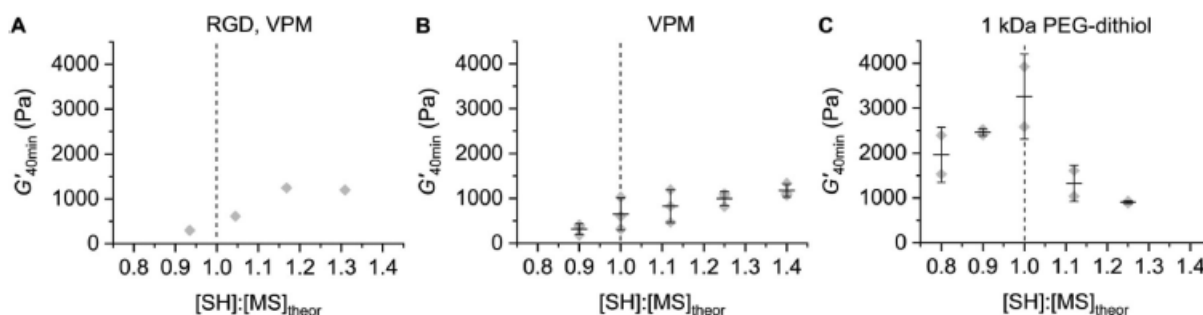


Figure 4. Effect of reactive group stoichiometry on G'_{40min} for A) PEG-4TzMS pre-functionalized with c[RGDFc] followed by VPM crosslinking at pH 7.0 (identical to R6 at $[SH]:[MS] = 0.95$), $N = 1$, B) PEG-4TzMS crosslinked with VPM at pH 8.0 (identical to R5 at $[SH]:[MS] = 1$), $N = 3$, and C) PEG-4TzMS crosslinked with 1 kDa PEG-dithiol at pH 8.0 (identical to R4 at $[SH]:[MS] = 1$), $N = 2$. The vertical dotted line shows theoretical 1:1 stoichiometry. For B) and C), the mean \pm standard deviation values are shown in addition to individual data points.

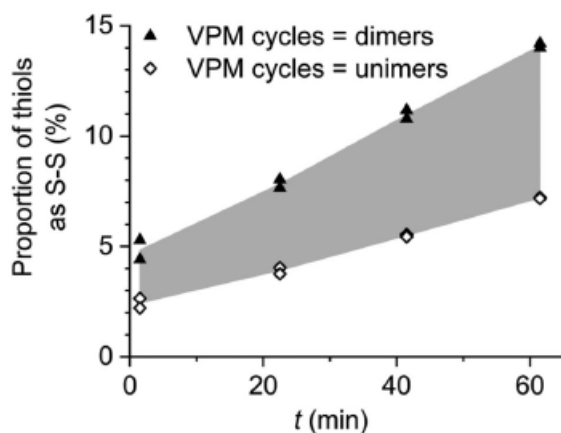


Figure 5. Quantification of VPM, linear VPM dimer, and cyclic VPM species (unimer or dimer) over time at pH 8.0 by LC/ESI QTOF-MS, $N = 2$. The composition of the solution was as used in R5 crosslinking experiment (pH 8.0). The shaded area shows the range between the two conditions, using the average of values from each condition as boundary lines.

and, consequently, in spatial defects at different length scales. For 3D cell encapsulation, spatial defects can translate to inconsistent cell responses, since cells can experience different local

crosslinking degrees and ligand densities through the gel volume. On a macroscopic scale, network defects decrease stiffness and strength, increase swelling, and decrease chemical stability. To minimize heterogeneity in step-growth hydrogel networks, telechelic prepolymers with defined molar masses and degrees of functionality, like the starPEGs used in this work, are used. This narrowly defined geometry disfavors the formation of back-biting loop structures and renders more homogeneous hydrogels compared to those obtained from polymeric precursors with higher dispersities and less regular geometries.^[19]

The internal structure and the properties of hydrogel networks are influenced by many factors including the polymer fraction, reactive group concentration, and the molar mass, architecture, length, and backbone composition of crosslinkers. The conversion and the kinetics of the crosslinking reaction, which are a function of pH in thiol-based nucleophilic crosslinking systems like thiol-MS, also influence the crosslinking degree and homogeneity of the network and impact the mechanical properties of the resulting hydrogel. In this work, we study the crosslinking kinetics and mechanical properties of PEG-4TzMS hydrogels formed at controlled pH values as a function of multifunctional thiol crosslinker structure and the degree of functionality varied by prefunctionalization with a bioactive ligand. For all experiments, we selected precursor compositions common in 3D cell culture with the aim of illustrating how typical changes in

compositional parameters can affect the properties of the resulting encapsulation matrix.

The crosslinking degree in a starPEG network is a function of the overall polymer concentration, the rate and efficiency of the crosslinking reaction, and the reactive partner stoichiometry. The impact of the overall polymer content on the properties in step-growth starPEG networks has been studied in depth by other authors.^[20–22] At concentrations close to the so-called overlap concentrations, the end groups of neighboring starPEG molecules are essentially touching, and the starPEG molecules exhibit an ordered packing arrangement throughout the volume. Covalent connection of the end groups via complementary reactive partners or short crosslinkers is spatially possible and leads to homogeneous gel networks. At concentrations significantly below the overlap concentration, short crosslinkers cannot link the star polymers efficiently, and at significantly higher concentrations the arm chains can entangle. Both cases give rise to network defects such as dangling chains or loops. For a 16 kDa PEG-4VS, the overlap concentration was reported to be 4.0% w/v as determined by dynamic light scattering (DLS) in PBS.^[23] The hydrogels in the present work were prepared at a constant total polymer concentration of 5% w/v. In **R1** and **R2**, the reactive partners are both 20 kDa starPEGs, meaning the total starPEG concentrations slightly surpass the overlap concentration to facilitate efficient crosslinking. In the systems using linear crosslinkers, starPEG concentration varied from 2.4% w/v when combined with 10 kDa PEG-dithiol (**R3**) to $\approx 4.5\%$ w/v when combined with the short linear crosslinkers 1 kDa PEG-dithiol or 1.7 kDa VPM (**R4–R6**). These starPEG concentrations straddle the overlap concentration, and were expected to allow efficient crosslinking when combined with the different length linear crosslinkers. Fixing the overall polymer content at 5% w/v, which has been applied for 3D cell encapsulations by us and others,^[3,5,6] should therefore give favorable compositions for obtaining fully crosslinked networks.

For step-growth crosslinking systems, network homogeneity is maximized under reaction-limited conditions, which allow complete mixing of the reactive partners before appreciable crosslinking has occurred as opposed to diffusion-limited conditions that lock reactive groups in the growing network at non-stoichiometric ratios to generate network inhomogeneities. Crosslinking reactions with pH-adjustable kinetics can offer reaction-controlled crosslinking and gelation on the minutes timescale within certain pH windows. Thiol-based Michael-type addition reactions are widely used in the 3D cell encapsulation community for this purpose, because such reaction kinetics are attainable within certain pH ranges by modulating the concentration of reactive species. Thiol-Mal crosslinking is notoriously rapid and typically generates inhomogeneous networks at physiological pH, but more homogeneous networks at pH values below 7 or by other strategies such as decreasing the concentration of available Mal groups through complexation.^[7] Thiol-VS crosslinking is slow and requires higher pH values to gel within desired timescales. In our previous work, thiol-MS showed gelation on a minutes time scale at near-physiological pH values. Under these conditions, thiol-MS hydrogels form more homogeneous networks than thiol-Mal and avoid the cell sedimentation during gel formation observed for thiol-VS.^[3] For TzMS, the second-order rate coefficient ($17 \text{ M}^{-1} \text{ s}^{-1}$ at pH 7.5)^[24] is sim-

ilar to that reported for reaction-limited starPEG gelation systems exhibiting high homogeneity.^[25] In the present work, we refined the buffering conditions to mitigate the effect of released methanesulfonic acid byproduct and maintain a stable pH during crosslinking. The selected buffer, comprising of 20 mM HEPES and 40 mM sodium carbonate, is based on common cell culture conditions,^[11] and provided excellent pH maintenance for the reactive group concentrations up to 8 mM used in our systems. The enhanced buffering capacity allowed the crosslinking reactions to reach higher conversions, exemplified by system **R2** reaching $G' = 5.6 \text{ kPa}$ versus **R1** reaching 0.65 kPa at pH 7.0. Methanesulfonic acid was shown to not impact cell viability in previous work,^[3] and the cytocompatible buffer adopted in the present work now resolves the question^[26] of how it may influence pH and crosslinking degree.

Gelation kinetics and mechanical properties are affected by changes in functionality, concentration or molar mass of reacting species, an issue typically disregarded despite its importance to reproducible 3D cell encapsulation outcomes.^[3,7] Overall, we see that gelation time and final stiffness of gels crosslinked with star or linear PEG crosslinkers in this work correlate with the concentration of starPEG in the precursor mixture, which determines the density of network points. The concentration of network points decreases in the order **R2** > **R4** > **R3**. The $t_{50\text{Pa}}$ values increase, and the $G'_{40\text{min}}$ values decrease correspondingly. Changing the architecture and molar mass of PEG-based thiol crosslinkers therefore provides a convenient means of tuning the crosslinking rate and final stiffness of hydrogels at fixed overall polymer content and crosslinking conditions. To impart the degradability necessary for cell proliferation, MMP-degradable peptide VPM is a common dithiol-bearing degradable peptide used in 3D cell culture.^[12,13,27,28] and served as a representative degradable crosslinker for comparison with the PEG crosslinkers in this work. Our work highlights important differences in crosslinking hydrogels with 1 kDa PEG-dithiol (**R4**) and VPM crosslinker (**R5**). Although $t_{50\text{Pa}}$ values were almost identical in both systems, $G'_{40\text{min}}$ values were threefold lower (0.8–1.1 kPa) in VPM crosslinked hydrogels. The starPEG and reactive end group concentrations were slightly lower in the VPM hydrogel due to the higher molar mass of VPM (1.7 kDa), but the density of network points was similar in both systems and, therefore, the differences in $G'_{40\text{min}}$ cannot be completely explained by starPEG concentration and crosslinker length. Mass spectrometry studies highlighted a significant loss of thiol functions through disulfide formation (i.e., thiol coupling) in VPM solutions. This loss could be compensated by adding excess VPM to the formulation without affecting the crosslinking ability of the system. This can be a pragmatic solution to obtain VPM-crosslinked thiol-TzMS hydrogels with higher stiffness for cell culture. Other important features observed in RGD-functionalized and enzymatically-degradable thiol-TzMS PEG hydrogels (**R6**) were that the values for $t_{50\text{Pa}}$ ranged from just under 1 min at pH 8.0 to 4 min at pH 7.5 and 6 min at pH 7.0, and that the $G'_{40\text{min}}$ values were in the 240–320 Pa range. These timescales allow comfortable handling and mixing of precursor and cellular components around physiological pH, and the achieved stiffnesses are suitable for 3D cell culture.^[4] Although this work has focused on the thiol-TzMS crosslinking system, some of the observed features have positive practical implications for other thiol-based nucle-

ophilic crosslinking systems and step-growth hydrogels more broadly.

4. Conclusion

Thiol/PEG-4TzMS hydrogels at compositions typically used for 3D cell culture allow comfortable handling during the experimental procedure. We previously demonstrated high cytocompatibility and >2 week gel longevity for fibroblast encapsulation in thiol/PEG-4TzMS gels, without exploring how composition influences the kinetics and mechanics of gel formation that are important for practical implementation of the system. The present work provides details on the expected gelation kinetics and mechanical stability of such networks, and how these vary with changes in the hydrogel formulation that are typically needed to match network properties such as stiffness and degradability with cellular requirements. Buffer containing 20 mM HEPES and 40 mM sodium bicarbonate satisfactorily maintained stable pH values throughout gelation in all systems, negating the effects of released methanesulfonic acid. This pH stability is important for controlling the gelation kinetics, and places the thiol-MS crosslinking alongside other thiol-based nucleophilic crosslinking reactions in which pH also remains stable during crosslinking. We obtained a gelation time of ≈ 4 min for the most biologically relevant system that was pre-functionalized with cell-adhesive ligand and crosslinked with degradable peptide VPM at pH 7.5. This timescale is very appealing for 3D cell encapsulation under near-physiological conditions to facilitate complete mixing and homogeneous cell distributions. The relatively low G' of ≈ 300 Pa is suitable for many 3D hydrogel applications, and could be increased to >1 kPa by introducing an excess of VPM crosslinker. Disulfide formation in the VPM system was identified as a contributing factor to lower stiffness values, which is relevant to many hydrogel systems that employ this peptide as crosslinker. We envisage that the properties of the thiol-crosslinked PEG-4TzMS system could be advantageous for automation of 3D cell cultures, where gelation kinetics are well adapted for the timescales of typical mixing protocols in pipetting robots.

5. Experimental Section

Materials: PEG-4SH (20 kDa) was purchased from JenKem Technologies (Texas, USA). PEG-dithiols (10 and 1 kDa) were bought from Creative PEGworks (North Carolina, USA), and VPM was purchased from GeneCust (France). Buffers were freshly prepared before each rheology experiment by dissolving HEPES and sodium bicarbonate from Sigma-Aldrich (Germany) in Milli-Q water and adjusting the pH value to the target (8.0, 7.5, and 7.0) using 1 M NaOH from Alfa Aesar (Massachusetts, USA). Solvents for ^1H NMR spectroscopy were purchased from Deutero (Germany). PEG-4TzMS (20 kDa) was synthesized following the previously established protocol.¹⁴

Equipment: pH measurements were performed with a Eutech Elite pH Spear (Thermo Scientific). Nuclear magnetic resonance (NMR) spectroscopy was performed with a Bruker Avance 300 MHz equipped with a He cooled 5 mm TCI-CryoProbe (a proton-optimized triple resonance NMR "inverse" probe with external water-cooling unit (CP TCI 500S2, H-C)/N-D-05 Z) from Bruker (Massachusetts, USA). All measurements were done at 298 K. The chemical shifts were recorded in parts per million (δ ppm) with the NMR solvent peak used as reference. Spectra were analyzed using Bruker's TopSpin software. Analytical high-performance liquid chro-

matography (HPLC) was performed with a JASCO 4000 (Japan) equipped with a Reprosil C18 column (250 \times 5 mm) and a UV/Vis detector. A gradient elution profile using Solvent A (water + 0.1% v/v TFA) and Solvent B (ACN/water 95:5 v/v + 0.1% v/v TFA) was employed over 40 min at 1 mL min⁻¹, going from 5% to 95% v/v Solvent B. Rheology was performed on a Discovery HR-3 rheometer (TA Instruments, USA) using 12 mm parallel plates and a Peltier stage temperature control system. Measurements were performed with $T = 25$ °C, gap = 300 μm , strain = 1%, and frequency = 1 Hz. Mass spectrometry was performed with a 6545 Accurate-Mass Quadrupole Time-of-Flight (LC/Q-TOF-MS) with electrospray ionization from Agilent (California, USA). Aliquots of 1.0 μL of sample were autoinjected into the LC system that contains a Poroshell HPH-C18 column (3.0 mm \times 50 mm, 2.7 μm) and a guard column (3.0 mm \times 5 mm, 2.7 μm) with column temperature set to 45 °C. The mobile phase consisted of two component solutions: A) water + 0.1% v/v formic acid and B) acetonitrile (ACN) + 0.1% v/v formic acid at a flow rate of 500 μL min⁻¹. The eluent composition over time was as follows: 0–0.5 min: 5% B; 0.5–5.5 min: 5–50% B; 5.5–7 min: 50–5% B; 7–12 min: 5% B at increased flowrate of 2.0 mL min⁻¹ for column washing; 12–13 min: 5% B at reduced flowrate of 500 μL min⁻¹ ready for the next sample. After separation, the LC flow entered the dual Agilent Jet Stream (AJS) ESI source set to 3,500 V as capillary voltage, 40 psi nebulizer gas pressure, and 7 L min⁻¹ dry gas flow, and 300 °C dry gas temperature. The TOF parameters used were an extended dynamic range (2 GHz), 140 V fragmentor voltage, and 45 V skimmer voltage. The mass spectra were acquired in the time interval of 1–5 min in full scan mode in the range of 200–1,700 m/z and with a spectra rate of 4 s⁻¹. To determine the formation of S–S bonds, the triply charged adduct of VPM (m/z 566.243), the linear dimeric VPM with loss of 2H, i.e., containing 1 S–S bond (m/z 565.905) and cyclic VPM (unimeric or dimeric, both with m/z 565.571 m/z) were extracted and automatically integrated using Mass Hunter software.

Quantification of the Degree of Functionalization and Molar Mass of Starting Materials: The degrees of functionalization for the NHS-, TzMS-, RGD-, and SH-terminated PEGs were abbreviated F_{NHS} , F_{TzMS} , F_{RGD} , F_{SH} throughout the manuscript. The F_{TzMS} was quantified by ^1H -NMR spectroscopy (Figure S1, Supporting Information) using the spectrum of the precursor PEG-4NHS and its reported F_{NHS} (from the supplier) as references. The molar masses of the thiol-bearing PEGs were determined in a similar manner (Figure S2, Supporting Information). See the captions of these figures for details of the calculations.

Functionalization of PEG-4TzMS with c[RGDFC] Peptide: A stock solution of PEG-4TzMS ($F_{\text{TzMS}} = 0.964$, $M_n = 22.2$ kDa) was prepared by dissolving the polymer (16.59 mg, 7.46×10^{-7} mol polymer) in freshly prepared Buffer 2 (171.3 μL) at pH 8.0. The solution was vortexed for 30 s to fully dissolve the polymer. A stock solution of c[RGDFC] was prepared by dissolving the peptide (0.98 mg, 1.69×10^{-6} mol) in Buffer 2 (280 μL) at pH 8.0. An aliquot of the c[RGDFC] stock (78.7 μL , 4.74×10^{-4} mmol, 0.16 equiv. relative to TzMS, targeting $F_{\text{TzMS}} = 0.80$ after reaction) was added to the stock solution of PEG-4TzMS (39.2 μL) in an Eppendorf tube at room temperature, vortexed for 30 s, then allowed to react for 60 min, reaching a final pH of 8.06. For purification, the pH was decreased to pH 5 using 1 M HCl, and the solution was dialyzed against water and freeze dried. The F_{TzMS} and F_{RGD} were determined by ^1H NMR spectroscopy, with the doublet at 7.6 ppm corresponding to the aromatic protons nearest to the unreacted TzMS units (Figure 2, signal b) and the doublet at 7.5 ppm corresponding to the aromatic protons after replacement of MS with RGD.

Simulating the Distribution of Functional Species in PEG-4TzMS: The distribution of stars bearing 0, 1, 2, 3, and 4 functional chain ends was derived for PEG-4TzMS ($F_{\text{TzMS}} = 0.964$) and its RGD-functionalized derivative ($F_{\text{TzMS}} = 0.833$) by Python simulations using the NumPy library (1.23).¹²⁹ Since kinetics do not affect the distributions and functionalization steps can be treated as subsequent events, the distributions are directly related to the probability of the individual arms in each system being attacked by a reaction partner. There are two limiting cases that define the bounds of this process: 100% diffusion control, in which all star molecules react with the same probability independent of the number of active arms they bear, and 100% chemical control, in which all active arms react with the same probability no matter the star to which they are attached.¹³⁰

For both distributions, the functionalization process was simulated according to all possible limiting pathways for systems with 200 000 macromolecules reacting with the reaction partner until the target stoichiometry was reached. In each step, an arm was selected for reaction. In the diffusion control case, a random macromolecular star was selected with equal probability, and in the chemical control case, the probability to be selected was equal for all arms in the system, making molecules with more active arms more likely to react. The $F_{TzMS} = 0.964$ was assumed to be reached through a functionalization process (i.e., starting from zero functionality, as would be expected in the synthesis of the commercial precursor PEG-4NHS). The $F_{MS} = 0.833$ system was then deduced through defunctionalization starting from the two limiting cases for the $F_{TzMS} = 0.964$ system. Average values were calculated from 100 000 sets of simulations. The values in this paper are precise in the reported significant figures.

Rheological Characterization of Hydrogel Crosslinking: First, the masses of PEG-4TzMS and crosslinker required in each experiment were determined from Equation 3 (see Supporting Information), which ensures that the overall polymer content is 5.0% w/v and the SH:MS ratio is 1.00. The concentration of the stock solutions of PEG-4TzMS and crosslinker were then determined by imposing equal volumes to facilitate mixing on the rheometer plate. The protocols from the **R2** and **R6** systems at pH 8.0 as representative examples were described here in full. For **R2** (initial pH 8.0), a stock solution of PEG-4TzMS ($F_{TzMS} = 0.964$, $M_n = 22.2$ kDa) was prepared by dissolving the polymer (10.34 mg, 4.65×10^{-7} mol polymer) in freshly prepared buffer (193.8 μ L) containing 20 mM HEPES and 40 mM NaHCO_3 (called Buffer 2) and set to pH 7.7–7.8. The initial pH of this and all other stock solutions for the rheology experiments was pre-determined experimentally to give the target initial pH ± 0.1 units after dissolving each compound, and are summarized in Table S2 (Supporting Information). The PEG-4TzMS solution was vortexed for 30 s to fully dissolve the polymer. A stock solution of PEG-4SH ($F_{SH} = 0.914$, $M_n = 20.4$ kDa) was prepared similarly by dissolving the polymer (11.67 mg, 5.71×10^{-7} mol polymer) in freshly prepared buffer (225.2 μ L) adjusted to pH 7.9. Rheology was then performed within 10 min after solution preparation. An aliquot of PEG-4TzMS solution (18.0 μ L) was pipetted onto the bottom plate, followed by addition of the PEG-4SH solution (18.0 μ L) directly into the first drop using a fresh pipette tip. The solution was mixed thoroughly by pipetting up and down for ≈ 20 s directly on the plate. The upper plate was lowered to a gap of 300 μ m, silicone oil was added around the sample to avoid evaporation, and a purge gas cover was placed to avoid disturbance during measurement. The total time required for sample loading until the start of the measurement was 60 s, and measurements were conducted for 40 min. The linear cross-linked systems **R3–R5** were prepared similarly. Note that the pH of the buffer needed to be significantly raised when dissolving VPM (**R5**), in order to reach the target initial pH values before rheology (see Table S2, Supporting Information). The **R1** systems used 10 mM HEPES (Buffer 1) at the target initial pH value prior to dissolving the solids, and was otherwise identical to **R2**. For **R6**, functionalization of PEG-4TzMS with c[RGDFC] was performed identically to described above, up to the purification step. After the 60 min reaction time, a final pH of 8.06 was reached. Note that the pH 7.5 and 7.0 systems required the addition of 1 M HCl (2.5 and 5.0 μ L, respectively) to attain the targeted initial pH value. Additional Buffer 2 (39.1, 36.7, or 34.1 μ L for pH 8.0, 7.5, and 7.0 systems, respectively) at the target pH value was added to make up the required volume. As crosslinker, VPM peptide (1.36 mg, 8.01×10^{-7} mol) was dissolved in Buffer 2 (124.5 μ L) pre-adjusted to initial pH of 9.93, 9.41, or 9.01 (for pH 8.0, 7.5, and 7.0 systems, respectively) and rheology was performed by adding the two solutions to the rheometer as described for **R2**.

pH Tracking During Hydrogel Formation: For each composition described in Table 1, a solution of the thiol component (80 μ L) was added to a solution of the PEG-4TzMS component (80 μ L) in an Eppendorf tube. The stock solutions were prepared with identical concentrations to in the rheology experiments. After vortexing for 30 s, the pH-meter probe was introduced into the solution and the Eppendorf tube with the probe inside was sealed with Parafilm. Values for pH were manually recorded over 40 min.

Supporting Information

Supporting Information is available from the Wiley Online Library or from the author.

Acknowledgements

S.P. and A.D.C. received funding from the European Union's Horizon 2020 research and innovation program under the FET PROACTIVE grant agreement no. 731957 (Mechano-Control) and the Senatsausschuss Wettbewerb (SAW) Leibniz-Transfer program under project uTissueFab. J.I.P. received funding from the Deutsche Forschungsgemeinschaft (DFG, project no. 422041745).

Open access funding enabled and organized by Projekt DEAL.

Conflict of Interest

The authors declare no conflict of interest.

Data Availability Statement

The data that support the findings of this study are available from the corresponding author upon reasonable request.

Keywords

cell culture, cell encapsulation, crosslinking, gelation, hydrogel

Received: October 5, 2022

Revised: November 17, 2022

Published online: December 11, 2022

- [1] S. Correa, A. K. Grosskopf, H. Lopez Hernandez, D. Chan, A. C. Yu, L. M. Stapleton, E. A. Appel, *Chem. Rev.* **2021**, *121*, 11385.
- [2] L. G. Griffith, M. A. Swartz, *Nat. Rev. Mol. Cell Biol.* **2006**, *7*, 211.
- [3] J. I. Paez, A. Farrukh, R. Valbuena-Mendoza, M. K. Włodarczyk-Biegun, A. Del Campo, *ACS Appl. Mater. Interfaces* **2020**, *12*, 8062.
- [4] J. I. Paez, A. De Miguel-Jiménez, R. Valbuena-Mendoza, A. Rathore, M. Jin, A. Glaser, S. Pearson, A. Del Campo, *Biomacromolecules* **2021**, *22*, 2874.
- [5] E. A. Phelps, N. O. Enemchukwu, V. F. Fiore, J. C. Sy, N. Murthy, T. A. Sulchek, T. H. Barker, A. J. García, *Adv. Mater.* **2012**, *24*, 64.
- [6] J. Kim, Y. P. Kong, S. M. Niedzielski, R. K. Singh, A. J. Putnam, A. Shikanov, *Soft Matter* **2016**, *12*, 2076.
- [7] B. Xue, D. Tang, X. Wu, Z. Xu, J. Gu, Y. Han, Z. Zhu, M. Qin, X. Zou, W. Wang, Y. Cao, *Proc. Natl. Acad. Sci. USA* **2021**, *118*, e2110961118.
- [8] M. Mours, H. H. Winter, *Macromolecules* **1996**, *29*, 7221.
- [9] M. Kurakazu, T. Katashima, M. Chijiishi, K. Nishi, Y. Akagi, T. Matsunaga, M. Shibayama, U.-I. Chung, T. Sakai, *Macromolecules* **2010**, *43*, 3935.
- [10] N. E. Good, G. D. Winget, W. Winter, T. N. Connolly, S. Izawa, R. M. Singh, *Biochemistry* **1966**, *5*, 467.
- [11] J. Michl, K. C. Park, P. Swietach, *Commun. Biol.* **2019**, *2*, 144.
- [12] M. P. Lutolf, J. L. Lauer-Fields, H. G. Schmoekel, A. T. Metters, F. E. Weber, G. B. Fields, J. A. Hubbell, *Proc. Natl. Acad. Sci. USA* **2003**, *100*, 5413.
- [13] J. Patterson, J. A. Hubbell, *Biomaterials* **2010**, *31*, 7836.
- [14] L. M. Weber, K. N. Hayda, K. Haskins, K. S. Anseth, *Biomaterials* **2007**, *28*, 3004.

- [15] M. J. O'melia, A. Mulero-Russe, J. Kim, A. Pybus, D. Deryckere, L. Wood, D. K. Graham, E. Botchwey, A. J. García, S. N. Thomas, *Adv. Mater.* **2022**, *34*, 2108084.
- [16] C. A. Deforest, E. A. Sims, K. S. Anseth, *Chem. Mater.* **2010**, *22*, 4783.
- [17] C. M. Madl, B. L. Lesavage, R. E. Dewi, C. B. Dinh, R. S. Stowers, M. Khariton, K. J. Lampe, D. Nguyen, O. Chaudhuri, A. Enejder, S. C. Heilshorn, *Nat. Mater.* **2017**, *16*, 1233.
- [18] T. Sakai, *Polym. J.* **2014**, *46*, 517.
- [19] Y. Akagi, T. Matsunaga, M. Shibayama, U.-I. Chung, T. Sakai, *Macromolecules* **2010**, *43*, 488.
- [20] W. Liu, X. Gong, Y. Zhu, J. Wang, T. Ngai, C. Wu, *Macromolecules* **2019**, *52*, 8956.
- [21] X. Li, S. Nakagawa, Y. Tsuji, N. Watanabe, M. Shibayama, *Sci. Adv.* **2019**, *5*, eaax8647.
- [22] M. Tosa, K. Hashimoto, H. Kokubo, K. Ueno, M. Watanabe, *Soft Matter* **2020**, *16*, 4290.
- [23] J. Wang, F. Zhang, W. P. Tsang, C. Wan, C. Wu, *Biomaterials* **2017**, *120*, 11.
- [24] X. Chen, H. Wu, C.-M. Park, T. H. Poole, G. Keceli, N. O. Devarie-Baez, A. W. Tsang, W. T. Lowther, L. B. Poole, S. B. King, M. Xian, C. M. Furdul, *ACS Chem. Biol.* **2017**, *12*, 2201.
- [25] K. Nishi, K. Fujii, Y. Katsumoto, T. Sakai, M. Shibayama, *Macromolecules* **2014**, *47*, 3274.
- [26] Y. Gao, K. Peng, S. Mitragotri, *Adv. Mater.* **2021**, *33*, 2006362.
- [27] M. D. Hunckler, J. D. Medina, M. M. Coronel, J. D. Weaver, C. L. Stabler, A. J. García, *Adv. Healthcare Mater.* **2019**, *8*, 1900371.
- [28] A. Farrukh, J. I. Paez, A. Del Campo, *Adv. Funct. Mater.* **2019**, *29*, 1807734.
- [29] C. R. Harris, K. J. Millman, S. J. Van Der Walt, R. Gommers, P. Virtanen, D. Cournapeau, E. Wieser, J. Taylor, S. Berg, N. J. Smith, R. Kern, M. Picus, S. Hoyer, M. H. Van Kerkwijk, M. Brett, A. Haldane, J. F. Del Río, M. Wiebe, P. Peterson, P. Gérard-Marchant, K. Sheppard, T. Reddy, W. Weckesser, H. Abbasi, C. Gohlke, T. E. Oliphant, *Nature* **2020**, *585*, 357.
- [30] B. Ebeling, M. Eggers, P. Vana, *Macromolecules* **2010**, *43*, 10283.

Supporting Information

Gelation kinetics and mechanical properties of thiol-tetrazole methylsulfone (TzMS) hydrogels designed for cell encapsulation

*Adrián de Miguel-Jiménez, Bastian Ebeling, Julieta I. Paez, Claudia Fink-Straube, Samuel Pearson, * Aránzazu del Campo **

A. de Miguel-Jiménez, J. I. Paez, C. Fink-Straube, S. Pearson, A. del Campo
INM – Leibniz Institute for New Materials, Campus D2 2, 66123 Saarbrücken, Germany.
Email: samuel.pearson@leibniz-inm.de; aranzazu.delcampo@leibniz-inm.de

A. de Miguel-Jiménez, A. del Campo
Saarland University, Chemistry Department, 66123 Saarbrücken, Germany.

B. Ebeling
Kuraray Europe GmbH, Advanced Interlayer Solutions, Competence Center for Innovation & Technology, Mülheimer Str. 26, 53840 Troisdorf, Germany.

J. I. Paez
Current address: Department of Developmental BioEngineering, Technical Medical Centre, University of Twente, Enschede, The Netherlands.

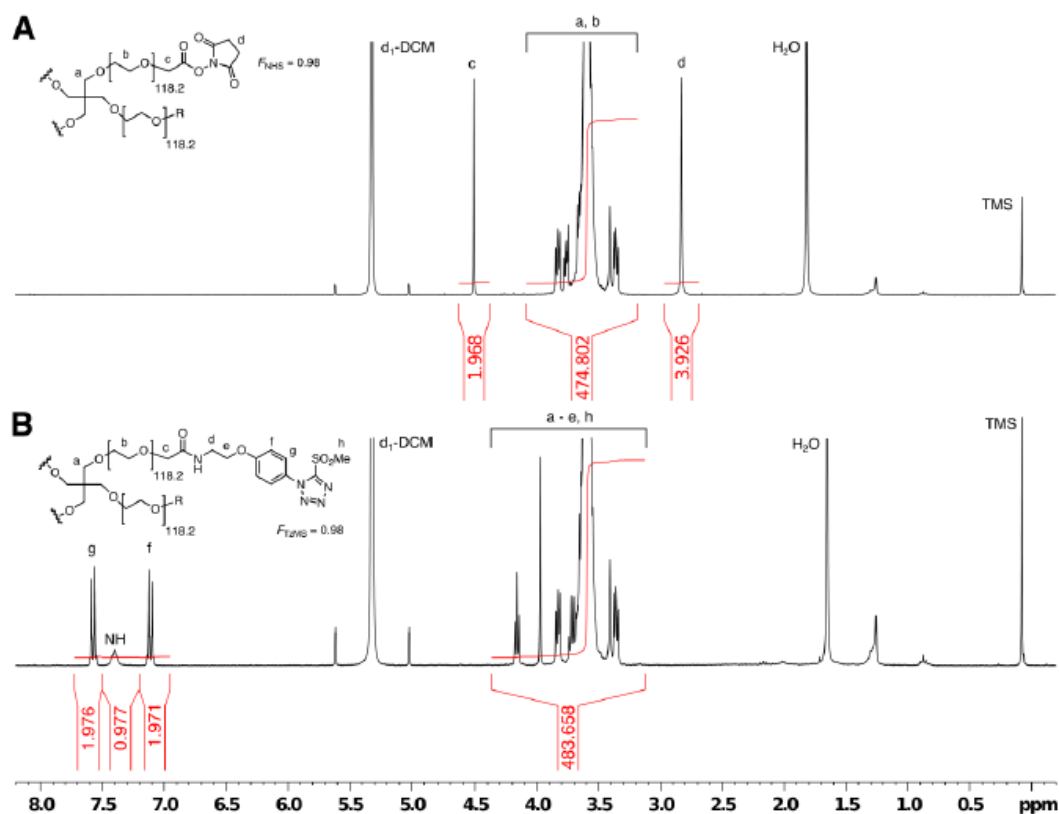


Figure S1. ^1H NMR of A) PEG-4NHS and B) PEG-4TzMS. For A), the $F_{\text{NHS}} = 0.984$ from the supplier was taken as the reference value for the integral of proton signal 'c' (4.5 ppm), i.e. $I_c = 2 \times F_{\text{NHS}} = 2 \times 0.984 = 1.968$. The integral of proton signals 'a' and 'b' from the PEG repeat units and 4-arm core was then used to determine the number of monomer repeat units n , i.e. $n = I_b / 4 = (I_{a,b} - I_a) / 4 = (474.802 - 2.00) / 4 = 118.2$. The molar mass of the polymer ($M_n = 21.6$ kDa) was then determined from the molecular structure, assuming that the non-functional end groups were carboxylic acid groups. For B), the integral for proton signals 'a - e, h' was set to the value of I_{a+b} plus expected values from protons 'c', 'd', 'e', and 'h', assuming that all the NHS groups had been converted to TzMS groups. Signals from protons 'c', 'd', 'e', and 'h' are negligible compared with I_{a+b} and this assumption is therefore reasonable even if conversion was not quantitative. The F_{TzMS} was then calculated from the signals of the aromatic protons 'f' and 'g' (7.1 and 7.6 ppm), i.e. $F_{\text{TzMS}} = (I_f + I_g) / 4 = (1.971 + 1.976) / 4 = 0.986$, which we took to be 0.984 given it cannot exceed F_{NHS} . The molar mass was then calculated in the same manner as for PEG-4NHS, giving $M_n = 22.2$ kDa.

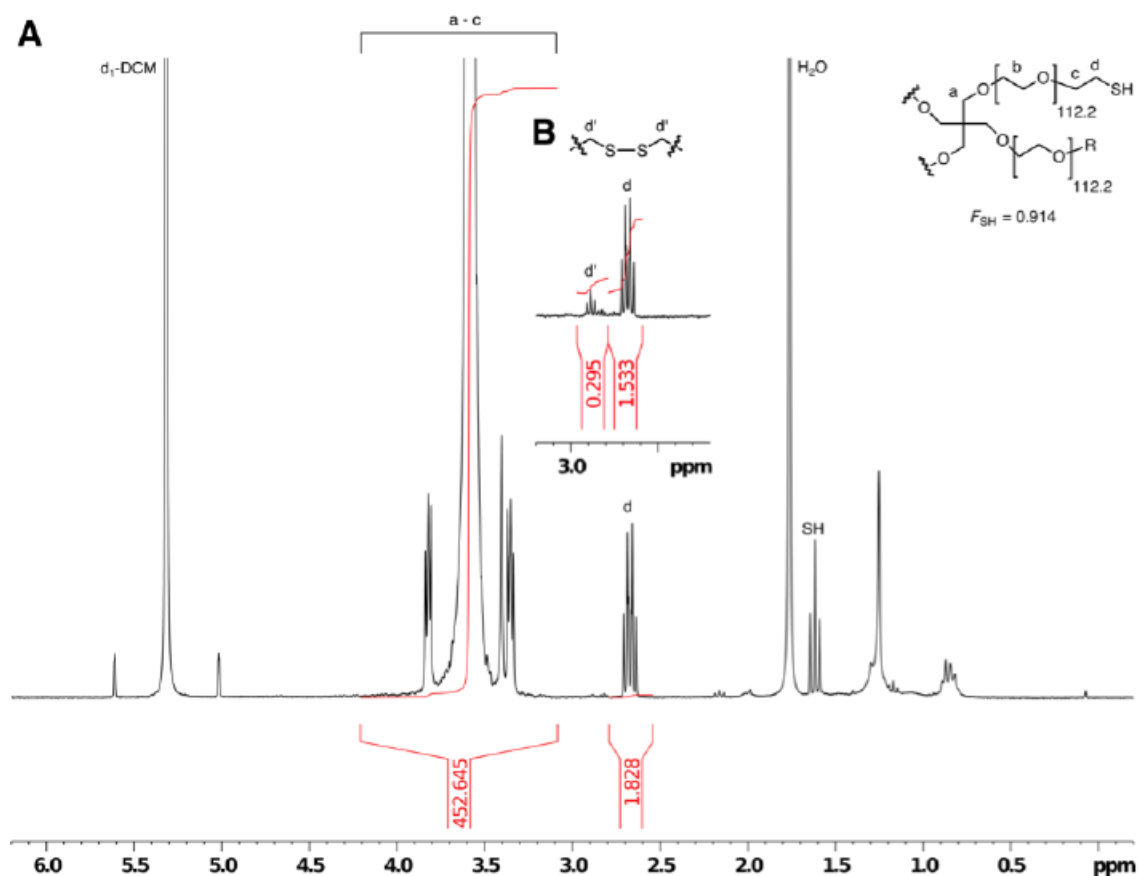


Figure S2. A) ^1H NMR of commercial PEG-4SH. The integral of the signal from the methylene protons 'd' adjacent to the SH terminus were set based on the reported degree of functionality, i.e. $I_d = 2 \times F_{\text{SH}} = 2 \times 0.914 = 1.828$. The integral of the signals from the star core and arms 'a-c' (3.1 – 4.2 ppm) was then used to determine the number of repeat units per arm, i.e. $n = I_b / 4 = (I_{a,b,c} - I_a - I_c) / 4 = (452.645 - 2.000 - 1.828) / 4 = 112.2$. The molar mass of the polymer ($M_n = 20.1$ kDa) was then determined from the molecular structure, assuming that the non-functional end groups were hydroxyl groups. The same protocol was followed for the linear PEG-dithiols. B) ^1H NMR spectrum of PEG-4SH in which ca. 20 % of the thiols had been converted to disulfides after long-term storage (under Ar, -20 °C, > 12 months).

Table S1. Degree of functionality and molar mass of PEG polymers used in this study.

Species	Degree of functionality from supplier (%)	Molar mass by ¹ H NMR spectroscopy (Da)
PEG-4NHS 20 kDa	98.4	21 579
PEG-4TzMS 20 kDa ^{a)}	98.4 / 96.4	22 243 / 22 219
PEG-4SH 20 kDa	91.4	20 127
PEG-dithiol 10 kDa	95.0	12 072
PEG-dithiol 1 kDa	99.0	996

^{a)} Two different batches of PEG-4TzMS were used in this work.

Table S2. Purity of peptides used in this study as determined by HPLC. ^{a)}

Species	Purity (%)
c[RGDfC]	97.3
VPM	98.8

^{a)} Peaks from the 220 nm channel were integrated for the quantification. Analysis conditions are described in the Experimental section.

Calculation of prepolymer concentrations for rheology experiments

In all rheology experiments, we imposed equal moles (n) of methylsulfone (MS) and thiol (SH) functional groups:

$$n(\text{MS}) = n(\text{SH})$$

This can be re-expressed as:

$$n(\text{P} - \text{MS}) \cdot a(\text{MS}) \cdot F(\text{MS}) = n(\text{P} - \text{SH}) \cdot a(\text{SH}) \cdot F(\text{SH})$$

where $n(\text{P} - \text{MS})$ is the number of moles of PEG-4TzMS, $n(\text{P} - \text{SH})$ is the number of moles of thiol-containing crosslinker, a is the number of chain ends per molecule, and F is the degree of functionality, i.e. the proportion of chain ends carrying the desired function.

This equation can be re-expressed as:

$$\frac{m(\text{P} - \text{MS}) \cdot p(\text{P} - \text{MS})}{M_n(\text{P} - \text{MS})} \cdot a(\text{MS}) \cdot F(\text{MS}) = \frac{m(\text{P} - \text{SH}) \cdot p(\text{P} - \text{SH})}{M_n(\text{P} - \text{SH})} \cdot a(\text{SH}) \cdot F(\text{SH})$$

where m is the mass, p is the purity (on a mass basis), and M_n is the number-average molar mass of each polymer component P-MS and P-SH.

Rearranging gives:

$$m(\text{P} - \text{MS}) = \frac{M_n(\text{P} - \text{MS}) \cdot p(\text{P} - \text{SH}) \cdot a(\text{SH}) \cdot F(\text{SH})}{M_n(\text{P} - \text{SH}) \cdot p(\text{P} - \text{MS}) \cdot a(\text{MS}) \cdot F(\text{MS})} \cdot m(\text{P} - \text{SH}) \quad (1)$$

In all rheology experiments, we also imposed a total polymer mass fraction (x) of 0.05 in the final rheology solutions, i.e.

$$x(\text{P} - \text{MS}) + x(\text{P} - \text{SH}) = 0.05$$

That is:

$$\frac{m(\text{P} - \text{MS})}{m_{\text{solution}}} + \frac{m(\text{P} - \text{SH})}{m_{\text{solution}}} = 0.05$$

Rearranging gives:

$$m(\text{P} - \text{SH}) = 0.05 \cdot m_{\text{solution}} - m(\text{P} - \text{MS}) \quad (2)$$

Substituting (2) into (1) gives:

$$m(\text{P} - \text{MS}) = \frac{M_n(\text{P} - \text{MS}) \cdot p(\text{P} - \text{SH}) \cdot a(\text{SH}) \cdot F(\text{SH})}{M_n(\text{P} - \text{SH}) \cdot p(\text{P} - \text{MS}) \cdot a(\text{MS}) \cdot F(\text{MS})} \cdot [0.05 \cdot m_{\text{solution}} - m(\text{P} - \text{MS})]$$

Rearranging gives an expression for the mass of P-MS required in a given mass of rheology solution:

$$m(\text{P} - \text{MS}) = 0.05 \cdot m_{\text{solution}} \cdot \frac{\left[\frac{M_n(\text{P} - \text{MS}) \cdot p(\text{P} - \text{SH}) \cdot a(\text{SH}) \cdot F(\text{SH})}{M_n(\text{P} - \text{SH}) \cdot p(\text{P} - \text{MS}) \cdot a(\text{MS}) \cdot F(\text{MS})} \right]}{\left[1 + \frac{M_n(\text{P} - \text{MS}) \cdot p(\text{P} - \text{SH}) \cdot a(\text{SH}) \cdot F(\text{SH})}{M_n(\text{P} - \text{SH}) \cdot p(\text{P} - \text{MS}) \cdot a(\text{MS}) \cdot F(\text{MS})} \right]} \quad (3)$$

The mass of P-SH can then be found from (2).

In order to facilitate mixing of the two reactive components, we also targeted equal volume aliquots of each precursor solution, which defined the concentrations of stock solutions of P-MS and P-SH.

Table S2. Buffer 2 pH values prior to dissolving PEG-4TzMS and the crosslinkers in order to attain the target initial pH values for rheology experiments.

Compound	Target initial pH	Initial buffer pH without compound	pH after dissolving compound
PEG-4TzMS	8.0	7.80	7.95
	7.5	7.20	7.59
	7.0	6.59	7.09
PEG-4SH	8.0	7.90	8.02
	7.5	7.27	7.54
	7.0	6.59	7.10
PEG-dithiol 10 kDa	8.0	7.98	8.03
	7.5	7.36	7.58
PEG-dithiol 1 kDa	8.0	8.04	8.06
	7.5	7.35	7.53
VPM	8.0	9.97	7.93
	7.5	9.47	7.50

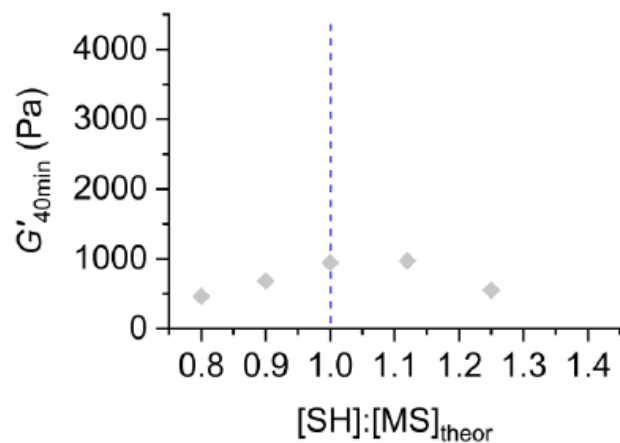


Figure S3. Effect of reactive group stoichiometry on $G'_{40\text{min}}$ for PEG-4TzMS crosslinked with 10 kDa PEG-dithiol at pH 8.0 (identical to **R3** at $[\text{SH}]:[\text{MS}] = 1$), $n = 1$. The vertical dotted line shows theoretical 1:1 stoichiometry.

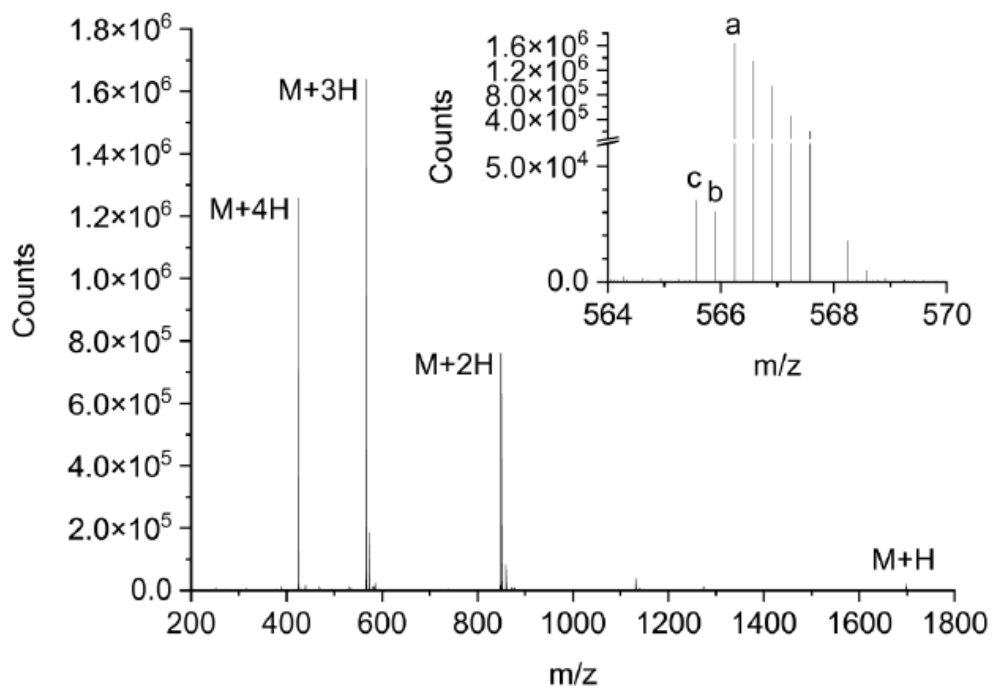


Figure S4. ESI-QTOF-MS spectrum of 61.5 min VPM solution, taken at 3.126 min retention time in the liquid chromatogram. The inset shows the region corresponding to a) VPM, b) Linear VPM dimer, and c) Cyclic VPM.

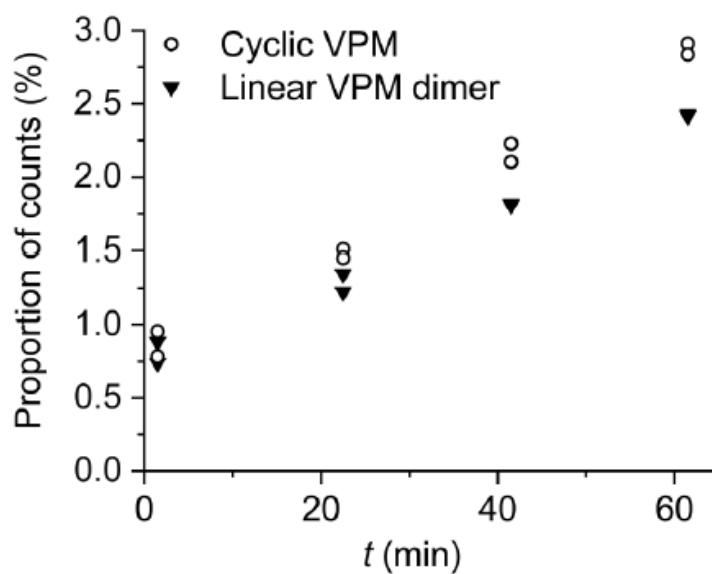


Figure S5. Detector counts for linear ($m/z = 565.905$) and cyclic ($m/z = 565.571$) disulfide, divided by the sum of counts for VPM ($m/z = 566.243$) and the disulfide species. The VPM solution was prepared identically to in the **R5** rheology experiment at pH 8.0.

5 Automated hydrogel preparation in pipetting robot

5.1 Introduction

5.1.1 Automated liquid handling in high throughput screening of pharmaceuticals

High throughput screening (HTS) in drug delivery research involves the evaluation of extensive libraries of chemical and/or biological compounds to investigate their bioactivity towards a specific target. HTS requires the use of automated pipetting robots to handle the large number of samples. The following advantages are associated with automated handling vs. manual preparation at lower throughput:

- i. **Reproducibility.** Automation can effectively reduce human errors associated with manual pipetting, thereby reducing variability, including user-to-user variability. Standardized protocols lead to more consistent and reliable results across multiple experiments.
- ii. **Accuracy and precision.** Automated systems can dispense a wide range of volumes, from milliliters to microliters accurately. In addition, liquid handling instruments are enclosed systems that do not require direct manipulation for liquid dispensing. This enables longer calibration intervals compared to manual instruments.
- iii. **Efficiency.** Automated liquid handling helps minimize experimental time and increase overall throughput. By streamlining the pipetting processes, pipetting tasks can be performed in a rapid and consistent manner, which is particularly beneficial when working with a large number of samples.

HTS using 3D cell co-cultures and organoids from human cells representing different tissues or disease states are used as advanced models for drug testing with expected high predictive potential for drug screening and to replace animal models.¹ In such processes, in situ forming hydrogels are primary support materials for the encapsulation of cells in 3D culture and organoids² and need to be handled in HTS formats. The utilization of automated liquid handling systems for cell and organoid encapsulation using in situ forming hydrogels offers the following advantages:

- i. A consistent and thorough mixing process leads to more uniform network formation across the sample, enhancing the reproducibility across multiple

hydrogel replicates. It also ensures homogeneous cell distribution throughout the hydrogel, thereby increasing the reliability of the outputs.

- ii. The consistent and consecutive dispensing of liquid mixtures into a specific well position is facilitated by the position calibration of the pipetting channels within the wells. This calibration translates into uniform 3D shape of the hydrogels, improving the reproducibility. Furthermore, the shape of the hydrogels may impact subsequent assays, including photometric measurements of active molecules contained in the hydrogel.³ This aspect is crucial in the present study, as the analysis of variability relies on this type of measurements.
- iii. Accurately pipetting volumes from stock solutions ensures the maintenance of a constant concentration during preparation of the hydrogels. In the context of thiol-MS hydrogels used in this chapter, maintaining the targeted ratio between MS and thiol groups is crucial for the formation of consistent 3D networks and achieving comparable stiffness, which directly affects cell behavior.^{4,5}
- iv. The capability of accurately dispensing volumes below 10 μL enables rapid diffusion of molecules within the hydrogel due to the reduced volume compared to larger volume hydrogels.¹ This feature could benefit the embedded cells by facilitating their access to essential molecules required for proper functioning and survival.
- v. Preparing multiple hydrogels within shorter timeframes, for example, 60 hydrogels in 10 minutes as demonstrated by Kletzmayr *et al.*,⁶ or even 96 hydrogels in 5 minutes as shown by Brooks *et al.*,⁷ offers the advantage of minimizing stability concerns associated with handling sensitive precursor solutions. In our case, this is relevant for thiol aqueous solutions, as they form disulfide bonds over time.

5.1.2 Design of experiments (DoE) to identify working parameters and establish robust pipetting protocols at minimum effort

Traditionally, experiments involving multiple factors are performed by one-factor-at-a-time (OFAT) approach. This method consists of changing one factor while keeping the others constant. This process is successively repeated over the desired range of levels until the best settings of the factor under study are found. However, this approach can be ineffective and imprecise, resulting in the inability to find the optimal conditions and

obtain a thorough understanding of the impact of each factor or their interactions on the process being analyzed. These limitations can lead to erroneous conclusions and suboptimal settings for the process being analyzed.⁸

In HTS experimentation, the high number of parallel experiments requires the use of statistical experimental design to screen for the different variables (i.e. factors). Design of experiments (DOE) is an advanced experimental design methodology that addresses the limitations of the OFAT approach. DOE involves systematic variation of multiple factors simultaneously, in a controlled and structured manner, to explore the effects of each factor and their interactions on the process being investigated. This approach aims to minimize the number of combinations tested while still reliably providing an accurate understanding the complete design space (**Figure 1**), by maximizing the amount of information extracted from each tested condition and minimizing the amount of resources and time required.⁸⁻¹⁰

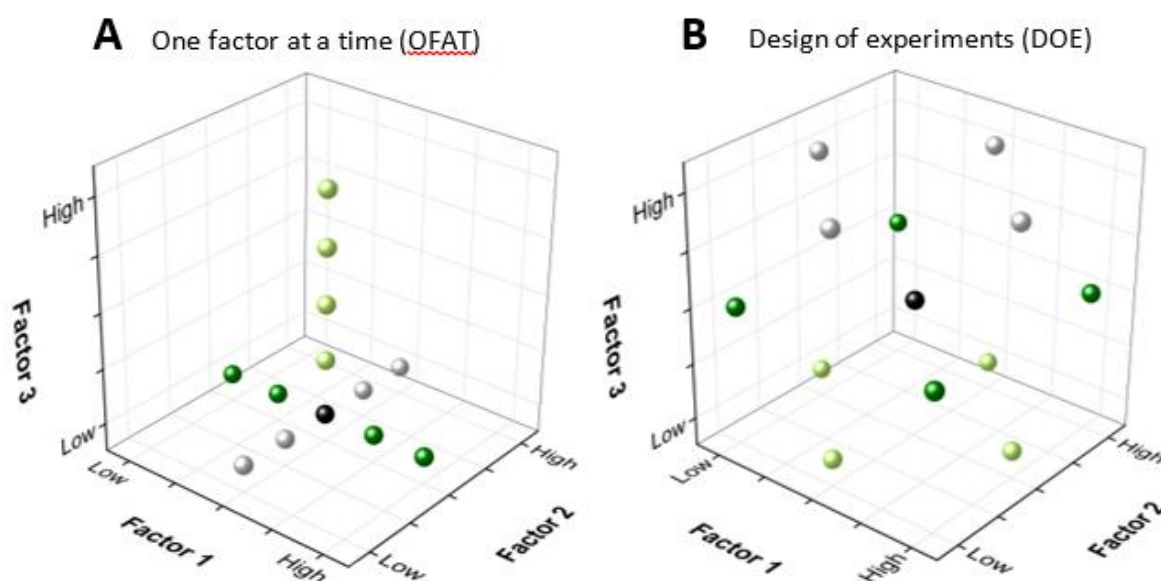


Figure 1. A) One factor at a time and B) Design of experiments.

In this chapter, a robust pipetting protocol for the preparation of cell encapsulating hydrogels with different mechanical and biochemical properties will be established using the DOE approach. The impact of various pipetting parameters on the variability of hydrogel preparation will be examined, aiming to optimize the reproducibility of the automated pipetting method for MS hydrogel preparation.

5.2 Objectives

The methylsulfone (MS) – thiol (SH) crosslinked hydrogels characterized in Chapter 4 of this Thesis were used for manual 3D encapsulation of cells in the group. For these encapsulation experiments, hydrogels of 10 μL volume were manually prepared in 15-well plates. In this chapter, the development of an automated protocol/method intended for automated 3D encapsulation of cells at larger throughput is described. The following individual objectives were pursued during the study:

- i. Parallel preparation of 5 μL hydrogel samples in a 384-well plate format.
- ii. Reproducibility of consecutively prepared hydrogels with a coefficient of variation (CV %), limited to a minimum of 2 % when pipetting 5 μL volumes with the Microlab Nimbus, (automation system used in this work) and even / odd ratio % from sequential pipetted volumes (ratio between the second and first dispense) below 10%.

The targeted composition, according to previous work in the group, corresponded to hydrogels with 5 wt% polymer content composed of PEG-4TzMS and VPM with [MS]:[SH] = 1. The buffer used for gel preparation was HEPES 20 mM + NaHCO_3 40 mM with a pH 7.5 – 7.6. Under these conditions, hydrogels were expected to form within 2 minutes, which was considered appropriate for the automated hydrogel preparation protocol.

5.3 Results and discussion

5.3.1 Steps in the development of an automated pipetting method

A previously prepared automated pipetting method in the group of Prof. Carsten Werner (IPF, Dresden) developed by Dr. Manfred Maitz, Dr. Nicholas Dennison and Dr. Maximilian Fusenig for the automated preparation of heparin-based hydrogels in 384-well format and specifically developed for a Tecan Fluent 480 instrument (from Tecan Group Ltd), was used as starting point. This protocol was adapted to the 8 channels Microlab Nimbus liquid handling robot from Hamilton at INM. The following steps were undertaken and are discussed in more detail in the next sections.

- i. The method was programmed using a drag-and-drop option in the Hamilton software development kit (SDK).

- ii. The method was programmed with two main principles in mind: modularity and minimum material waste.
- iii. The code was virtually and physically tested by pipetting water. Code errors were identified and initial values of pipetting parameters were set.
- iv. Pipetting parameters for each step were step-by-step optimized using PEG-4TzMS and VPM precursor solutions. In this way, pipetting errors, such as air aspiration, bubble formation, splashing or dripping were corrected.
- v. The variability of the prepared hydrogels was photometrically quantified by mixing labelled hydrogel precursor solutions. Stepwise modifications of the pipetting parameters from the automated method were investigated using a design of experiments (DOE) approach and applied to reduce variability to the targeted maximum threshold.

5.3.2 Design of the pipetting workflow

The semi-automated pipetting method for the preparation of MS hydrogels with the Microlab Nimbus liquid handling robot (**Figure 2**) reproduced the steps of the protocol for manual preparation of 10 μ l PEG-4TzMS/VPM hydrogels that had been established in the group. In this method, hydrogels were prepared by mixing given volumes of PEG-4TzMS and VPM precursor stock solutions and crosslinking in the well plate. The cells were mixed and resuspended with the PEG-4TzMS solution in a previous step.

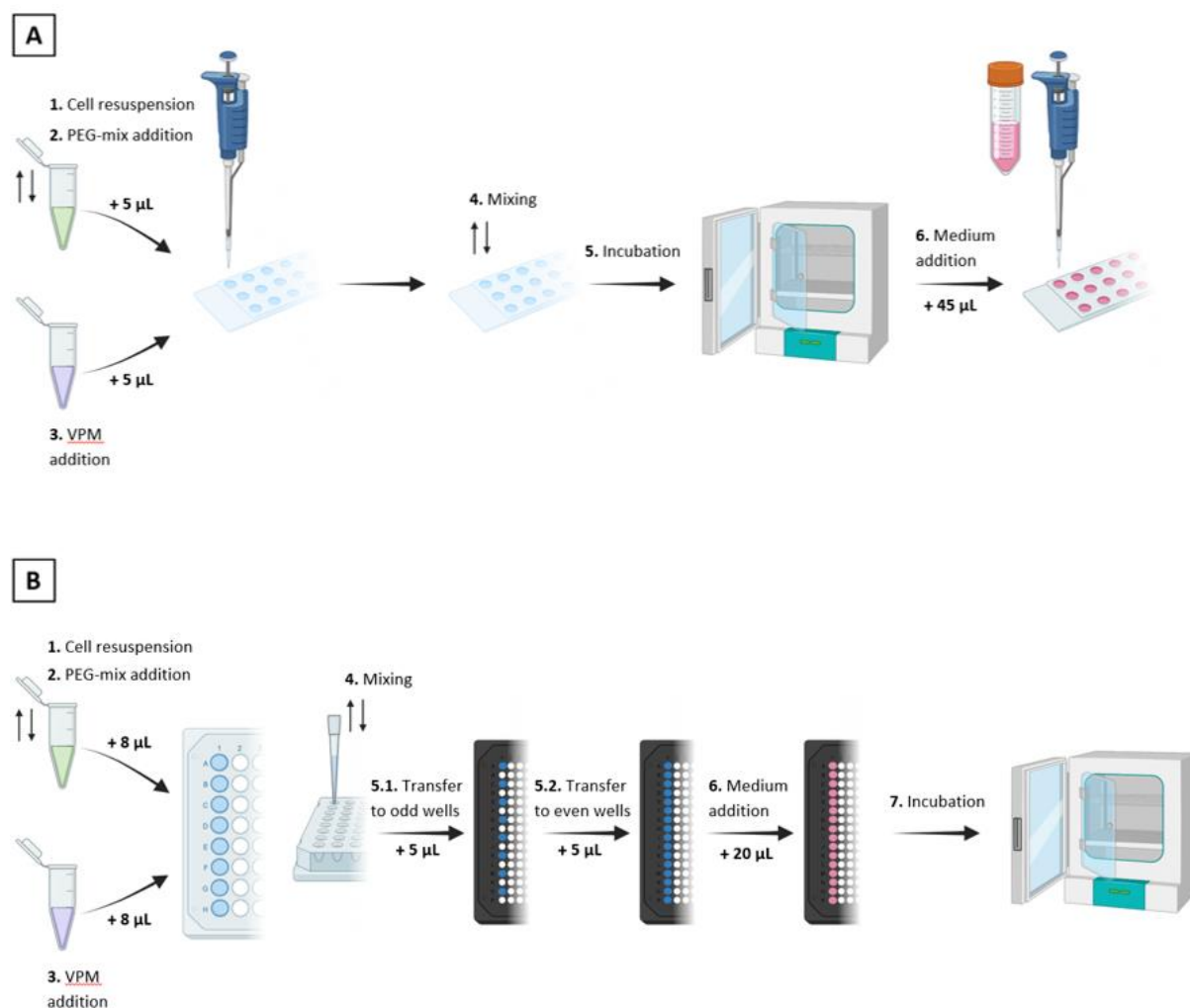


Figure 2. Manual (A) vs automated (B) hydrogel preparation. In the automated protocol, all pipetting steps were done by the robot, including the medium addition after hydrogel is made, while the transferring to an incubator was done by hand. *Created with BioRender.*

The available protocol for the Tecan instrument (IPF, Dresden) was taken as basis and reprogrammed to be adapted to the Microlab Nimbus pipetting robot (from Hamilton Company) at INM. The group at IPF successfully demonstrated robotic preparation of 5 μL hydrogels from Maleimide-SH precursors and encapsulation of mesenchymal stem cells with a coefficient of variation below 5 %. A volume of 5 μL was targeted for the automated preparation of MS hydrogels as well. The small volume of the samples favors the diffusion of molecules in the hydrogels, such as nutrients for the cells.¹

Following the experience in the IPF group, a 2 μL excess volume per stock precursor solution was used in the first aspiration step. This provided better mixing results and reduced the risk of air aspiration in the experiments at IPF. To maintain a small excess of liquid inside the tip after the final dispensing into the 384-well plate (to avoid potential air dispense), 1 μL extra volume was aspirated from each precursor solution as well. As a result, an excess volume of 3 μL per stock solution (8 μL of MS and SH in total) was used for the preparation of each 5 μL hydrogel.

A major factor that influences the variability of in situ prepared hydrogels from reactive precursor solutions is gelation kinetics. In fast crosslinking systems (i.e. gel formation within 2 mins to avoid cell sedimentation during hydrogel formation), the instantly increasing viscosity once the reactive precursors are in contact hampers pipetting of equal and consecutive volumes of the reactive mixture during consecutive pipetting and dispensing steps, creating a potential source of variability. To minimize this effect, the number of hydrogels per iteration of the pipetting process were restricted (showed in **Figure 2B**) to one column of the well plate (16 wells). With this design, 16 replicates of the one column would be created within the 384-well plate, which were considered enough for performing the statistical analysis.

To prepare the 16 gels within a single column, the transfer process to the 384-well plate was divided into two consecutive dispensing steps (8 + 8). This division was necessary because the instrument was equipped only with eight channels. An alternating pattern (odd and even wells) of dispensing was implemented (**Figure 2B**) to accommodate the arrangement of channels in the robot arm. This arrangement requires a minimum distance between consecutive channels, which is greater than the spacing between the center points of two adjacent wells in the 384-well plate.

An alternative strategy to reduce the impact of increasing viscosity was considered by using two separated pipetting iterations. However, this strategy doubles the time needed for hydrogel preparation, and could lead to aging effects of the stock solutions containing thiol crosslinkers.

As an intermediate step during the pipetting process, a 96-well plate was used for parallel mixing of 8 wells (containing a mixture of the two precursor solutions) at a time by using

the 8 independent pipetting channels from the robot. PCR wells with a convex shape that allowed mixing small volumes with less bubbles formation than flat bottom wells were selected.

Another factor to consider in the design of the automated pipetting protocol is the elapsed time, which is the time between the mixing of the precursor solutions and the final dispense into the even wells from the 384-well plate. The pipetting method was designed to minimize the elapsed time by the preparation of one column in two consecutive dispensing steps per iteration, and the virtual configuration of the labware so that the robotic arm followed a sequential movement.

5.3.3 Programming of the pipetting robot

The pipetting method was programmed using the Hamilton Method Editor application. Drag-and-drop programming was applied. Functions were selected from a library and placed within a numbered set of lines in a logical order. For the construction of the protocol, pipetting functions for liquid handling (e.g. tip pick up, aspirate, dispense, and eject tip), were combined with general functions (e.g. variable assignment, loop, or if, else). When adding a new function to the code, the menu allows introduction of the experimental values for each parameter necessary to run the function. For example, for liquid aspiration function, the aspiration volume, the channel number, the source, and the target labware were specified. As a starting point, arbitrary values within the default ranges of the instrument were selected.

Other parameters dependent on the specific properties of the handled liquid, such as viscosity or surface tension, were addressed separately. These parameters include aspiration and dispense flow rate (speed) and were introduced in a separate file accessed through the Hamilton CO-RE Liquid Editor application. The list of these parameters was grouped in the so-called “liquid class” and the numerical values were manually entered. If any of these parameters needed to be adjusted, there was no direct shortcut available within the main Hamilton Method Editor, so they had to be individually changed from the previously mentioned application.

The desired labware (tips, well plates, Eppendorf tubes and Falcon tubes) was defined in the deck layout through the HAMILTON Labware Editor. The labware was arranged from left to right, aligning with the instrument's sequential movement between steps. This arrangement was designed in such a way that the necessary channels could access the targeted labware during each pipetting step, and aimed to minimize the potential risk of contamination that could arise from dripping.

To maintain a comprehensive record of experimental details and potential errors, a logfile containing instrument details, experimental specifications such as the date and time, and the code itself, was generated and stored after each execution of the pre-programmed code. The level of detail concerning the code in the logfile depended on the inclusion of tracing functions during the method development. To ensure a record of all steps in the pipetting method, including the values of all defined variables, trace functions were employed to display these values within the logfile.

During the programming of the method, “Run Control” application was used to check for potential errors that required further adjustments in the program. Three errors were frequently encountered:

- Mismatching variable names causing inconsistencies and incorrect data assignments.
- Syntax errors led to programming issues.
- Incompatibility between specific functions or features and the chosen labware was a recurrent issue. For instance, the liquid level detection feature (see next section) was not compatible with the targeted small volumes and labware. Therefore, an alternative strategy was followed, specified below.

Overall, the pipetting method was programmed with two key principles in mind: modularity, to make it applicable to other hydrogel compositions, and waste minimization, which will be described in sections 5.3.3.2 and 5.3.3.3.

5.3.3.1 Liquid level detection of small volumes

In aspiration and dispensing steps, the HAMILTON software requires setting a “height value” for positioning the tip within the liquid container from which the step will be carried

out. In liquid handling robots, two options are available: liquid level detection (LLD), which will detect the surface of the liquid and then position the tip at an appropriate height below the surface; and fixed height, which consists of setting the desired height manually.

Two options for liquid level detection were available in the HAMILTON equipment and tested: capacitive liquid level detection (cLLD) and pressure liquid level detection (pLLD).

- Capacitive liquid level detection (cLLD) utilizes conductive tips and measures the change in capacitance, when the tip is introduced into the liquid, to determine the position of the liquid surface. This method relies on the different dielectric constant between the liquid and air. The capacitance value depends on factors such as the tip, the liquid container, the container holder, the instrument's base where the holder is placed, the volume and the liquid conductive properties. The cLLD option was experimentally not feasible in the Microlab Nimbus due to the incompatibility of the Eppendorf holder from HAMILTON and volumes below 100 μL in the wells.
- Pressure liquid level detection (pLLD) senses pressure to identify the position of the liquid surface. In this method, the pressure is monitored as the tip approaches the liquid, and the instrument detects a drop in pressure when the tip enters the liquid. The position of the tip at the pressure drop is considered the position of the liquid surface. However, the liquid that is aspirated during the process of determining the liquid surface is abruptly dispensed, leading to splashing and the formation of bubbles. Consequently, this technique was not utilized.

An alternative to the liquid level detection techniques was to set a fixed height from which the tip aspirates or dispenses the liquid. In this case, the tip remains stationary regardless of the liquid being aspirated, potentially resulting in inadvertent air intake. To reduce this risk, the selected height was 1 mm away from the bottom, enabling maximal utilization of liquid volume (thus minimizing dead volume) while simultaneously preventing air aspiration. However, the immersion of the tip inside the liquid and close to the bottom increases the likelihood of liquid adhering to the outer part of the tip and resulted in material loss. Thus, the aspiration height was set for each individual aspiration step,

varying depending on the available liquid and the volume that would be aspirated, as specified in section 5.3.5.

Regarding the mixing of the precursor solutions in the current method, the liquid was pipetted up and down at a specified flow rate (identical for both aspiration and dispensing) from a fixed height. Although this mixing process may be considered less accurate than liquid level detection, effective mixing was achieved, as described in the subsequent sections.

5.3.3.2 Modularity of the pipetting method

A modular pipetting protocol allows modification or exchange of individual steps and provides flexibility for the adaptation of the method to other hydrogel mixtures. The following levels of modularity were implemented in the protocol:

- Submethods. The pipetting method was structured in 7 different submethods: Method, Initialization, Variables, Preparation, Pipetting, Termination and On Abort. The Method and On Abort are created by default, and they must always be enabled in the software. The other submethods perform specific functions and can be individually enabled or disabled and modified as desired.
 - i. Preparation. This submethod was programmed for the optional filling of the outer wells from the well-plate with water and minimize evaporation of the dispensed liquids.⁶
 - ii. Variables. To allow easy changes in the pipetting parameters, such as handled volume or aspiration or dispensing height, all variables used in the pipetting method were gathered in a single submethod.
 - iii. Pipetting. All pipetting steps shown in **Figure 2B** were incorporated into this submethod as individual steps. These steps could be individually enabled or disabled, allowing for the isolation and study of specific steps without the influence of others when necessary.
- Loops were incorporated to the code to iterate the method and prepare hydrogels in different columns of the well. The loop counter's value was selected to align with the desired number of columns to be prepared.

- Duplicated labware. To enable the utilization of different stock solutions for the preparation of hydrogels in different columns by using the same pipetting step, the deck layout was modified to include “multiple labware sources”.

5.3.3.3 Minimizing material waste

Minimization of material waste included maximizing the utilization of prepared solutions and reusing labware, such as tips. In our case, the following specific measures were implemented to reduce material wastage:

- A 96-well PCR plate with convex-bottom wells was utilized for the mixing of the precursor aliquots. The cone-shaped bottom has a smaller dead volume than a flat bottom well. For the same reason, 1.5 mL Eppendorf tubes were utilized for preparing precursor solutions.
- To maximize utilization of well plates, an additional code was implemented to enable the instrument to recognize previously used wells. This allowed continued use of well plates until all positions were occupied.
- The same tips were utilized for the mixing step and the final transfer of the pre-hydrogel mixture to the 384-well plate, allowing for a reduction in tip usage and minimizing the time between the mixing and the final transfer stages.

5.3.4 Pretesting of the pipetting parameters using water

To set the starting values of the flow rate in the aspiration and dispense steps, and the tip height from which these steps are performed, a preliminary study using water was performed. This step helped finding and solving pipetting errors like:

- Air aspiration when using a fixed tip height during a pipetting step and the liquid level is below the selected 1-2 mm tip height.
- Splashing and bubble formation due to too high flow rate. The maximum flow rate supported by the Microlab Nimbus was 500 $\mu\text{L}/\text{s}$. In our experiments, 250 $\mu\text{L}/\text{s}$ was initially tested as flow rate for the aspiration and dispense steps. However, after observing splashing on the well walls of the 96-well plate and occasional bubble formation, a decrease to 140 $\mu\text{L}/\text{s}$ and finally to 60 $\mu\text{L}/\text{s}$ was necessary. At the latter flow rate, splashing was successfully eliminated.

- Regarding the dispense mode, two options were available in the Microlab Nimbus instrument: *jet empty tip*, which was designed for dispensing into empty wells by setting a certain fixed height, and *surface empty tip*, designed for dispensing liquid on top of another liquid by sensing the liquid surface, either inside or outside of it. Depending on the availability or absence of liquid in the container where the dispense would take place, the dispense mode was selected.

5.3.5 Pipetting with hydrogel precursor solutions

Once the basic pipetting parameters were identified using water, experiments with the hydrogel precursor solutions were started. As described in the previous section, the initial flow rate was set to 60 $\mu\text{L/s}$ and the tip height to 1 mm for the aspiration and dispensing speed. However, these parameters required adjustment since the precursor solutions have higher viscosity than water.

The optimization of the pipetting method required adjusting the values of the pipetting parameters listed in **Table 1**. Each step of the pipetting process (**Figure 1**) was individually tested and the parameters were modified based on visual analysis as specified in this section.

Table 1. Pipetting parameters which depend on the liquid handling process (column on the left) or the properties of the liquid (column of the right).

Liquid handling related parameters	Liquid properties related parameters
Dispense mode	Flow rate ($\mu\text{L/s}$)
Tip height (mm)	Mixing flow rate ($\mu\text{L/s}$)
Volume (μL)	Air transport volume (μL)
Mixing cycles	Swap speed (mm/s)
Mixing volume(μL)	Stop back volume (μL)

i. Transference of stock solutions to 96 PCR well plate

In the aspiration step for the transfer of the two stock solutions to the 96 PCR-well plate, the tip height was adjusted according to the available liquid and the volume to be aspirated at each stage of the method. At each aspiration step, the tip height was positioned 1-2 mm below the liquid surface, based on a preliminary visual study. As the stock solution volume decreased after preparing one column of hydrogels, the tip height

in the next aspiration step was lowered. This measure minimizes the liquid that remains attached to the outer part of the tip when it retracts from the liquid.

For dispensing of the MS stock solution, a 1 mm tip height, worked well, while for dispensing the SH aliquot, the tip height was readjusted to 1.5 mm since the MS solution was already in the well. These conditions avoided bubble formation.

Using 60 $\mu\text{L/s}$ dispensing flow rate, bubble formation was observed, probably due to the higher viscosity of MS solutions than water solutions. Lower flow rates (36 and 12 $\mu\text{L/s}$) were tested and neither bubbles nor splashing was observed. Since opaque black conductive tips were used, the behavior of the liquid inside the tip could not be observed during the aspiration step. To minimize risk of viscous liquid “jumping” inside the tip, a slow flow rate (12 $\mu\text{L/s}$) for both aspiration and dispensing was selected.

The formation of small drops at the end of the tip during the transport of the MS aliquot from the Eppendorf to the PCR 96-well plate was observed. This dripping effect was neither observed during the optimization with water, nor during the transfer of the SH aliquot to the same well plate, and was therefore attributed to the higher viscosity of the MS solution. To prevent the resulting contamination and material loss, the *air transport volume* function was activated. This function allows aspiration of a small volume (1 μL in this case) of air immediately after the desired volume, after the withdrawal of the tip from the liquid.

It was also observed that a liquid layer remained on the external surface of the tip when retracting from the stock solutions. This is due to the slow flow of the viscous solution and the good wetting properties of the tip surface, potentially resulting in uptake of larger volumes than desired. To mitigate this issue, the tip retraction speed (*swap speed*) was set to 20 mm/s for the MS solution and 30 mm/s for the SH solution. At this speed, a very thin layer of liquid was still observed for the MS aliquot, while no liquid was visible in the case of the SH solution.

Dispense mode by jet empty tip was used for the MS aliquot since it was the first stock solution to be dispensed into an empty well. Surface empty tip was selected for the dispense of the SH aliquot on top of the MS aliquot.

ii. **Mixing in 96 PCR well plate**

For the mixing step, the default mixing option available in the software was employed, which included three pipetting parameters: flow rate, volume, and cycles.

An equal flow rate (12 $\mu\text{L/s}$) was applied for the aspiration and dispensing steps, according to experience in the previous step of the method (transference of the stock solutions).

During the mixing process, the tip position was fixed to a default tip height of 0 mm from the bottom of the well based on the calibrated position. However, variation of 0.2 to 0.4 mm was observed between the calibrated height and the actual position of the well bottom.

The mixing volume was initially set to 70 % of the volume inside the well based on the experience at IPF. Visual inspection of the mixing process showed that less than 50 % of the liquid was being aspirated and dispensed under these conditions. The difference was due to the proximity of the tip and the bottom of the well which created a vacuum effect and resulted in incomplete aspiration of the targeted volume during aspiration. Therefore, 90 % of the volume inside the well was set as mixing volume.

The number of mixing cycles, which involved one aspiration and consecutive dispensing for each cycle, was initially set to 7 attending to IPF experience with similar systems.

iii. **Transference of pre-hydrogel mixture to 384-well plate**

In the final step of the method, aliquots of the hydrogel precursor mixture (5 μL) were transferred to a 384 low volume well plate with wells of 25 μL and a truncated cone shape. The truncated cone shape required low dispensing speed to avoid misplace of the dispensed volume. The higher viscosity of the precursors mixture, since the gelation starts immediately upon mixing, required lower aspiration (9 $\mu\text{L/s}$) and dispensing (8 $\mu\text{L/s}$) flow rates.

The parameter *stop back volume* was used in the dispensing step to aspirate a small air volume (set to 2 μL) right after dispensing the targeted volume to achieve accurate

delivery. This step eliminated dripping during the movement of the tip from the first to the second dispense in odd and even wells.

In the final dispensing step, which involved dispensing the remaining liquid into empty wells in two consecutive steps (odd and even wells), the *jet partial volume* mode was used as dispensing mode, allowing consecutive dispensing in the different wells. The swap speed for this step was fixed to 150 mm/s (without option to be modified).

Formation of some hydrogels on the wall of the wells was observed in less than 10 % of the wells. To prevent dispensing onto the walls, calibration of the center position of the wells was necessary.² In addition, a slower swap speed (i.e. retraction speed of the tip) leads to a gradual spreading of the drop on the surface of the liquid inside the well during the dispensing step. Higher retraction speeds led to drop sticking to the tip and falling into a different part of the well. Since the swap speed could not be varied in the same method, the tip height was modified. By lowering the tip height from the 1 mm position above the bottom (selected during optimization with water) to 0.3 mm, the issue was overcome. Lower tip heights facilitate contact and adhesion between the drop and the bottom surface of the well while the tip is retracted from the well.

The optimization of the process with polymer solutions based on visual observation led to a working pipetting method without apparent splashing, bubble formation or dripping in any of the steps. However, because of the use of non-transparent, the flow of the liquid in the interior part of the tip could not be observed.

5.3.6 Establishment of mixing parameters for PEG-4TzMS hydrogel preparation using a Design-of-Experiments approach

A design of experiments (DOE) approach was employed to systematically investigate and the influence of three different parameters of the mixing step in the variability of the final hydrogels. This approach enables the examination of the significance of the individual factors involved, as well as the interactions between these factors. The studied parameters are listed in **Table 2**.

Table 2. Pipetting parameters that influence the mixing process during automated pipetting method.

Mixing flow rate	Speed at which both aspiration and dispensing are performed during mixing.
Mixing volume	Percentage of the volume contained in the well, which will be used for mixing.
Mixing cycles	Number of consecutive aspiration and dispensing steps.

To quantify the variability of the prepared hydrogels, fluorescence spectrophotometry was selected. Two fluorescent dyes with different emission wavelengths were added to the stock solutions and the fluorescence signal from each dye in the final hydrogel was quantified with a plate reader. It was assumed that variations in the pipetted volumes or in the homogeneity of the mixed volumes would lead to differences in the fluorescence signal.

The variability was evaluated using two statistical parameters: the coefficient of variation in % (CV%) and the difference in % between the signal from even and odd wells (even / odd ratio %). The coefficient of variation has been used to study the variability of pipetted volumes in both automated and manual liquid handling,^{3,11,12} while the even / odd ratio % arises from the need to evaluate the variability between the two consecutive dispensing steps in odd and even wells.

For this study, a CV% and even / odd ratio % below 10 % was considered as a reasonable target according to previous works.¹³

5.3.6.1 Selection of the fluorescent dyes for detection

Two dyes with sufficient difference in their emission wavelength were initially selected: fluorescein and rhodamine B. It was observed that the fluorescence emission of rhodamine B became one order of magnitude lower in the presence of fluorescein, most probably because of a quenching effect, similar to the case described by J. Petersen and J. Nguyen.³

Consequently, Atto 488 biotin and Atto 594 biotin dyes were taken as (more expensive) alternative. The excitation and emission spectrum curves of these two dyes exhibit minimal overlap (see **Figure 3**), making them suitable for simultaneous use and enabling the fluorescence emission signal of a single dye to be studied without interference from

the other. The biotin does not interact with the PEG-MS or VPM molecules and therefore it should not impact crosslinking.

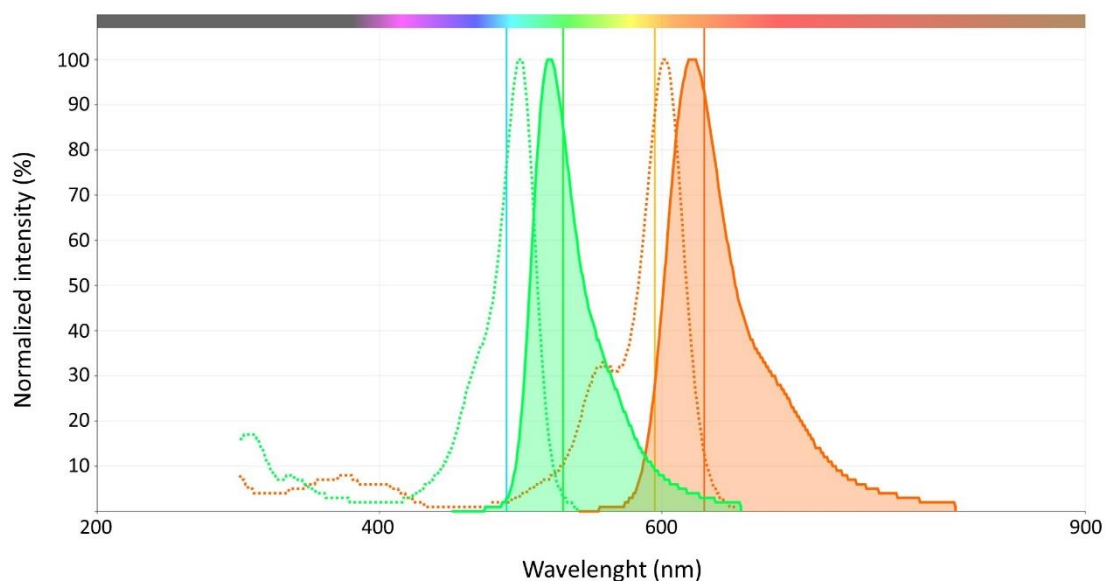


Figure 3. Spectrum of Atto 488 (green) and Atto 594 (orange) dyes. The dotted line (unfilled) corresponds to the excitation curve and the solid line (filled) to the emission curve. The first vertical line of each pair corresponds to the selected excitation wavelength (490 nm for Atto 488 and 590 nm for Atto 594) and the second vertical line of each pair to the selected emission wavelength (530 nm for Atto 488 and 630 nm for Atto 594). Created with AAT Bioquest's interactive Spectrum Viewer.

Prior to conducting the DOE experiments, the experimental parameters for fluorescence detection of the two dyes were selected. The final values for the different parameters can be found in **Table 3**.

Table 3. Parameters for the fluorescence emission measurement of the Atto dyes contained in the final hydrogels.

	Atto 488 biotin	Atto 594 biotin
Excitation Wavelength (nm)	490	595
Emission Wavelength (nm)	530	630
Excitation Bandwidth (nm)	9	9
Emission Bandwidth (nm)	20	20
Gain	70	80
Number of Flashes	25	25
Integration Time (μs)	20	20
Z-Position (μm)	8000	10000

5.3.6.2 Impact of flow rate, volume, and cycles on the mixing

To maximize the information about the system and considering the relatively low number of experiments required with a three-factor analysis, a full factorial design was preferred over a fractional design.

The factors studied were the flow rate, volume and cycles from the mixing step (**Table 2**). Two levels were selected for each parameter, low and high (**Table A** from **Figure 4**). The low values for the three parameters were obtained from the previous study on the pipetting protocol using polymer solutions (section 5.3.5). A flow rate of 36 $\mu\text{L/s}$, previously tested along with 12 $\mu\text{L/s}$ (section 5.3.5), was chosen as it did not result in splashing or bubble formation. Regarding the high value of the mixing volumes, a test with 100, 120, 130, and 140 % was run. 100% and 120% did not produce bubbles, but they were considered insufficient in terms of the volume of liquid aspirated during the mixing process. At 140%, no bubbles were observed even if the entire liquid volume was aspirated. However, aspirating all the liquid could potentially lead to inadequate turbulence formation, and random bubble formation may occur. Thus, a volume percentage of 130 % seemed a good compromise. Approximately 10 % of the liquid volume contained in the well remained after aspiration, which was considered sufficient for generating turbulence when dispensing the remaining 90 % on top during the mixing process. Finally, the high value for the mixing cycles was arbitrarily selected.

A center point was included to investigate the impact of using the middle values of the selected factors. Additionally, an extra data point (highlighted in red in **Figure 4C**) was added to the experiment, which was not part of the original design, with the purpose of examining the impact of mixing volume (middle level) along with high settings for the other factors, as it was hypothesized that the mixing volume would play a major role in the mixing process. The reason behind using high levels for the other two factors was that a higher flow rate would create stronger turbulence, and a higher number of cycles would help to ensure thorough mixing. Therefore, the extra data point was set to the high levels of flow rate and cycles, along with a medium level of volume.

For each condition a column of 6 gels was prepared using the protocol in **Figure 2B**, giving 3 “odd” gels and 3 “even” gels.

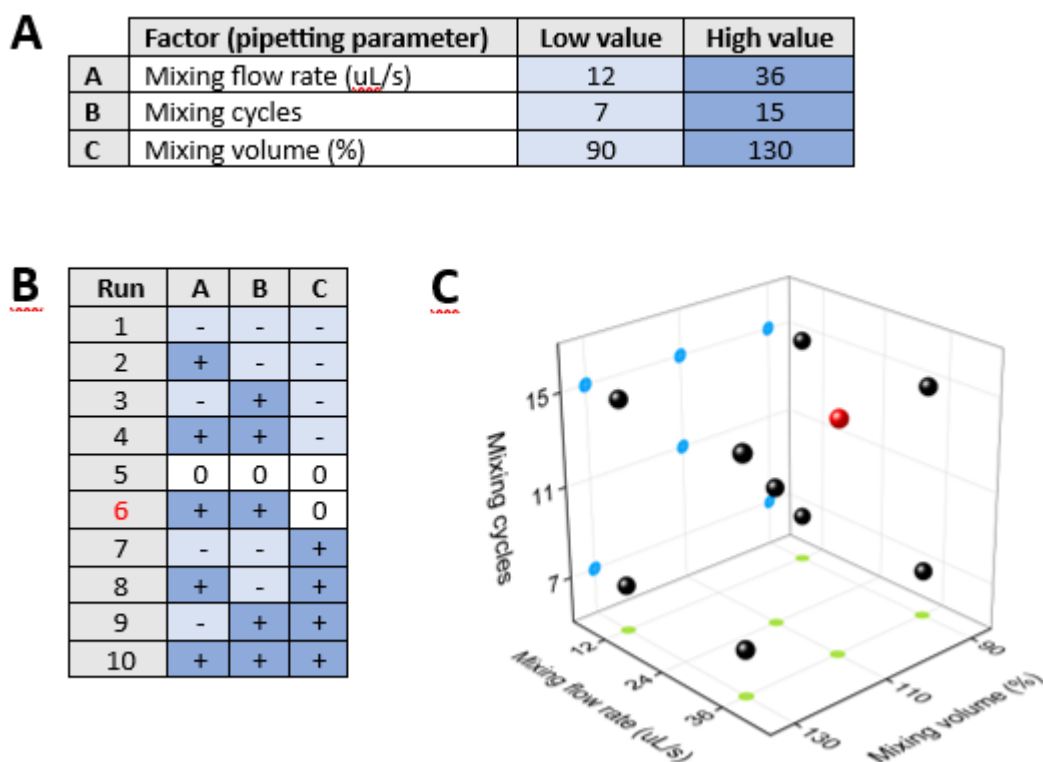


Figure 4. Full factorial design to optimize the mixing step. A) Factors and respective levels (low and high), B) Randomized design table showing the reference number of each run (extra point of interest not included in the design marked in red), and C) Visual representation of experiment conditions.

To have enough data for statistical analysis, each experimental point or condition was repeated twice. In addition, the preparation of the hydrogels followed a randomized order for the different columns.

After hydrogel preparation, the fluorescence signal of the resulting hydrogel samples in the wells was measured, and the CV % and even / odd ratio % for the gels prepared under different conditions in the 2^3 full factorial design were calculated and analyzed (**Figure 5**).

A CV > 10 % was obtained for the hydrogels prepared with 90 % mixing volume according to the variability of the fluorescence signal corresponding to the two Atto dyes (**Figure 5**). Within the 4 different conditions that were tested, the one where the three factors under study had low values showed the highest CV %. The combinations with 36 $\mu\text{L/s}$ flow rate showed lower CV % values than the combinations with 12 $\mu\text{L/s}$. Furthermore, the samples with 36 $\mu\text{L/s}$ and 15 mixing cycles showed the lowest CV %.

The center point showed a CV around 20 % according to the Atto 488 measurements, but only 3 and 9 % according to the Atto 594 fluorescence value. The extra point with high values for both mixing flow rate and mixing cycles, and medium for mixing volume, showed even lower CV % values.

Samples prepared with a mixing volume of 130 % showed a lower CV %. Run 7, in which just the volume percentage was set to a high value, gave similar results to run 4 (opposite values) with a CV % between 20 and 25 % for Atto 488 and between 10 and 15 % for Atto 594, while the rest of the runs (8, 9 and 10) had a lower CV %. Run 10 showed a CV % <10 % for both dyes.

In most runs, a significant difference was observed between the CV % of the two Atto dyes, with the CV % of Atto 488 being higher in most cases. This disparity decreased in the samples prepared with 130 % mixing volume.

The % of fluorescence difference between the emission in odd and even wells varied in consonance with the CV % (**Figure 5**). Additionally, in accordance with the CV % results, a significant difference was observed in the even / odd ratio % between Atto 488 and Atto 594, with values reaching 164 % and 66 % respectively. This distinction can be observed in **Figure 5**, where the ratio % of Atto 488 tended to be much higher compared to the optimal value of 100 %, while the ratio % of Atto 594 was relatively closer. Particularly, in run 10, the even / odd ratio % for both dyes was very similar, with a difference of 8.3 % for Atto 488 and 4.3 % for Atto 594 in runs 10 and 10' respectively.

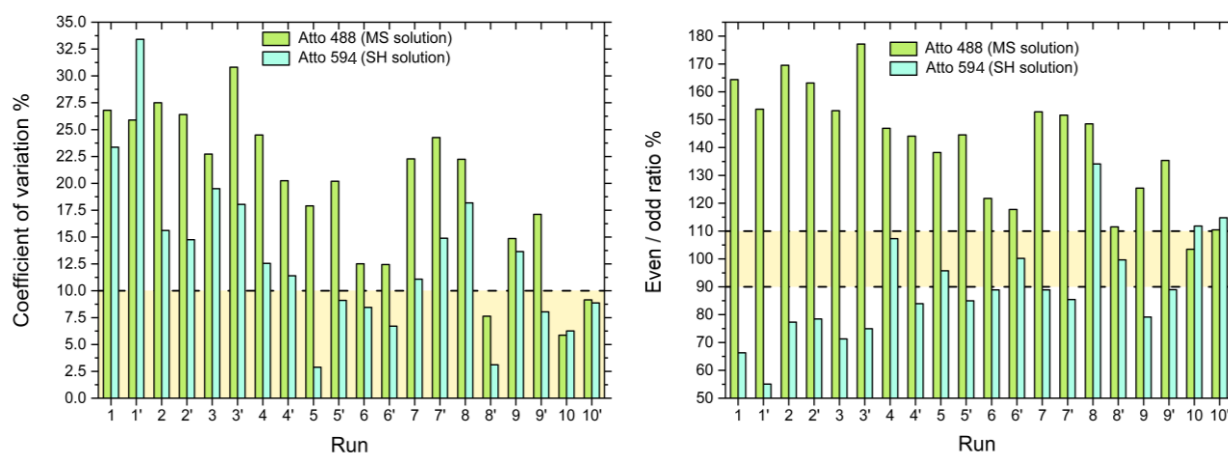


Figure 5. Plots showing coefficient of variation % and even / odd ratio % from raw fluorescence of Atto 488 (MS aliquot) and Atto 594 (SH aliquot). Each replicate (run) corresponds to 6 hydrogels (3 odd + 3 even), 12 hydrogels per condition.

A tendency to lower CV % and even / odd ratio % was observed by moving from low to high levels of the 3 mixing factors.

By varying the mixing parameters while keeping the pipetting parameters from other steps of the method constant, the impact of effective or ineffective mixing could be analyzed. Furthermore, by enhancing mixing through higher levels of the mixing parameters, both dyes (and hypothetically, the stock solutions) were more evenly distributed in the pre-hydrogel mixture and equally dispensed across all wells, leading to a decrease in CV % and improved homogeneity in the final hydrogels. However, high flow rates could cause stress to cells in future experiments.² Therefore, it will be necessary to study the effect of these high settings in cell viability.

Fluorescence measurements revealed an unequal distribution of the two dyes in odd and even wells. In odd wells, the concentration of Atto 594 was higher, while Atto 488 was more concentrated in even wells. This discrepancy is attributed to the sequence of addition of the stock solutions and to incomplete mixing. Before mixing, PEG-4TzMS is dispensed first into the well, while VPM is dispensed on the top. If incomplete mixing occurs, the PEG-4TzMS volume is expected to concentrate at the bottom of the well, while the VPM volume remains at the top. During the subsequent aspiration of the mixture from the bottom of the well (**Figure 6**), the position of the PEG-4TzMS and VPM rich volume are interchanged inside the pipette tip. Therefore, a higher volume of the stock solution containing Atto 594 is dispensed into odd wells, while a higher volume of the stock solution containing Atto 488 is dispensed into even wells.

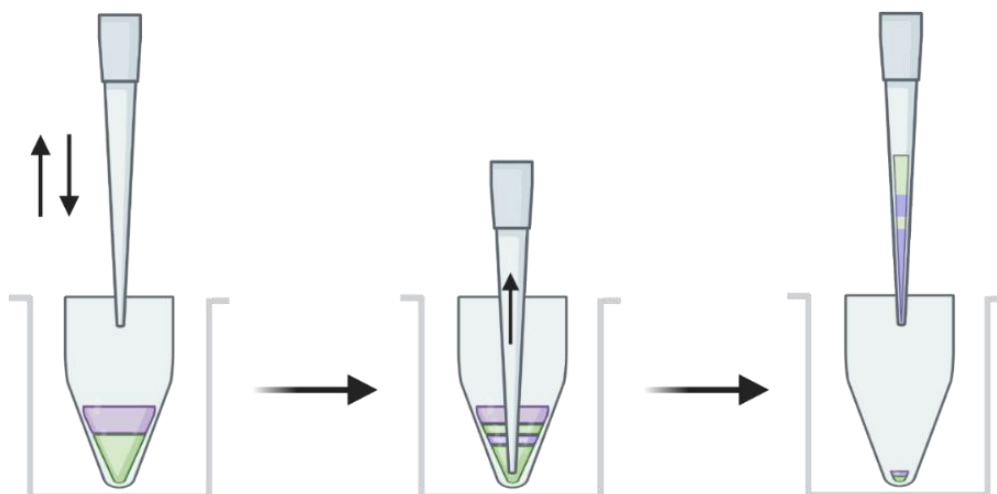


Figure 6. Scheme of an incomplete mixing of the two precursor aliquots in a well from the PCR 96-well plate, leading to aspiration of inhomogeneous mixture. After the aspiration from the last transfer, PEG-4TzMS (green) is mostly located in the lower part of the tip, and most of the VPM (purple) is situated on the top part. *Created with BioRender.*

With increasing mixing, the difference in concentration between the two dyes almost disappeared (run 10, **Figure 5**), which is associated with the improved homogeneity of the mixture achieved before dispensing it into the individual wells of the 384-well plate.

Despite the described trends observed in **Figure 5**, the statistical analysis of the data from **Figure 5** with the Minitab software did not lead to consistent results.

When considering the CV % and even / odd ratio % as response variables, none of the effects were significant for either Atto dye, as indicated in the Pareto chart in **Figure 7**. The boxes representing the factors or their interactions are below the threshold of significance (represented by the red dotted line). Furthermore, the factors exhibiting a greater effect are different according to the responses of Atto 488 to Atto 594. An example is the mixing volume, that appears to have a stronger effect on the responses of Atto 488, while the interaction between the mixing volume and the mixing cycles is the most influential factor for Atto 594.

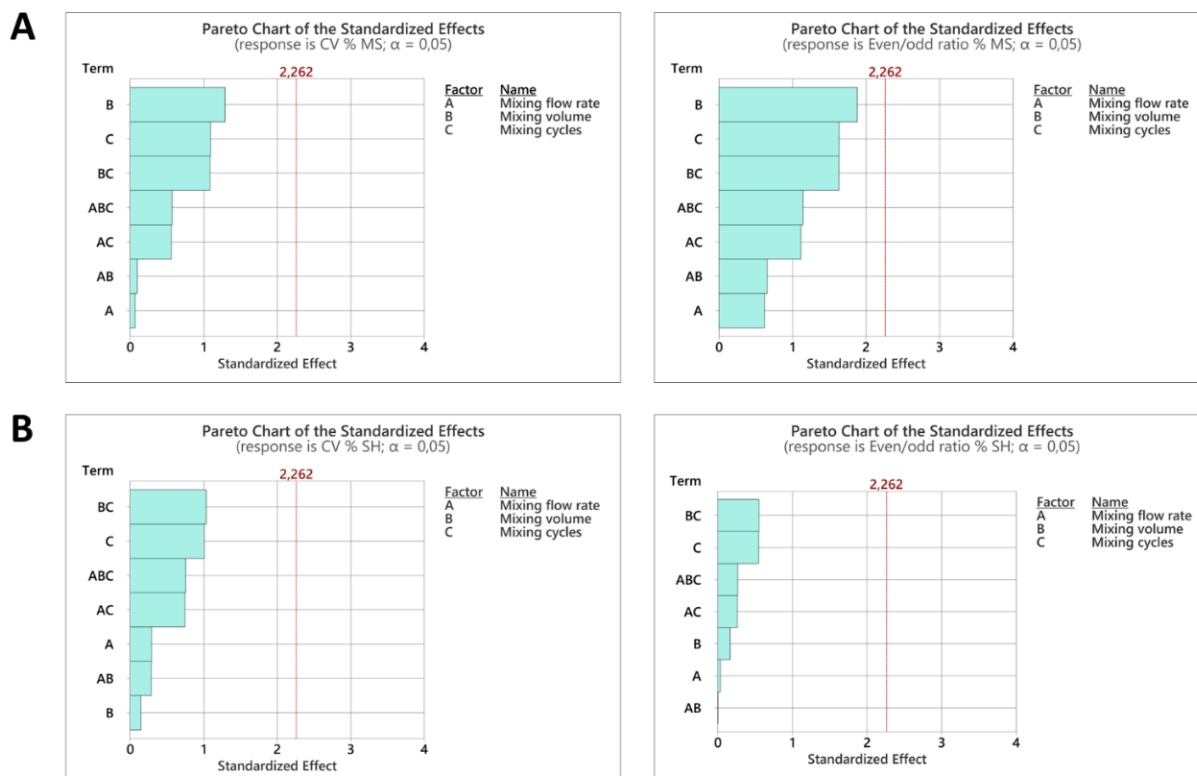


Figure 7. Pareto charts displaying the standardized effects of the 3 mixing factors and their interactions. The chart represents the results of the DOE experiment’s analysis, with a 95 % confidence interval and an α level of 0.05. A) Responses of the CV % and the even / odd ratio % of Atto 488, B) Responses of CV % and the even / odd ratio % of Atto 594.

A similar scenario was observed when considering the emitted fluorescence as the response variable for both Atto dyes (**Figure 8**). In this case, the mixing flow rate showed the highest effect on both dyes, but its significance differed between Atto 488 and Atto 594. The mixing flow rate was found to be not significant for Atto 488, while it was significant for Atto 594. In addition, the effects of the other factors and their interactions varied between the responses of Atto 488 and Atto 594, resulting in inconsistency regarding the effect of the mixing parameters from the DOE experiment.

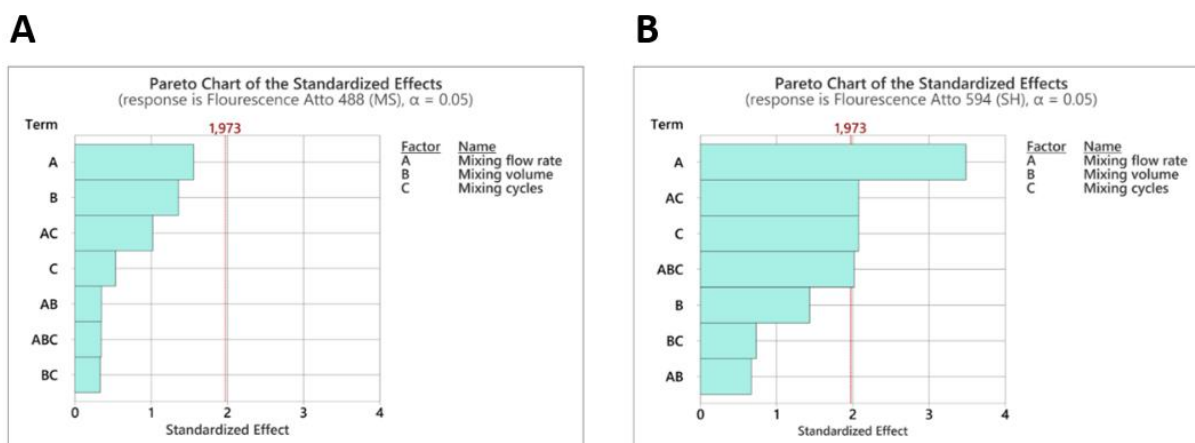


Figure 8. Pareto charts displaying the standardized effects of the 3 mixing factors and their interactions. The chart represents the results of the DOE experiment's analysis, with a 95 % confidence interval and an α level of 0.05. A) Response of the fluorescence from Atto 488, B) Response of the fluorescence from Atto 594.

The analysis of the results from the DOE experiment shows that no conclusive statements can be drawn regarding the significance of the effects of the different mixing factors. This is attributed to the presence of uncontrolled parameters affecting the pipetting process beyond the mixing stage. The uncontrolled parameters may include the internal organization of the mixture (previously discussed), the progressively increasing viscosity following the mixing of the precursor solutions, or the aspiration and dispensing steps involved in the different steps of the pipetting method. It became necessary to isolate each individual pipetting step for an in-depth analysis, aiming to draw conclusions without the interference from other steps. By isolating a specific pipetting step, the suspected parameters that influence the variability could be studied to assess their impact on the CV % and even / odd ratio %, enabling the optimization of the entire pipetting method and increasing the reproducibility of the final hydrogels.

5.3.7 Insights from the two consecutive dispensing steps into the 384-well plate

Apart from the mixing step, a possible source of variability could be the low accuracy during the aspiration and dispensing involved in the two other key steps of the automated method (**Figure 2B**): the transfer of the stock solution to the PCR 96-well plate and the final transfer of the pre-hydrogel solution to the 384-well plate. However, among these

two pipetting steps, the last transfer step seemed more likely to introduce variability because of the following reasons:

- i. First dispensing effect. The final transfer takes place in two consecutive dispensing steps. Possible variations between these two steps are dryness of the tip during the first dispensing step, the different remaining volume inside the tip between each dispensing step, or the air gap resulting from the *blowout volume*, which was implemented to prevent dripping during the transition from the odd to the even wells.

What was defined as “first dispensing effect” in the current work, has been previously reported as “first shot or “last shot” in other works,¹² pointing out that there could be differences between the first and last dispense steps of a sequential dispensing process. The first dispense could result in a higher inaccuracy than the consecutive dispensing steps within a sequential dispense.¹⁴

- ii. The viscosity increase that occurs after mixing the two hydrogel precursors can potentially impact the two consecutive dispensing effect. Note that there are 3 – 4 seconds delay between the first and second dispense steps.
- iii. In the aspiration and dispensing of low volumes, small deviations have a big impact in variability. During the last transfer step, 5 μL are dispensed into each well. The pipetting robot used in this work presented an accuracy of 2.5 % (regarding the accepted value) and a precision of 2.0 % (coefficient of variation) for volumes of 5 μL (using 50 μL tips).

Different solutions were studied to minimize the effects of the listed factors on the variability of the final hydrogels, such as using sacrificial wells to avoid the first dispensing effect, varying the gelation time to modify the viscosity, or using asymmetric volumes to compensate the dispensing deviation during the two consecutive dispensing steps.

5.3.7.1 Isolation of the final dispensing step by manual mixing

The automated transfer of the hydrogel precursors mixture from the PCR 96-well plate to the 384-well plate was isolated from the other pipetting steps by modifying the automated protocol (**Figure 9**). The transfer of stock solution aliquots and vortex mixing

were conducted manually, whereas the final transfer step was carried out by the robot. Despite using the same automated protocol, the manual steps were disabled in the revised pipetting method.

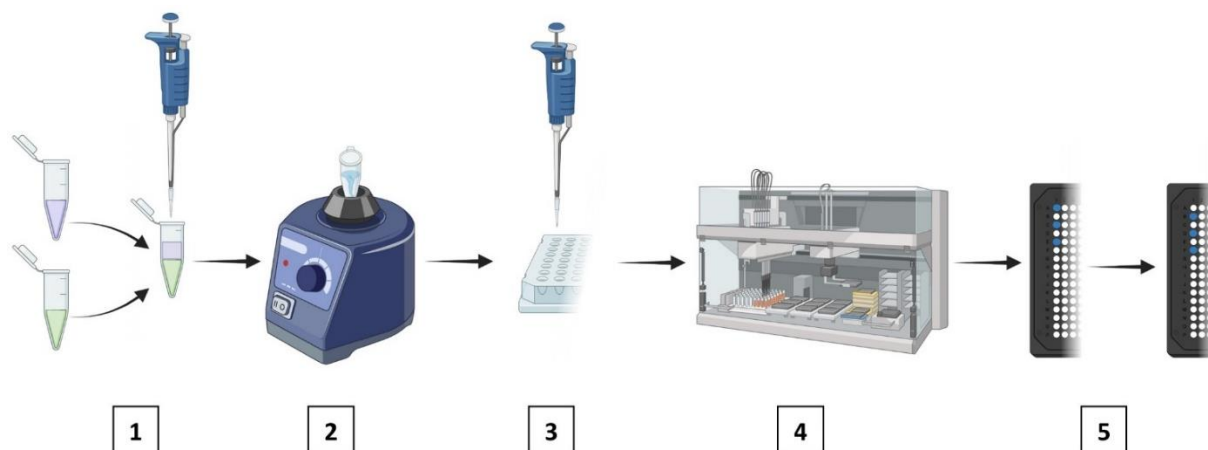


Figure 9. Simplified protocol. The 96-well PCR plate was manually prepared by pipetting stock solutions into a 1.5 mL Eppendorf tube, vortexing for 25 seconds, and manually transferring the fully mixed solution into the 96-well PCR plate. This process takes approximately 80-90 seconds, which is comparable to the time it would take for a robot to complete the same task. *Created with BioRender.*

5.3.7.2 First dispensing effect: the impact of using sacrificial wells

To mitigate the potential differences between the first and second dispense, sacrificial wells were employed. This approach involved aspirating an additional volume of 4 μL (per channel) from the mixed pre-hydrogel solution and introducing an extra 4 μL dispensing step before dispensing into the odd and even wells (**Figure 10**). Lower dispensing volumes could not be dispensed with the equipment.

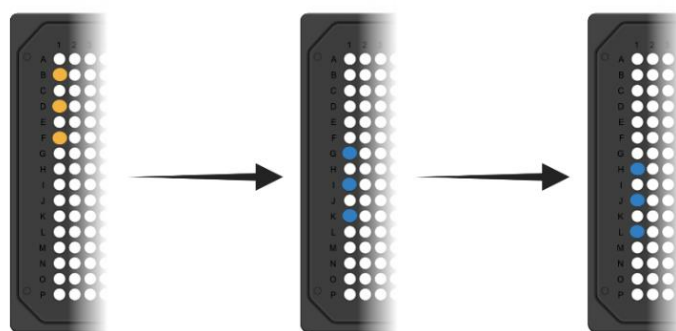


Figure 10. Sacrificial wells (yellow) which are filled before the consecutive dispensing in odd and even wells (blue). *Created with BioRender.*

When sacrificial wells were employed, an overall odd and even difference of 4 % was observed (**Figure 11A**). On the other hand, when sacrificial wells were not used, the overall odd and even difference was 7.5 % (**Figure 11B**).

The CV % consistently remained below 10 % for all four repetitions of the experiment. Furthermore, in three out of these four repetitions, the CV % dropped below 5 % (**Figure 11C** top). The CV % was also below 10 % in the experiment without the sacrificial well, but only in one repetition did it go below 5 % (**Figure 11D** top). These results were in consonance with the even / odd ratio %, where all the four repetitions were below the 10 % when using sacrificial wells (**Figure 11C** bottom). However, when not using sacrificial wells, the even / odd ratio % slightly surpassed the targeted 10 % by 2 % in two out of four repetitions (**Figure 11D** bottom).

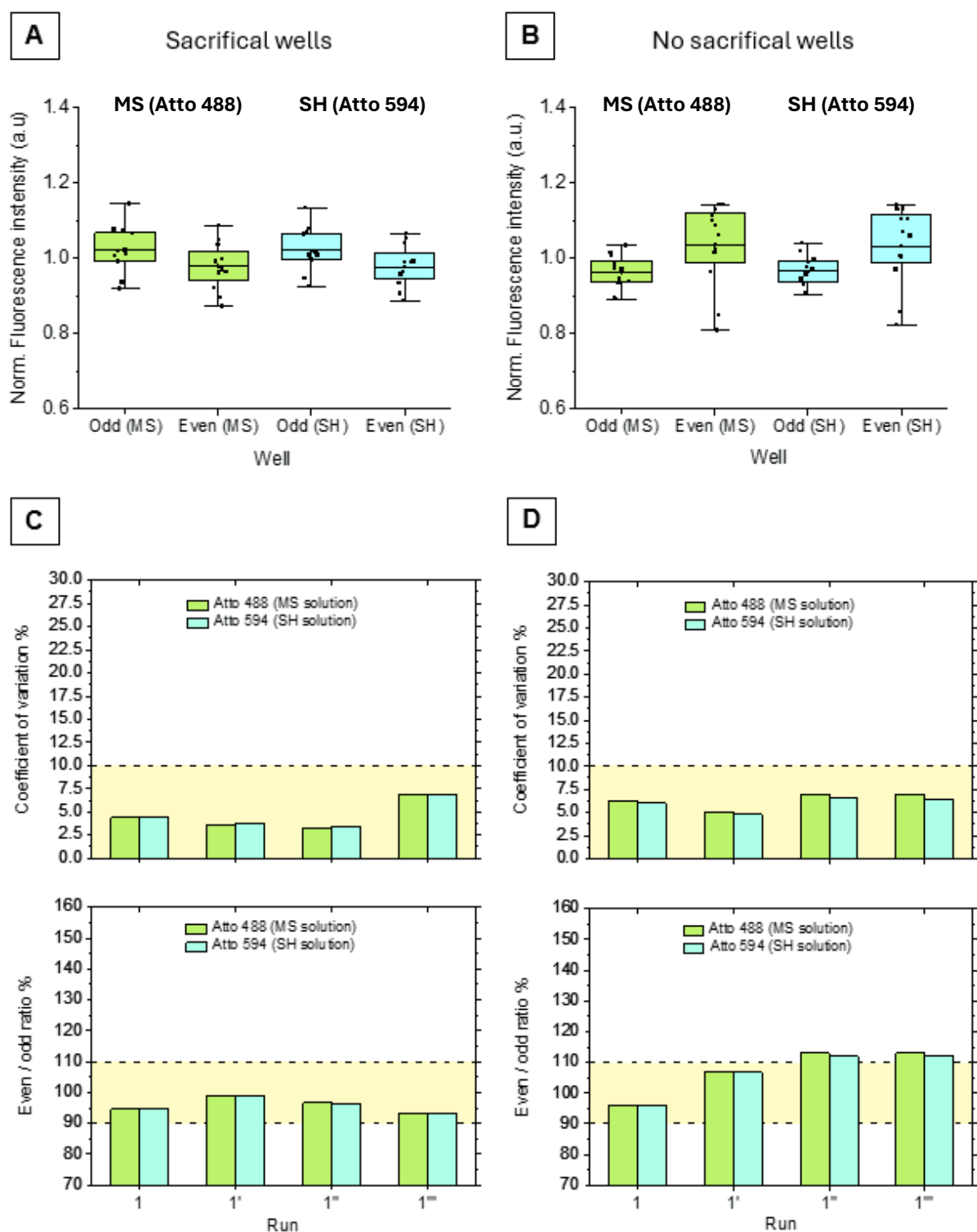


Figure 11. A, B) Distribution of normalized fluorescence data from two different dyes, Atto 488 (MS aliquot) and Atto 594 (SH aliquot). Each pair of boxes corresponds to one dye, with one box for the odd wells and one box for the even wells. The data shown in the box plots correspond to the fluorescence signal obtained from 12 replicates of each dye in each type of well (odd or even) for a total of 24 hydrogel per box plot and condition. A)

Sacrificial wells, and B) No sacrificial wells. Middle and bottom plots correspond to coefficient of variation % and even / odd ratio % from raw fluorescence of Atto 488 and Atto 594 in both types of well (odd and even) using sacrificial wells (C) or not (D). Each replicate corresponds to 6 hydrogels (3 odd + 3 even), 24 hydrogels per condition.

Using sacrificial wells translated into a decrease of the difference between the odd and even consecutive dispense, it was seen by the decrease of 3.5 % between the overall odd and even difference in both scenarios. The unknown first dispensing effect was therefore minimized by using sacrificial wells. The similarity between the second and third dispense, when using sacrificial wells (which is considered the first dispense then), became higher, increasing the precision of the dispensing in odd and even wells.

In addition, it was evident that the mixing achieved through vortexing was effective, in contrast to most of the runs observed in the DOE experiment. This is apparent in all plots presented in **Figure 11**, as the fluorescence signal for both Atto dyes are very similar within each well. The points are evenly dispersed and distributed in the box plots (**Figure 11A, B**), and the boxes significantly overlap in the bar plots (**Figure 11C, D**), indicating consistent mixing across the wells.

While sacrificial wells offered benefits in terms of reducing variability, it is important to consider the increased material waste.

5.3.7.3 Increasing viscosity: study on the effect of gelation time

Another factor that affects all pipetting steps is the increasing viscosity of the precursor mixture from the moment the two precursors are mixed, which could difficult the transfer step into the 384-well plate that occurs 5 – 10 s after mixing.

To investigate the impact of variable viscosity during the last dispense, precursor mixtures with three different gelation times were tested: 1 minute and 40 seconds, 2 minutes, and 4 minutes (**Figure 12A,B,C** respectively). The varying gelation times were achieved by changing the pH of the VPM precursor solution to 7.70 7.40 and 7.00 respectively. The higher the pH, the faster the gelation and the increase in viscosity, and therefore the expected impact in the transfer step.

Increasing the gelation time translated into a decrease of the overall odd and even difference (**Figure 12** left). Following the same trend, longer gelation times translated into lower CV %. A gelation time of 4 min rendered a CV of 2.6 % vs 1 min 40 sec that showed a CV of 12.5 % (**Figure 12D**).

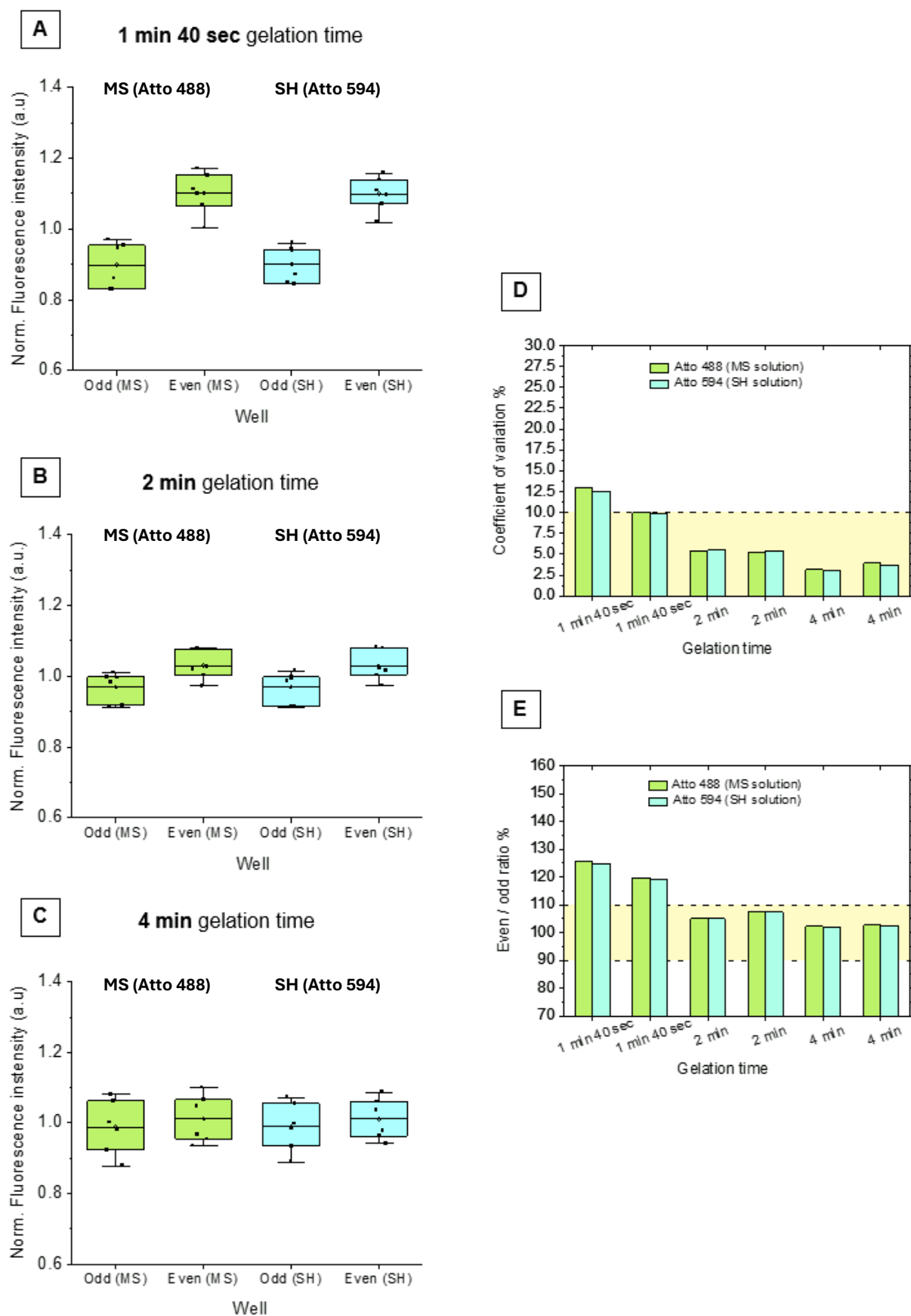


Figure 12. A, B, C) Distribution of normalized fluorescence data from the two different dyes, Atto 488 (MS aliquot) and Atto 594 (SH aliquot). Each pair of boxes corresponds to

one dye, with one box for the odd wells and one box for the even wells. The data shown in the box plots correspond to the fluorescence signal obtained from 6 replicates of each dye in each type of well (odd or even) for a total of 12 hydrogels per box plot and condition. A) Gelation time of 1 min 40 sec, B) Gelation time of 2 min, and C) Gelation time of 4 min. Plots on the right correspond to D) Coefficient of variation % and (E) even / odd ratio % from raw fluorescence of Atto 488 and Atto 594 in both types of well (odd and even). Each replicate corresponds to 6 hydrogels (3 odd + 3 even), 12 hydrogels per condition.

A decrease in the odd and even overall difference from 22 % to approximately 2.6 % was achieved by increasing the gelation time from 1 min and 40 sec to 4 min. Fast gelation times resulted in larger differences between the first and second dispense (left **Figure 12**). This disparity in dispensed volumes between odd and even wells was also evident in the higher CV % and even / odd ratio % observed at lower gelation times for the different runs (right **Figure 12**).

Higher volumes were dispensed in even wells than in odd wells. This is not expected to be a consequence of the rising viscosity since the liquid from the second dispense into even wells, which occurs 3 to 4 seconds after the first, should have a higher viscosity and eventually result in lower volumes. This could be explained by a combined effect of the “stop back volume” parameter, which involves reversing the plunger to aspirate air after dispensing a volume (previously explained in this chapter), and the increasing viscosity, which could lead to an incomplete first dispense.

Pipetting problems arising from viscosity can be avoided by leaving the tip inside the dispensed liquid for longer time, but this option is not available in jet partial dispense mode (used for dispensing in empty wells). Therefore, after the first dispense and the subsequent air aspiration, while viscosity is increasing, the remaining liquid inside the tip would move down and reduce the air gap between the tip bore and the liquid inside. As a result, during the second dispense into even wells, the 2 μL air volume aspirated as stop back volume would be dispensed first, but since the liquid inside the tip pushed out some air, the actual amount of air dispensed would be less than 2 μL , resulting in some extra volume being dispensed in even wells.

The possibility of tuning the gelation rate within the physiological pH, from 7.0 to 8.0, makes the MS hydrogels suitable for the adaptation to an automated protocol with minimized impact of viscosity in the pipetting process. However, long gelation times lead to cell sedimentation and should be avoided. Thus, a gelation time between 2 and 4 minutes could be a good compromise.

5.3.7.4 Low precision dispensing: offsetting the even / odd difference at short gelation times by dispensing asymmetric volumes

In the previous two experiments involving manual vortexing for mixing, a difference of 6.2 % and 7.5 % was observed in the fluorescence signal emitted by the two Atto dyes in odd and even wells. This discrepancy was observed at a gelation time of 2 minutes, which was considered a reasonable time with both the CV % and the even / odd ratio % below the targeted 10 %. It was hypothesized that the 7 % variation between odd and even wells was due to an inherent systematic pipetting error of the instrument.

To investigate this hypothesis, asymmetric volumes of the stock solutions were pipetted to compensate the 7 % disparity between consecutive dispensing steps. Two different scenarios were tested: introducing a 3.5 % excess volume in odd wells (5.2 μL) and a 3.5 % deficit in even wells (4.8 μL), as well as doubling that amount (5.4 and 4.6 μL respectively). The expectation was that compensating for the pipetting error by adding a 3.5 % difference in volumes between even and odd wells would rectify the issue. Conversely, it was expected that doubling the necessary volume would produce the opposite outcome compared to using equal volumes of 5 μL in both odd and even wells, which was the normal volume used in all previous experiments.

Using equal volumes for the two consecutive dispensing steps led to a 12 % overall difference between odd and even wells in the new experiment, with the even wells exhibiting higher fluorescence emission (**Figure 13A**). Introducing a 3.5 % excess volume in odd wells and a 3.5 % deficit volume in even wells resulted in a 0.4 % difference (**Figure 13B**). Lastly, employing a 7 % excess volume in odd wells and a 7 % deficit volume in even wells produced a difference of 8.5 %, with odd wells displaying higher fluorescence emission (**Figure 13C**).

The corresponding calculated CV % and even / odd ratio % are represented in **Figure 13D, E**. When equal volumes or a 7 % volume excess and deficit were employed, the CV % ranged between 5 % and 10 %. On the other hand, when a 3.5 % volume difference was used, the CV % remained below 2.5 %. Regarding the even / odd ratio %, it exceeded the targeted 10 % but remained below 15 % for both extreme cases. On the contrary, the 3.5 % volume excess in odd wells and deficit in even wells resulted in an even/odd ratio below 2 %.

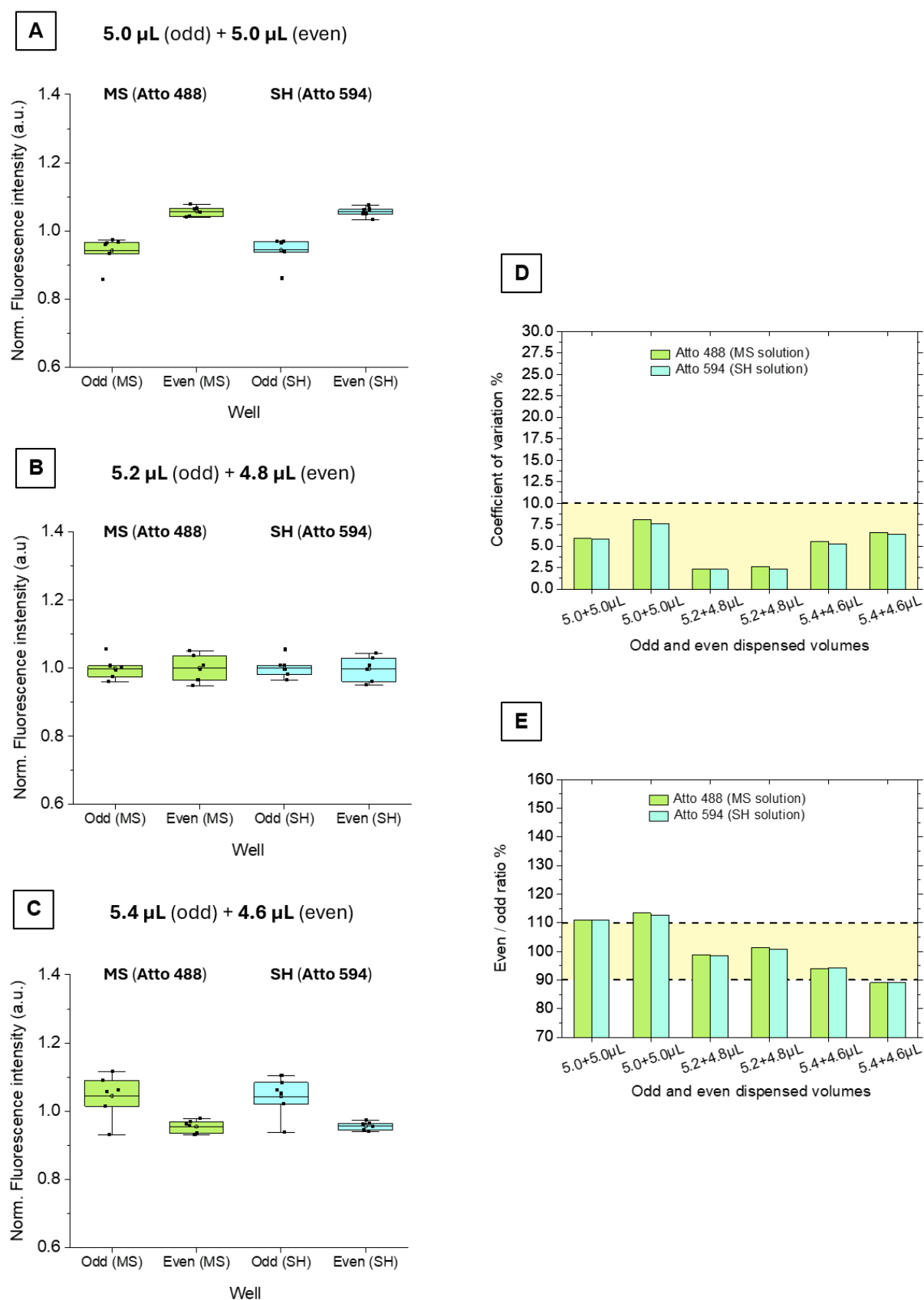


Figure 13. A, B, C) Distribution of normalized fluorescence data from the two different dyes, Atto 488 (MS aliquot) and Atto 594 (SH aliquot). Each pair of boxes corresponds to

one dye, with one box for the odd wells and one box for the even well. The data shown in the box plots correspond to the fluorescence signal obtained from 6 replicates of each dye in each type of well (odd or even) for a total of 12 hydrogel per box plot and condition. (A) Equal volumes of 5 μL dispensed in odd and even wells. (B) 5.2 μL dispense in odd wells and 4.8 μL dispense in even wells. (C) 5.4 μL dispense in odd wells and 4.6 μL dispense in even wells. Plots on the right correspond to (D) Coefficient of variation % and (E) even / odd ratio % from raw fluorescence of Atto 488 and Atto 594 in both types of well (odd and even). Each replicate corresponds to 6 hydrogels (3 odd + 3 even), 12 hydrogels per condition.

The difference between odd and even wells was mostly eliminated, reaching a 0.4 %, by using asymmetric volumes and compensating for the 7 % of fluorescence difference observed between odd and even wells when using equal volumes and performing a thorough mixing by vortexing.

5.4 Conclusions and outlook

A pipetting protocol for the automated preparation of in situ crosslinked thiol – methylsulfone – based hydrogels was programmed and tested. The automated method was successfully applied to the preparation of 5 μL MS hydrogels in a 384-well plate format. To study the variability across different hydrogels, fluorescence spectroscopy was applied by introducing two different dyes in the precursor solutions. After establishing a pipetting protocol, a design of experiments (DOE) approach was used to optimize the reproducibility of the prepared hydrogels by systematically modifying the pipetting parameters from the mixing step, translating into a better mixing of the two hydrogel precursors. By doing this, the targeted CV and even / odd ratio % of ≤ 10 % was reached. In addition, two different strategies, sacrificial wells and asymmetric volumes, have been successfully used to further minimize the difference between the two consecutive dispense steps. By using asymmetric volumes, the CV % went to the instrument imprecision limit of 2 %, while the even / odd ratio % was decreased to less than 2 %. Finally, gelation time was found to be a crucial parameter to carefully control and keep the variability at low values, due to the increasing viscosity from the mixing step and the higher difficulty to pipette viscous solutions.

After the successful development and preliminary optimization of the automated pipetting, it will be used for the 3D cell encapsulation of cells and organoids. However, new challenges may emerge from the cell encapsulation process since cells will be subjected to stress during the resuspension and mixing steps that could result in low viability. In order to not compromise the complete mixing of the precursor solutions, while keeping a high viability, different alternatives could be tested, such as decreasing the mixing flow rate and increasing the mixing cycles. Furthermore, additional modules such orbital shaker could be used to avoid resuspension of the cell-containing stock solution by pipetting up and down. On the other hand, organoids must be carefully manipulated to not disturb the cell agglomerate, which could be facilitated by using wide-bore tips and low flow rates during the automated pipetting method.

Cell culture analysis protocols, such as viability and functional assays, could also be adapted to 384-well plate format to expand the automation and save time. Challenges may also be encountered when performing simple steps like staining and washing in the small wells from the low volume 384-well plates used in this work, which have a maximal volume of 25 μ L. Special protocols or even changing the low volume 384-well plates for normal 384-well plates with higher volumes may be needed to improve washings.

Homogeneity across 3D cell-laden scaffolds, both for the cells and hydrogel precursors, could also be studied by attaching fluorescent molecules and analyzing the outputs in existing automated microscope compatible with 384-well plate format. Moreover, in more sophisticated workstations, confocal microscopes, as well as incubators, can be integrated into the pipetting robot ecosystem to highly increase the versatility and drastically decrease the experimental time.

The cell encapsulation process will be followed by the mechanical characterization of the hydrogels using techniques such as nanoindentation, which has already been successfully demonstrated for MS hydrogels in our research group, utilizing the 384-well plate format.

5.5 Materials and methods

5.5.1 Materials and equipment

A Microlab Nimbus pipetting robot from Hamilton Company (US), featuring 8 independent channels, capable of pipetting volumes ranging from 1 to 1000 μL , and CO-RE paddles was employed for the automation of MS hydrogels preparation. The instrument was the enclosed version, with a deck provided of 20 positions (136 cm L x 28 cm W x 89 cm H) which could hold up to 12 well plates, depending on the use of tips and liquid reservoirs. It was equipped with a HEPA filter and two UV lamps on each top side (left and right) of the enclosure.

The closed-source software from Hamilton was utilized to develop the pipetting protocol for the automated casting of MS hydrogels. The software was formed by different applications among which the Hamilton Method Editor, Hamilton CO-RE Liquid Editor, Hamilton Run Control and Hamilton Labware Editor were mainly used for building up the pipetting protocol.

For the fluorescence measurements, Atto 488 biotin and Atto 594 biotin (from ATTO-TEC, DE) were selected. Regarding the equipment, an Infinite 200 PRO plate reader (from TECAN, CH), integrating a support for ANSI SLAS standard format to hold the desired well plate, was used. The instrument was equipped with a Quad4 Monochromator for wavelength selection between 280 and 850 nm and automated z-focusing for high sensitivity top fluorescence measurements in low volume 384 well plates. The Tecan i-control, version 2.0.10.0, software was employed to set the experiment and perform the measurements.

Transparent 96 PCR well plates for the mixing step, as well as black 384 low volume well plates with transparent bottom from Greiner (DE) bottom for the preparation of hydrogels were used.

DOE experiments were designed with Minitab (US) software and analyzed with both Minitab and DesignExpert (from Statease, US) software.

5.5.2 Methods

5.5.2.1 Programming the pipetting method for thiol-TzMS hydrogels automated preparation

The labware to be used during the experimental protocol was virtually placed on the desired position of the deck layout (**Figure 14**) through the Hamilton Method Editor, which allowed the robot to recognize the physical location of the labware inside the instrument.

The selection of the “sequences” or available positions of the labware (e.g., different wells from a well plate) and their order of use within the pipetting method was done on the same screen of the Hamilton Method Editor, prior to initiating the method-building process.

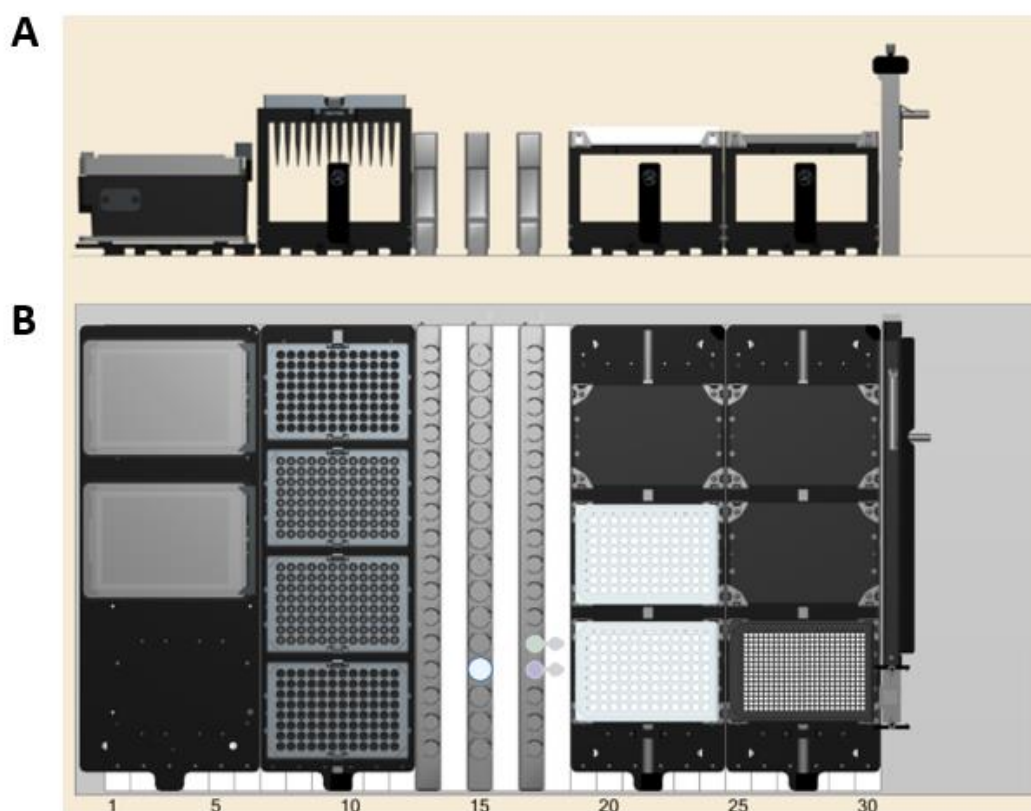


Figure 14. Screenshot from the deck layout in Hamilton Method Editor, showing the disposition inside the instrument of the labware used for building up the MS hydrogels casting protocol. A) Front view of deck layout, and B) Upper view of deck layout. From left to right: 384-well plate, 96 PCR well plates (x2), 1,5 mL Eppendorf tubes for stock

solutions (PEG-4TzMS and VPM), falcon tube for cell medium or buffer, and racks with 50 and 300 μL tips (x2 each).

Labware definition was available in files provided by Hamilton, but some specific pieces of labware like the 384 low volume well plate used in this work were not available. Changes to the existing labware, as well as creating new labware was done through the Hamilton Labware Editor (**Figure 15**).

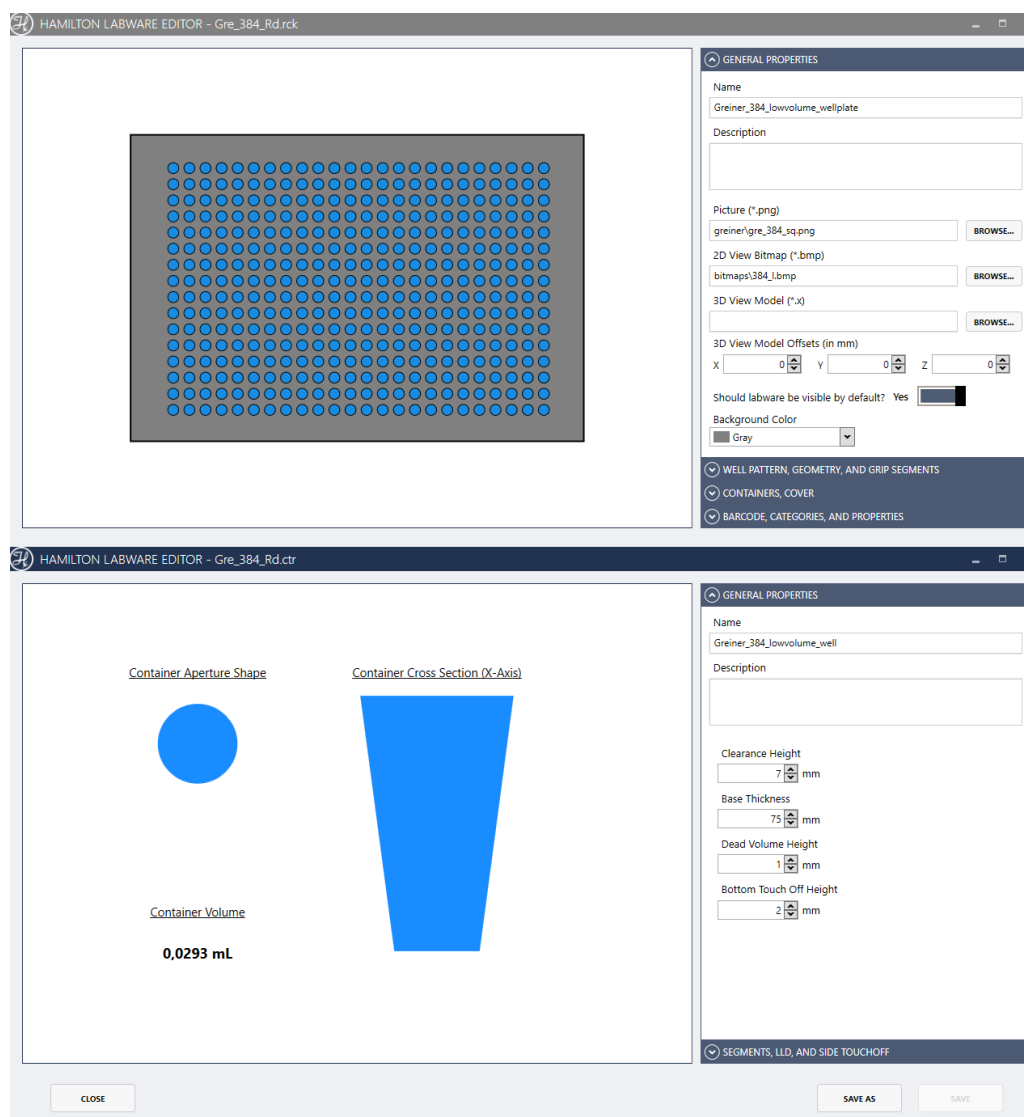


Figure 15. Screenshot from the Hamilton Labware Editor, showing the modified definition of the 384 low volume well plate used in the building protocol. The dimensions of both the well plate (upper image) and the liquid container, or well, (lower image) can be created or modified.

The pipetting method was developed using the Hamilton Method Editor software (**Figure 16**). This application allowed for drag-and-drop programming, where functions from a library were selected and placed into the code by dragging them to the desired line.

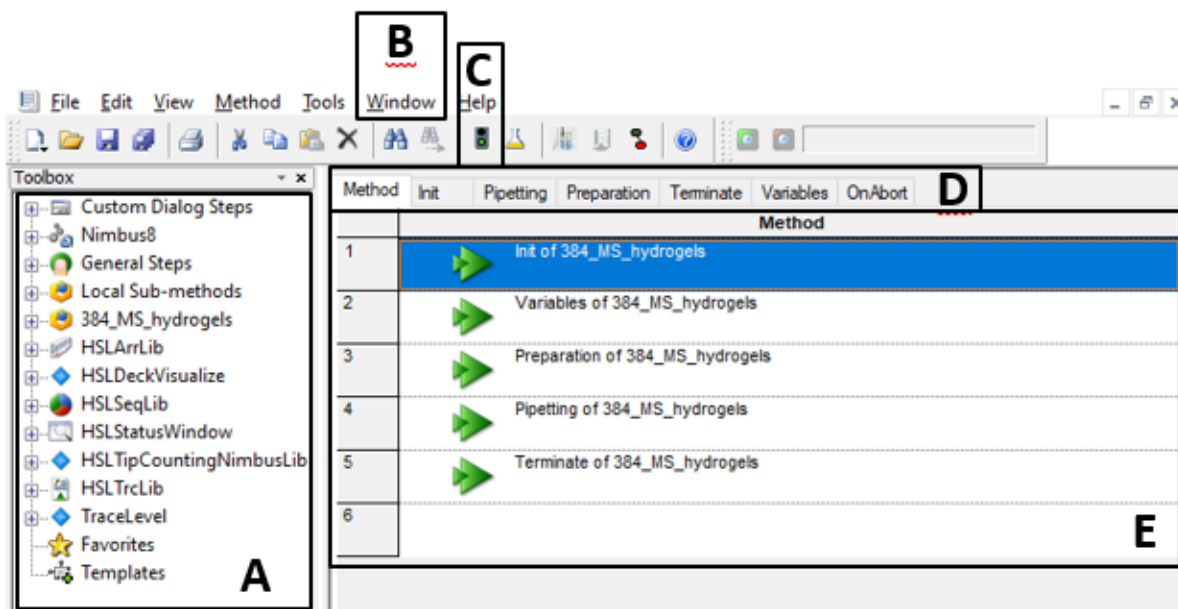


Figure 16. Screenshot from the Hamilton Method Editor showing the main screen highlighting the steps most used functionalities. A) Libraries section, showed as a drop-down menu of libraries containing all necessary functions to build up a method, B) Window selection tool to change between the different files that constitute the method, C) Run Control shortcut to access the application with the same name, with which the programmed method can be run, D) Sub-methods, or subsections, that form the main method file (.med), and E) Lines from the code produced by drag-and-drop programming.

Liquid handling parameters specific to the properties of the liquid were selected in the “liquid class” menu, accessible through the Hamilton CO-RE Liquid Editor (**Figure 17**). These parameters ranged from the dispensing mode to the liquid detection technique. When programming the pipetting method, the liquid class was selected in a drop-down menu that appears when certain functions are programmed in the code, such as the “aspirate” or “dispense” functions.

The screenshot displays the 'Liquid Details' tab in the Hamilton CO-RE Liquid Editor. The configuration is as follows:

- Liquid Device:** 1000ul Channels
- Liquid:** Water
- Tip type:** 50ul Tip with filter (Ham org. name) (23)
- Dispense mode:** Surface Empty Tip

The 'Liquid parameters' section is divided into 'Aspirate' and 'Dispense' columns, with units indicated on the right:

Parameter	Aspirate	Dispense	Unit
Flow rate:	0	0	μl/s
Mix flow rate:	0	0	μl/s
Air transport volume:	0	0	μl
Blowout volume:	0	0	μl
Swap speed:	0	0	mm/s
Settling time:	0	0	s
Over-aspirate volume:	0		μl
Clot retract height:	0		mm
Stop flow rate:		0	μl/s
Stop back volume:		0	μl

Additional settings include:

- Pressure LLD sensitivity:** Medium
- Max height difference [mm]:** 0
- Set version...** button
- Original Liquid Class

At the bottom, there are four buttons: 'Aceptar' (highlighted), 'Cancelar', 'Aplicar', and 'Ayuda'.

Figure 17. Screenshot from the liquid class drop-down menu in Hamilton CO-RE Liquid Editor, displaying the different pipetting parameters based on the type of liquid being dispensed.

The Run Control application was utilized to execute the programmed pipetting method (**Figure 18**). In this application, the code behind the method could be read line by line, and errors could be analyzed. There were available two different modes: simulation (seen in **Figure 18**), used to check whether there were errors in the code after finalizing the programming, and connection to robot, used to run the programmed method in the instrument when the code was free of errors.

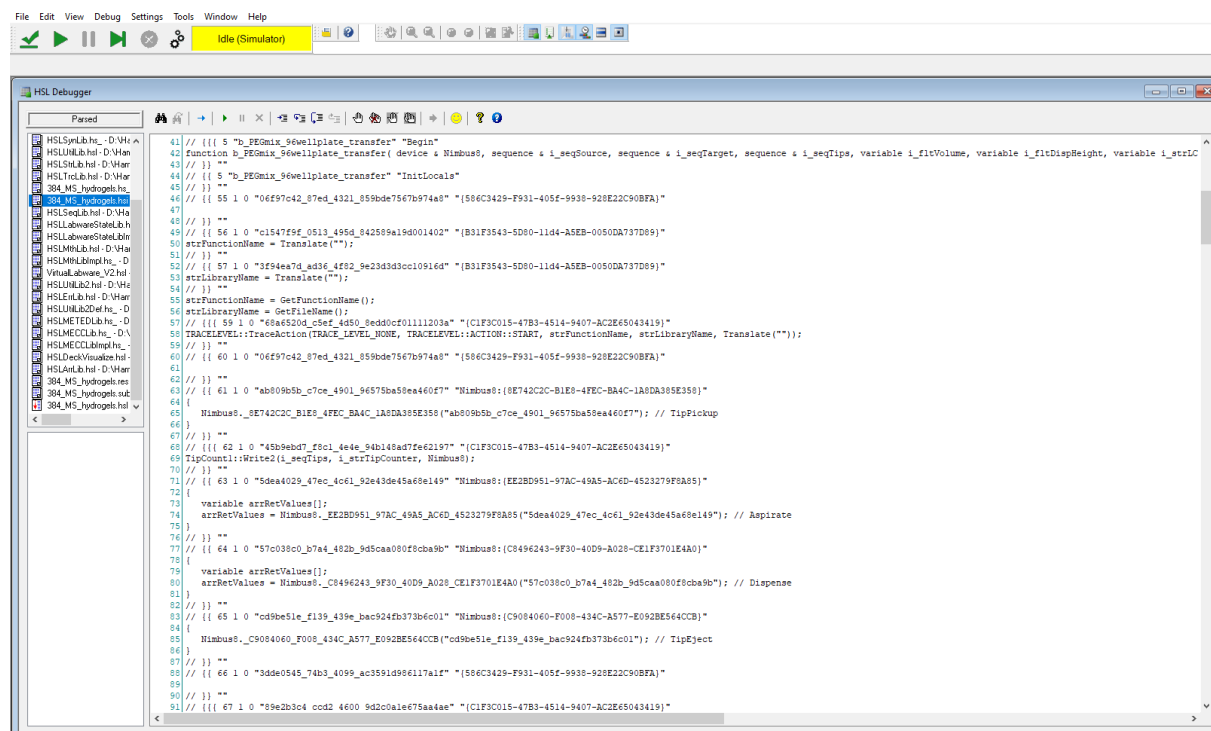


Figure 18. Screenshot from the Run Control application in simulation mode (yellow label on top). The main section displays the code generated from the drag-and-drop programming of the pipetting protocol. On the left side, there is a list of available files that can be executed by the application.

5.5.2.2 Protocol optimization using blank aqueous solutions

In order to check the correct functioning of the instrument when running the pipetting method, two colored aqueous solutions were used. For that, a buffer stock solution of HEPES 20 mM + NaHCO₃ 40 mM was freshly prepared in a 1.5 mL Eppendorf tube. Subsequently, two separate solutions were derived from this buffer, wherein each solution contained a distinct dye, fluorescein or rhodamine B. After thorough mixing in the vortex until homogeneity was reached, the two Eppendorf tubes, containing the colored solutions, were situated in the correspondent holder in the instrument.

Run Control application was then used to test the method in connection mode. To change pipetting parameters related to functions, such as the pipetting height or the volume, Hamilton Method Editor was used. On the other hand, Hamilton CO-RE Liquid Editor was used to modify parameters related to the liquid, such as the flow rate or the

swap/retracting speed, among several other functionalities which depend on the liquid properties (**Figure 17**).

The utilization of two solutions with different dyes facilitated the tracking of the pipetting process. This allowed for convenient detection of any issues, such as leakage or inadequate mixing, that could arise during the method.

5.5.2.3 Preparation of precursor solutions for hydrogel optimization

For the automated preparation of hydrogels, two precursor solutions containing the PEG-4TzMS backbone, pre-functionalized with the cell adhesion peptide c[RGDfC], and the peptide crosslinker VPM were prepared following a modified version of the recipe from R6 experiment, described in Chapter 4.

To prepare a single column of 6 hydrogels, a 54 μL stock solution of each precursor (PEG-4TzMS and VPM) was prepared. Out of this total volume, 24 μL were designated for the hydrogel preparation process, while the remaining volume accounted for the extra amount needed for the dead volume of the 1.5 mL Eppendorf tube (ca. 20 μL), and the potential loss of volume that may occur when the tip retracts from the liquid after each aspiration step from the automated pipetting method.

To this purpose, the stock solution of each precursor was firstly prepared at pH 8.0. Then, to the MS stock solution, an aliquot of 0.130 μL from a 5 mg/mL Atto 488 biotin stock solution in PBS was added per 100 μL of MS solution. Same was done for the VPM stock solution, but in this case Atto 594 biotin was used.

The gelation time was adjusted to allow sufficient time for the robot to mix and transfer the pre-hydrogel mixture to the 384 well plate within approximately 1 minute and 10 seconds, while minimizing any significant increase in viscosity, by decreasing the pH of the SH stock solution by adding HCL 1 M. Aliquots of 1 - 5 μL were added to the VPM stock solution until 2 ± 0.17 minutes gelation time was reached. To set the gelation time, an aliquot of 3 μL from each precursor solution was mixed until pipetting up and down was not possible anymore. The final pH of the VPM stock solution ranged from 7.1 to 7.3, depending on the exact gelation time.

5.5.2.4 Protocol optimization for hydrogels

Following the verification of the proper functioning of the new automated pipetting method using blank aqueous solutions, the subsequent step involved working with polymer solutions. This was done to consider the viscosity of the system throughout the entire pipetting process.

To configure the instrument, the desired pipetting and liquid parameters were defined using the Hamilton Method Editor and Hamilton CO-RE Liquid Editor, respectively. Subsequently, 50 μL and 300 μL tips racks, along with 96-well PCR plates and a 384-well plate, were positioned in their predefined locations on the instrument's deck layout.

Once the instrument was prepared, precursor solutions were freshly prepared as described in the previous section, just before initiating the method in the Run Control application. The gelation time was established after the preparation of the stock solutions, resulting in a time gap of approximately 25 minutes between dissolving the precursors and starting the automated hydrogel preparation.

The prepared stock solutions were placed in the designated holder of the liquid handling robot, the door of the enclosure was manually closed, and the method (**Figure 2B**) was initiated through the Run Control application.

5.5.2.5 Assessment of hydrogel variability

The variability of hydrogels prepared using the liquid handling robot was evaluated by measuring the fluorescence emitted by the dyes incorporated into the precursor stock solutions. Two different approaches were employed depending on the optimization stage:

- i. After preparing a single column consisting of 6 hydrogels, the method was paused using an infinite timer (which could be disabled when desired) and the enclosure door was opened. This extra step was performed by including a 4 lines step in the programmed code. The 384-well plate was covered to prevent any disturbances to the hydrogels and it was transported to the plate reader.
- ii. After preparation of 20 columns of 6 hydrogels each (totaling 120 hydrogels, which was the maximum capacity achievable with the pipetting method employed

during optimization), the method was finished. This triggered the automatic opening of the enclosure door, and the 384-well plate was subsequently transported to the plate reader after covering it.

The definition of the 384 low volume well plate was added to the database using the Tecan i-control software and fluorescence measurement mode was chosen for the analysis. The specific parameters for the measurement of the two different dyes were selected either from the drop-down menus or manually entered the designated fields on the measurement screen.

5.5.2.6 Design of Experiments

The optimization experiment for the mixing parameters was designed using Minitab software. To do this, the DOE option in the Statistics drop-down menu was chosen. A new full factorial design was created with two levels (high and low), three factors (mixing flow rate, mixing volume, and mixing cycles), one center point, and two replicates per factorial point.

For the analysis of the experiment, within the DOE menu, the "analyze factorial design" option was selected. First, the desired responses were chosen, which included the CV %, even / odd ratio %, or the raw fluorescence signal from each of the two Atto dyes. Subsequently, terms up to the 3rd order (1st and 2nd order were also tested) were selected. A bilateral confidence interval of 95% was chosen, and the desired plots, such as the Pareto Chart and Half normal plot of the effects, were also selected for visualization of the significance.

The final plots from the DOE analysis were modified by using the same Minitab software.

5.5.2.7 Alternative protocol for the isolation of the final dispense into 384 well plate

To ensure the isolation of the final transfer step to the 384-well plate from the other steps of the pipetting method, an alternative mixing protocol was implemented (**Figure 8**).

For the preparation of a single column of 6 hydrogels, a 40 μL stock solution of each precursor (PEG-4TzMS and VPM) was prepared as explained in section 5.5.4. Similar to previously described, 24 μL were allocated for the actual hydrogel preparation, and the

rest accounted for the dead volume of the 1.5 mL Eppendorf tube and the possible loss of volume that may adhere to the walls of the tube after mixing in the Vortex.

An aliquot of 34 μL from each precursor solution was pipetted into an empty 1.5 mL Eppendorf tube and vortexed for 25 seconds. The resultant pre-hydrogel mixture was rapidly transferred to 3 wells of the 96 PCR well plate, which was placed into the liquid handling robot as fast as possible, to avoid high viscosity during the following transfer into the 384 well plate. Finally, the door of the robot was manually closed, and the last step of the pipetting method was started through the Run Control application.

5.5.2.8 Modifying the pipetting method for the study of sacrificial wells

This experiment followed the same protocol as described in sections 5.5.2.3 to 5.5.2.5 of this chapter, with one modification made to the code of the pipetting method. Using the Hamilton Method Editor, an additional dispense step of 4 μL (with the exact same parameters as the subsequent dispensing steps in odd and even wells) was added through drag-and-drop programming before the dispensing in odd and even wells.

5.5.2.9 Setting different gelation times

The same protocol as described in sections 5.5.2.3 to 5.5.2.5 from this chapter was used in this experiment. Thus, a single stock solution of PEG-4TzMS with a pH of 8.0 was prepared, along with three different stock solutions of VPM to obtain three distinct gelation times. A solution of VPM with a pH of 7.70 was prepared to achieve a gelation time of 1 minute and 40 seconds. Another solution of VPM with a pH of 7.40 was prepared to achieve a gelation time of 2 minutes. Finally, a solution of VPM with a pH of 7.00 was prepared to achieve a gelation time of 4 minutes.

To minimize the disulfide formation, each VPM solution was freshly prepared before starting the preparation of the hydrogels in the liquid handling robot, which was done by following the previously described protocol.

Bibliography

- (1) Leung, B. M.; Moraes, C.; Cavnar, S. P.; Luker, K. E.; Luker, G. D.; Takayama, S. Microscale 3D Collagen Cell Culture Assays in Conventional Flat-Bottom 384-Well Plates. *J Lab Autom.* **2015**, *20* (2), 138–145. <https://doi.org/10.1177/2211068214563793>.

- (2) Rimann, M.; Angres, B.; Patocchi-Tenzer, I.; Braum, S.; Graf-Hausner, U. Automation of 3D Cell Culture Using Chemically Defined Hydrogels. *J Lab Autom.* **2014**, *19* (2), 191–197. <https://doi.org/10.1177/2211068213508651>.
- (3) Petersen, J.; Nguyen, J. Comparison of Absorbance and Fluorescence Methods for Determining Liquid Dispensing Precision. *Journal of the Association for Laboratory Automation* **2005**, *10* (2), 82–87. <https://doi.org/10.1016/j.jala.2005.01.009>.
- (4) Luo, T.; Tan, B.; Zhu, L.; Wang, Y.; Liao, J. A Review on the Design of Hydrogels With Different Stiffness and Their Effects on Tissue Repair. *Frontiers in Bioengineering and Biotechnology* **2022**, *10*.
- (5) Xue, B.; Tang, D.; Wu, X.; Xu, Z.; Gu, J.; Han, Y.; Zhu, Z.; Qin, M.; Zou, X.; Wang, W.; Cao, Y. Engineering Hydrogels with Homogeneous Mechanical Properties for Controlling Stem Cell Lineage Specification. *Proceedings of the National Academy of Sciences* **2021**, *118* (37), e2110961118. <https://doi.org/10.1073/pnas.2110961118>.
- (6) Kletzmayer, A.; Clement Frey, F.; Zimmermann, M.; Eberli, D.; Millan, C. An Automatable Hydrogel Culture Platform for Evaluating Efficacy of Antibody-Based Therapeutics in Overcoming Chemoresistance. *Biotechnol. J.* **2020**, 1900439. <https://doi.org/10.1002/biot.201900439>.
- (7) Brooks, E. A.; Jansen, L. E.; Gencoglu, M. F.; Yurkevicz, A. M.; Peyton, S. R. Complementary, Semiautomated Methods for Creating Multidimensional PEG-Based Biomaterials. *ACS Biomater. Sci. Eng.* **2018**, *4* (2), 707–718. <https://doi.org/10.1021/acsbomaterials.7b00737>.
- (8) Wahid, Z.; Nadir, N. Improvement of One Factor at a Time Through Design of Experiments. **2013**.
- (9) Czitrom, V. One-Factor-at-a-Time versus Designed Experiments. *The American Statistician* **1999**, *53* (2), 126. <https://doi.org/10.2307/2685731>.
- (10) Montgomery, D. C. *Design and Analysis of Experiments*; John Wiley & Sons, 2017.
- (11) Albert, K. J. *Automated Liquid Handlers As Sources of Error*. BioProcess International. <https://bioprocessintl.com/upstream-processing/assays/automated-liquid-handlers-as-sources-of-error-183663/> (accessed 2023-06-21).
- (12) Albert, K. J.; Bradshaw, J. T. Importance of Integrating a Volume Verification Method for Liquid Handlers: Applications in Learning Performance Behavior. *JALA: Journal of the Association for Laboratory Automation* **2007**, *12* (3), 172–180. <https://doi.org/10.1016/j.jala.2006.10.005>.
- (13) Taylor, P. B.; Ashman, S.; Baddeley, S. M.; Bartram, S. L.; Battle, C. D.; Bond, B. C.; Clements, Y. M.; Gaul, N. J.; McAllister, W. E.; Mostacero, J. A.; Ramon, F.; Wilson, J. M.; Hertzberg, R. P.; Pope, A. J.; Macarron, R. A Standard Operating Procedure for Assessing Liquid Handler Performance in High-Throughput Screening. *SLAS Discovery* **2002**, *7* (6), 554–569. <https://doi.org/10.1177/1087057102238630>.
- (14) Bradshaw, J. T.; Knaide, T.; Rogers, A.; Curtis, R. Multichannel Verification System (MVS): A Dual-Dye Ratiometric Photometry System for Performance Verification of Multichannel Liquid Delivery Devices. *JALA: Journal of the Association for Laboratory Automation* **2005**, *10* (1), 35–42. <https://doi.org/10.1016/j.jala.2004.08.012>.

6 Conclusions and outlook

In this doctoral thesis, hydrogels formed by the crosslinking of aryl methylsulfone and thiol functionalized PEG precursors were developed and characterized for their use as matrices in medium/high-throughput 3D cell culture. The main conclusions from the presented work are as follows:

The crosslinking kinetics and the final mechanical properties of hydrogel formulations as a function of the polymer precursor concentration, stoichiometry, thiol-crosslinker structure, functionalization degree and pH were analyzed by rheology. Hydrogels with tunable kinetics from seconds to minutes and variable shear modulus between 6 and 0.3 kPa were obtained. Among the different variants, a hydrogel formulation containing cell adhesive molecules (RGD) and a degradable dithiol crosslinker with a gelation time of >1 min and a shear modulus of 321 ± 94 Pa (at pH 8.0) was considered appropriate for cell encapsulation and the establishment of 3D cultures for automated medium/high-throughput workflows. Using a liquid handling robot, a protocol for the preparation of 5 μ l hydrogels in 384-well plate format was developed.

- i. A synthesis protocol for 4-arm PEG-TzMS precursor with 95% end-group functionalization was upscaled to 0.6 g with a cost reduction of 68 %. The instability of the intermediate Tz-4 in the Tz-MS synthesis protocol remained the major bottleneck for the synthesis of the polymer precursor. Although the 0.6 g scale was sufficient to establish the automated hydrogel formation protocol, it is not sufficient for the use of these hydrogels for HTP 3D cell cultures in the future. Alternative protocols need to be explored in the future.
- ii. A variety of potential alternative protocols for the synthesis of PEG-TzMS were described. However, the stringent criterium of end-group functionalization >95% required for stable hydrogel formation forces the use of highly reactive MS intermediates which can lead to instability of reaction intermediates and similar bottlenecks in the alternative pathways.
- iii. The release of methanesulfinic acid as byproduct of the crosslinking of PEG-TzMS with dithiols induces a continuous decrease in the pH of the reaction medium. The decrease in pH leads to a deceleration of the crosslinking rate as the reaction

progresses and could affect cell viability in a real system. The 20 mM HEPES + 40 mM NaHCO₃ buffer was sufficient to keep the pH constant during crosslinking of 5 wt% PEG-4TzMS hydrogels in the present study and allowed formation of stable networks in minutes within the pH range of 7.0 to 8.0. Monitoring of the pH during crosslinking is recommendable when exploring MS-Thiol chemistry for a real application.

- iv. An increasing gelation time and decreasing mechanical stability were observed in our PEG-MS/thiol hydrogels as the concentration of the tetra-arm PEG concentration decreased. By keeping the polymer solid content and crosslinking conditions constant, gelation kinetics and mechanical properties from MS-SH hydrogels can be tuned by modification of the crosslinker's chemical and structural architecture. The obtained results can be explained in terms of crosslinking density as it varies with the polymer and crosslinker concentration, length and functionality. This suggests that the formed hydrogel is homogeneous and the gelation proceeds in a reaction-controlled mechanism. The multiple parameters available to tune the reaction rate and the final properties allow to adapt the properties of the hydrogel to the needs of the cell culture.
- v. The potential formation of disulfide bonds by dithiol crosslinkers leads to a lower concentration of available thiols in the medium for crosslinking and represents a drawback in thiol-based crosslinking systems. In particular, disulfide formation led to lower mechanical stability of hydrogels when using the enzymatically degradable peptide crosslinker VPM. This could be counteracted with an excess of VPM, which resulted in stiffer hydrogels.
- vi. Pre-functionalization of synthetic backbones with cell-adhesion ligands is necessary to improve cytocompatibility of PEG-based hydrogel networks. In the MS hydrogels, this can be done with a simple preincubation step of the PEG-MS with the thiol containing ligand. The incorporation of the RGD motif translated into lower concentration of available MS end-groups for crosslinking and into hydrogels of lower stiffness due to lower concentration of crosslinking points.
- vii. Preparation of low volume (down to 5 μ L) hydrogels based on the MS-SH crosslinking reaction can be automated by using a liquid handling system and 384-well plates. This opens the possibility to use the MS hydrogels for medium/high-

throughput 3D culture applications, provided the synthesis of the PEG-TzMS derivative can be upscaled in the future.

- viii. This work introduces a novel in situ crosslinked hydrogel designed for 3D cell encapsulation and compatible with automated liquid handling systems within medium/high-throughput frameworks. The developed hydrogel formulation in this Thesis with a gelation time between >1 min at pH 8.0, 4 min at pH 7.5 and 6 min at pH 7.0 is sufficient to allow aspiration, mixing and dispensing steps in an automated liquid handling system.

The pH-dependent thiol-TzMS crosslinking chemistry, presenting gelation times from seconds to minutes at near physiological pH (7.0 – 8.0), is a step forward in filling the existing gap in the library of thiol-mediated biocompatible chemistries for hydrogel crosslinking. The reaction's high selectivity, tunable kinetics, and stability of the final adduct make it a highly promising alternative for hydrogel crosslinking. Although the thiol-TzMS reaction releases methanesulfinic acid as a side product, this does not significantly affect cell viability in presence of sufficient buffering capacity, remaining the viability remarkably comparable to established thiol-maleimide and thiol-vinyl sulfone chemistries. Furthermore, the straightforward synthesis of the tetrazole-MS hydrogel precursor, optimized and upscaled in this thesis, enhances its potential for its application in medium/high-throughput formats where compatible hydrogels are currently limited.

As for the use of MS hydrogels in 3D cell culture after encapsulation, their low stiffness of approximately 0.3–6.0 kPa (under the tested conditions) makes them ideal for encapsulating cells from relatively soft tissues such as adipose, brain, lung, and even muscle. Moreover, the tunability of their stiffness by modifying the crosslinker architecture at a given polymer concentration, as well as by potentially altering their polymer content, broadens their applications for 3D cell encapsulation of various cell types. This flexibility in adjusting mechanical properties allows MS hydrogels to be tailored to specific cellular environments, enhancing their utility in a wide range of tissue engineering and regenerative medicine applications, among other possible fields.

For similar systems involving stoichiometric crosslinking reactions between complementary reactive groups, this study highlighted the importance of carefully controlling the concentration of hydrogel precursors. The research demonstrated, through a stepwise study involving techniques such as LC-MS and rheology, that thiol-mediated chemistries using thiol-containing crosslinkers must pay special attention to thiolated molecules, which may form disulfide bonds. These bonds can disrupt the stoichiometric ratios, leading to variability in hydrogel formation and potentially affecting cell behavior.

The lack of automated protocols for medium/high throughput 3D cell encapsulation, as well as compatible and temporary cell supports like hydrogels, hinders the potential application of these systems in fields such as drug discovery and development. Therefore, the introduction of the TzMS hydrogel with tunable gelation times at near-physiological conditions and compatibility with automated liquid handling systems represents a significant advancement. In addition, the developed semi-automated protocol can be implemented for other systems involving more than one hydrogel precursor whose crosslinking occurs under similar conditions. This development enhances reproducibility in medium/high-throughput formats and paves the way for a more standardized 3D encapsulation of cells in hydrogels. Thus, this study not only broadens the range of available biocompatible hydrogels but also facilitates more efficient and reproducible 3D cell culture studies in automated workflows.

To expand the impact of this study, future efforts should prioritize the integration of cells and further refinement of the semi-automated protocol. Incorporating cells could alter the properties of the pre-hydrogel mixture, affecting viscosity and flow, necessitating adjustments in pipetting parameters such as aspiration and dispensing speeds. Additionally, pipetting steps such as mixing, involving consecutive aspiration and dispensing steps that create turbulence, may subject cells to shear stress, potentially impacting cell viability and requiring optimization of parameters.

Exploring the mechanical properties of hydrogels, as well as cell behavior in medium/high-throughput formats will require adapting techniques like nanoindentation and microscopy to such workflows. Challenges may arise in nanoindentation due to the

Conclusions and outlook

size constraints of wells in 384- or 1536-well plates. Similarly, cell assays involving staining, such as fluorescence microscopy, may face difficulties during washing steps due to well size limitations, necessitating the development of alternative protocols.

7 List of publications

The work presented in this PhD thesis contributed to the publications listed below:

- (1) **de Miguel-Jiménez A**, Ebeling B, Paez JI, Fink-Straube C, Pearson S, del Campo A. Gelation Kinetics and Mechanical Properties of Thiol-Tetrazole Methylsulfone Hydrogels Designed for Cell Encapsulation. *Macromol. Biosci.* 2023; 23; 2200419; doi: 10.1002/mabi.202200419.

- (2) Paez JI, **de Miguel-Jiménez A**, Valbuena-Mendoza R, Rathore A, Jin M, Gläser A, Pearson S, Del Campo A. Thiol-Methylsulfone-Based Hydrogels for Cell Encapsulation: Reactivity Optimization of Aryl-Methylsulfone Substrate for Fine-Tunable Gelation Rate and Improved Stability. *Biomacromolecules.* 2021; 22(7): 2874-2886; doi: 10.1021/acs.biomac.1c00256.

- (3) Trujillo S, Kasper J, **de Miguel-Jiménez A**, Abt B, Bauer A, Mekontso J, Pearson S, del Campo A. Cytocompatibility Evaluation of PEG-Methylsulfone Hydrogels. *ACS Omega.* 2023; 8(35); 32043-32052; doi: 10.1021/acsomega.3c03952.